A STUDY OF THE INFLUENCE OF WALL FLEXIBILITY ON PRESSURE IN RECTANGULAR SILOS

A thesis submitted for the degree of Doctor of Philosophy

by

Neil Dennis Jarrett

Department of Mechanical Engineering, Brunel University

May, 1991

ABSTRACT

The pressure exerted by the stored material on rectangular planform flexible walled silos is investigated during filling and discharge. Tests on a large scale steel model silo with a pyramidal hopper showed that the stress state of the stored material is significantly influenced by the wall flexibility and boundary conditions. The measured wall pressures were very different to pressures predicted by traditional theories and existing design codes. This is because traditional theories were developed for rigid walled circular silos and they ignore the effects of stored material/structure interaction.

In this thesis the results of tests to measure the stress state throughout the contents of a flexible silo and pyramidal hopper are presented and compared with measurements of the structural response. The tests show that the redistribution of stresses within the stored material is extensive and is influenced by the corners in non-circular silos and horizontal and vertical stiffeners. As wall flexibility increases, there is increased freedom for stresses imposed by the stored material to redistribute and reduce the structural forces in the wall. The measured pressures in the corners of the model silo were up to nine times the pressures at the centre of the wall at the same level. The failure to incorporate the redistribution into the model design led to a considerable over estimate of the wall stresses.

Many existing measurements of pressures in the stored material in silos were weakened because of inaccurate instrumentation. In this study, considerable care was taken during the selection of pressure cells, calibration and equilibrium checks to ensure the accuracy of measured data. Pressure was measured in four directions at forty eight positions in the model to determine the total stress state throughout the stored material. The results showed that wall pressures were influenced by five different arching phenomena.

It is concluded that the existing theory is not accurate for pressure calculation in flexible non-circular silos. The use of a more accurate theory for the calculation of wall pressure can lead to extensive savings in the cost of the silo structure.

Acknowledgements

The author would like to thank Mr C.J. Brown of the Mechanical Engineering Department, Brunel University and Dr D.B. Moore of the Structural Design Division, Building Research Establishment for their guidance and support throughout this project. Advice and the loan of pressure cells from Dr J. Nielsen and Dr J. Munch-Andersen of the Danish Building Research Institute and Prof. V. Askegaard of the Technical University of Denmark is gratefully acknowledged. Finally special thanks are owed to Geraldine for her patience and understanding over the past three years.

List of Contents

Notation

a,b = Side length

d = Diameter of silo

d_p = Mean particle diameter

f = Particle shape constant

g = Gravitational acceleration

h = Depth

k = Buckling constant

q = Wall frictional force per unit area

t = Wall thickness

x,y,z = Cartesian co-ordinate axes

A = Cross sectional area

C = Perimeter

D = Diameter

E = Elastic modulus

F = Force

F_{cr} = Critical buckling load

H = Dimensionless depth h/d

K = Ratio of horizontal to vertical pressure

K_a = Active ratio of horizontal to vertical pressure

K_o = At-rest ratio of horizontal to vertical pressure

L = Outlet size

P = Pressure

P_h = Horizontal pressure

P_i = Inclined pressure

P_{max} = Maximum pressure

P_n = Pressure normal to the wall

P_v = Vertical pressure

P_{vtrans} = Vertical pressure at the hopper/bin transition

P_{wi} = Inclined wall pressure

R = Hydraulic radius (A over C)

T = Geometry constant (Reimbert's equations)

V = Volume

W_d = Discharge rate

α = Angle of wall from the horizontal

β = Angle of sloping backfill from the horizontal

γ = Angle of wall to the vertical

ρ = Unit Weight

δ = Angle of wall friction

ψ = Angle of critical shear surface to the horizontal

μ = Poissons ratio

σ_h = Static vertical pressure at depth h

σ_n = Normal stress

σ_p = Stress parallel to the wall

σ_v = Vertical stress in the stored material

τ = Shear stress

τ_w = Shear stress at the interface of wall and stored material

ϕ = Internal angle of friction

1. Introduction

Silos usually consist of a vertically sided section on top of a section with inclined sides (Figure 1.1). They can be used to store grain, coal, cement, mineral ores and many other materials in quantities up to one hundred thousand tonnes. The majority are constructed from either steel or reinforced concrete.

Figures 1.1(a) to 1.1(d) illustrate four different types of silo. This project aims to determine the pressure on the walls of steel silos with an aspect ratio similar to that illustrated in Figure 1.1(a). They are referred to as square silos. They are not necessarily square in plan-form but the ratio of length to width will be less than that of the trough shaped silo illustrated in Figure 1.1(b).

A number of analytical methods has been developed for the determination of the pressure upon the walls of silos. Each method is based upon different assumptions and is only applicable to a certain type of silo. Whereas reinforced concrete and circular steel silos have received considerable attention, the stresses within the stored material in rectangular steel silos remain less well determined. Traditionally the static wall pressure in square and rectangular silos has been calculated using the Janssen theory [1] , the Reimbert theory [2] or earth pressure theories such as those presented by Rankine [3] or Coulomb [4]. The resulting pressures are multiplied by a safety factor to prevent failure due to any pressure deviations which may occur during discharge. The methods provide two dimensional solutions, and ignore any variation in wall deformation at constant depth. They consider that the wall is rigid and non-deforming or that it deforms by rotation about the lower boundary only. The walls of square silos carry load from the stored material by a combination of membrane and bending action. Deformation is greater in the centre of a silo wall than at the corners and because the imposed pressures are dependent on wall deformation, a non-uniform pressure distribution results.

The interaction of a flexible silo wall and stored material has been modelled by Chandrangsu [5] , Ibrahim [6] , Ooi [7] A. Mahmoud [8] and M. Mahmoud [9, 10]. They all considered axisymmetric or plane strain problems and assumed no pressure differential on a horizontal section. Other authors [11, 12] have investigated the effect of different modes of rigid wall deformation on wall pressure but only a few studies have considered the interaction of soil and a flexible wall. Stroyer [13] proposed a

theory for the redistribution of pressure on flexible sheet pile walls restrained along their upper boundaries by ground anchors. He found that the outward deflection of the middle of the wall mobilised shear stresses within the stored material and resulted in a transfer of pressure from the deformed centre of the wall to the supports at the upper and lower boundaries. Stroyer's theory was disputed by Rowe [14] who stated that the ground anchors yield sufficiently to mobilise an active state of pressure behind the wall. Non-circular silos have very stiff corners and relatively flexible walls and so it is possible that the phenomenon described by Stroyer for retaining walls is manifested in non-circular silos. If so, it would generate a redistribution of pressure from the centre of the silo wall to the corners.

The results of most of the experiments carried out to investigate the effect of wall flexibility on wall pressure are unreliable mainly due to the inaccurate pressure measurement equipment used. It is only recently that pressure cell design has advanced sufficiently to enable the accurate measurement of pressure in a granular medium. Two types of Pressure Cell have been developed. Cells which are built into the wall and measure pressure at the interface of the wall and stored material and cells embedded in the stored material. Wall cells can now be designed to minimise any disturbance of the stored material and hence a high level of accuracy is possible. Embedded cells are sensitive to the method of placement. They are less accurate than wall cells because both the placing and the presence of the cell changes the stress field of the surrounding material.

Experimental studies of soil-structure interaction have been conducted on rigid walls and flexible retaining walls [11, 12, 13, 14, 15]. Although many studies have been carried out on rigid cylindrical silos, only Pieper [16] , Reimbert [2] , Walker and Blanchard [17] , Tattersall and Schmidt [18] and Moran [19] have investigated pressures on non-circular flexible silos and they all neglected to consider any pressure variation over a horizontal cross section. Pressure away from the silo wall has been measured by Askegaard [20] and Munch-Anderson [21] to investigate the stress state of the stored material during mass flow discharge in deep rigid walled silos. There is no work which has attempted to determine the horizontal distribution of pressure on the walls of square silos. The purpose of this project is to determine the factors affecting wall pressure and to propose a theory for pressure calculation.

The project has four distinct sections:

(1) The appraisal of existing theories for earth pressure and soil structure interaction, and the identification of possible phenomena that affect pressure in non-circular flexible silos.

(2) The assessment of existing silo and hopper wall pressure theories for application to flexible non-circular silos.

(3) The measurement of pressure within a large-scale model silo, and comparison of the results with existing theory.

(4) The measurement of wall strains to establish the effect of wall flexibility on wall stresses.

The remainder of this chapter describes the common forms of silos and the influence of the silo aspect ratio and wall structural material on design. Chapters 2 and 3 discuss existing theory, while Chapters 4 and 5 outline the design and instrumentation of the test rig. The remainder of the project is devoted to the discussion and analysis of test results.

1.1. Silo Classification

1.1.1. Silo Forms

In this thesis the vertical walled section of the silo is referred to as the 'bin'. The word 'silo' is used to describe the entire structure and the hopper is the lower section with inclined walls. Silos are classified by the height to width ratio, plan-form, wall structural material and the type of flow during discharge of the contents.

Height to width ratio

Silos may be classified as shallow or deep. As an approximate guide, shallow silos are defined as those in which the height does not exceed one and a half times the diameter or shorter side length. Deep silos have a height to diameter ratio greater than that of shallow silos [22].

Plan-form

Silo plan-forms are usually circular or rectangular. Often the circle is the most economical shape for a silo, and if the loads are axially symmetric silos are designed to withstand tensile forces only. If the silo is designed to withstand eccentric loads then the walls have to withstand bending forces and consequently the circle may not be the most economic form, and square silos that carry their loads by bending can provide an economical solution [23].

Wall structural material

A silo wall is subjected to horizontal and vertical forces. The horizontal forces are due to the lateral thrust from the stored material and the vertical forces (which are a function of the lateral thrust) result from friction between the wall and stored material. Reinforced concrete silos carry vertical compressive forces with relative ease and so tend to fail in tension due to high lateral thrusts [24,25,26,27]. Circular plan-form steel silos usually carry the lateral forces by hoop tension, and they are more prone to failure by buckling under excessive vertical forces [28]. Square steel silos and trough bunkers are usually stiffened plate structures. Horizontal and wall friction loads result in a combination of in-plane axial and out-of-plane bending forces, the ratio of which depends upon the plate thickness [29]. These silos have a low rate of failure but tend to be conservatively designed [30].

The increase of horizontal and vertical pressure with depth is shown in Figure 1.2. Increases in

horizontal pressure may be negligible beyond a certain depth and therefore concrete silos are more efficient if they are tall, whereas steel silos tend to be shallow squat structures.

Flow type

Several types of flow have been identified [31]. For the purpose of this thesis, it is sufficient to limit the description to the two principal types and they are mass flow and funnel flow (Figure 1.3). Mass flow occurs mainly in deep silos with steep hopper walls. All the contents of the silo flow as a single mass. Funnel flow occurs in squat silos with shallow hopper walls. The material flows down a central core of stationary stored material. The flow type required in a silo depends on the stored product. For perishables, mass flow is preferable.

Jenike [32] developed a method for determining the flow type within a silo of any plan-form. He found that it is a function of the strength of the stored material, the coefficient of friction between the silo wall and stored material, and the angle of inclination of the hopper. The relationship between these parameters is presented graphically in Figure 1.4.

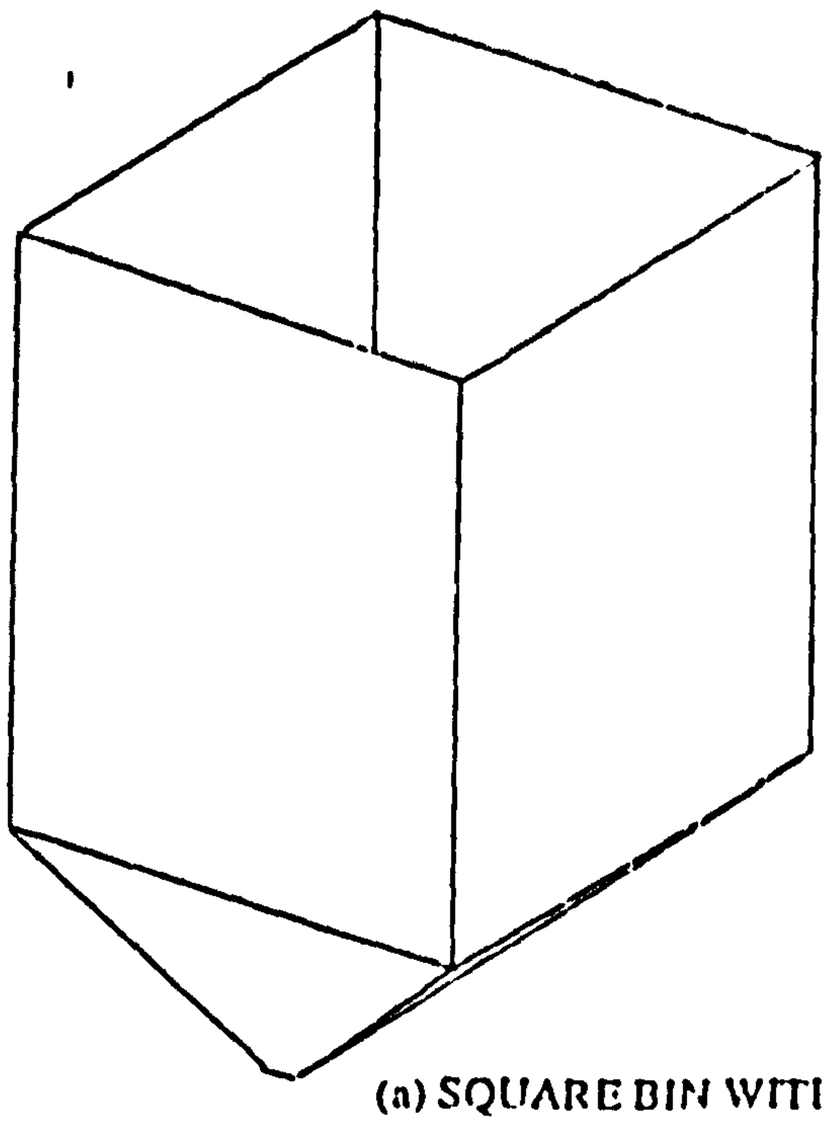

(a) SQUARE BIN WITH PYRAMIDAL HOPPER

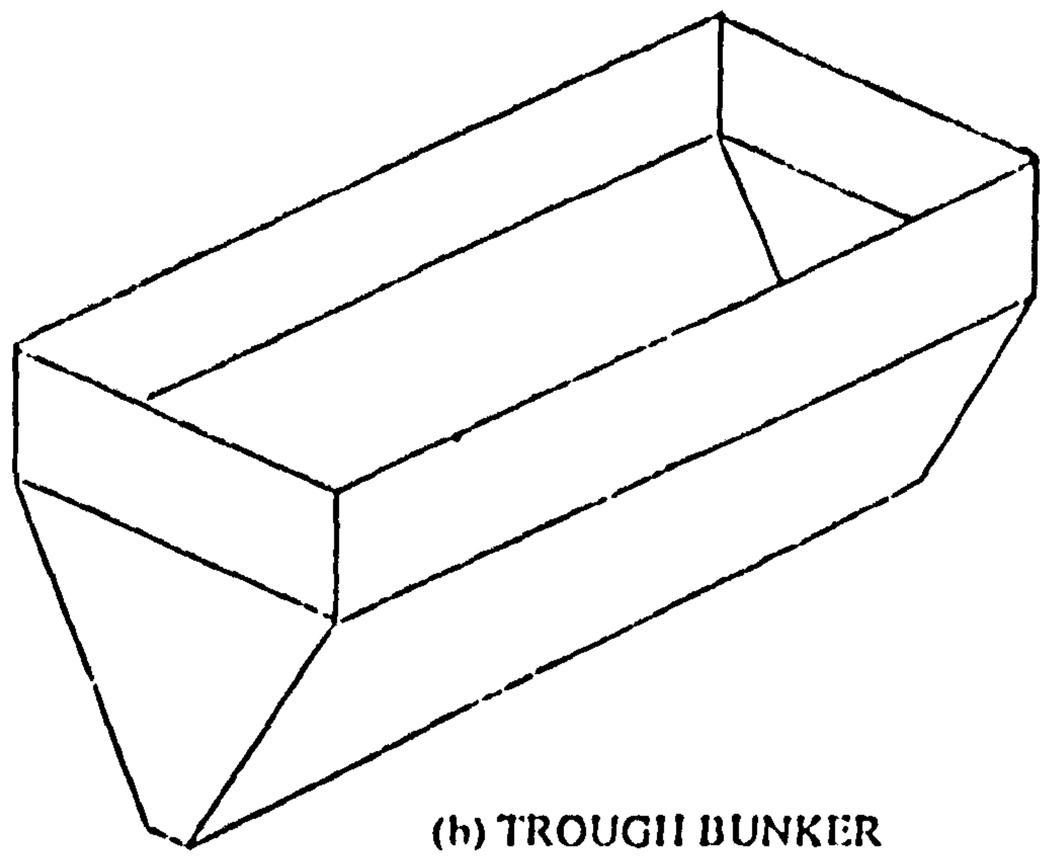

(b) TROUGH BUNKER

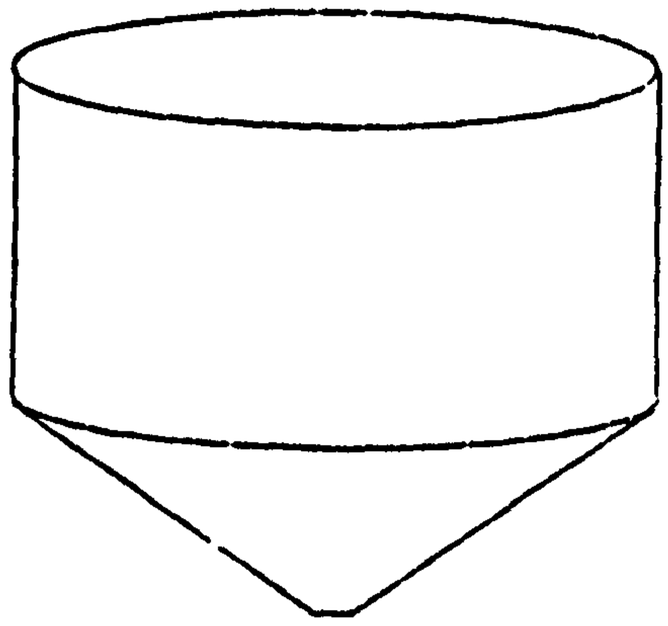

(c) SHALLOW, FUNNEL FLOW CYLINDRICAL BIN WITH CONICAL HOPPER

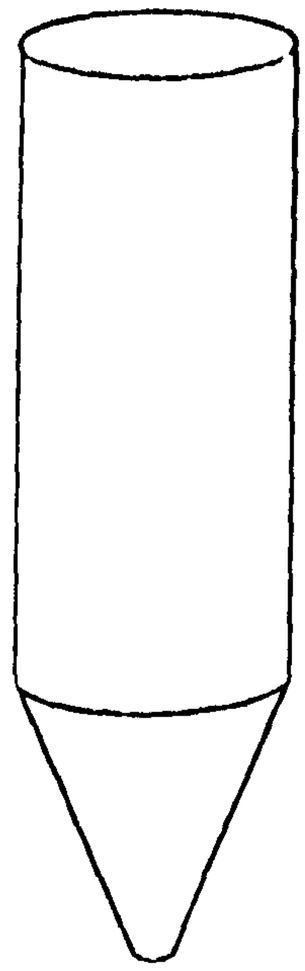

(d) DEEP MASS FLOW BIN

Figure 1.1

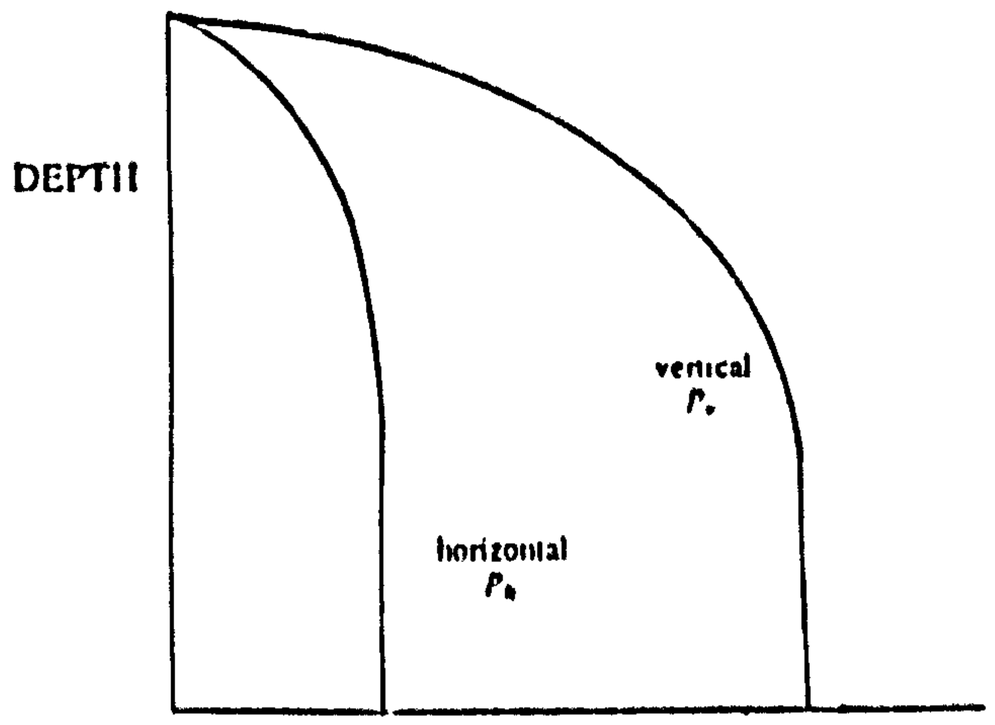

Figure 1.2 DISTRIBUTION OF HORIZONTAL AND VERTICAL PRESSURE AGAINST DEPTH OF STORED MATERIAL

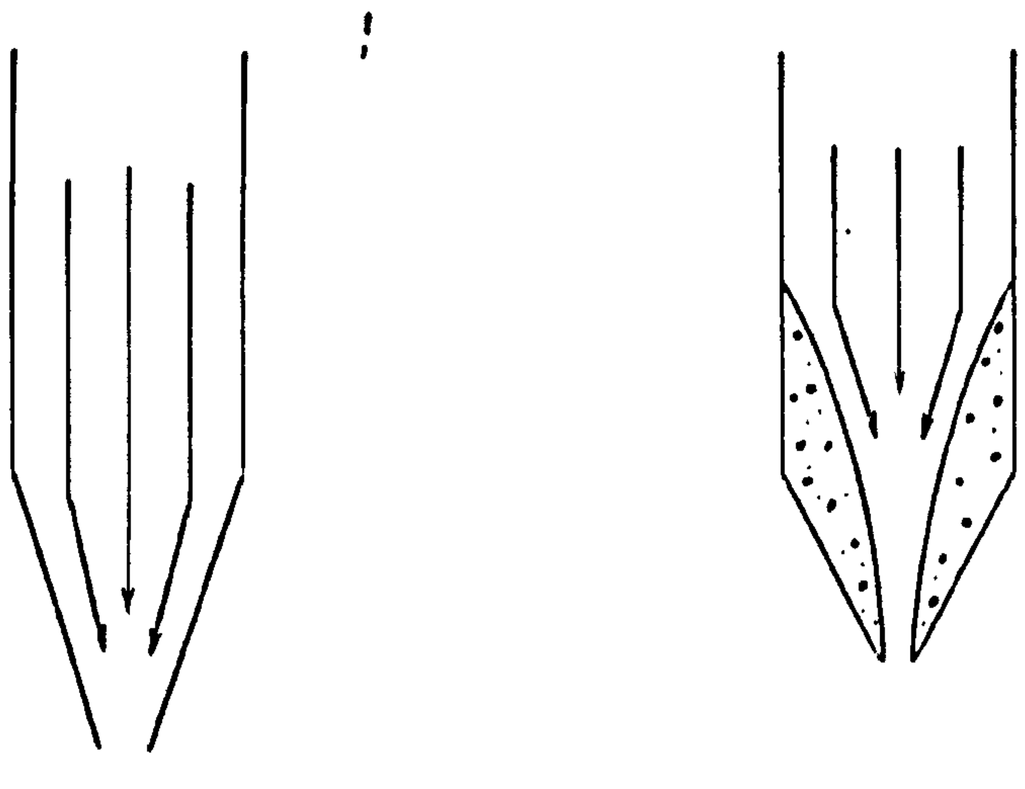

Figure 1.3 FLOW TYPES

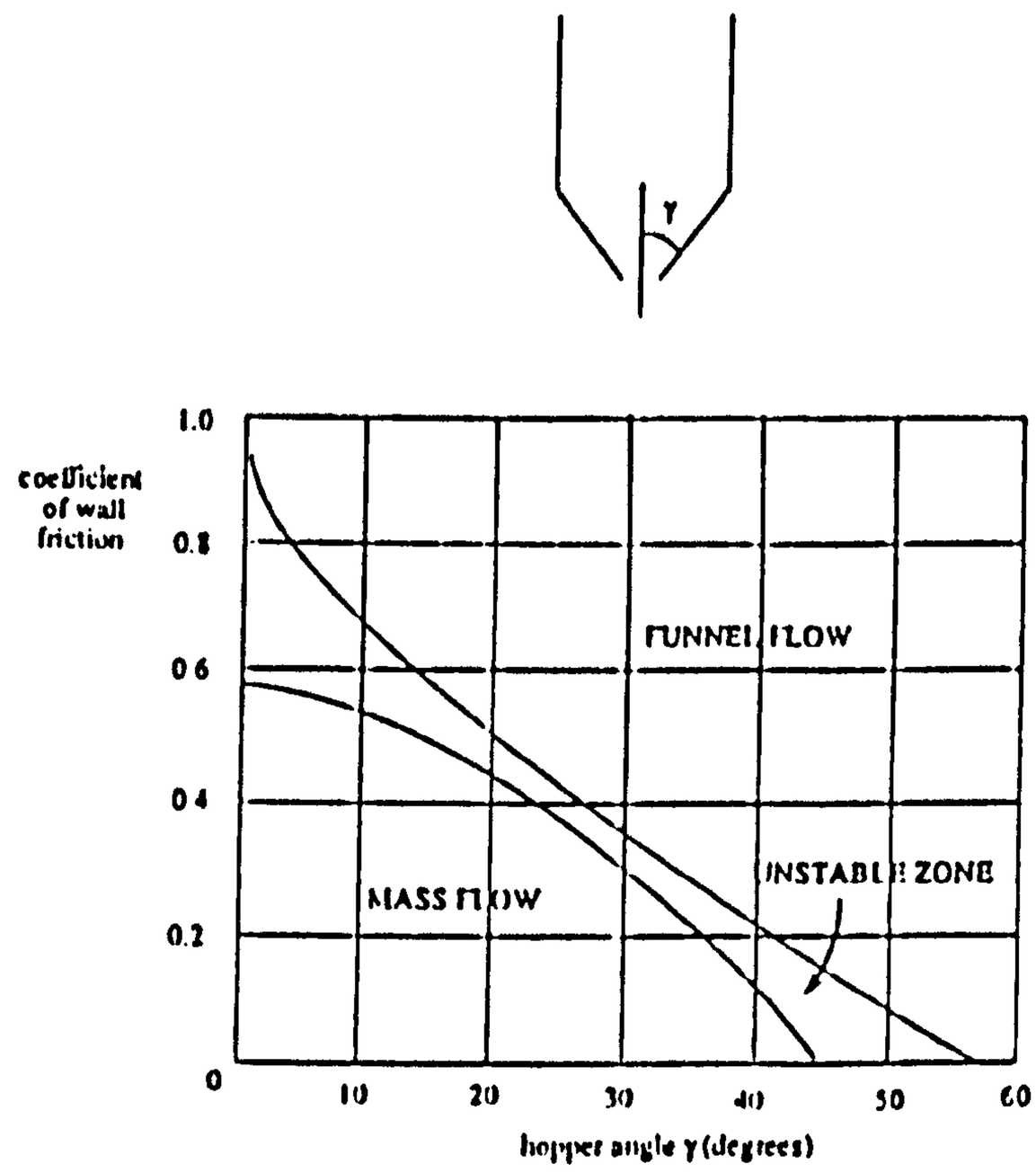

Figure 1.4 RELATIONSHIP BETWEEN HOPPER ANGLE, COEFFICIENT OF WALL FRICTION, AND FLOW TYPE FOR CONICAL HOPPERS
SOURCE: JENIKE

2. Stress states within the silo stored material

The pressure exerted on a silo wall by the stored material is different when the material is flowing and when it is stationary. For design purposes it is necessary to determine the stress at the silo wall during filling of the silo, when the stored material is static and when the material is discharging. Each of these cases is discussed below. The discussion includes other factors which affect pressure such as moisture content, temperature variation and segregation and degradation of the stored material.

2.1. Static stress state

The stored material in a silo will be either in a state of elastic or plastic equilibrium. The active and passive states are the two limiting states. They are plastic states of equilibrium, and are reached after lateral expansion of the stored material (active state) or lateral contraction of the stored material (passive state) when a critical combination of shearing and normal stress leads to shear failure. Every state between the active and passive states, including the at-rest state, is a state of elastic equilibrium. Shear failure is defined by the Mohr-Coulomb criterion. For cohesionless materials this reduces to

$$\tau = \sigma_n \tan\phi \qquad (2.1)$$

where τ is the maximum shear stress at failure within the stored material, and σ_n is the stress normal to the failure plane.

The stress state at any point within the silo contents will depend upon the distance to the surface of the stored material, the material properties, the wall roughness and the wall deformation.

2.1.1. Silo with rigid walls

When a granular mass is deposited into a silo with rigid walls the material may assume an elastic state [33] as the wall has not moved. Because of symmetry there will be no shear stress in the vertical plane at the centre line of the silo and the vertical pressure will be the major principal pressure. Alternative views [34,35] suggest that the stored material assumes a plastic stress state and is represented by the Mohr's circle 'C-D' in Figure 2.1. Friction between the wall and stored material will change the direction of the maximum principal stress from the vertical. The stress at the wall is represented by the Mohr's circle 'A-B' in Figure 2.1. It follows that the stress at any point between the centre of the silo and the wall and at the same depth will be represented by a circle lying between these circles.

The major and minor principal stresses are approximately related by Jaky's [36] coefficient K_0 which can be presented in simplified form as

$$\frac{\sigma_h}{\sigma_v} = K_0 = 1 - \sin\phi \tag{2.2}$$

Compressible materials deposited into the hopper will consolidate as the level of the stored material rises during filling. Since the walls are inclined, the material will compress laterally as well as vertically and will approach a passive state of plastic equilibrium [37].

2.1.2. Silo with deformed walls

The soil behind a rigid wall which has rotated about its base is shown in Figure 2.2(a). The failed soil is illustrated as a series of layers inclined at an angle equal to $45 + \frac{\phi}{2}^{o}$ from the horizontal. Each layer has slipped over the layer below. The stored material is in a plastic state of equilibrium and pressure varies linearly with depth as shown in Figure 2.2(b) [38]. Pressure at the wall is influenced by the wall

deformation and the stiffness of the stored material. The wall pressure may be calculated by either the Rankine (equation 3.15) or Coulomb (equation 3.21) theories if wall friction can be ignored.

Figure 2.3 illustrates the deformation required to fully mobilise the active and passive stress states for sand [39]. The rotation required to mobilise the plastic state in a stored material behind a wall pivoting about its base will depend upon the stress/strain characteristics of the stored material. Figure 2.3 shows that the wall rotation required to mobilise the active state is much less than that required to mobilise the passive state.

The shear stress-strain curve for a dense cohesionless material is shown in Figure 2.4. Terzaghi [33] stated that the drop in strength of the stored material is due to dilation. He noted that once a surface of failure has developed, the material dilates. This reduces the interlock between particles along the failure plane and hence reduces the shear strength during further sliding. It is unlikely that the peak strength of the stored material will be mobilised at the same instant throughout the failure plane. Rowe and Peaker's analogy [15] of a shear surface behind a retaining wall and the corresponding positions on the shear stress-strain curve are shown in Figure 2.5. Positions *a* to *c* are in a state of plastic equilibrium whereas positions *c* to *f* have not reached shear failure. Wall friction causes a change in the direction of the principal stresses (discussed in Section 2.1.1.) and consequently a re-orientation of the failure surface close to the wall. This is shown in Figure 2.1.

In practice, silo walls are unlikely to deform in the manner described above. They may be flexible and restrained at the top and bottom. Terzaghi [38] and Fang [12] have investigated the pressure distribution behind rigid walls for different modes of deformation. They found that horizontal translation or rotation of the wall about the upper edge result in a pressure distribution similar to that shown in Figure 2.6. Terzaghi presented a theory for the calculation of pressure behind walls which deform in this manner. Terzaghi's general wedge theory is described by Clayton [39]

> "The [stored material] close to the base of the wall will have mobilised its full shear resistance, and will attempt to move downwards. Because the [stored material] above has not yet reached failure, it will be partially suspended by the shear forces on the final shear

> surface and the top of the back of the wall. The [stored material] will 'arch' between the wall and the shear surface, and the centre of pressure will be moved upwards relative to its position as if the wall had rotated about its base."

The arching phenomenon is not limited to these few modes of wall deformation. It occurs in a number of situations where there is interaction between a yielding structure and a particulate medium (such as the stored material in a silo). The consideration of the arching phenomenon is essential to the correct prediction of pressure in flexible square silos.

2.1.2.1. Arching in soils

In this Section, the arching phenomenon is discussed with reference to common examples from soil mechanics texts. The term 'soil' is used because the examples are related to specific problems of soil-structure interaction. Arching is a transfer of pressure from a yielding mass of soil onto adjoining relatively stationary parts. A simple description of arching is given by Terzaghi's [33] prediction of the stress distribution in the soil above a yielding strip (Figure 2.7).

Before yield of the strip the vertical pressure is equal to the product of the unit weight of the soil and the depth of soil above the strip. As the strip yields, the descent of the column of sand located above it is resisted by shearing stresses along the boundaries A-A and B-B. The load on the strip decreases and the friction force on the planes increases. The soil has arched over the yielding strip.

Costes [40] investigated arch formation over underground ducts. He found that the planes of sliding are not vertical but are curved. At the surface of the soil their spacing is greater than at the yielding strip. He also stated that during subsidence of the strip, horizontal layers within the yielding soil mass do not remain plane and the surfaces of equal normal pressure are not plane but are curved like arches.

Terzaghi assumed that the yielding strip deforms sufficiently to mobilise the full shear strength of the soil over the entire length of the shear planes. This may result in an underestimation of the load on the yielding strip since the degree of mobilisation of the shear strength will depend upon the magnitude of

deformation of the strip relative to the deformation of the floor and the stiffness of the soil. The mobilised shear strength will also decrease with distance from the yielding strip. The vertical friction planes will not extend to the surface of the soil if the surface is at a sufficient distance from the strip. Costes describes a plane of equal settlement. Above the plane, the settlement is uniform over any horizontal layer of the soil. Below the plane, frictional stresses increase from zero at the plane to the full shear strength of the soil at some distance below.

Stroyer [13] studied the arching of soil behind a flexible sheet pile wall. Such a wall is shown in Figure 2.8 and the soil is represented by a series of strips. The anchor at the top of the wall prevents horizontal translation and movement of any layer is outwards in relation to the layer above. Near the bottom, the movement of any sliding strip is outwards in relation to the layer below. Towards the middle, the soil slides outwards in relation to the strips both above and below. The centre strips are restrained from movement by friction on adjacent strips. Some outwards force is transferred from the centre strips to the strips above and below. In the same manner the adjoining strips are restrained from sliding by adjacent layers, to which they in turn transfer some of their force. Ultimately, a certain part of the pressure on the wall is transferred through internal friction to the upper and lower supports.

Similarly arching may occur in a square planform silo with flexible walls. Figure 2.9 shows a plan and side elevation of the deformed walls of a loaded silo. It is possible that an arch will form over the deformed wall. Pressure will be relieved in the centre of the wall and increased in the corners. A second possibility is that vertical arches will form between a stiff ring beam at the top of the hopper and the hopper outlet. Other vertical arches may form between horizontal stiffeners or between a ring beam at the top of the hopper and a ring beam at the top of the silo.

There are no existing experimental or theoretical data to demonstrate the formation of arches within silos (other than arches formed by friction at the interface of the wall and stored material and described by Janssen [1]. These are discussed in Chapter 4). If arches do occur, the static state of stress in the silo may be very different to that predicted by existing theory.

Figure 2.10 shows a summary of the most probable modes of arching in the silo. All the arches are due to the same phenomenon which is a transfer of pressure from a yielded part of the stored material to a non-yielding boundary. The non-yielding boundary may be a part of the silo structure or the stored material. Each type of arch has been named and is described below. They will be referred to by these names throughout this work.

1. The Janssen arch (Figure 2.10a)

The Janssen arch forms after consolidation of the stored material. It introduces shear at the interface of the silo wall and the stored material and across any horizontal section of the stored material. The arch results in a transfer of vertical pressure from the consolidated stored material to the wall. Janssen [1] developed a rational theory for pressure on a silo wall and incorporated the effects of this arch. It is described in Chapter 3.

2. The horizontal arch (Figure 2.10b)

This leads to a pressure transfer across any horizontal plane behind a wall where there is variable wall deformation. The deformation of the centre of the wall is greater than that at the edges and this results in a pressure transfer from the centre to the edges.

3. The vertical arch (Figure 2.10c)

This occurs behind a wall on a vertical plane, but only when the deformation of the upper and lower boundaries is restricted. The example given in Figure 2.10c is a vertical section through a hopper wall. The upper boundary is restrained by a stiff ring beam and the lower boundary is restrained by the outlet. Wall deformation leads to a pressure transfer from the middle of the wall to the boundaries.

4. The Terzaghi arch (Figure 2.10d)

The Terzaghi arch was described in Section 2.1.2. It forms behind a deformed wall when the upper boundary of a wall is restrained. At some distance away from the wall, the stored material does not yield and an arch forms between the wall and the non-yielded stored material. The arch relieves pressure in the yielded region and increases it at the wall and in the non-yielded region.

2.2. Dynamic Stress State

2.2.1. Filling pressures

Experimental work [2,16,41,42,43,31,44] has shown that conventional static theories are reasonable for the prediction of horizontal wall pressure during filling. This is because the pressure exerted by the stored material on the silo wall when the silo is full is unlikely to be exceeded during filling. Janssen's [1] formulae (discussed in chapter 4) have been adopted by design codes with the assumption that solids are charged into a silo without significant impact and that powders are charged at a sufficiently low rate that they de-aerate.

The static and dynamic stress states are influenced by the method of filling of the silo. The stored material may be charged into a silo centrally or eccentrically through a chute, or it may be dropped uniformly over the surface. Nielsen [31] found that the method selected will affect the voids ratio and particle orientation of the stored material. If a distributed filling method is adopted (the material is poured in a uniform manner so that the level of the stored material increases at the same rate over the entire area of the silo), a homogeneous isotropic medium might be expected, but as filling through a chute can result in particles orientated in the same direction, the medium may be anisotropic and will result in a non-uniform pressure distribution.

2.2.2. Discharge loads

The stress state within a stored material will change as flow commences. Material expands vertically in the bin and hopper and in the hopper contracts laterally [41]. The stress field changes so that orientation of the direction of the maximum principal stress changes from vertical when the stored material is stationary towards horizontal during discharge. In mass flow, the stress state of all the stored material in the silo changes. In funnel flow, only the material within the flow channel experiences such a major stress change, and so the wall pressure in mass flow and funnel flow silos must be determined using different criteria.

2.2.2.1. Mass flow

In a mass flow silo the boundaries of the flow channel coincide with the silo wall and so the channel is defined and constant. (In a funnel flow silo, the flow channel is not defined because it forms within the stored solid). Many authors [45,34,35,46,47,48] have proposed methods for the calculation of pressures in mass flow silos. Other investigations of the pressures at the walls of mass flow silos have been conducted [49,50,51,52,53] and have highlighted the erratic behaviour during flow. The walls are subjected to high localised pressures of short duration. Research studies [41,44,54,55,56] have identified two types of overpressure during discharge. Both are due to a re-orientation of stress within the stored material. The first is known as the switch, which occurs at the start of flow as the material changes from one stress state to another. It is only significant in the hopper and is discussed in more detail in Chapter 4. The second type of overpressure is attributed to a local stress reorientation within the flowing stored material as it passes imperfections on the silo walls. Such imperfections may be formed by welds in steel silos or formwork seams in reinforced concrete silos. Jenike [41] developed a method of analysis based upon strain energy for determining such overpressures.

Evidence suggests that overpressures may still be exerted against the silo wall when discharge has ceased but some material is retained in the silo. Walker [34] measured high overpressures under static conditions at the mid height of a hopper which was drawn half empty of solid, then refilled with the outlet closed. Van Zanten [47] measured continuing high pressure at an irregularity even though flow had stopped.

Munch-Andersen [57] noted that if a silo wall is sufficiently rough, the angle of friction between the wall and stored material may be higher than the internal angle of friction. A stationary layer of stored material will form along the wall of the silo and reduce the effect of wall imperfections, and hence reduce the overpressures.

Although overpressures and their fundamental causes have been identified, they are difficult to quantify and so it is common practice for designers of mass flow silos to multiply the calculated static pressure by a constant derived from experimental data. The overpressure factor has traditionally been applied to the static pressure without any regard to the structural response of the silo. Since the overpressures only affect local areas, they result in a pressure variation which may result in a worst stress state in the silo wall than a high uniform pressure. Therefore the assumption of a high but constant pressure at any level is not necessarily safe.

2.2.2.2. Funnel flow

The flow channel will expand from the outlet to meet the wall if the silo is sufficiently tall. This meeting point is referred to as the 'effective transition'. Jenike [41] states that if a silo has a height to diameter ratio exceeding five there will always be an effective transition. The upper section will comply with mass flow criteria and the lower section with funnel flow criteria. The location of the transition is defined not only by the shape of the silo but also by the flow properties of the solid. It is improbable that there will be a transition in shallow silos and consequently flow pressures are unlikely to exceed

static pressures, but if the flow channel does reach the walls then any overpressure will be insignificant [58].

Jenike stated that pressures measured during the discharge of a funnel flow silo are similar to the static pressures but that there will be some variation because the flow channel is not well defined. Van Zanten [47] observed distinct zones within the flowing channel and measured a scatter in the lateral pressure during flow. Shamlou [59] states that the mean of the discharge pressures was equal to static pressures and so it is acceptable to design the structure to resist static pressure alone. In this assumption, he fails to allow for the possible adverse effect of a pressure variation on the silo wall. Some recent code writers recognised that the discharge pressures may be greater than the static pressures and so they recommended a constant factor of safety [60,61]. They failed to allow for pressure variation across a horizontal level and this may contribute to the continuing structural failures of funnel flow silos.

2.2.2.3. Eccentric flow

Most theories assume that the pressure distribution around the perimeter of a silo is uniform at any given depth. If the discharge outlet is positioned eccentrically to the centre of a silo or a non-concentric filling technique is adopted, the pressure distribution will be non-uniform [62]. Eccentric loading leads to particular problems with circular silos as they are generally designed to resist membrane forces only. Jenike [63] noted that many designers failed to allow for additional bending due to eccentric loading often with the the result that the silo wall buckled toward the flow channel. Nielsen's experiments [31] show that there will always be a non-uniformity of loading as a consequence of deviations from perfect cylindrical geometry or the influence of eccentric loading and discharge, while Pieper [42] observed that pressures due to eccentric discharge are erratic and may be higher or lower than the static pressure predicted using Janssen's formulae. Ooi [64] found that the total pressure

exerted upon a silo wall was the same during discharge as when the stored material was stationary. High pressures are always balanced by low pressures elsewhere and so design for the highest pressures is not necessarily safe.

2.3. Other Loading Considerations

Pressure distributions can be affected by factors which may either increase or decrease wall loads. Such factors are difficult to quantify, and will be more noticeable in some silo cases than others. A limited list is given below.

Temperature variation

Thermal contraction of a silo wall will be restrained by the stored material. The magnitude of the resulting increase in lateral pressure will depend upon the temperature drop, the difference between temperature coefficients of the wall and stored material, the number of temperature changes, the stiffness of the stored solid and the stiffness of the silo wall.

Consolidation

Consolidation of the stored material may be due to release of air causing particles to compact (a particular problem with powders) physical instability due to changes in surface moisture and temperature, chemical instability due to chemical changes at the face of the particles, and vibration of the silo contents. The accurate determination of wall pressures requires a knowledge of the variation of bulk density and the angle of internal friction with depth.

Moisture Content

An increase in the moisture content of the stored material can increase cohesive forces or cause the formation of links between the particles of water soluble substances [65]. The Australian

code [61] recommends that wall friction for calculations should be determined using both the driest and wettest material likely to be encountered.

Segregation

Solids with a wide range of particle sizes and blends, containing particles with a wide range of density, size and shape, tend to segregate. The greater the height of free fall on filling the greater the segregation. This may create areas of dense material. More seriously, coarse particles may flow to one side of a silo and fine cohesive particles remain on the opposite side. An eccentric flow channel can form leading to unsymmetrical loads on the wall.

Degradation

A solid may degrade on filling. Particles may be broken or reduced in size due to impact, agitation and attrition. Silos for the storage of silage are a particular problem. Material degradation will result in a changing pressure field which tends towards hydrostatic.

Corrosion

Stored solids may chemically attack the storage structure altering the angle of wall friction and wall flexibility.

Abrasion

Large granular particles such as mineral ores can wear the wall surface resulting in problems similar to those described for corrosion. A lining may be provided to the structural wall, but care should be taken to ensure that wall displacement does not cause damage to the lining.

Impact Pressures

The charging of large rocks can lead to high impact pressures. Unless there is sufficient material to cushion the impact, special protection must be given to the hopper walls. In silos with flow problems, strong Janssen arches may form. They bridge across the silo and prevent flow of the

contents above the arch whilst material below continues to flow. Collapse of the arch can lead to severe impact pressures. In this case preventive action at the geometric design stage is required.

Rapid Filling and Discharge

The Australian code [61] warns that the rapid discharge of bulk solids having relatively low permeability to gasses can induce negative air pressures in the silo. Rapid filling can lead to greater consolidation, the effects of which are discussed above.

Powders

The rapid filling of powders can aerate the material and lead to a temporary decrease in bulk density, cohesiveness, internal friction and wall friction [66]. In an extreme case, the pressure from an aerated stored material can be hydrostatic.

2.4. Summary

The method of calculation of stresses at the silo wall is influenced by the stored material stress state. This is a function of the material properties and the boundary conditions and is different when the stored material is stationary to when it is flowing. The method of static pressure calculation must be selected in accordance with the mode of wall deformation. The same method will be used irrespective of the filling technique but the type of filling will influence the compaction and particle distribution within the stored material. The filling method must be considered when the material properties are determined and may lead to complications of the analysis if, for example, it generates an anisotropic medium.

An analysis of the pressure during the discharge of a funnel flow silo is not usually necessary since the flowing contents have a negligible effect on the stationary material near the wall (provided that the flow channel is concentric). In mass flow silos, the wall pressure may be much greater during discharge and

this should be incorporated into the method of analysis. There are no proven methods to determine the mass flow pressure state and so it is usual practice to apply a safety factor to the pressure calculated under static conditions.

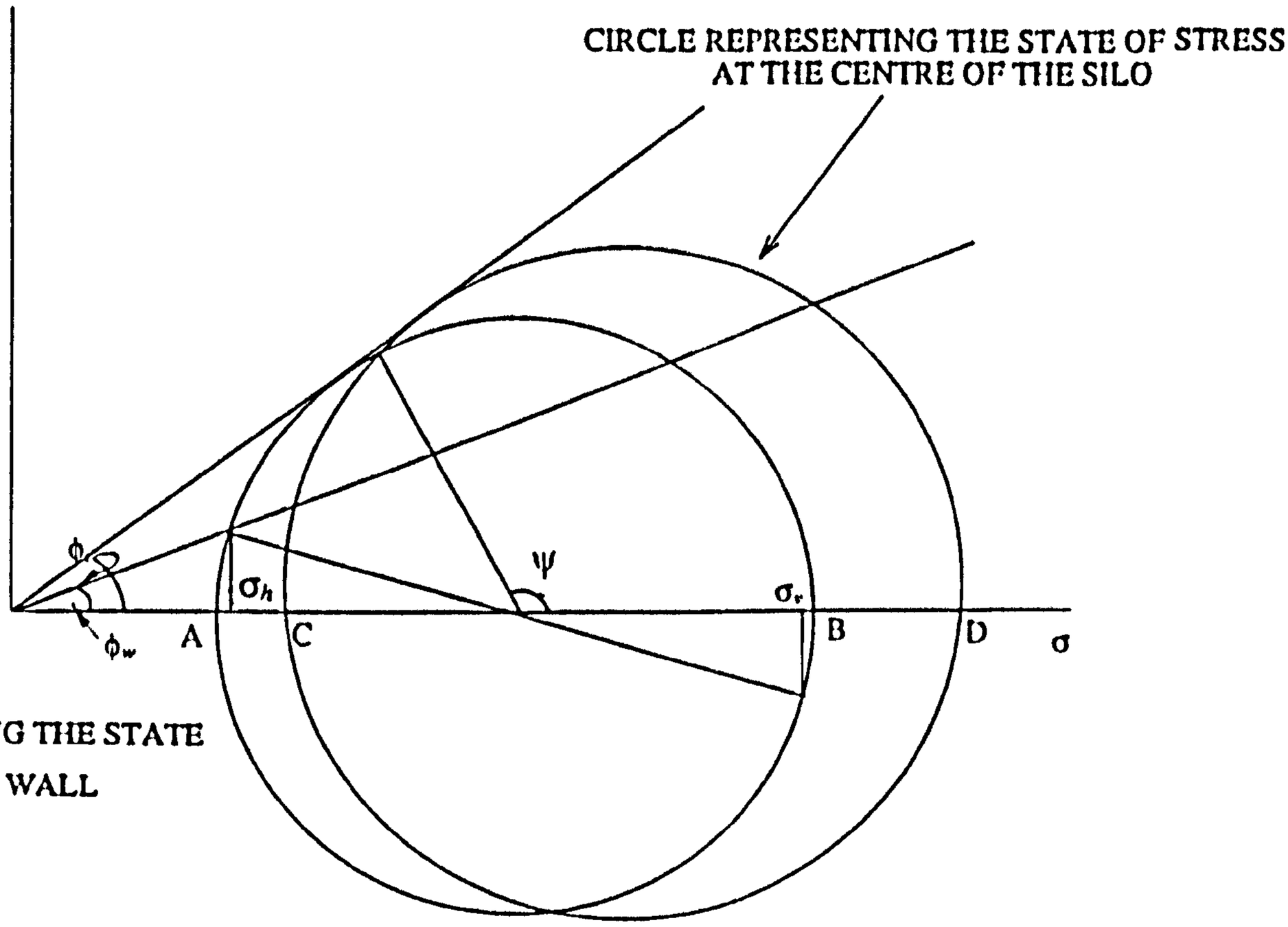

Figure 2.1 STRESS CONDITIONS AT THE WALL (AB) AND IN THE CENTRE (CD) OF THE SILO

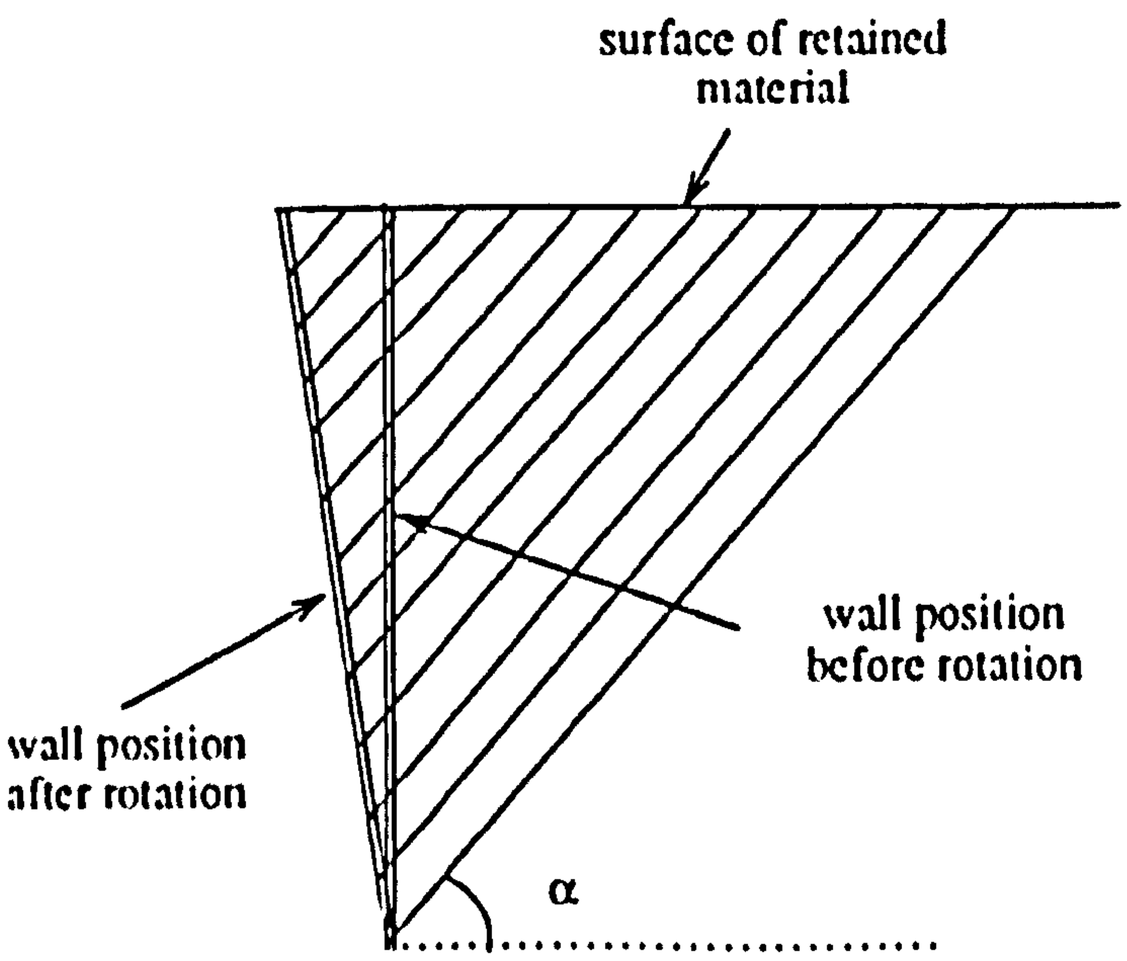

(a) SLIP PLANES BEHIND A RIGID WALL ROTATING ABOUT THE BASE

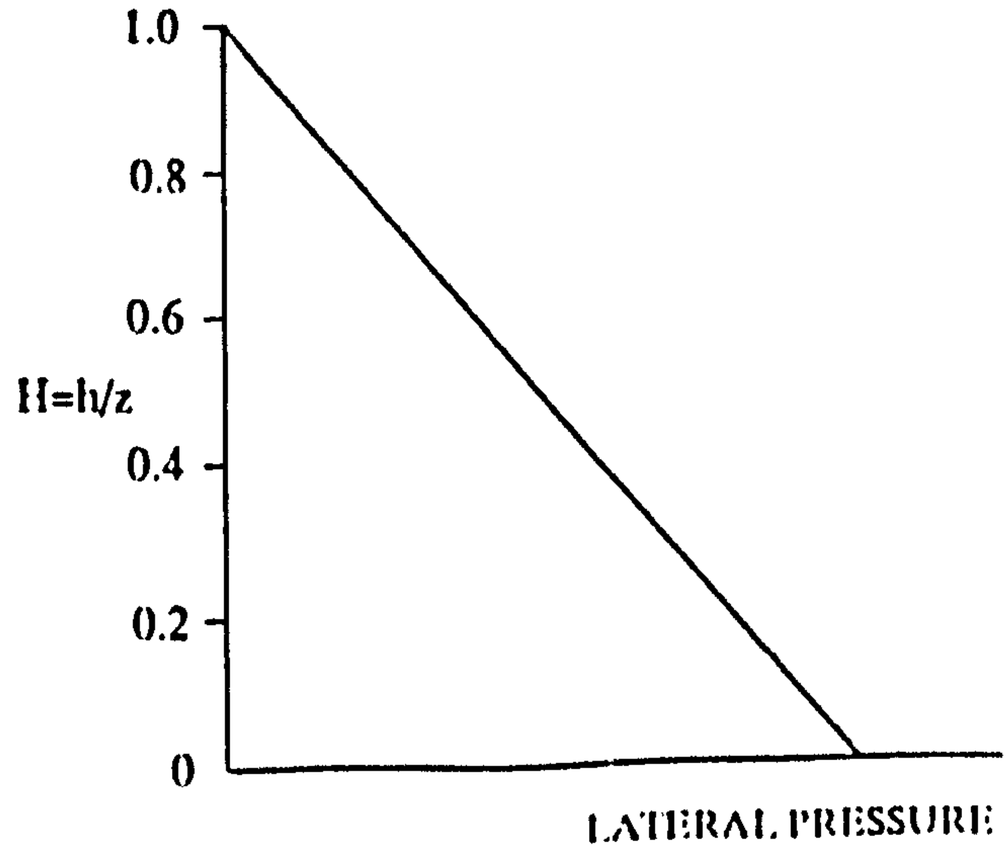

(b) PRESSURE DISTRIBUTION WITH DEPTH

Figure 2.2

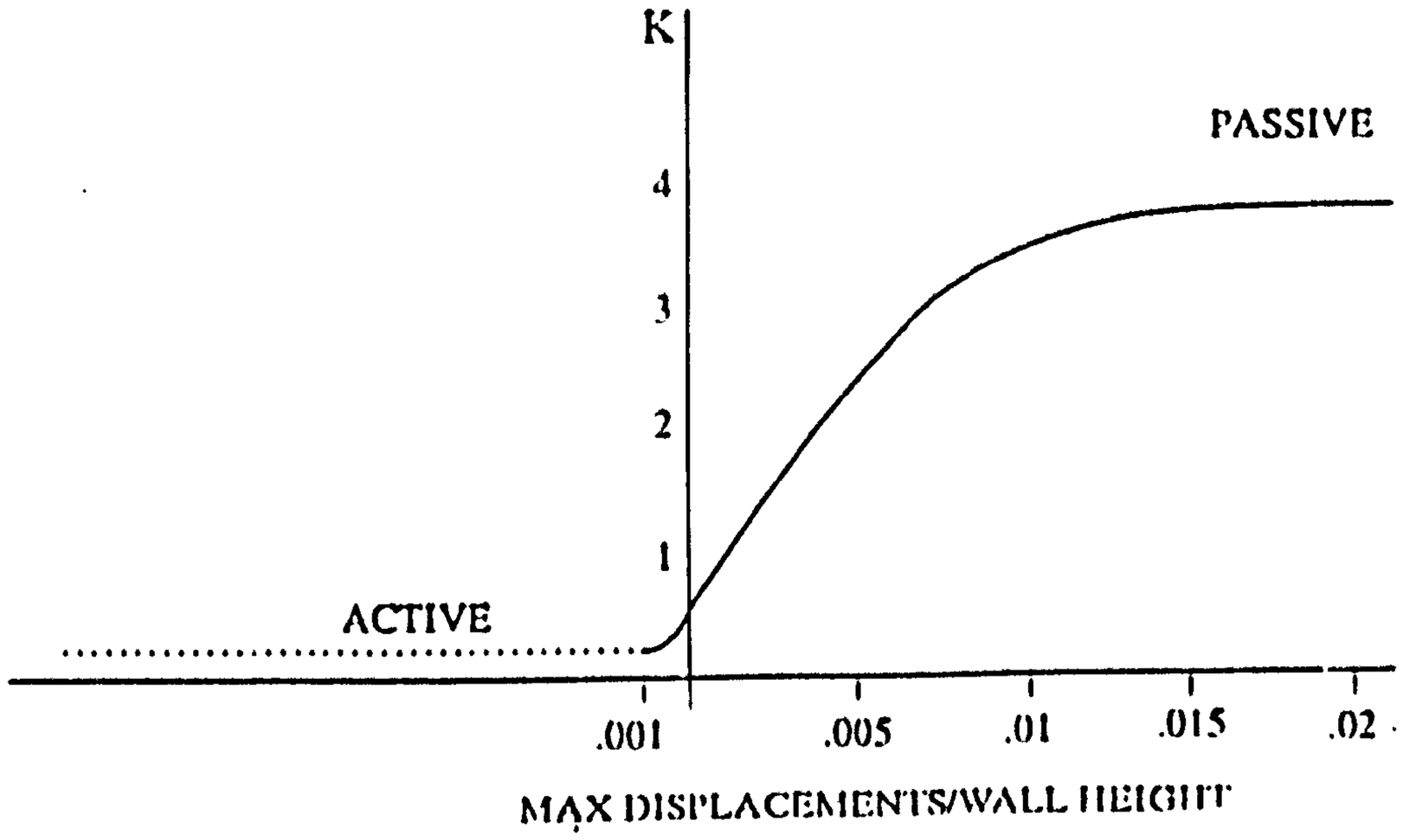

Figure 2.3 DISPLACEMENT REQUIRED TO MOBILISE THE PLASTIC STRESS STATES IN SAND

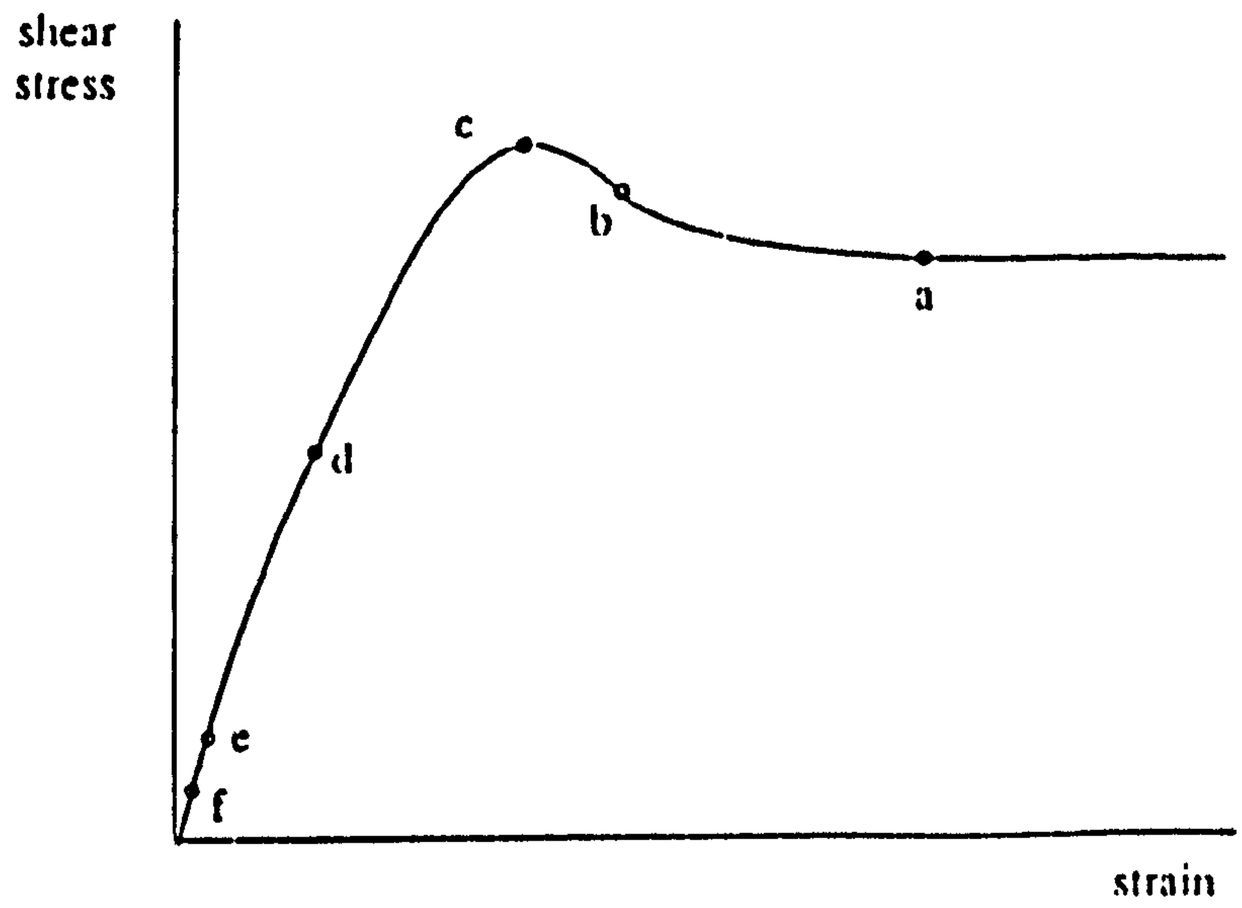

Figure 2.4 SHEAR STRESS/STRAIN RELATIONSHIP FOR DENSE SAND

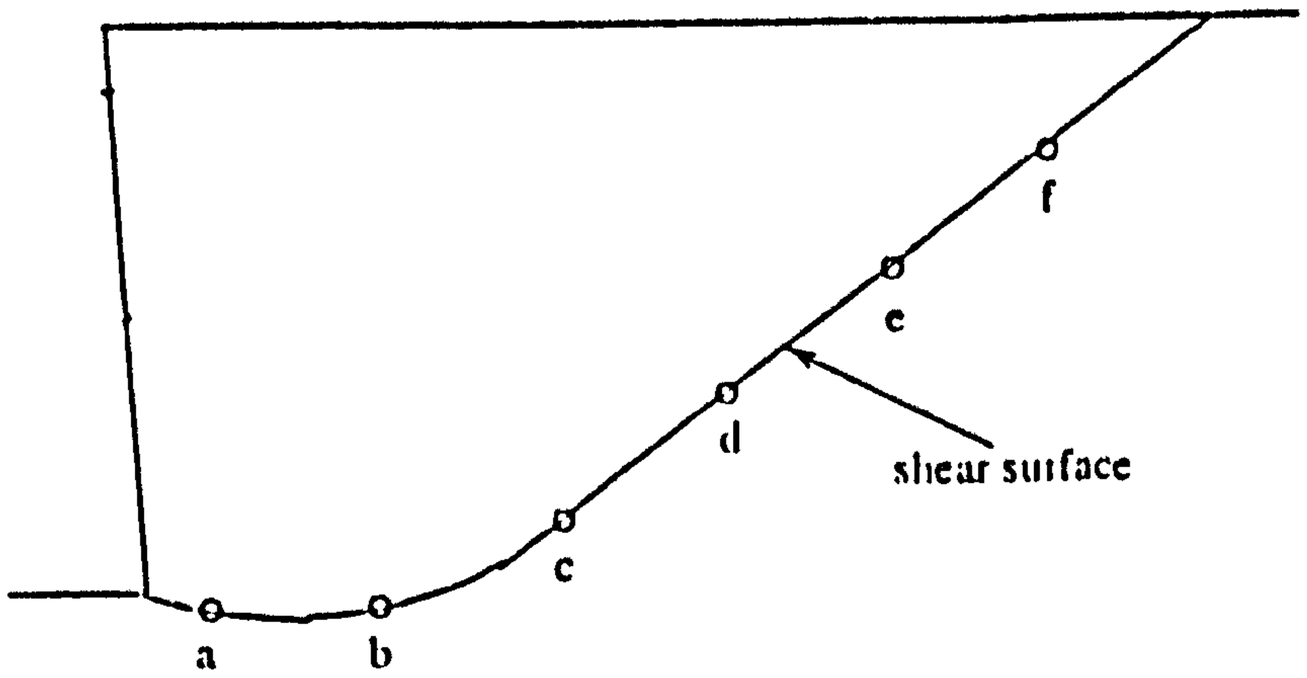

Figure 2.5 ROWE AND PEAKER'S ANALOGY OF SHEAR STRESS ON THE SLIP PLANE
SOURCE; ROWE AND PEAKER (15)

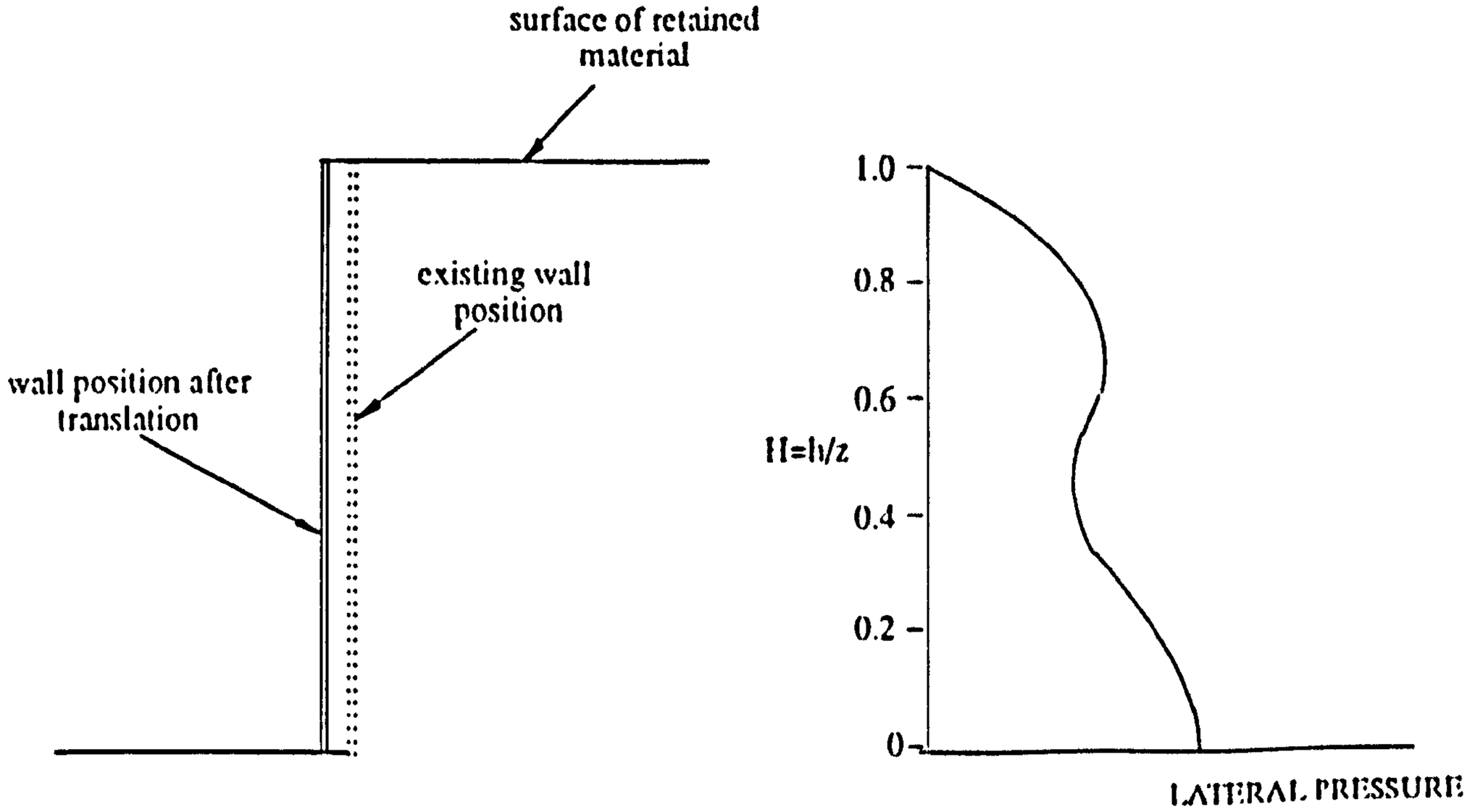

Figure 2.6 PRESSURE DISTRIBUTION WITH DEPTH FOR WALL TRANSLATION

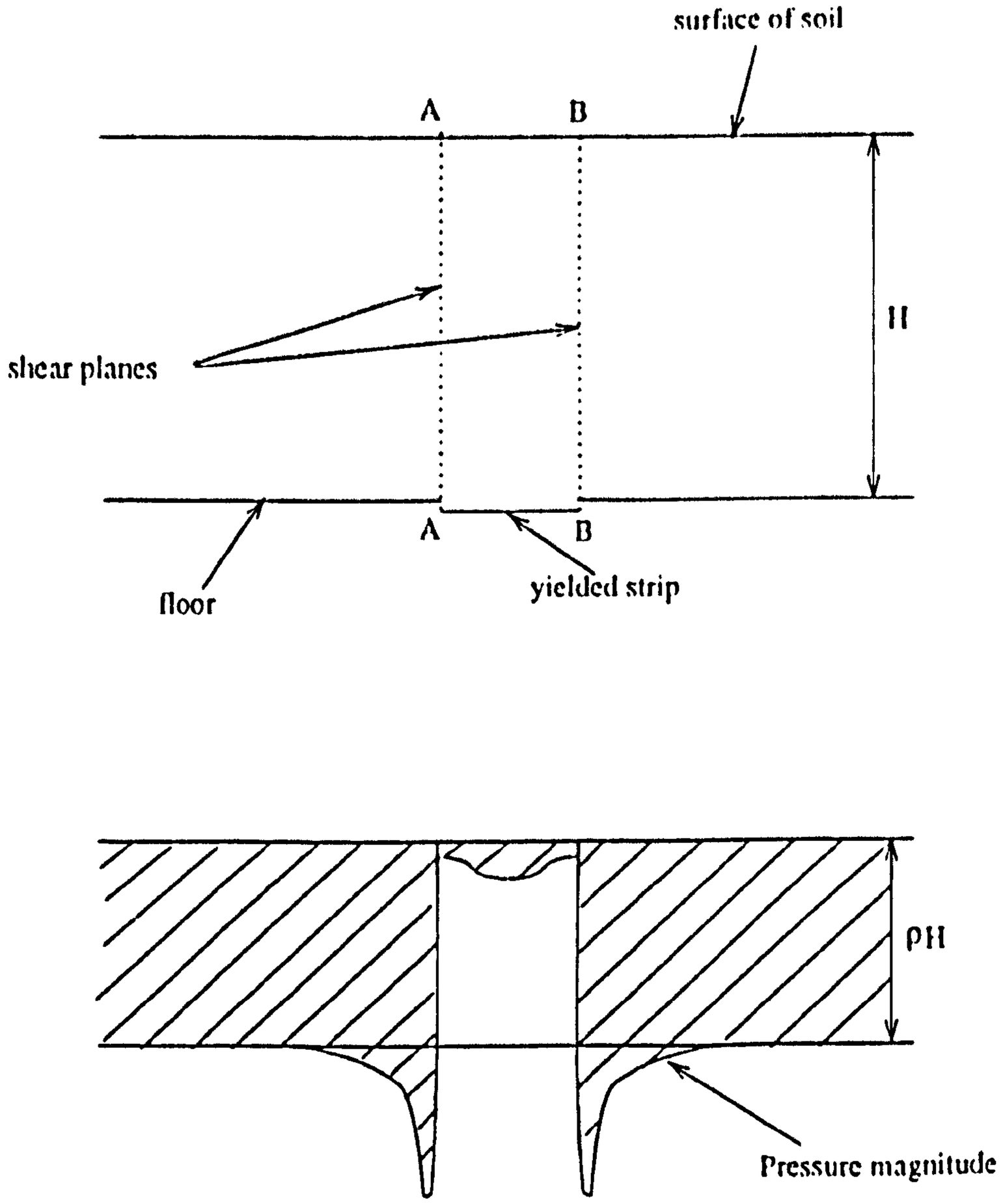

Figure 2.7 TERZAGHI'S PRESSURE DISTRIBUTION FOR SOIL OVER A YIELDING STRIP
SOURCE; TERZAGHI

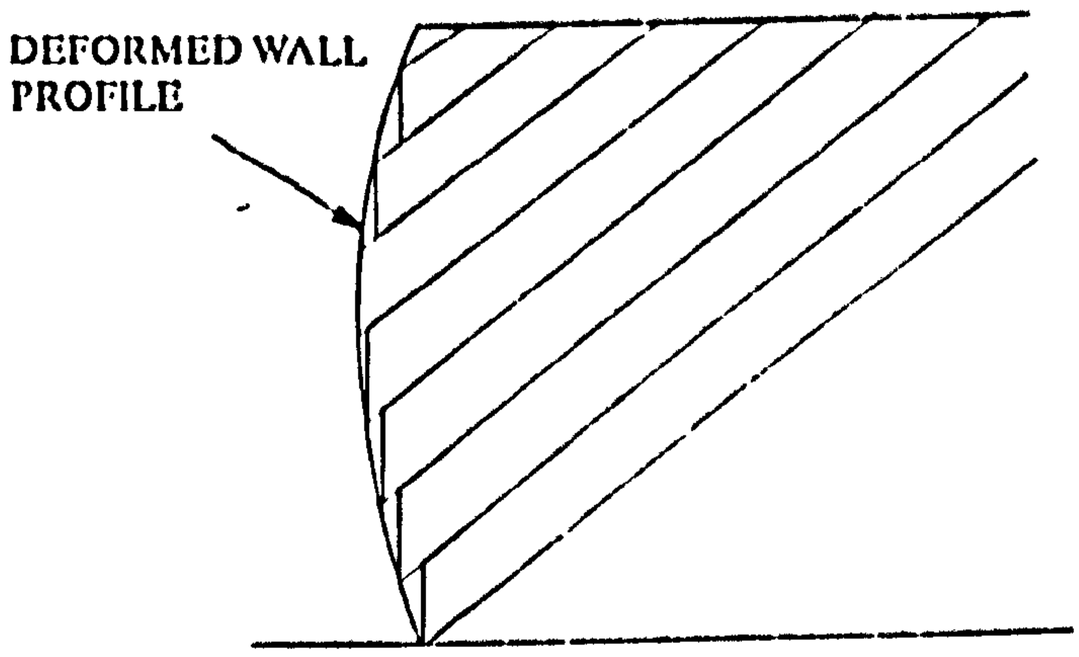

Figure 2.8 STOYER'S ANALOGY OF SHEAR PLANES BEHIND A FLEXIBLE WALL

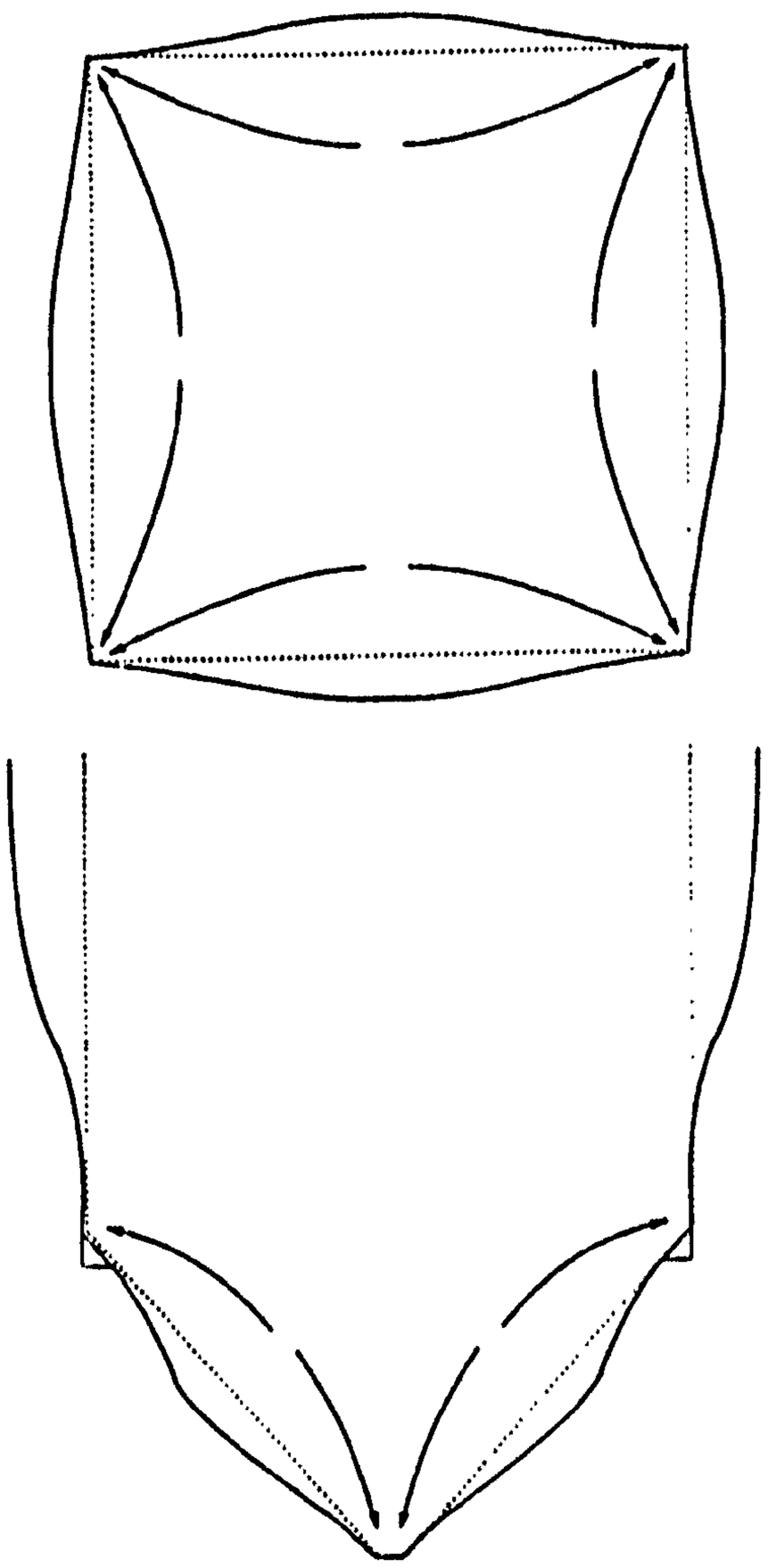

Figure 2.9 ARCHING POSSIBILITIES IN A SQUARE FLEXIBLE SILO

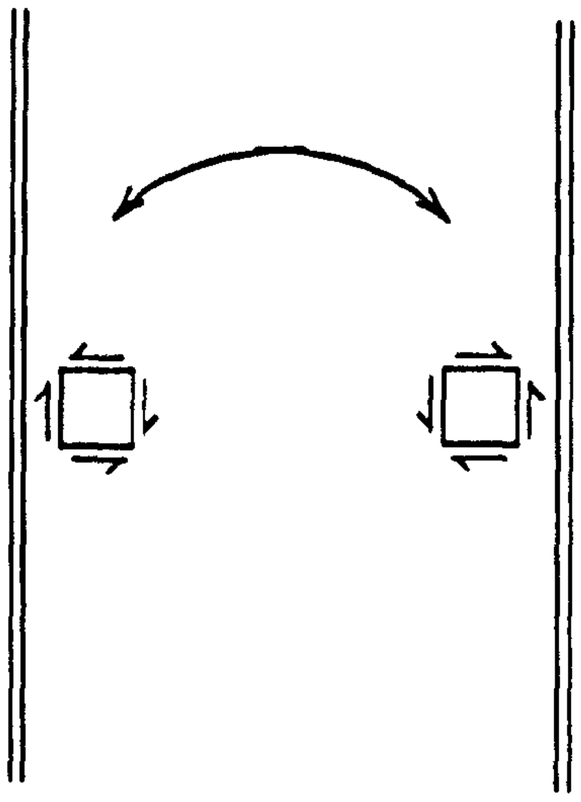

(a) Janssen Arch

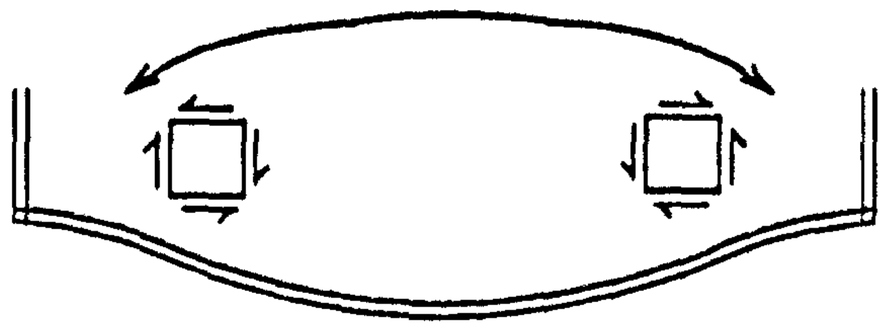

(b) Horizontal Arch

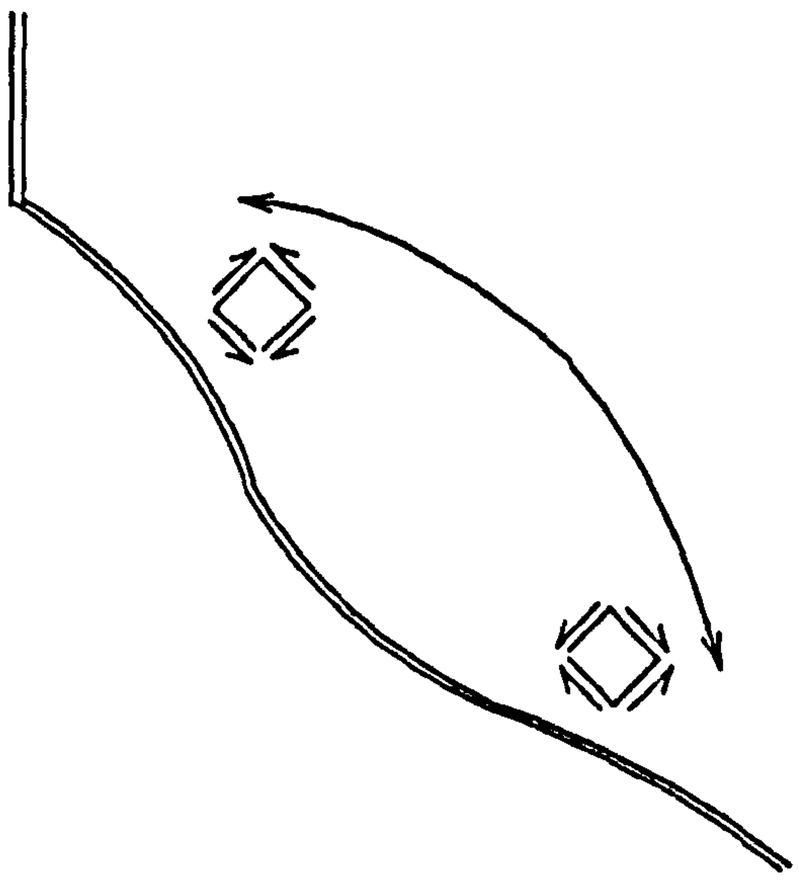

(c) Vertical Arch

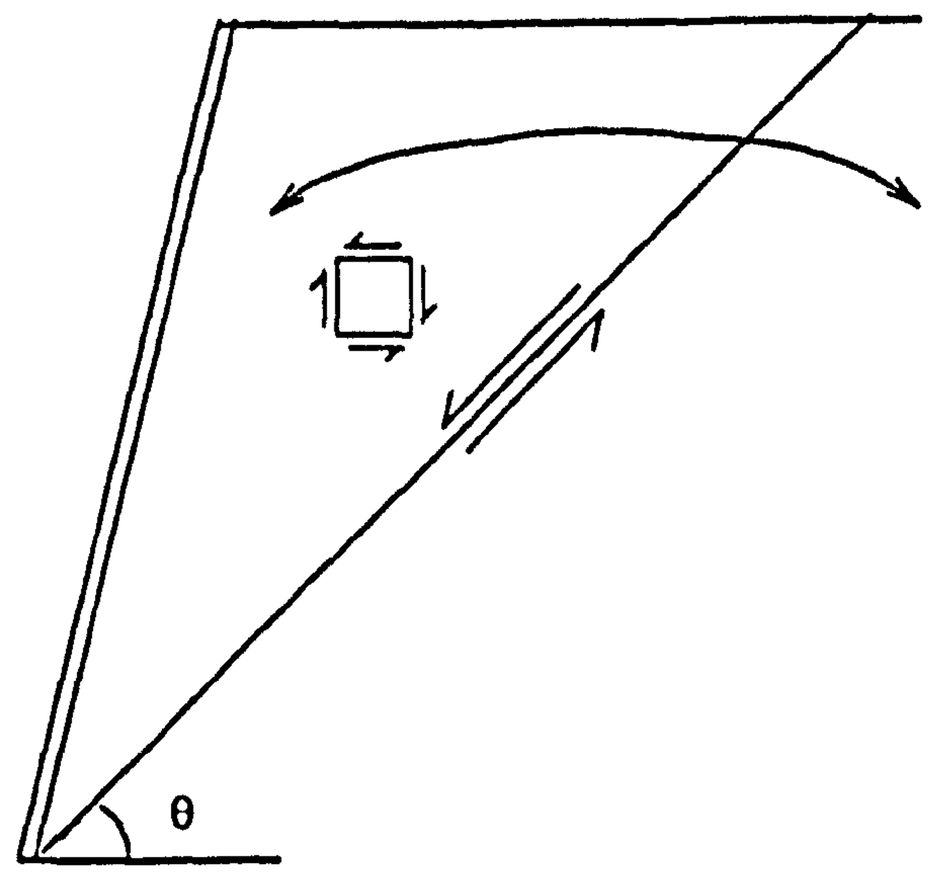

(d) Terzaghi Arch

Figure 2.10 TYPES OF ARCH

3. Theories for the calculation of wall pressure

3.1. Introduction

The stresses within the contents of a flexible walled silo will be a function of the interaction between the flexible wall and the stored material. In square bins with pyramidal hoppers wall deformation varies at constant depth and a three dimensional stress analysis is required. This is not the case for either circular silos, which can be reduced to a two dimensional problem based upon the assumption of symmetry, or for long trough bunkers in which it is acceptable to assume plane strain. Since there are not any theories for the calculation of wall pressure in square silos, methods formulated for cylindrical silos or retaining walls have been applied to square silos without consideration of the true mode of wall deformation. Many different theories have been developed for the calculation of bin and hopper wall pressures and these have been reviewed extensively elsewhere [27,29,67,59,68,69]. Only the most widely used methods are described below. The assumptions of each are discussed and their suitability for the calculation of pressures on square silos is briefly assessed.

3.2. Existing methods for the calculation of wall pressure

3.2.1. Static pressures

Pressures in deep silos of circular or square plan form are usually calculated by the Janssen [1] theory.

Janssen considered the vertical equilibrium of a horizontal slice through the stored material in a silo (Figure 3.1),and obtained the following relationship:-

$$A\left[\sigma_v + d\sigma_v\right] + C\,\mu\,K\sigma_v dh = A\,\sigma_v + \rho\,A\,dh \tag{3.1}$$

where C is the silo perimeter. Rearranging and solving the first order differential equation gives the Janssen equation for vertical pressure

$$P_v = \frac{\rho R}{\mu K}\left[1 - e^{-K\mu\frac{h}{R}}\right] \tag{3.2}$$

The hydraulic radius, R, allows the Janssen method to be applied to silos with different plan shapes. It is only applicable to deep silo structures where Janssen arching of the stored material between the silo walls is possible. The accuracy of the method is dependent upon the selection of a value for the ratio of horizontal to vertical pressure K. K is usually assumed to be constant throughout the silo contents, but, factors such as friction at the wall-material interface and wall deformation will alter the value of K in the vicinity of the silo wall. Analytical methods which allow for the variation of K due to wall friction have been derived by Nanninga [45] , Lvin [70] and Takami [71] , but they do not have a significant effect upon the resulting pressure prediction and so they have not been widely adopted by designers. Other researchers [41,42,61,72,73,74] have considered that sufficient accuracy can be achieved by the use of a single value for K. These include Jenike's suggestion of 0.4 and Jaky's [36] ratio for earth pressure at-rest

$$K_0 = 1 - \sin\phi \tag{3.3}$$

which is used for silos with rigid walls. The Rankine active ratio

$$K_a = \frac{1 - \sin\phi}{1 + \sin\phi} \tag{3.4}$$

is frequently adopted by designers and may be acceptable for the design of flexible walled silos if the wall deformation is sufficient to develop the full active state of pressure and wall friction is negligible. In the case of rough walled silos, Walker [34] stated that the ratio becomes

$$K_a = \frac{1 - \sin^2\phi}{1 + \sin^2\phi} \tag{3.5}$$

Another method that is frequently used for the calculation of silo wall pressure was developed by M. and A. Reimbert [2]. They carried out experiments to investigate the increase in wall friction with depth. Their tests showed that the relationship was in the form of Curve 2, Figure 3.2 and was accurately approximated by the following function.

$$Q_R = \frac{\rho A h^2}{h + T} \tag{3.6}$$

where Q_R is the wall friction force, and T is given as

$$T = \frac{P_{v\,max} - P_{v0}}{\rho} \tag{3.7}$$

Figure 3.2 shows that the function of wall friction tends towards an asymptote. The asymptote represents the wall friction assuming that all the stored material at every level in the silo is carried by wall friction alone. T is shown in Figure 3.2. and is defined by the intersection of the friction asymptote and the zero pressure axis. It is, amongst other things, a function of the vertical pressure imposed by the conical surcharge of stored material (P_{v0} Figure 3.2) and the maximum vertical pressure in the silo $P_{v\,max}$. At great depth in a silo, all the vertical pressure due to the mass of any horizontal slice is carried by wall friction. Therefore, at some depth in the silo the vertical pressure reaches a maximum and does not increase beyond this level. It is shown by the vertical asymptote in Figure 3.2 and is equal to

$$P_{v\,max} = \frac{\rho R}{\mu K} \tag{3.8}$$

Substituting the equations for P_{v0} and $P_{v\,max}$ the constant T becomes:

For circular silos

$$T = \frac{D}{4 \tan\delta K} - \frac{h}{3} \tag{3.9}$$

and for rectangular silos

$$T = \frac{a}{\pi \tan\delta K} - \frac{h}{3} \tag{3.10}$$

Having determined the function of wall friction from experimental data and assuming that $q = P_h \tan\phi$, the Reimberts were able to derive the following expressions for vertical and horizontal pressure.

$$P_v = \rho \left[h \left[\frac{h}{T} + 1 \right]^{-1} + \frac{h}{3} \right] \tag{3.11}$$

$$P_h = P_{h\,max} \left[1 - \left[\frac{h}{T} + 1 \right]^{-2} \right] \tag{3.12}$$

Where $P_{h\,max}$ is the maximum asymptotic value of horizontal pressure. For circular silos

$$P_{h\,max} = \rho \frac{D}{4 \tan\delta} \tag{3.13}$$

and for rectangular silos

$$P_{h\,max} = \rho \frac{a}{4 \tan\delta} \tag{3.14}$$

The Reimbert equations allow for the difference in geometry between the silos, but they do not incorporate any difference due to wall deformation because all their experiments were carried out in silos with very stiff walls.

Static loads in shallow silos are usually determined by either the Coulomb [4] or Rankine [3] earth pressure theories. Rankine's theory considers the stress in a granular material when it reaches a state of plastic equilibrium, and establishes that

$$P_n = K_a \sigma_v \tag{3.15}$$

where K_a is defined in equation 3.4. Rankine's theory assumes that the stored material extends infinitely and is therefore not correct for circular or square silos. It does not allow for wall friction and is thus conservative in the prediction of wall pressure, and fails to account for surcharge due to the cone of stored material. In the cases of silos with stiff walls, the wall deformation will not be sufficient to fully mobilise the active state of pressure, and consequently loads will be underestimated. The effect of stiff corners will also change the pressure distribution from that predicted by Rankine.

Coulomb's theory assumes a single plane of failure, and that the material behind a wall will fail by sliding as a rigid wedge-shaped block. Coulomb's original expression ignored the effects of wall friction and assumed a horizontal surface to the stored material. These boundary conditions produced the same value of horizontal thrust as that obtained by the Rankine method. The Coulomb method was extended by Mayniel (referenced in Clayton [39]) to allow for wall friction and by Muller-Breslau (again referenced in Clayton [39]) to allow for a sloping backfill, inclination of the back of the wall, and wall friction. Muller-Breslau's solution was obtained by resolving the forces (Figure 3.3) parallel and perpendicular to the shear surface and substituting the Mohr Coulomb relationship between shear and normal stress at failure.

$$\tau = \sigma_n \tan\phi \tag{3.16}$$

Thus an expression was derived for the maximum value of thrust, considering a unit length of the wall.

$$F = \frac{1}{2} \rho h^2 \frac{f_1}{\sin\alpha \cos\delta} \tag{3.17}$$

where F is the force per unit length acting at an angle δ to the wall, W is the vertical force per unit length, N is the force per unit length normal to the wall and

$$f_1 = \frac{\sin^2(\alpha+\phi)\cos\delta}{\sin\alpha \sin(\alpha-\delta)\left[1+\sqrt{\left[\frac{\sin(\phi+\delta)\sin(\phi-\beta)}{\sin(\alpha-\delta)\sin(\alpha+\beta)}\right]}\right]^2} \tag{3.18}$$

The volume of surcharge (backfill) on a silo is limited by the width of the silo and interaction with the opposite wall. Therefore, the incorporation of a sloping backfill considerably overestimates the pressure on a silo wall for both a conical or wedge shaped surcharge. Therefore, a more accurate prediction of pressures in shallow silos may be possible if the stored material surface is assumed to be horizontal ($\beta=0^{\circ}$) and the wall is vertical ($\alpha=90^{\circ}$). If these geometric conditions are realistic, the simplified solution becomes

$$F = \frac{1}{2}\rho h^2 \left[\frac{\cos\phi}{\sqrt{\cos\delta} + \sqrt{\sin(\delta+\phi)\sin\phi}}\right]^2 \tag{3.19}$$

Ingold [75] showed that the solution can be further simplified without significant inaccuracy if the critical angle of the shear surface (Figure 3.3) is assumed to be

$$\psi = 45 + \frac{\phi}{2} \tag{3.20}$$

The normal thrust is then

$$F = \frac{1}{2}\rho h^2 \left[\frac{1-\sin\phi}{\cos\delta + \sin(\delta+\phi)}\right] \tag{3.21}$$

The modified Coulomb theories may lead to errors if there is a surcharge from the stored material. If the surcharge is included in the calculations using equation 3.18, the pressures are overestimated. If the surcharge is not considered in the calculation the pressures will be underestimated. Further inaccuracies are possible when the heights of the bin and hopper are similar because it is only possible to include one angle of wall inclination in the calculations.

The Janssen, Reimbert, Rankine and modified Coulomb theories are only a few of the many theories developed for the calculation of static pressures normal to silo walls. They are the most commonly used but are based upon assumptions which limit their applicability to certain types of silos. Their suitability for the calculation of pressure in square flexible silos is discussed further in Section 3.4.

3.2.2. Hopper Static pressures

The hopper walls carry all the weight of the stored material in the silo other than that carried by wall friction in the vertical section. Knowledge of the vertical pressure at the transition between the vertical walled section and the hopper is required to define the loading on the hopper.

Static pressures normal to the inclined walls of bunkers are usually calculated by either the Rankine theory [3] (modified by the NCB [76] or Lambert [22]) or the Coulomb [4] theory. In deep silos the hopper wall pressure is frequently calculated by Janssen's [1] or Reimbert's [2] method and the resulting forces resolved to give the normal and frictional components on the hopper wall. Alternatively Walker's [34] static and dynamic theories extended by Walters [35] and Enstad [46] , Jenike's [77] or Pieper's [16] theories are used.

Other theories have been developed for the calculation of hopper wall pressures [68,78,79] , but experimental evidence [41, 17, 68] does not suggest that they are more accurate than the methods listed above and so they have not been presented here.

Pieper [16] presented formulae for the calculation of normal and frictional wall pressures on the hopper wall following a series of tests on pyramidal hoppers. He found that for the purpose of design it was sufficient to assume that the pressure distribution upon a hopper wall subjected to surcharge from a bin decreased linearly from the transition to the outlet. The pressure normal to the hopper wall at the transition was equal to

$$P_n = \frac{P_v \sin^2\gamma + P_{h\,trans}\cos^2\gamma}{\sqrt{\tan\delta}} \tag{3.22}$$

and pressure at the outlet equals

$$P_n = P_v \sin^2\gamma \tag{3.23}$$

Walker [34] assumes that the shear stress on vertical planes is zero and so the vertical pressure at any level is equivalent to the hydrostatic pressure due to the head of material above it. For any silo and stored material combination, the pressure normal to the hopper wall is equal to the vertical pressure multiplied by a constant. The constant will be a function of the hopper wall angle and the angle of wall friction.

The Mohr's circle in Figure 3.4 represents the stress at a point adjacent to the hopper wall. The vertical stress σ_v is equal to the head of material ρh. Stress normal to the wall, which is at an angle γ to the vertical is represented by P where P is a point on the wall yield locus at an angle 2γ around the circle from point Q. Q represents the minimum principal stress. The pressure normal to the wall can be found from the geometry of the Mohr's circle

$$P_n = P_v \frac{\sin 2\gamma \cos\delta}{\sin(\delta+2\gamma) + \sin\delta} \tag{3.24}$$

The theory is only valid to the point where the plane representing the normal to the wall becomes tangent to the material locus. Walker's theory will give a conservative estimation of pressure due to the assumption of zero shear stress on vertical planes [80].

Walters [35] extended Walker's theory and assumed that shear due to wall friction varies linearly from the wall to the centre of the silo. Consideration of the equilibrium of the horizontal element of the hopper shown in Figure 3.5 gives the following differential equation.

$$\frac{d\sigma_v}{dh} + \frac{1}{A}\frac{dA}{dh}\sigma_v + \frac{C\ (\tau_w + \sigma_n \tan\gamma)}{A} = \rho \tag{3.25}$$

Stresses at the wall and in the centre of the silo are represented by the Mohr circles in Figure 2.1. Walker used a distribution function 'D' to relate the vertical stress at the wall to the average vertical stress. Walters defined 'D' as a function of the angle of internal friction of the stored material (ϕ), the angle of wall friction (δ) and the angle of inclination the hopper wall to the vertical (γ). The shear stress τ_w and stress normal to the hopper wall σ_n were defined as functions of the vertical stress (σ_v), ϕ,

δ and γ. Finally the area was put in terms of depth and the angle of inclination of the hopper wall. Walters solved equation 3.25. His final solution for stress in a hopper is valid for the static and mass flow states of stress. It is limited to the calculation of pressures in steep mass flow hoppers and so is not presented here.

Jenike (in Arnold [67]) assumed a linear distribution of stress up the hopper wall. Firstly an equation was derived for the vertical equilibrium of the entire hopper. The total weight of the stored contents is equal to the sum of the vertical components of wall friction and wall normal force.

$$\rho H^2 \tan\gamma \left[\frac{H}{3}\right] = 2(\tan\gamma + \tan\delta) \int_0^H \sigma_n \, h \; dh \tag{3.26}$$

The wall pressure distribution is assumed to increase linearly from zero at the transition to a maximum at the outlet. Integrating equation 3.26 and solving for σ_n gives the following expression for the calculation of pressure normal to a hopper wall.

$$P_n = \rho \frac{D}{2(\tan\gamma + \tan\delta)} \tag{3.27}$$

Where D is the diameter of the silo. Equation 3.27. is modified to include surcharge from the stored material in a bin. The surcharge pressure is distributed linearly from a maximum at the transition ring beam to a minimum at the apex of the hopper and added to the pressure distribution determined from equation 3.27. P_n at the ring beam of conical hoppers becomes

$$P_n = \frac{3 P_{v\,trans} \tan\gamma}{2 (\tan\gamma + \tan\delta)} \tag{3.28}$$

3.2.3. Discharge Pressures

Walker [34] stated that the stress at any point in a solid during discharge can be represented by the Mohr's circle shown in Figure 2.10. He suggested a method of analysis which was originally derived for application to mass flow silos. Funnel flow hoppers are designed to carry static pressures although these may be multiplied by a constant to compensate for eccentricity of the flow channel.

Higher pressures have been measured in the hopper at the start of discharge in mass flow hoppers when the material changes stress state. The change is referred to as the "switch". It occurs when the material moves from a static (active pressure) to a dynamic (passive pressure) state. Many authors [35,52,69,78,81,82] have derived formulae to calculate the resulting overpressure which moves rapidly up from the hopper outlet after the start of flow and locks at the transition during flow. The switch overpressure will be partially or totally absorbed by the layer of stationary material in funnel flow hoppers and so is less severe than in mass flow hoppers. Rotter [83] argues that the switch pressure is not detrimental to the structural safety of the hopper. The ring beam at the transition between the hopper and the vertical section is in compression due to the inward force from the inclined walls of the hopper. The switch pressure acts against the compressive force and so it may actually increase the load which maybe carried by the hopper during discharge.

3.3. Comparison of theories

Figure 3.7 shows a comparison of the Janssen [1] , Reimbert [2] , Rankine [3] and Coulomb [4] theories for the calculation of horizontal pressure on the vertical walls of the silo shown in Figure 4.2a. The values of the density, angle of internal friction of the stored material, and angle of wall friction are given in Table 3.1. Two Janssen pressure distributions are shown to illustrate the affect of K, the ratio of horizontal to vertical pressure, on wall pressure. $K1$ is the active ratio equal to $1 - \sin\phi / 1 + \sin\phi$

and $K2$ is the at-rest ratio equal to $1-\sin\phi$. All the other theories incorporate the active ratio. The figure shows that there is very little difference between the theories and the only significant deviation from the mean pressure is due to the variation of K.

Angle of wall friction (δ)	33°
Angle of internal friction (ϕ)	43.5°
Angle of hopper wall (γ)	43.8°
Bulk density (ρ)	$16.29 kN/m^3$

TABLE 3.1 - Stored material properties adopted for the comparison of wall pressure theories.

Figures 3.8 and 3.9 show a comparison of the Janssen [1] , Coulomb [4] Pieper [16] , Walker [34] and NCB [76] methods for the calculation of pressure normal to the hopper wall. Figure 3.8 shows the pressures normal to the hopper wall for the silo filled to the top of the hopper. The Coulomb method predicts the highest pressures. This is because it was developed for retaining wall applications. It is based upon the assumption that the stored material extends infinitely away from the wall and so it does not allow for the affect of opposite walls. The pressures predicted by the Janssen, Walker and Jenike theories are all similar and approximately one third lower than the Coulomb prediction. The Pieper and N.C.B. pressure distributions are considerably lower than all the others.

Figure 3.9 shows a comparison of the methods of pressure calculation for the same silo filled to two metres above the top of the hopper. The vertical surcharge pressure was calculated using Janssen's equation. The figure shows little correlation between existing theories. Some theories predict maximum pressures at the top of the hopper and others predict the highest pressures at the outlet.

3.4. Assumptions of the existing theories

The major assumptions used in many or all the above theories are summarised and discussed below:

1. The stored material is isotropic and homogeneous. Tests [31,44] have shown that this is rarely the case and that anisotropy may lead to significant changes to the static and discharge pressures from those predicted by existing theories.

2. The angle of internal friction is used to describe the strength of the stored material. Soil strength is dependent on the stress path to failure. The stress path is determined by the silo aspect ratio and the silo wall stiffness. The angle of internal friction represents the strength for a single stress path to failure and so it does not necessarily represent the strength of all the material in the silo.

3. Many theories assume that the major principal stress aligns with the vertical axis and the minor principal stress aligns with a horizontal axis perpendicular to the bin wall when the stored material is static. Some researchers [34,35] have incorporated a distribution factor to allow for the effect of wall friction on the direction of the principal stresses but none have allowed for any change due to wall slope on a horizontal plane.

4. The ratio of horizontal to vertical pressure is usually assumed to be constant with the stored material in either an at-rest or an active state of equilibrium. This is not however a limitation of the theories, but users have generally adopted a single value of K which suggests that the walls are rigid and non-deforming or that they are rigid and rotate about the base. Other modes of wall deformation have not been incorporated into design calculations.

5. Wall friction is usually assumed to be constant and fully mobilised at every point on the wall although again this is not a limitation of the theory.

6. The stored material is assumed to be incompressible. This may lead to errors in the calculation of hopper pressures. In compressible stored materials consolidation during or after filling will cause slip along the inclined hopper walls. Lateral contraction of the contents will change the stress state toward a passive plastic state of equilibrium.

7. The effect of discharge on the stored material stress state in the bin has usually only been incorporated into design using an overpressure factor applied to the static pressure. Two factors are

specified, one for mass flow and one for funnel flow. They are applied to all silos that fall within these categories without consideration of the structural form or susceptibility to different load conditions.

Many of these assumptions are reasonable for circular silos but they may all be incorrect for non-circular silos with flexible walls. Although the errors due to the assumptions described in 1, 2, 5 and 6 may be small, the neglect of others will lead to significant errors for some silo types. The emphasis of existing research into static pressures has been towards the correct determination of the ratio of horizontal to vertical pressure, and the variation in vertical pressure with distance from the silo wall due to the effect of wall friction. Few researchers have considered the effect of wall flexibility on pressures and those that have, have only considered plane strain or axisymmetric problems. There has been a similar neglect of the problems of wall flexibility during studies of wall pressures when discharging silos. In addition, the few experimental studies carried out on non-circular flexible silos have not given any information on the influence of wall flexibility.

The literature relating to other fields of soil mechanics and reviewed in Chapter 2 showed that arching generates a significant redistribution of pressure behind flexible walls. Based upon this evidence hypotheses were presented for arching in non-circular flexible silos. In order to investigate these hypotheses, and considering the lack of existing experimental data, an experimental study was undertaken on a model silo. The test programme had the following major aims.

1. To gain a comprehensive understanding of the phenomena that affect pressures in non-circular flexible silos.

2. To verify the existing methods of silo wall pressure calculation for non-circular flexible silos.

3. Pending the results of 2, to provide a basis for the development of improved theories to describe the general case of pressure on a flexible wall.

The following chapters describe the design and testing of the silo model.

$$\tau = \mu \sigma_h$$

$$\sigma_h = K \sigma_v$$

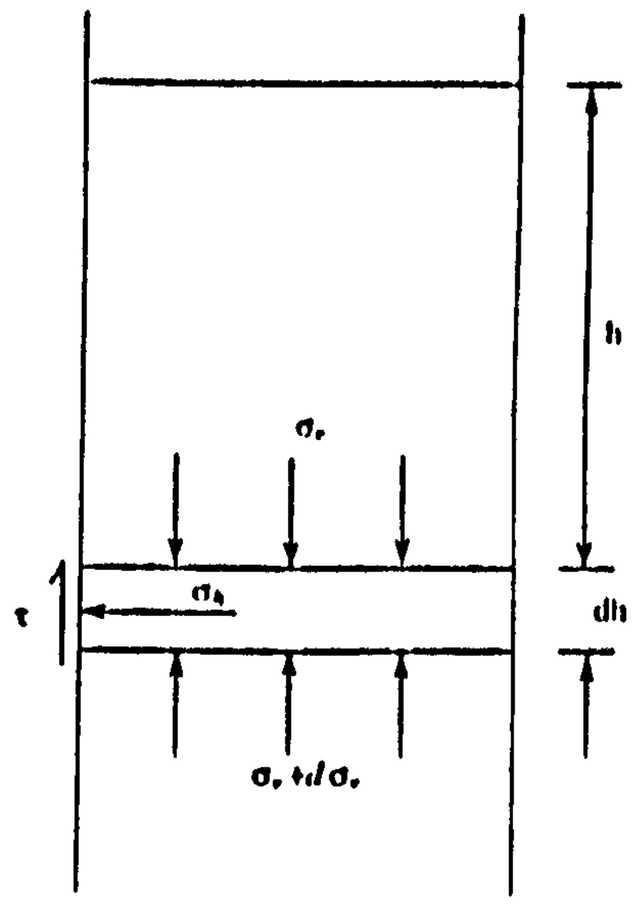

Figure 3.1 STRESSES ON A HORIZONTAL SLICE THROUGH THE SILO (JANSSENS THEORY)

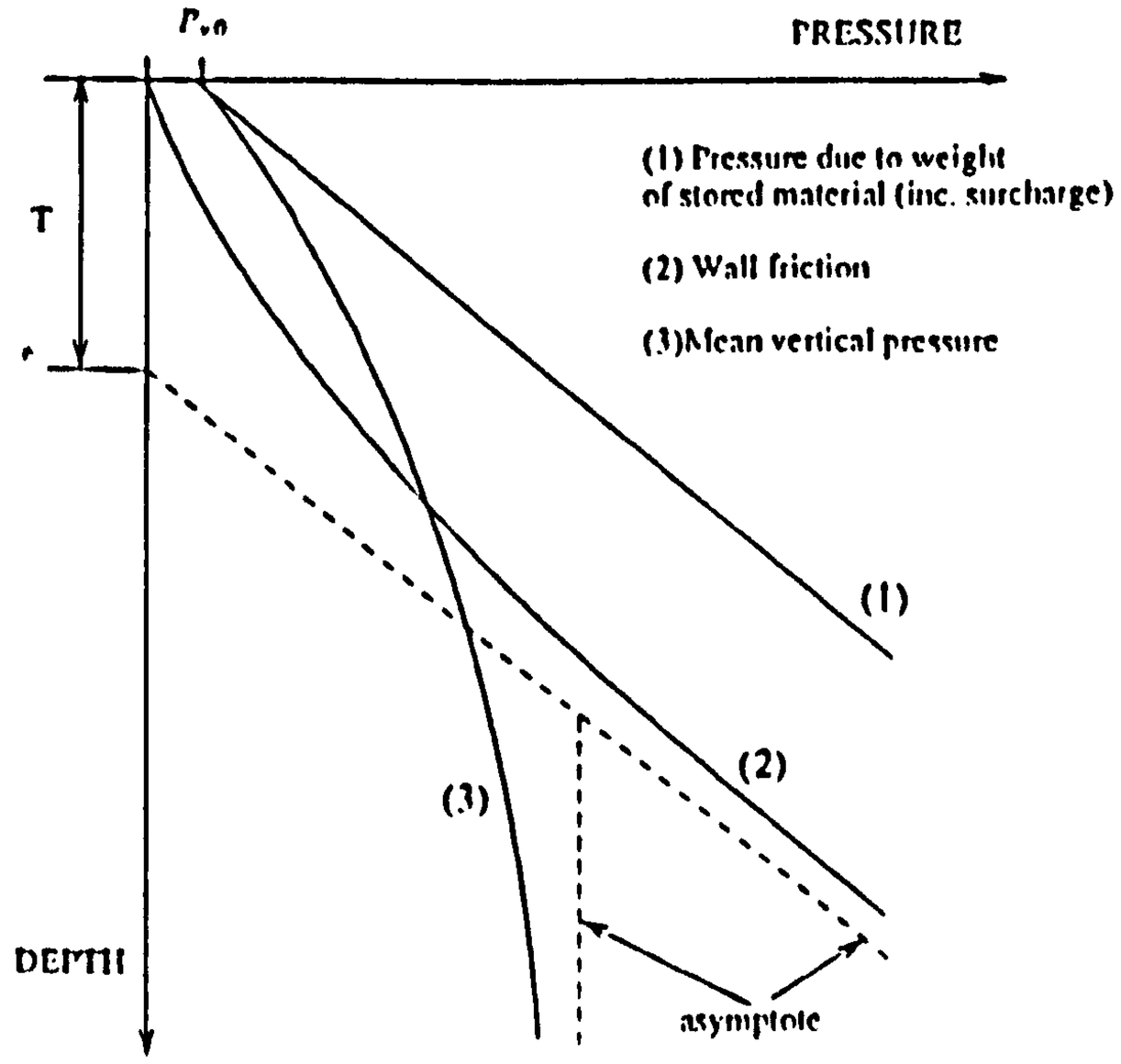

$P_{v\,max}$

Figure 3.2 PRESSURE CURVES USED IN DERIVING THE REIMBERT EQNS

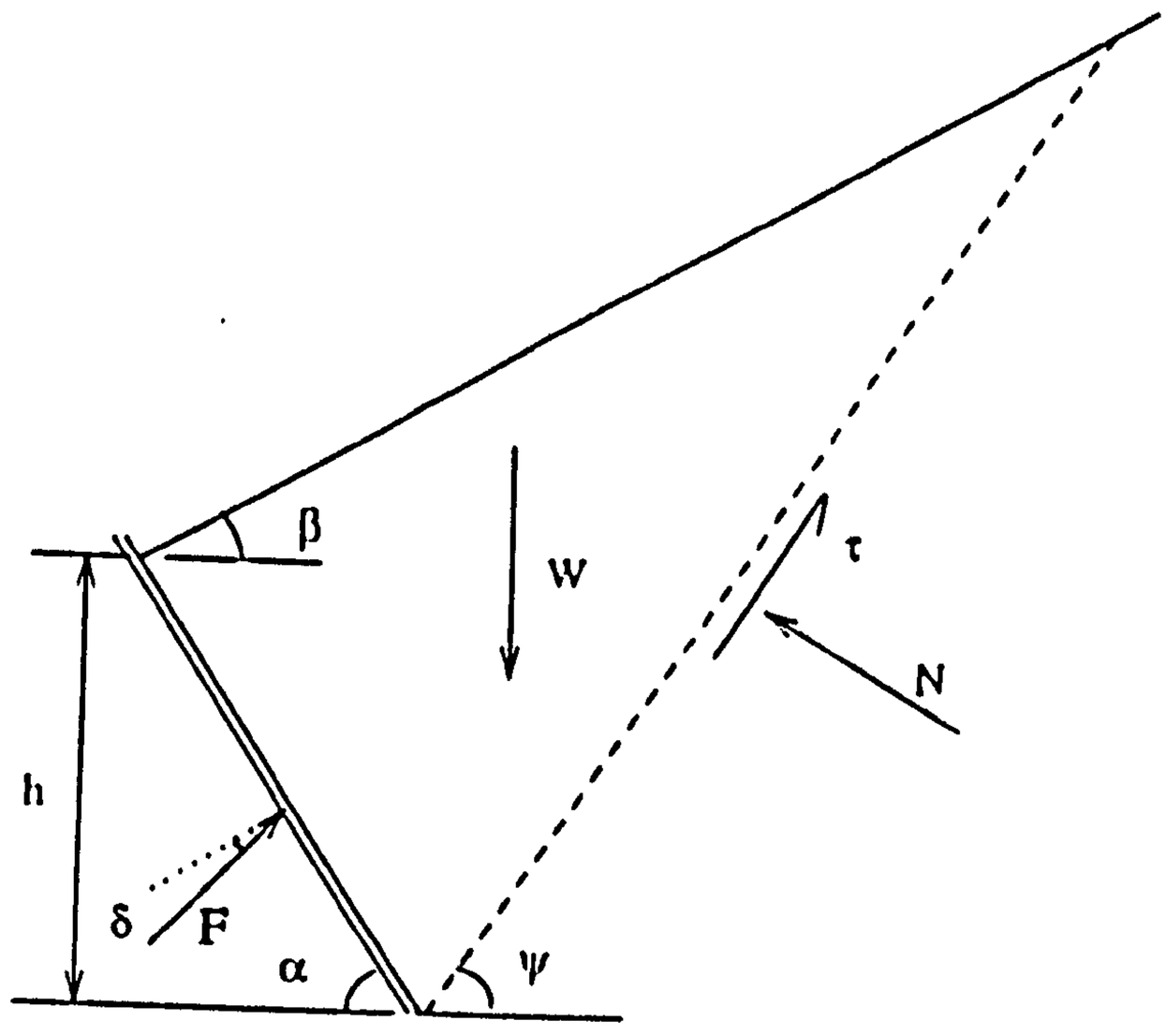

Figure 3.3 COULOMB WEDGE ANALYSIS

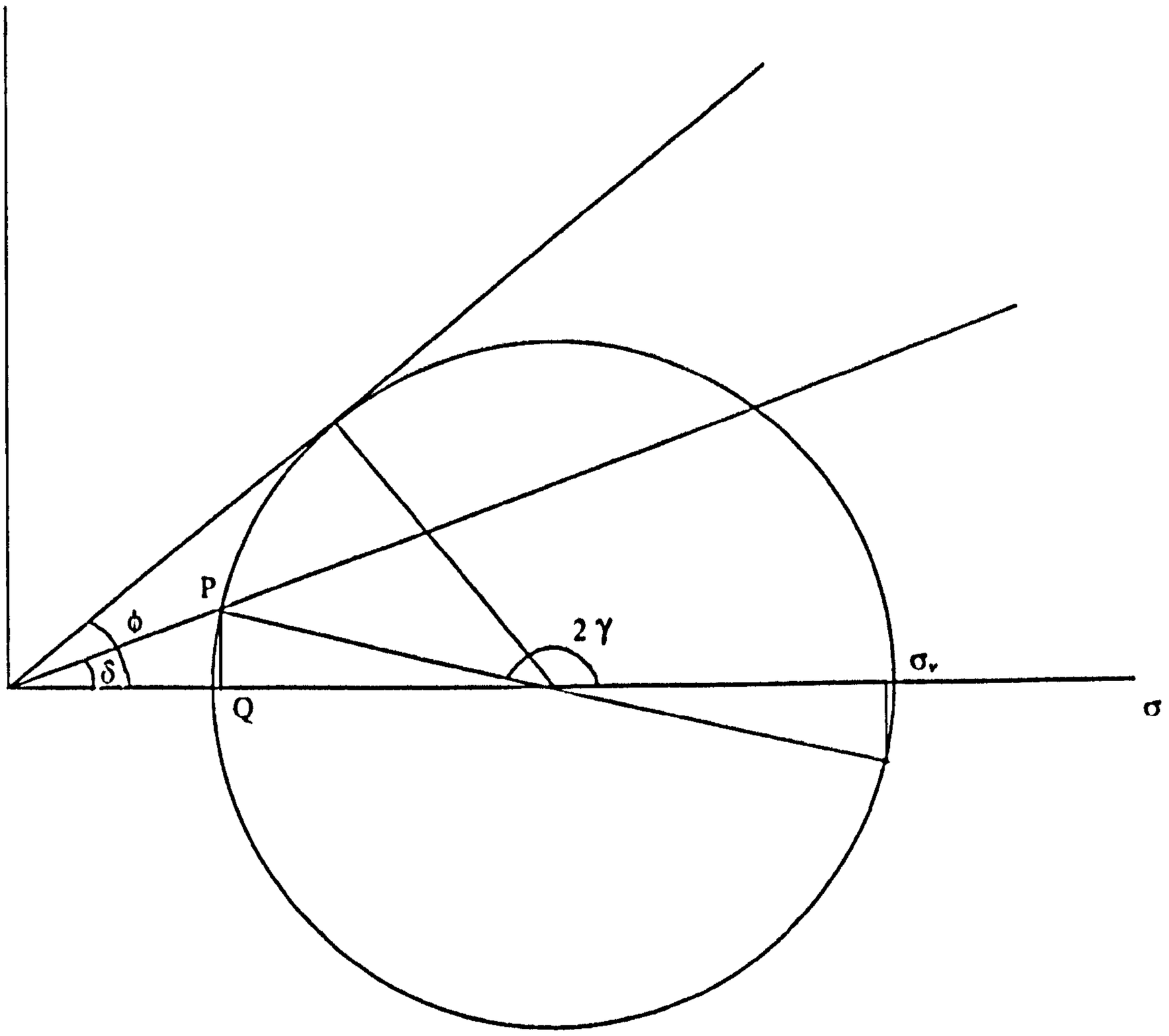

Figure 3.4 MOHR CIRCLE FOR MATERIAL (WALKER'S THEORY)

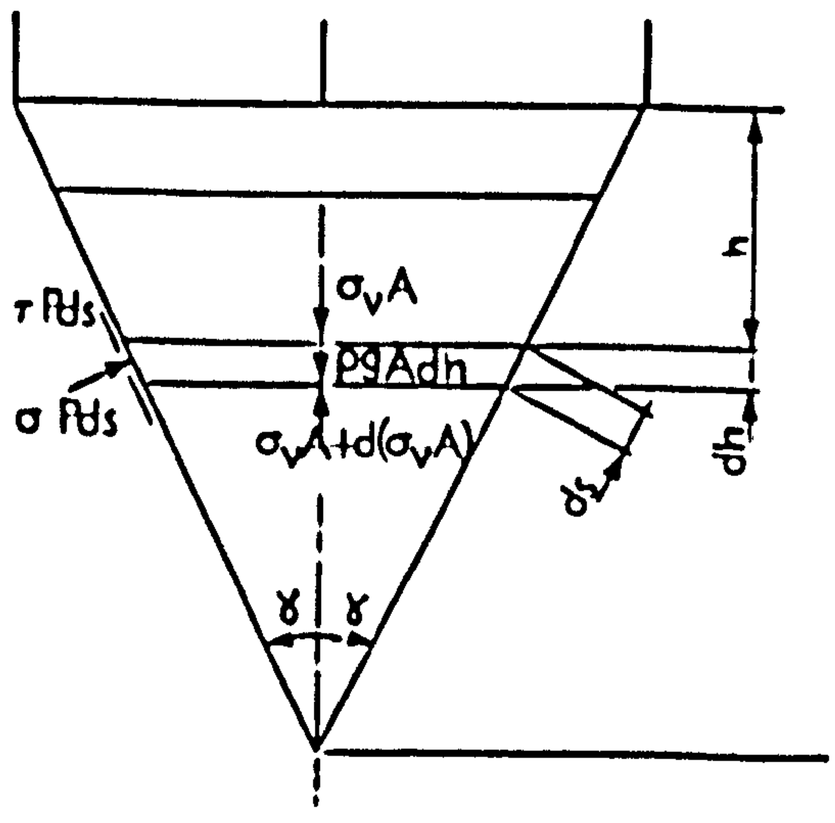

Figure 3.5 HORIZONTAL SLICE THROUGH THE HOPPER

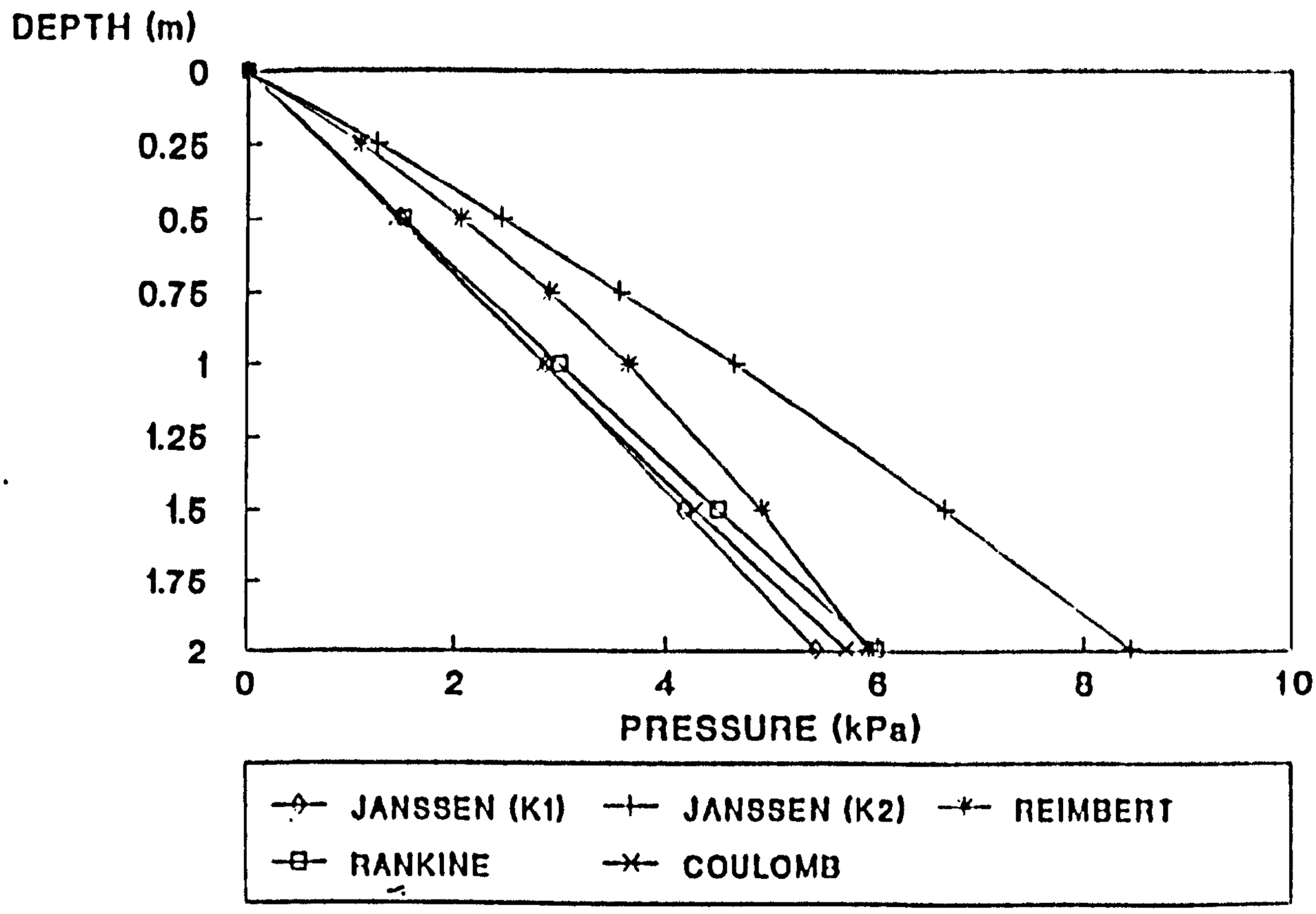

Figure 3.7 COMPARISON OF WALL PRESSURE THEORIES

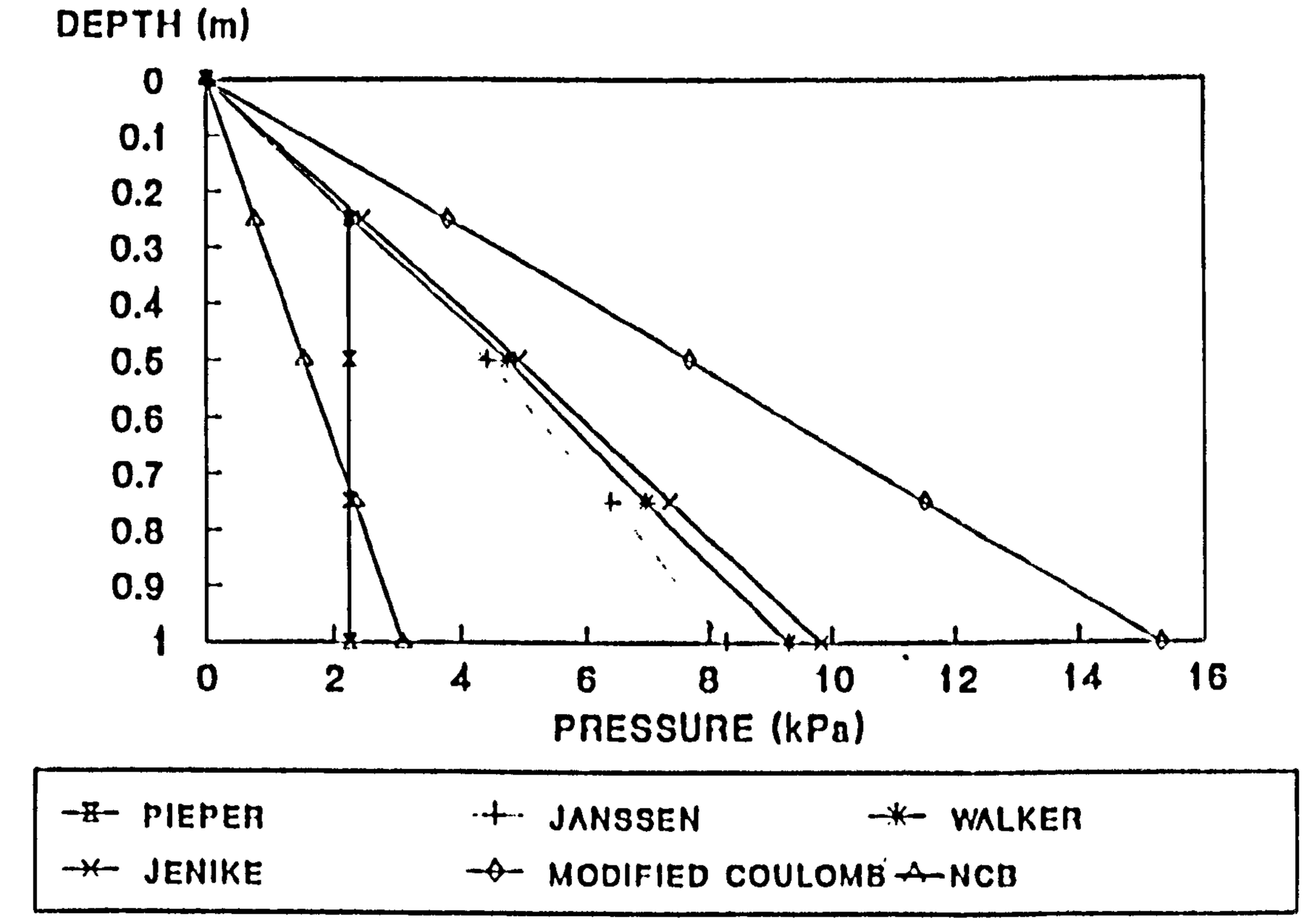

Figure 3.8 HOPPER PRESSURE NORMAL TO THE WALL,SILO FILLED TO TOP OF HOPPER

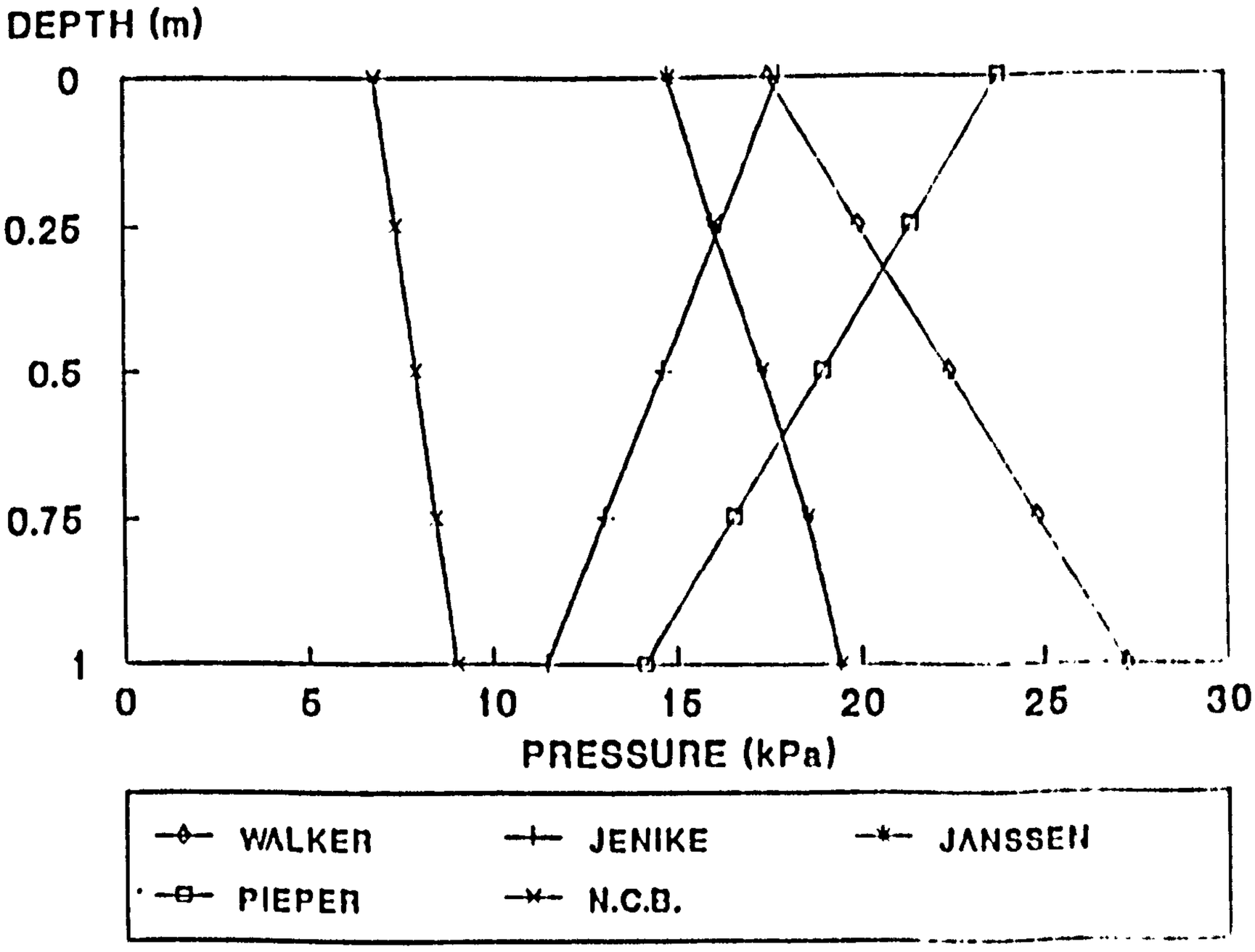

Figure 3.9 HOPPER PRESSURE NORMAL TO THE WALL,SILO FILLED

4. Design of the Experimental Apparatus

4.1. Introduction

A large scale model silo was constructed for testing at the laboratories of the Building Research Establishment. It was expected that the investigation of a single silo model would give an insight into the mode of interaction of the wall and stored material and the phenomena that affect pressure in flexible silos of different aspect ratios and wall and stored material stiffnesses during both filling and discharge.

The experimental rig is shown in Figure 4.1. It consists of the model silo, a storage silo, a timber filling box and filler box support structure, and a bucket elevator to transport the stored material between the test silo and the storage silo. The test model is detailed in Figures 4.2 and 4.3. Detailed reasons for each of the design decisions are given in Sections 4.3 to 4.5. and so only a brief description is given here. The model is Grade 43 steel, the geometry is shallow and was designed for funnel flow. The plan-form is 2.0m. by 2.0m. square. The height of the bin is 2.0m. and the height of the hopper is 1.0m. The granular stored medium was Leighton Buzzard sand. This is a poorly graded sand with well rounded particles. A steel frame was erected around the model to support a timber filler box. Twenty five holes were drilled at even spaces in the base of the box to give a distributed filling. The filling process is shown in Figure 4.4. A distributed filling method was selected in preference to the more common chute filling to minimise anisotropy of the stored material. Tests were conducted with the material in a static state and during discharge. Measurements of pressure, deformation and strain were recorded.

The detailed design and analysis of the test model and preliminary tests on the stored material are discussed below. The selection of instrumentation for the measurement of pressure, deformation and strain is discussed in Chapter 5.

4.2. Selection of model size and geometry

The model is not intended to be a scale replica of any particular structure and so the results will not be directly applicable to any silo other than the test model. The model was designed to indicate the pressure magnitude and distribution in square flexible silos other than very small silos in which the boundary conditions have a disproportionate effect on the pressure distribution.

The problems of scale errors from tests on reduced scale model silos have been investigated by Reimbert [2] , Hartlen [44] , Nielsen [84] , Pieper [16] and Munch-Anderson [85]. Most of the problems arose due to the difficulty of scaling the boundary conditions. Nielsen conducted tests on small scale models and found that it was necessary to increase the gravitational acceleration to overcome boundary affects. However, above a certain size, the behaviour of one silo could be used to predict the behaviour of another within the earth's gravitational field if the boundary conditions and aspect ratios were similar. He suggested that silos with a diameter or side length of two metres or more could be used to predict the behaviour of larger silos. A side length of two metres was selected for the test model. The silo height was selected to impose the maximum surcharge upon the hopper whilst still keeping within the restraints of the "shallow" classification (discussed in Chapter 1).

The hopper was designed for funnel flow since this was typical of shallow steel silos manufactured in practice. An angle of wall inclination of forty three degrees was selected to achieve funnel flow using Jenike's criteria [32].

4.3. Stored material selection

The stored material was selected to meet the following criteria:

(a) Dry and free flowing

(a) Uniform in size and shape to help achieve repeatable results.

(b) Cohesionless, and of sufficient particle size to prevent air entrapment, so that the parameters of creep and cohesion could be ignored.

(c) Have practical applications within the bulk solids handling industry.

The stored material chosen was Leighton Buzzard sand, particle size 0.5mm to 1.0mm. It is dry and free flowing. The particles are uniform in size and shape and it has often been used for research purposes and the results are widely acknowledged in both research and industrial circles.

4.4. Filling Method

The model filling technique and stored material were selected to minimise anisotropy of the stored material and to ensure consistency of compaction throughout the silo. Distributed filling produces a dense and nearly isotropic medium that can be simulated well in the shear box. The shear box tests for the determination of the lower and upper limits for the angle of internal friction are discussed in Section 4.7.3. The distributed filling method was expected to produce a dense medium close to the upper limit of the density range. The density of the medium in the silo will vary with depth due to the different distances of fall of particles from the filler box. The velocity of the particles during filling influences their lodgement at rest (Nielsen [86]). Since the velocity of particles charged into the bottom of the silo (when it is empty) is greater than that of particles landing at the top (when it is full), the particle packing will also vary. The difference in density of the stored material in the silo was measured using the techniques outlined in BS1377, 1975 at 0.25m. and 2.75m. above the outlet. The densities were $15.9 kN/m^3$ and $15.3 kN/m^3$ respectively. The difference is approximately four per cent. This is very small when compared with the variation in measured pressures throughout the silo (presented in Chapter 8). It suggests that the distributed filling method leads to a similar packing of the stored

material throughout the silo.

4.5. Model Design

Before carrying out the detailed analysis and design of the model silo, a literature survey [29,87,88,30,89,90,27,91,22] was conducted to determine the most common silo forms and analysis and design methods. The test model was designed so that features such as the support structure and ring beam were typical of existing structures. Three methods of analysis were reviewed and compared with experimental results obtained from a small perspex silo loaded by filling with water. Of the methods tested, only the Finite Element Method was in good agreement with the experimental results. The good correlation from this single test suggested that the Finite Element Method was suitable for the analysis of the test model.

4.5.1. Review of silo analysis and design techniques

4.5.1.1. Wall Plates

The design of silos has been discussed by Gaylord [29] , Troitsky [87,88] , Lightfoot [30] , Steel Designers Manual [89] , Skieller [90] , Safarian and Harris [27] , Rotter [91] and Lambert [22]. They consider steel silos reinforced with either horizontal or vertical stiffeners. Material loads in the silo are applied directly to the wall plate, and transferred via the plate to the stiffeners. The walls are subjected to bending and tensile membrane stresses. Frictional forces result in vertical compression of the wall and, because of the stiff corners and column supports, in-plane bending of the wall.

There are two main approaches to modelling the structural system. Either the silo is analysed as many isolated components or it is considered as a continuous folded plate structure. Most existing guides recommend the first approach. The walls are designed with assumed boundary conditions and interaction between individual plates is ignored.

Wall pressure is carried partly by flexural action of the plate in bending and partly by membrane action. Silo walls may be designed using either small or large deflection theories. If the wall deflections are small (less than the thickness of the plate), for design purposes it is acceptable to assume that the load is carried entirely by plate bending. If the deflections are large, membrane action is included.

Large deflection analysis

The large deflection analysis of a folded plate structure is complex because of the non-linear behaviour of the connected plate elements. A unique analysis is required for each plate configuration and a detailed analysis which considers the plate interaction and the in-plane and out-of-plane forces is only possible by numerical methods. Since little research work has been conducted in this area, it is more common to analyse the individual elements independently and ignore interaction between them.

Troitsky [87] describes the work of Lichtarnikov [92] in which the wall plate is treated as a membrane and a formula is derived to calculate the bending moment on a simply supported strip of unit width. The method does not consider the in-plane force and the plate boundary conditions are approximate.

Small deflection analysis

Three methods of analysis are commonly used. Wall plates between stiffeners with an aspect ratio greater than two to one are analysed as a beam bending in one direction only. The beam is assumed to span continuously over stiffeners and is fully fixed at the ends.

Plates with an aspect ratio less than two to one are designed from tabular data. Roark [93] and Timoshenko [94] provided data for the maximum stress in rectangular plates for different load cases and boundary conditions. Data are not given for the analysis of trapezoidal plates. The hopper wall is analaysed as a rectangular plate and its dimensions are calculated from formulae given in Roark.

Both of the methods described above are inaccurate due to the assumed plate geometry and boundary conditions. Numerical techniques such as the finite element analysis can be used to study the interaction of the various plate members subjected to in-plane and out-of-plane loads.

Plates are less efficient when subjected to out-of-plane loads than to membrane tension and so a plate structure designed by small deflection theory is less economical than one designed by large deflection theory. Despite the possible economies, designers have rarely adopted large displacement theory because of its complexity. The very large deformations that must exist, coupled with the lack of research leads most designers to take a more conservative approach.

Plate Instability

Levy [95] found that the buckling resistance of a flat plate is increased by the application of lateral pressure. He incorporated the increased buckling resistance into an empirical analysis for isolated plates. In practice a conservative stability analysis is usually adopted and the critical elastic buckling load is calculated assuming that the only loads acting are in the plane of the plate.

4.5.1.2. Transition ring beam

Hopper loads may be carried by the silo walls, or, entirely or in part by any ring beam present at the intersection between the bin and hopper. The second method is more often adopted for rectangular

hoppers. The ring beam has to carry the hopper weight and distribute the silo loads to the supports. At the start of filling the ring beam will act as a compression frame. It resists inward forces from the suspended hopper. As filling continues, the compressive forces will be offset by tension from the lateral pressure exerted by the stored material in the bin.

The ring beam may also have to carry loads from the following:

1. Vertical load from wall friction in the bin.

2. Axial compressive forces that arise from in-plane bending of the wall plates.

3. Axial tension due to forces from adjacent walls.

4. Torsion due to eccentricity of any of the above forces.

4.5.1.3. Support structure

The support structure for small silos is usually terminated at the ring beam. The walls of the structure above carry all the loads from the bin. This form of support is common in circular silos but in square silos the supports are usually continued from the transition ring beam to the top of the structure. Their function is to carry the vertical loads in the bin and provide resistance to buckling. A small ring beam is often positioned at the top of the silo to give additional restraint against horizontal forces. The support structure is braced to provide stability against externally applied lateral forces or non-symmetrical internal forces.

4.5.2. Assessment of the accuracy of the methods of analysis

The test model was designed using small displacement theory, as this is most frequently used in practice. The accuracy of the methods of analysis described in Section 4.5.1. was investigated by

comparison with test results from a perspex model silo. Strain gauges were attached to the model shown in Figure 4.5 and the model was filled with water. The measured stresses were compared with those predicted by traditional theories and the Finite Element method. Whilst there was good agreement between the theoretical values obtained using the Finite Element method and experimental results, the traditional calculations tended to produce conservative solutions. The maximum principal stresses in the centre of the hopper wall predicted by the Finite Element method were within approximately 15% of the maximum principal stress measured in the model. The maximum stresses predicted by the traditional theories were up to four times greater than the measured stresses.

The tests suggested that the simplified analytical methods used by the majority of designers lead to uneconomic designs. They also showed that the Finite Element model gave an accurate prediction of wall stresses from a known pressure field for this particular model.

4.5.3. Wall design

The walls of the test model were not stiffened because stiffeners have a local effect on the pressure distribution and could have confused the interpretation of the global pressure field.

The maximum wall stress and wall thickness were calculated by small displacement theory using the finite element method. The PAFEC 75 software package for finite element analysis was used and is described in Appendix A. The mesh generated for the analysis is shown in Figure A1. A model of a quarter of the test silo was analysed. Loads imposed on the bin were calculated using Janssen's equation and on the hopper using guidance in the Australian code [61]. As a factor of safety, the most conservative codified values of the ratio of horizontal to vertical pressure, 'K', were selected for each load case. Vertical restraints were applied to the bin-hopper transition. The Finite Element model was also restrained against rotation about the 'y' axis (Figure A1) along both vertical edges and vertically along the hopper/bin transition.

Displacement output is in the form of three translations and three rotations, each in or about the global 'x', 'y' and 'z' directions. The principal stresses on the top, middle and bottom surfaces of the element are found at each element centroid and each nodal point. The principal stresses predicted for a 10mm. thick wall plate were determined. The largest stresses were significantly lower than the yield stress of steel and so a 6mm. plate was analysed. The deformations of a wall constructed from 6mm. plate were over 9mm. and so were considered to be excessive when compared with the plate thickness and so 10mm. plate was selected for the test model wall.

The elastic critical buckling load was calculated from the following equation

$$F_{cr} = \frac{k\,\pi^2\,E}{12\left[1-\mu^2\right]\left[\frac{b}{t}\right]^2} \qquad (4.1)$$

No allowance was made for the increase in buckling resistance due to the horizontal pressure. The plate was assumed to be simply supported on all four edges and subjected to a linearly increasing load. A factor for k equal to 6.7 was taken from Brown [96] and the calculated total critical buckling load was 31.8 kN. This is much greater than the applied axial compressive load due to friction between the stored material and the wall and suggests that plates designed to carry lateral pressure by bending action in shallow silos are not in danger of buckling.

4.5.4. Silo support structure and ring beam

The support structure was designed for two load cases - the silo full and the silo filled to the top of the hopper. All members were designed in accordance within the guidelines of BS 5950. The silo is supported upon four columns that were designed to carry the weight of the structure and contents by axial compression. The transition ring beam was designed for bi-axial bending. It is required to resist lateral thrust from the stored material and vertical and inward forces from the hopper self weight and contents and from frictional drag on the bin wall. Figure 4.6 illustrates some of the possible details of

transition ring beams. The ring beam shown in Figure 4.3 was selected because it produces the lowest out-of-plane stress in the bin wall.

4.5.5. Connections

All plate connections are butt welds. Other connections are a mixture of fillet welds and bolts. Welded steel members are adversely affected by welding shrinkage and so particular care was taken during the fabrication of the hopper/bin connection and ring beam to minimise residual stresses.

4.5.6. Outlet size

The outlet dimensions were selected to allow a gravity discharge of the contents in approximately thirty minutes without the use of a feeder. The discharge time was calculated using the following formula taken from the B.M.H.B. code for silo design [60].

$$W_d = 1.03\,\rho g^{0.5}\,(L - f d_p)^{2.5}\;(cot\alpha)^{-0.35} \tag{4.2}$$

where

W_d is the discharge rate (kgs^{-1}), ρ is the bulk density (kgm^{-3}), g is the gravitational acceleration (ms^{-2}), L is the width of the outlet, f is a particle shape constant (taken as 1.8), d_p is the mean particle diameter, and α is the angle of the wall from the horizontal.

The accuracy of the formula has not been confirmed and so it was checked with results from a model test. The time for a known quantity of sand to pass through a number of different sized holes was measured. The experimental and theoretical results were in close agreement. A discharge orifice of

80mm. * 80mm. was selected for the test model. Equation 4.2 predicted a discharge time of thirty minutes to the nearest minute and the experiment predicted thirty four minutes. The discharge time for the silo model was approximately forty three minutes.

4.6. Tensile Tests

The Elastic Modulus and yield stress of the steel wall plate were determined from the mean results of five tensile tests. Specimens were cut to the dimensions recommended in BS 18 Part 2. The specimens were tested to failure in tension. Extension over a 150 mm. length of the specimen was recorded at regular intervals during loading.

Property	Mean	Standard Deviation
Elastic Modulus	216 kN/mm^2	9.1 kN/mm^2
Yield Stress	326 N/mm^2	16.7 N/mm^2

TABLE 4.1 - Mean results from five tensile specimens

4.7. Stored material properties

The stored material was Leighton Buzzard sand, with particles sizes ranging from 0.5mm. to 1.0mm. The effective size was 0.55mm. and the uniformity coefficient was 1.5. Knowledge of the angle of internal friction, angle of wall friction, angle of repose, and bulk density of the stored material was required for the model design.

4.7.1. Bulk Density

The bulk density of the sand was found when the sand was in a loose state and in a dense state. Each test was repeated three times. The loose specimen was prepared by pouring the sand from a container at a height of approximately twenty millimeters above the sand surface. The dense specimen was vibrated for forty seconds on a vibrating table. (Any further vibration did not affect the density.) The bulk densities are given in Table 4.2.

Loose sand	14.5 kN/m^3
Dense sand	16.29 kN/m^3

TABLE 4.2 - Sand Bulk Density

4.7.2. Angle of repose

The angle of repose checks the lower bound value of the internal angle of friction from the shear box tests. It was measured on a planar surface using a cylindrical drum, and was found to be 36°.

4.7.3. Shear box test

The angle of internal friction and angle of wall friction were determined from direct shear tests. The direct shear box has been severely criticised but Potts [97] points out that it remains popular due to its simplicity, and the results obtained from it are consistent with the results from other more sophisticated tests. In chapter three it was stated that results from the shear box are limited because it does not model the correct stress path to failure of the sand in the silo. The Geotechnical staff at the Building Research Establishment stated that it was unlikely that the shear strength in the silo would differ by

more than plus or minus four degrees from the shear strength in the shear box if the sand densities were similar. Since it is impossible to determine the precise shear strength at every point in the silo, the mean value achieved in the direct shear box is a compromise.

Square samples with a side length of ten centimetres were adopted for the shear box tests. Standard shear box test procedure recommends that tests are conducted with the sand in loose, medium and dense states of compaction. The extreme care required when placing sand in the shear box to obtain a loose state of compaction indicated that it was unlikely that such a condition could be obtained in a silo. For this reason tests were only conducted upon medium and well compacted samples.

The medium density samples were prepared by pouring the sand from a container no further than 50 cm. above the box. The surface of the sand was leveled with a flat plate. The dense samples were prepared by depositing the sand using a chute with 7.5 cm. diameter and 50 cm. height. The box was vibrated for one minute to achieve more compaction. Care was always taken to produce a uniform sample thickness.

The upper half of the shear box was displaced at a rate of 0.5 mm. per minute whilst the lower half remained stationary. To check the influence of strain rate on the results, three tests were conducted at a displacement rate of 0.15 mm. per minute. The difference from the mean was less than five per cent. Readings were taken for every 0.2 mm. of displacement. The vertical consolidating force was increased in intervals of 30 kN. from 30 kN. to 180 kN.

The angle of internal friction was found in the first series of tests. In the second series of tests a steel plate was inserted into the bottom half of the shear box and the angle of wall friction was measured.

During testing it was noted that the covering plate to the shear sample was rising. It appeared that the sample was not shearing in one plane, but that material was pushed in the direction of the applied load. An insert was added to the sample box to reduce the area of the shearing plane from 100 cm^2 to 36 cm^2. The insert did not appear to influence the results.

The mean results are given in Table 4.4.

Material property	Medium dense sand	Dense sand
ρ	14.9 kN/m^3	15.8 kN/m^3
ϕ	35.5°	43.5°
δ	28.6°	33.0°

TABLE 4.3 - Direct shear box test results

The results from the shear box tests were typical of those expected for dry sand and the angle of internal friction for the medium specimen agreed with the angle of repose. The angles obtained for the medium density and the dense specimens are the lower and upper bounds respectively. The filling method selected for the test model produces a density between 15.5 and 15.9 kN/m^3. Therefore the dense specimen in the shear box should give a reasonable prediction of the angles of friction in the silo.

Figure 4.1 TEST RIG

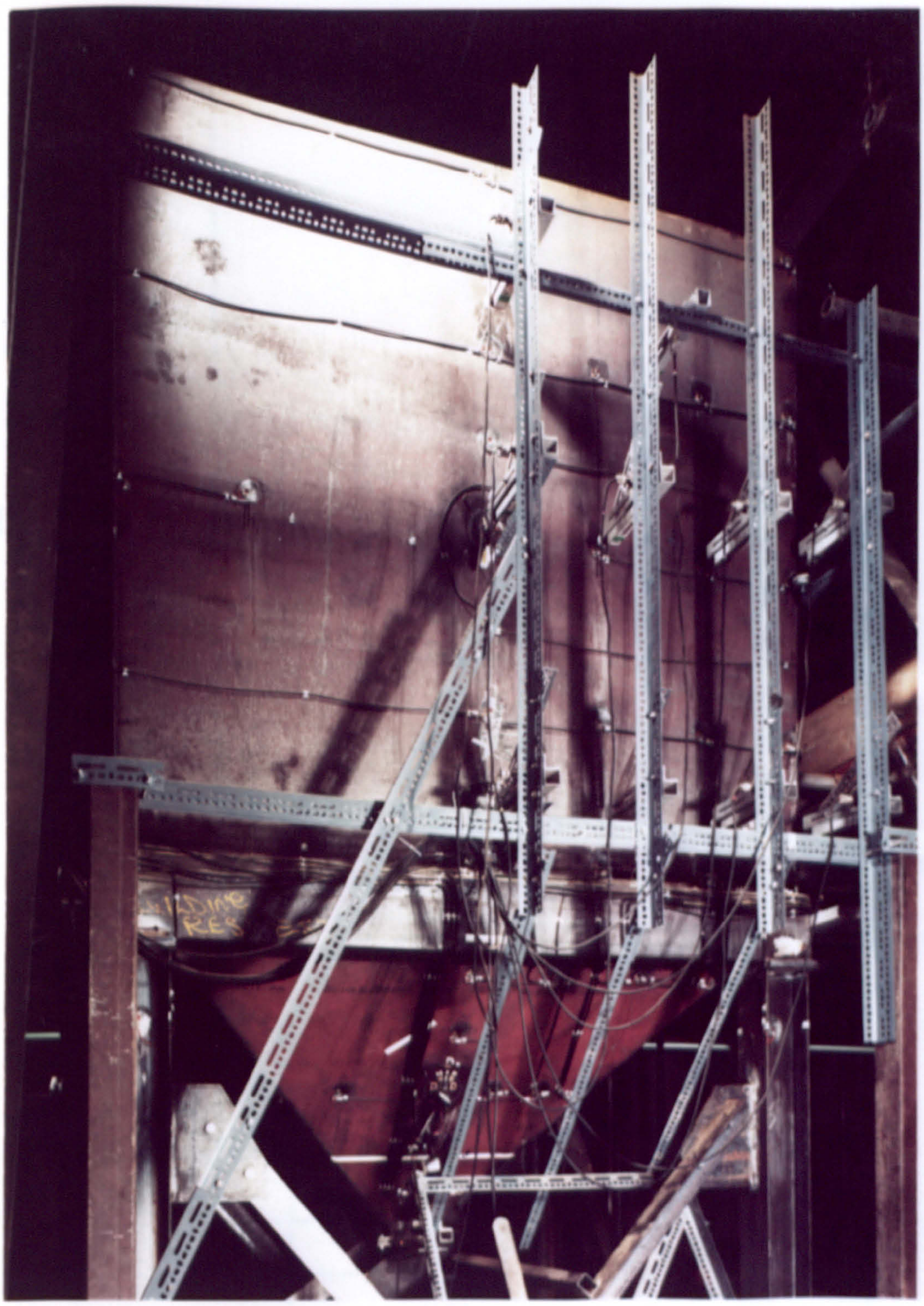

Figure 4.2a SILO MODEL

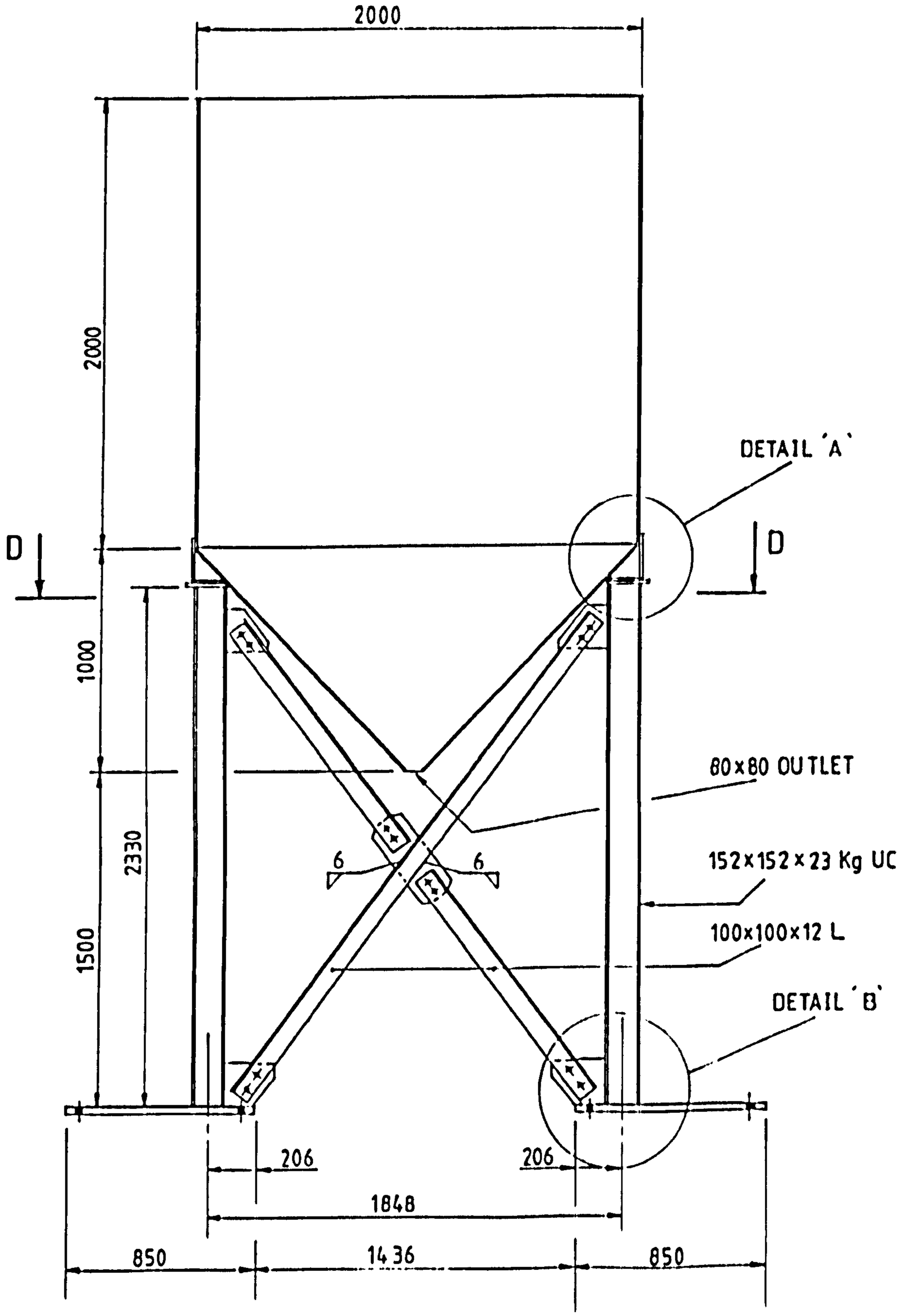

Figure 4.2b SILO MODEL DETAILS

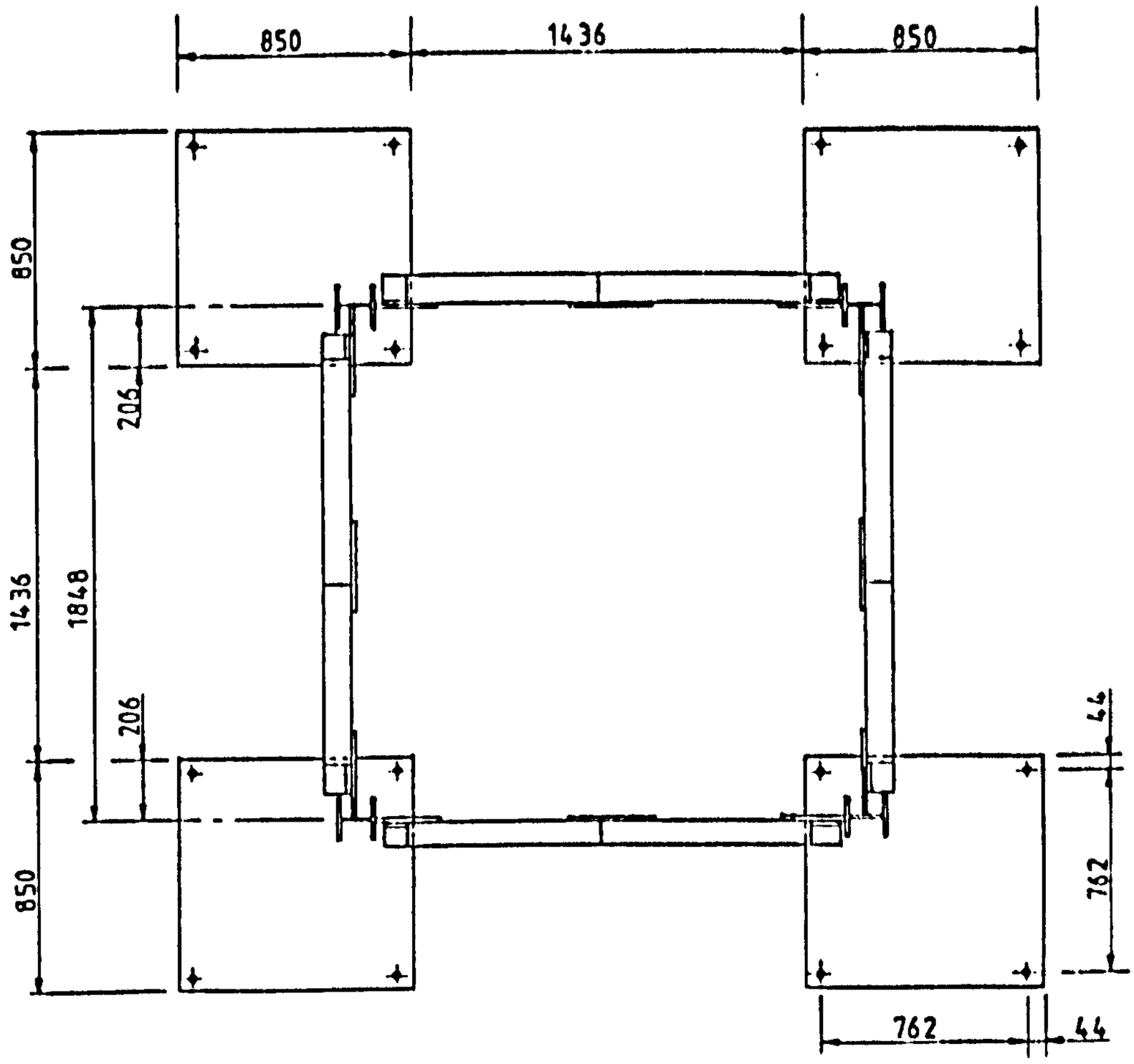

SECTION DD

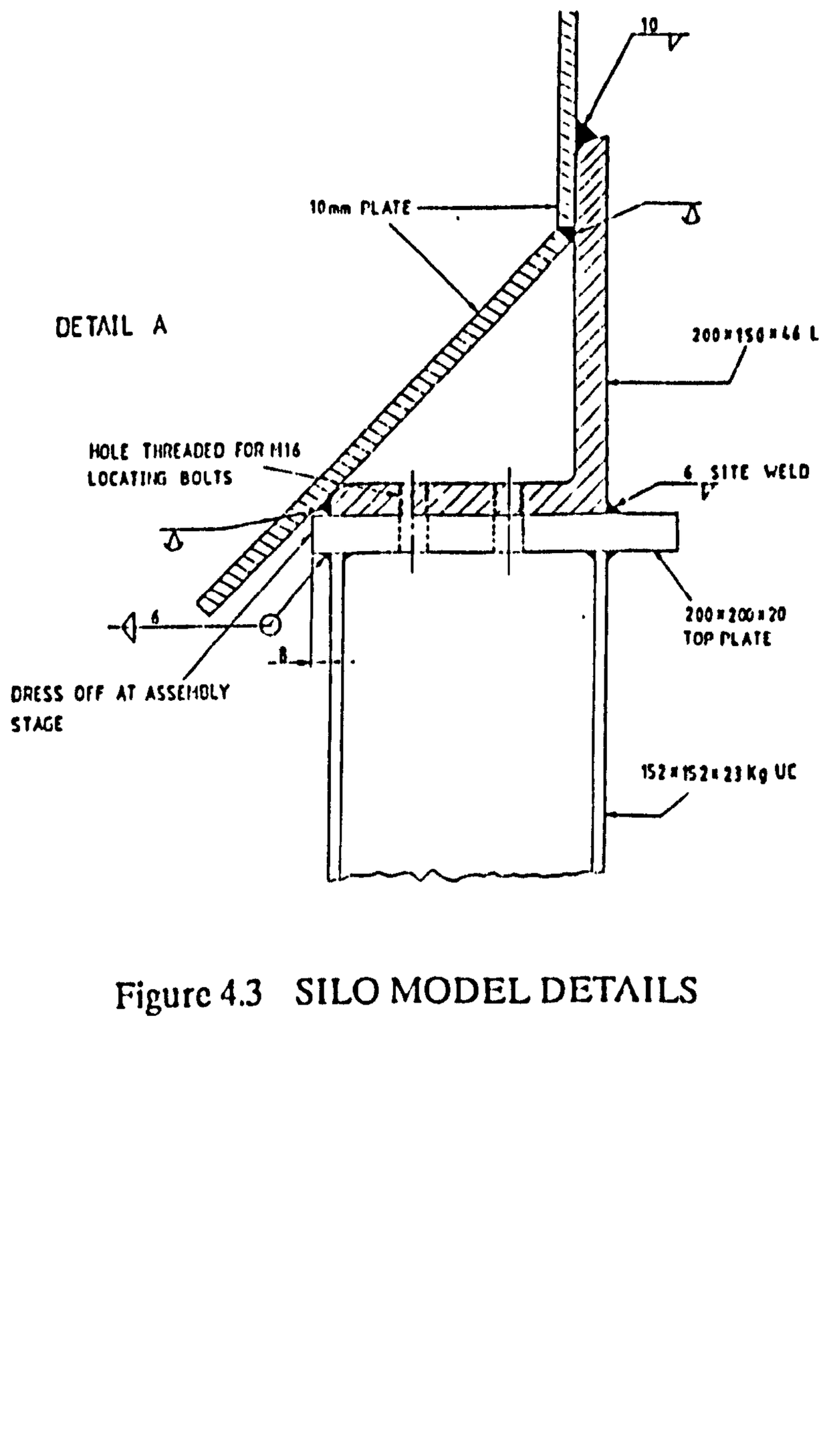

Figure 4.3 SILO MODEL DETAILS

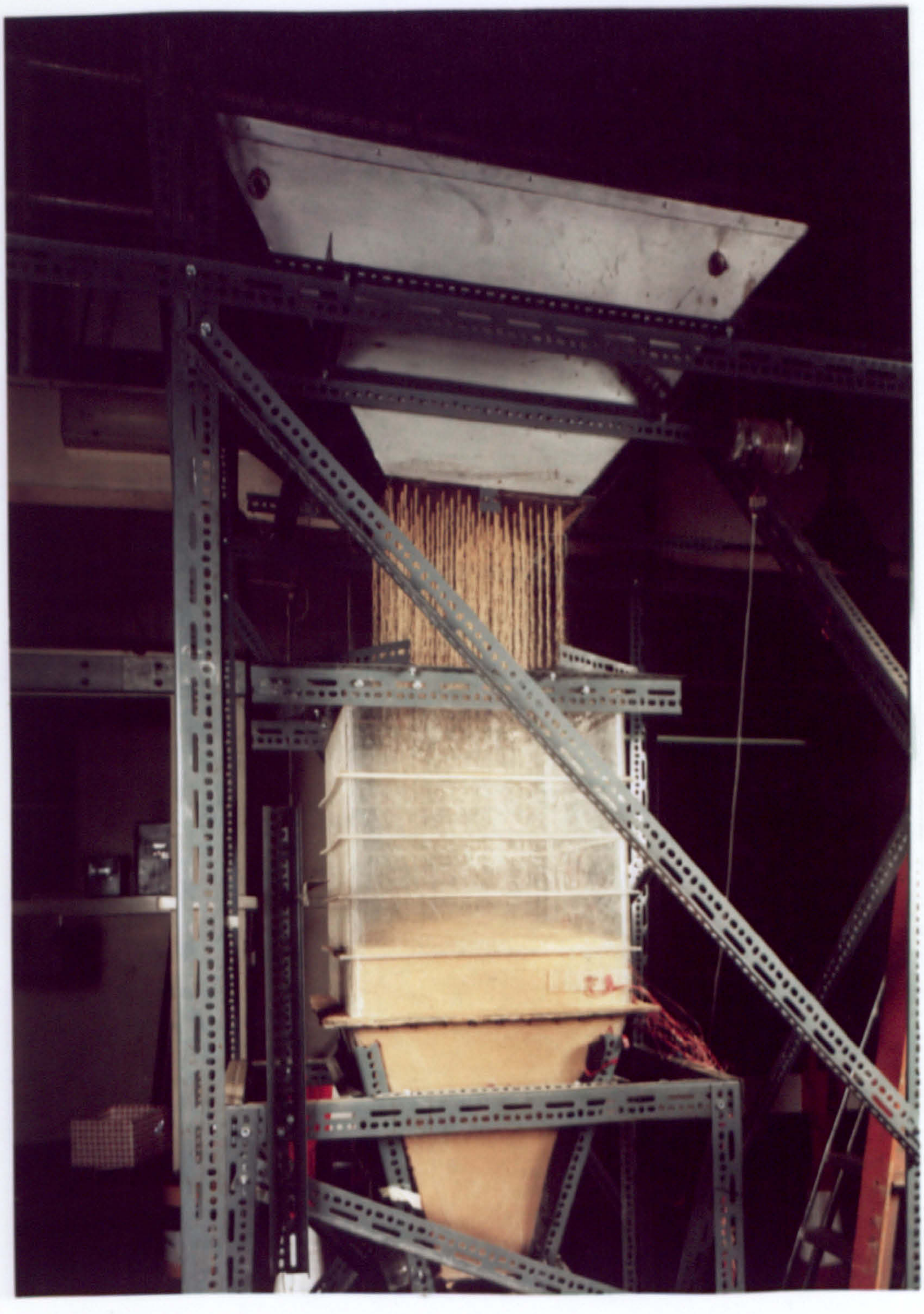

Figure 4.5 PERSPEX MODEL SILO

Figure 4.4(a) SILO FILLING

Figure 4.4(b) FILLER BOX AFTER DISCHARGE

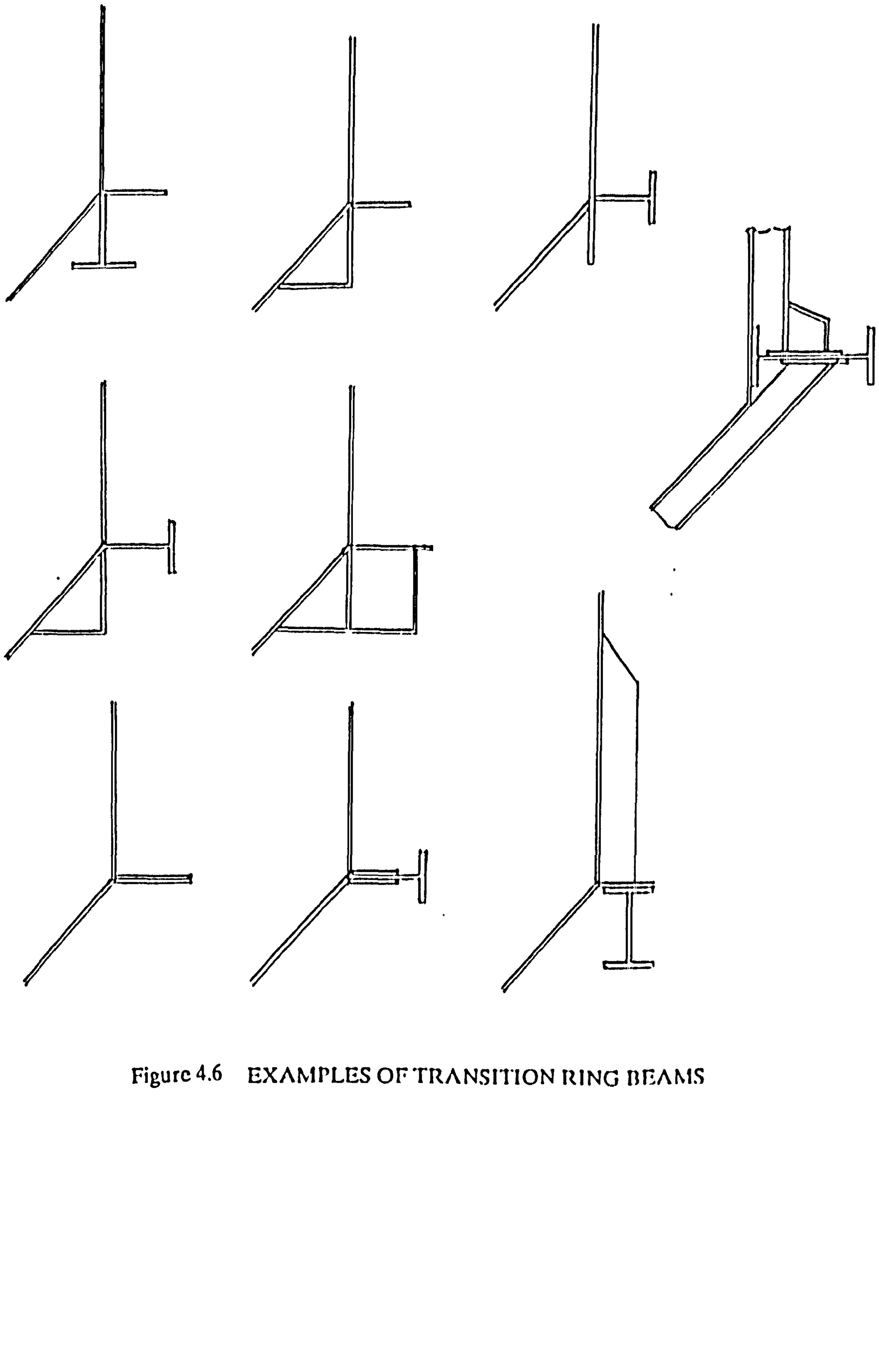

Figure 4.6 EXAMPLES OF TRANSITION RING BEAMS

5. Selection of Instrumentation

Measurements of strain, pressure and deformation were recorded during the test series. Strain gauges were attached to all four walls of the silo model in similar positions on each wall. They provided a check of the symmetry of loads exerted by the stored material on the silo wall and enabled a long term check on the consistency of wall stresses. They were also used (with results from a Finite Element analysis) to assess the effect of the difference between the measured and theoretical pressure distributions on the silo structure. Measurements of wall displacements were necessary to understand the effect of wall deformation on wall pressure. These were measured at selected positions on one wall only. Pressures in the stored material were measured at the interface of the wall and stored material and at intervals throughout the stored material to determine the total stress state.

5.1. Strain Measurement

A limited number of strain gauges were positioned on each wall of the silo to check the symmetry of the system. A greater number of gauges were adhered to one of the walls to investigate the stress distribution. Metal-foil electrical-resistance strain gauges were bonded to the outside of the silo wall in three element rectangular rosettes using a Cyanoacrylate adhesive. The gauge length was 5 mm, the nominal resistance was 120 ohms and the gauge factor was 2.18. They were monitored using a Solartron Orion 3516 data logger.

5.2. Deformation Measurement

Linear Voltage Displacement Transducers (L.V.D.T.'s) were assembled on an independent frame to measure deformation normal to one of the bin and one of the hopper walls. The influence of the mode

of wall deformation on pressure was discussed in Chapter 2. Many research projects have been conducted [11, 12, 13, 14, 15, 98] to establish the effect of different modes of rigid wall deformation and wall flexibility on wall pressure. The results of these projects and the deformation measurements in the test silo contribute to the understanding of the interaction of the flexible wall and stored material. In particular, the deformation measurements point out the degree of mobilisation of the plastic active state of pressure. In addition, the deformation of the upper boundaries at the centre of the bin and hopper walls indicates the probable linearity of the pressure distribution with depth and the possibility of vertical arches. The horizontal slope of the walls might indicate that horizontal arches form behind the flexible wall containing a granular stored material.

5.3. Pressure Measurement

The investigation of the interaction of a flexible silo wall and the stored material requires the determination of the total stress state at selected points throughout the silo contents. It is necessary to measure pressure in the vertical and horizontal directions and normal to an inclined plane.

Two types of pressure cell are currently in use,

a) cells that are fitted into the silo wall and measure pressure normal to the wall and

b) cells that are placed within the stored material.

The latter are referred to as embedded cells and they can be placed to measure any pressure normal to the cell face. Wall cells can be designed to minimise any disturbance of the stored material and a high level of accuracy is possible. Embedded cells are less accurate since the placing and the presence of the cell changes the stress field within the surrounding material. The error due to the presence of the embedded cell is systematic for tests in a single stored material. It is minimised by careful design and can be included in a calibration constant. The installation error is random. Its significance will vary

depending upon the stored material properties, the topography of the surface of placement, the hardness of the particles and the filling method. The randomness of the error can be reduced if care is taken to ensure that the placing method, pressure applied to the cell face and contact between the cell and stored material are the same for each test.

This chapter discusses the selection of pressure cells and the calibration and equilibrium checks carried out to achieve successful pressure measurements.

5.3.1. Cell design

A number of pressure cells have been developed for measuring pressure in a soil or stored material [12, 17, 99, 100, 101, 102, 103, 104, 105, 106].. The majority consist of a deflecting diaphragm and a means to measure the diaphragm deflection. The average pressure is related to the diaphragm deflection by a calibration factor. The deflection may be determined by electrical resistance strain gauges bonded to the rear of the diaphragm, or by the measurement of the pressure within a liquid confined behind the diaphragm.

Cells designed to measure shear stresses usually consist of a beam attached to the cell face and spanning perpendicular to the cell face. Bending strains at the outer flanges of the beam are measured by strain gauges and related to the shear stress by a calibration factor.

Some cells are designed on the basis that the error will be large but systematic, and can be included in a calibration factor. Most cells are designed to minimise their effect on the stored material stress state however, and the philosophy has been reviewed by Hanna [100] and Hvorslev [99].

5.3.1.1. Wall cell design

Accurate measurements of wall pressure can be gained if:

a) the cell face does not protrude from the wall,

b) the wall stiffness remains unchanged,

c) the cell face deflection is small, and

d) the angle of inclination of the cell face to the silo wall is small.

a, *b* and *d* are functions of the method of fixing the cell to the wall. The preferred situation occurs when the cell is mounted within the wall and its face is flush with the face of the wall. *c* and *d* are the major considerations for wall cell design. Cell face deformation causes local strains within the stored material in the region of the cell. Pressure will be relieved from the cell face, and the resulting error is a function of the stiffness of the stored material and the magnitude of cell face deformation.

Experiments have suggested that the maximum permissible deflection of a pressure cell should be less than 1/2000 of the diameter [99] or 1/5000 of the diameter [100]. Marchant [104] suggested that each micron of cell face displacement resulted in a measuring error of 1.5%, while Nielsen [31] found that a 0.01 mm. cell face deformation leads to a 10% error when the cell diameter is 50 mm. and the pressure from the stored material is 50 kPa. The error will be a function of the relative stiffnesses of the cell and stored material. Askegaard [102] used Gravesen's theory for a flexible membrane over a hole in a rigid wall. He stated that if the cell is suitably stiff, the cell error will be small for a range of values of stored material stiffness.

When measuring shear stresses, it is important that the coefficient of friction of the pressure cell face is the same as that of the surrounding wall.

Four wall cells were fitted into the wall in the positions shown in Figure 5.1. The wall cells measured normal and shear pressure. They served a number of purposes:-

a) Provided an accurate measurement of pressure normal to the wall and friction in the plane of the wall at four points.

b) Gave an indication of the actual variation of pressure between successive tests, and hence some indication of the variability of the testing procedure as a whole.

c) Provided an accurate datum from which the embedded cells could be calibrated.

5.3.1.2. Embedded cell design

Placement of a cell in a silo stored material will change the stress conditions in the surrounding material unless the cell and material have the same deformation properties. Embedded pressure cells are generally stiffer than the stored material and will measure pressures greater than the true pressure.

Tory and Sparrow [107] showed that for particular ratios of thickness to diameter of the cell, and cell stiffnesses, the measuring error is negligible and changes in soil stiffness can be catered for without appreciable errors.

Askegaard [102] stated that the measurement error of an embedded cell would be increased due to the effect of forces acting parallel to the cell face. He related the measured pressure to the true pressure normal to the cell face by the following expression

$$\sigma_{33} = A\,\sigma^{A}_{33} + B(\sigma^{A}_{11} + \sigma^{A}_{22}) \qquad (5.1)$$

where σ^{A} are the stress components in the surrounding medium and σ_{33} is the stress component measured normal to the cell face. A and B are constants dependent upon the Poisson's ratio, the thickness-diameter ratio of the inclusion and the ratio between the moduli of elasticity of the inclusion and the surrounding material. Askegaard stated that if a cell is made flat and thin enough, the measuring error can be made arbitrarily small whatever the properties of the stored material and cell. The ideal case exists when A=1 and B=0. The constants for Askegaard's cells vary from the ideal case but the true value can be determined from calibration tests.

Cells are usually designed with an inactive rim to reduce error due to the considerable overstress which occurs in a narrow zone near the edge, and must be of sufficient size overall to ensure that loading is

continuous over the cell face rather than from a few particles. Finally, the cell face deformation must be limited to prevent local strain of the stored material as described in section 2.1 above.

5.3.2. Cell selection

Askegaard's cells [102] were chosen for our experimental programme as they comply with all the requirements discussed above. For the wall cells, tests by Askegaard showed that they measure pressures to within 3% of the actual values for the pressure range anticipated in the model silo. For the embedded cells calibration tests determined the constants 'A' and 'B' in equation 5.1. Both types of cell have been used successfully in silos to measure static and dynamic pressures [21,44,108,109,110]. The selection of cell face diameter is a compromise. Small cells enable a more accurate measurement of changes in pressure profile normal to the wall than large cells but the larger the cell face, the smaller the error for the same cell face displacement. The embedded cells were 75mm diameter and the wall cells 100mm diameter. Very small cells were not considered necessary to measure the highly localised force which may occur during mass flow discharge because the model was designed for funnel flow.

5.3.3. Cell specification

5.3.3.1. Wall cell

The cell shown in Figure 5.2 has been designed using the principles described above. It is manufactured from steel plate cut from the silo wall to minimise any change in the wall stiffness. A front plate of mild steel 0.5 mm. thick and 98 mm. diameter was placed in a 0.7mm. deep recess. The 100 mm. diameter recess was turned into the steel wall piece. The front plate was laser welded to the steel piece near its centre and connected along the circumference by a flexible rubber seal. The cavity between the

front plate and the steel piece is 0.2 mm. thick and filled with silicone oil. The oil pressure corresponds to the normal stress on the pressure cell and is measured with a Honeywell 136PC 151G1L pressure transducer. Cell face deflection is less than 1 micron per 100 kPa and so the maximum cell face deformation within the pressure range anticipated in the model silo is 1/100000 of the diameter and is considerably less than the minimum recommended values [99, 100].

The relative displacement between the two plates in their plane is proportional to the shear stress transferred to the cell. The shear stress is measured by four semiconductor strain gauges attached to the central steel piece. They are combined in a full Wheatstone bridge.

The finished cell before installation is shown in Figure 5.3. It was mounted flush with the wall and screwed into place. The screws were fastened with araldite epoxy resin and ground to give a smooth finish.

5.3.3.2. Embedded cell

The embedded cells measured pressure normal to the cell face only. The geometry was selected to meet the criteria discussed above. The cells are shown in Figure 5.4. They are manufactured from brass and are 75 mm. diameter and 3 mm. thick. They consist of two plates brazed together. A 0.7 mm. deep recess was turned into one plate to form a 0.2 mm. cavity which was subsequently filled with silicone oil. Once again the oil pressure corresponds to the normal stress on the pressure cell and is measured with a Honeywell 136PC 151G1L pressure transducer. Cell face deflection is less than 2 microns per 100 kPa. (1/50000 of the cell diameter at the maximum anticipated pressure in the model silo). The cells have a 3mm inactive rim around the edge.

5.4. Placing of Embedded Cells

The errors due to cell placement have been reported by Hadala (referenced in Hvorslev [99]) Askegaard [108, 111] and Munch Andersen [21]. The inclusion stresses are sensitive to the method of placement. Askegaard found that they vary with each different person who places the cell.

Errors due to placing can only be incorporated into a calibration constant if the placing method adopted creates an identical disturbance around each cell placed. In reality, it is difficult to create the same disturbance with each test. The topography of the stored material may vary between tests and the stress field around the cell will vary for different cell orientations. The scatter of results between seemingly identical tests will be a function of the filling method, the care taken during cell placement, the cell orientation and the stored material and cell stiffnesses amongst other factors.

Only a few experimental investigations have been made to determine the effects of different methods of placement on measured pressures. Hadala recommended placing the cell on a planed surface of sand deposits. Askegaard recommended levelling the sand with a disk of the same diameter or slightly larger than the cell diameter. Hvorslev found that the application of a seating pressure during or after installation of the cell improved contact with the stored material and stabilised the stored material properties and cell error.

Hadala, Askegaard and Hvorslev each recommended a different method of placement. The most suitable technique for the test model was established after some comparative tests. The cells were initially placed on the stored material in the main test model without any surface preparation or seating pressure. The measured pressures varied by over 100% of the expected value. Although some variation between cell readings was expected due to variation in actual pressure, the magnitude of variation suggested that most of the scatter could be attributed to the installation technique. This may be due to the effects of wall friction, wall flexibility or the imprecise method of filling. It is difficult to calculate the effects of the wall friction and wall flexibility since they are unknown but it is unlikely that they would

lead to such a dramatic variation in pressure over a small part of the centre of the silo. Deviation from the mean pressure is partly due to variation in the surface of the sand. The surface level was found to vary from the intended level by up to one hundred millimetres, even though great care was taken with the filling process. This will lead to a significant error at a low head of sand, but at higher levels the percentage deviation in pressure due to a one hundred millimetre change in surface level will be small. This is particularly true for a cell placed in front of wall cell 'A' (Figure 5.1.) where the pressure increase is small after the head of sand has risen above one metre.

5.4.1. Tests to develop a consistent method of placement

The small Perspex model shown in Figure 4.5 was used to investigate the effect of different methods of cell placement. The model is 500mm x 500mm and 1100mm high. The small size enabled a number of tests to be conducted in a short period of time. The filling method and stored material were selected to minimise pressure variation between similar tests. A distributed method of filling reduced anisotropy of the stored material. For cells placed to measure horizontal pressure, the disturbance due to placement was negligible and the stored material contacted the cell over the entire face. The results produced were repeatable. The measurement of vertical pressure was more difficult. For the initial tests disturbance of the stored material around the cell was minimised. The installation procedure was to fill the silo to the required level and place the cell so that the flat face was in contact with the surface of the material. The sand was not disturbed and no pressure was applied to the cell during or after placement. It was noticeable that cells that recorded pressures in excess of the mean pressure at low levels of sand continued to record pressure higher than the mean and with a similar coefficient of variation for the entire test. This suggested that pressure variation is due to the manner of particle packing. The sand is not isotropic and homogeneous and so the initial stress field is influenced by the lodgement of particles after fall from the filler box. It is different for each test, but the variation from the mean will be constant for a test because the initial stress field influences the stress field throughout the test.

A number of reasons were hypothesised for the inconsistency. Munch-Andersen [21] found that results from the embedded cells improved when a layer of sand was glued to the cell. He believed that the higher coefficient of friction of the cell face prevented the formation of local rupture planes in the sand. A layer of sand was glued to the cells and some improvement was noticed but the results were still unsatisfactory.

The method of filling leaves the sand in a dense state. When the cell is rested upon the surface, minor undulations in the surface will prevent contact between the cell and the sand over all the face. Tests were conducted in which a forced hollow was created under the cell face. It gave results which were higher than those from a cell rested upon a smooth surface and suggested that contact over the entire face was essential for accurate results. The cells were used previously in tests by Munch-Andersen [21]. They were placed (without surface preparation or pressure) upon compressible media such as Wheat and Barley. The stored material compressed as the silo filled and resulted in contact over all of the cell face. Sand is a less compressible material than Wheat or Barley and so some surface preparation is required to achieve contact over the entire face. A number of different variations to the placement method were tried as follows.

1. Cell placed face up.
2. Cell twisted and pushed into the sand to ensure contact at all points.
3. Surface levelled with a disk and cell rested upon the level surface.
4. Surface prepared by pouring loose sand from a small container in the area in which the cell was to be placed.
5. Surface prepared by loosening the sand by hand and pushing the cell into the sand.

Slightly improved results were obtained when the cells were placed face up. Poor results were achieved when the cell was twisted and pushed into the sand. Consistent results were achieved with

methods 4 and 5, but method 5 was preferable to method 4 due to the speed of cell installation, and was adopted because it was felt that the smaller inclusion would result in greater accuracy. Although the method led to consistent results, the cell was expected to under-register due to the formation of an arch over the loose compressible inclusion. Equilibrium checks carried out are described below.

5.5. Cell calibration

Askegaard calibrated both the wall and embedded cells in a specially designed calibration chamber. The calibration constant relates true pressure to the supply voltage. The cells were embedded in sand within Askegaard's calibration chamber and a known air pressure was applied to the sand. A mean constant of 39.5 $\mu V/V/kPa$ with a standard deviation of 0.2 was determined for normal pressure applied to the four wall cells. The mean constant measured for the embedded cells was 135 $\mu V/V/kPa$. (The standard deviation was not given.)

The shear cells were calibrated using a weight suspended by a hook glued to the cell face. The mean constant was 371 $\mu V/V/kPa$ and the standard deviation was 3.0.

The inclusion error of a pressure cell can be incorporated in the calibration constant if the cell is calibrated in the same material as is used in the model and if the installation procedure is the same in the calibration chamber and the model silo. However, the filling and placement methods in the calibration chamber and the large scale model are necessarily different, and so the constants calculated in the chamber may not be correct for the embedded cells placed in the model.

Two calibration constants were calculated for the embedded cells. Firstly, the cells were loaded hydrostatically and the output voltage was related to the applied pressure. This constant did not allow for the inclusion effects, which were incorporated into a second calibration factor determined from a comparison of the embedded and wall cell measurements. The embedded cells were placed close to the wall cells to measure pressure normal to the face of the wall cell (direction 11), parallel to the wall (direction 22), and vertically (direction 33). Consideration of any two wall cell positions gives two

simultaneous equations from which the constants 'A' and 'B' in equation 5.1 can be established. Values of σ^{A}_{11}, σ^{A}_{22} and σ^{A}_{33} were the mean embedded cell readings from five tests. σ_{11} is the mean wall cell reading from twenty tests. To prevent any error due to the presence of the embedded cells, the twenty tests did not include those with the embedded cells placed adjacent to the wall cells.

Table 5.1 includes the mean pressures and standard deviations measured by the wall cells and the free field cells.

Position	Wall Cell		Embedded Cells					
	σ_{11}		σ^{A}_{11}		σ^{A}_{22}		σ^{A}_{33}	
	$\bar{x}$	σ_{n-1}	$\bar{x}$	σ_{n-1}	$\bar{x}$	σ_{n-1}	$\bar{x}$	σ_{n-1}
A	6.55	1.61	3.76	0.41	6.09	0.52	19.78	3.34
B	4.37	0.70	6.81	0.99	9.59	0.91	39.50	5.48
C	9.66	0.89	11.62	0.86	8.48	0.85	30.13	4.62
D	1.28	0.43	1.59	0.35	3.01	0.59	14.44	0.91

TABLE 5.1 - Mean Pressures (kPa) and Standard Deviations for Wall and Embedded Cells with the Silo Full

The consideration of pressures at positions 'C' and 'D' in Figure 5.1 at levels of 2.5, 2.75 and 3.0 metres of sand gave the following mean constants:

$A = 0.83$ standard deviation = 0.02

$B = 0.003$ standard deviation = 0.006

The standard deviation for the constant A is small because while the ratio of horizontal to vertical pressure was different for positions 'C' and 'D', it was similar at each of the load intervals.

The constants obtained from equations incorporating pressures from cell position 'B' were very sensitive to the value of σ^{A}_{11}. Measured values of normal pressure varied between 5.1 and 5.7 kPa, a

relatively small discrepancy, and yet the ill-conditioned nature of the system resulted in values for the constant 'A' which varied between 0.33 and 1.02. It is possible therefore that the position of the wall cell (in respect of the ratio of horizontal to vertical pressure) is highly critical in obtaining good calibration data from the actual test silo.

5.5.1. Applicability of calibration factors

The intrinsic weakness of calibration of embedded cells from wall cells is that wall cells necessarily occur at the edge of the material and the inclusion stresses may be sensitive to the proximity of the boundary. An equilibrium check is essential to confirm the accuracy of the calibration constant obtained from either of the methods described above. A check of the equilibrium of vertical forces was carried out at the level of the transition between the bin and the hopper. It confirmed the accuracy of the calibration constants and is described in Chapter 9.

The calibration factors given above were based upon the assumption that the inclusion stresses around the cell are the same when it is placed vertically or horizontally. If the same constant is to be used for cells placed to measure pressure normal to the inclined hopper wall, the inclusion created when placing the cell at an inclination should also be the same. A comparison of the wall cell and embedded cell measurements suggests that the inclusions may be different and so different calibration factors may be required for the inclined cell measurements. At cell position 'A', the data given in Table 5.1 shows that the wall cell measurements were higher than the embedded cell measurements. This contradicts the results from positions 'B','C' and 'D' in which the embedded cells predicted higher pressures than the wall cells. The difference may be because particles of sand cannot fall directly behind an inclined embedded cell and must be deflected from the silo wall or surrounding medium. Since all the inclined cells are placed in the same manner, this error is expected to be systematic and so it can be included in a calibration constant.

The true calibration constant can only be determined from two or more wall cells placed to measure pressure parallel and normal to the wall cell in different proportions. Unfortunately, only one wall cell was inserted in the hopper wall and so the true value of the calibration constant for the inclined pressure measurements cannot be determined from the wall cells. Since pressure measurements normal to the hopper wall are of fundamental importance to the study, alternative methods were considered.

a. Apply a linear factor to all measurements. The factor may be obtained by comparison of the results from the inclined wall cell and a single embedded cell placed in front of the wall cell .

b. Apply a linear factor calculated from a check of the vertical equilibrium of the loaded hopper.

The constant A from equation 5.1 (if B is assumed equal to zero) calculated by method 'a' is :-

$$\frac{Wall\ cell}{Embedded\ cell} = \frac{6.45}{3.76} = 1.72$$

The vertical equilibrium of the hopper was checked (method 'b') for the silo filled to the top of the hopper and the silo full. The equilibrium check is detailed in Chapter 9. It was concluded that the check with the silo full was most accurate and this led to a constant A of 0.87 if B is assumed to be zero. This is close to the value selected for the embedded cells placed to measure horizontal and vertical pressure. For simplicity, it was decided to adopt a single constant for A of 0.83 for all embedded cell results. Because of the problems, the results presented for hopper pressures should be treated as somewhat less certain than bin pressures.

5.6. Summary

It is apparent that the two most important factors to achieve consistency of measurement with embedded cells are to ensure contact of the stored material over the entire cell, and to create an identical inclusion around each cell placed. The placement inclusion should be minimised but it is more

essential to create an identical inclusion for each test, since this can be included in a calibration constant. Reasonable results can be obtained if such constants are calculated from the mean of a large sample of data.

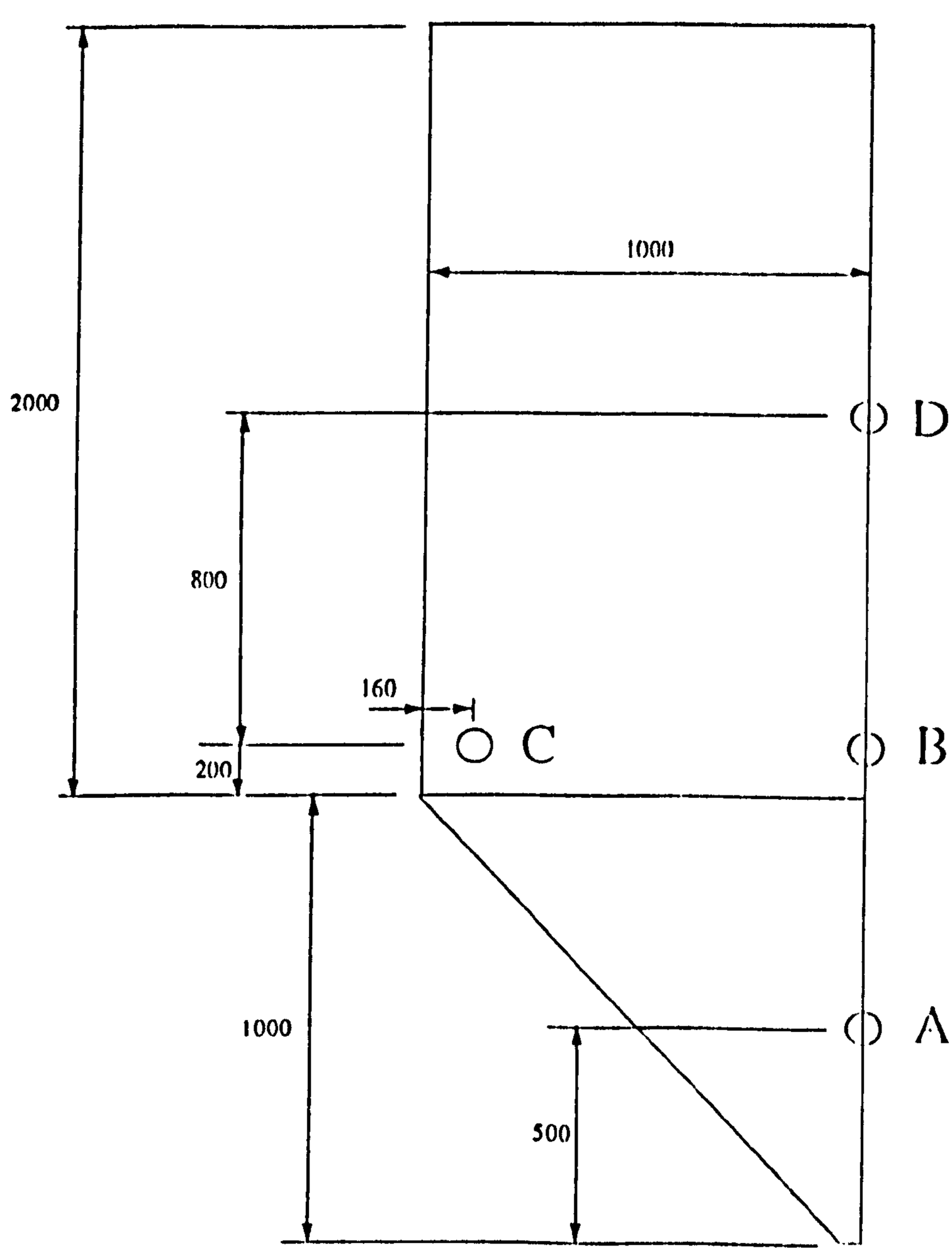

Figure 5.1 WALL CELL POSITIONS

(Dimensions in mm)

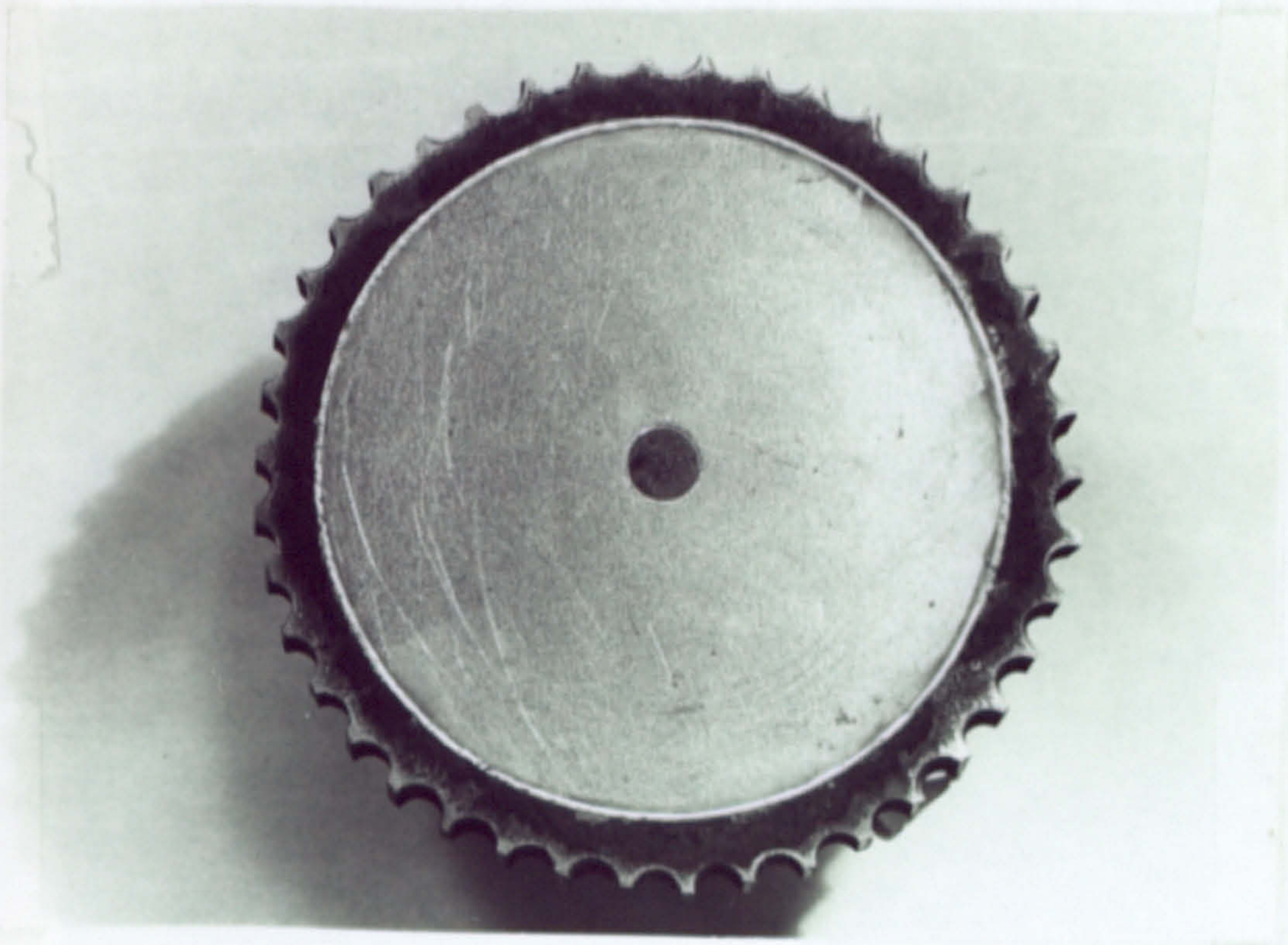

Figure 5.2 WALL CELL BEFORE INSTALLATION

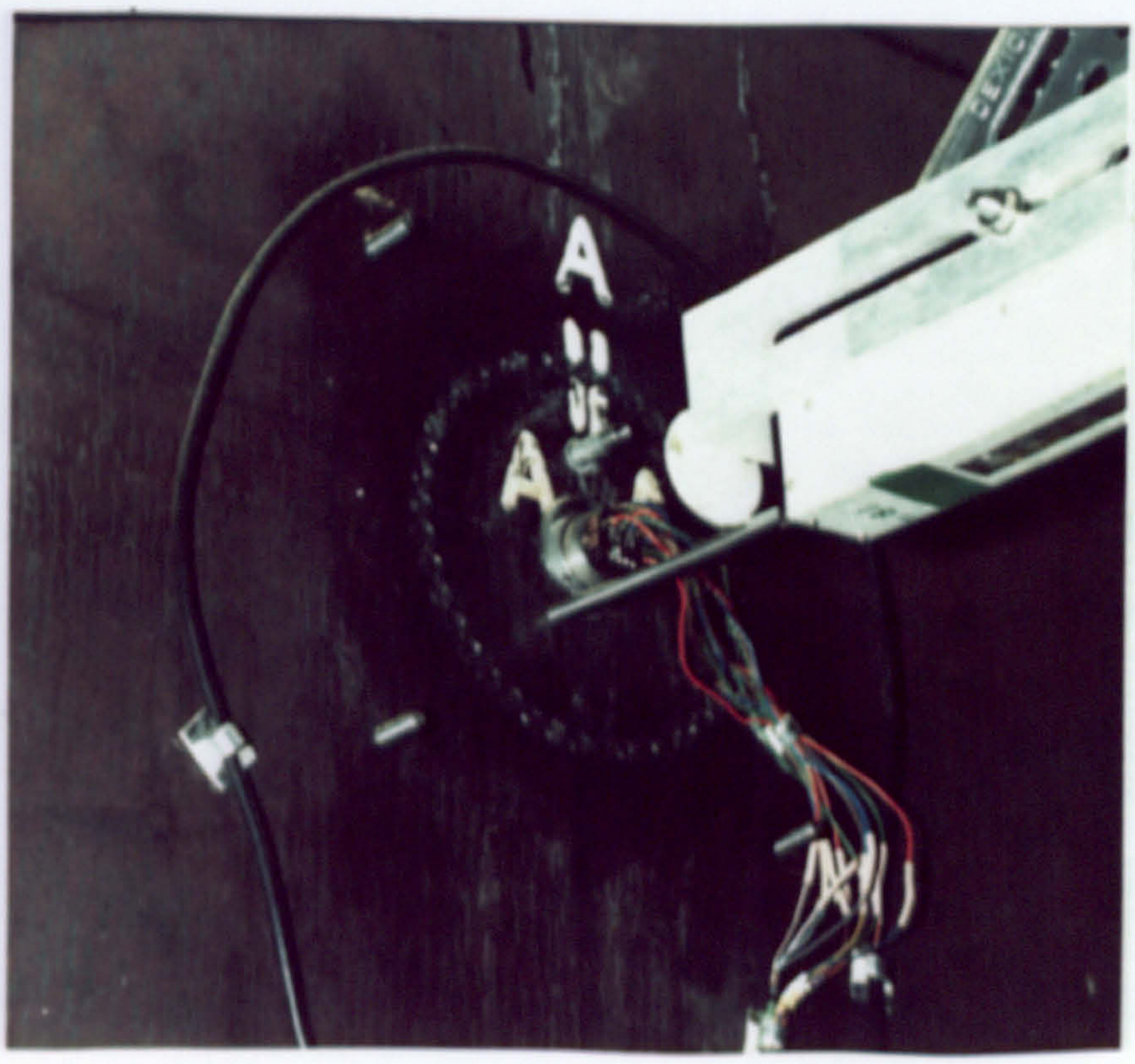

Figure 5.3 INSTALLED CELL (EXTERNAL FACE OF SILO WALL)

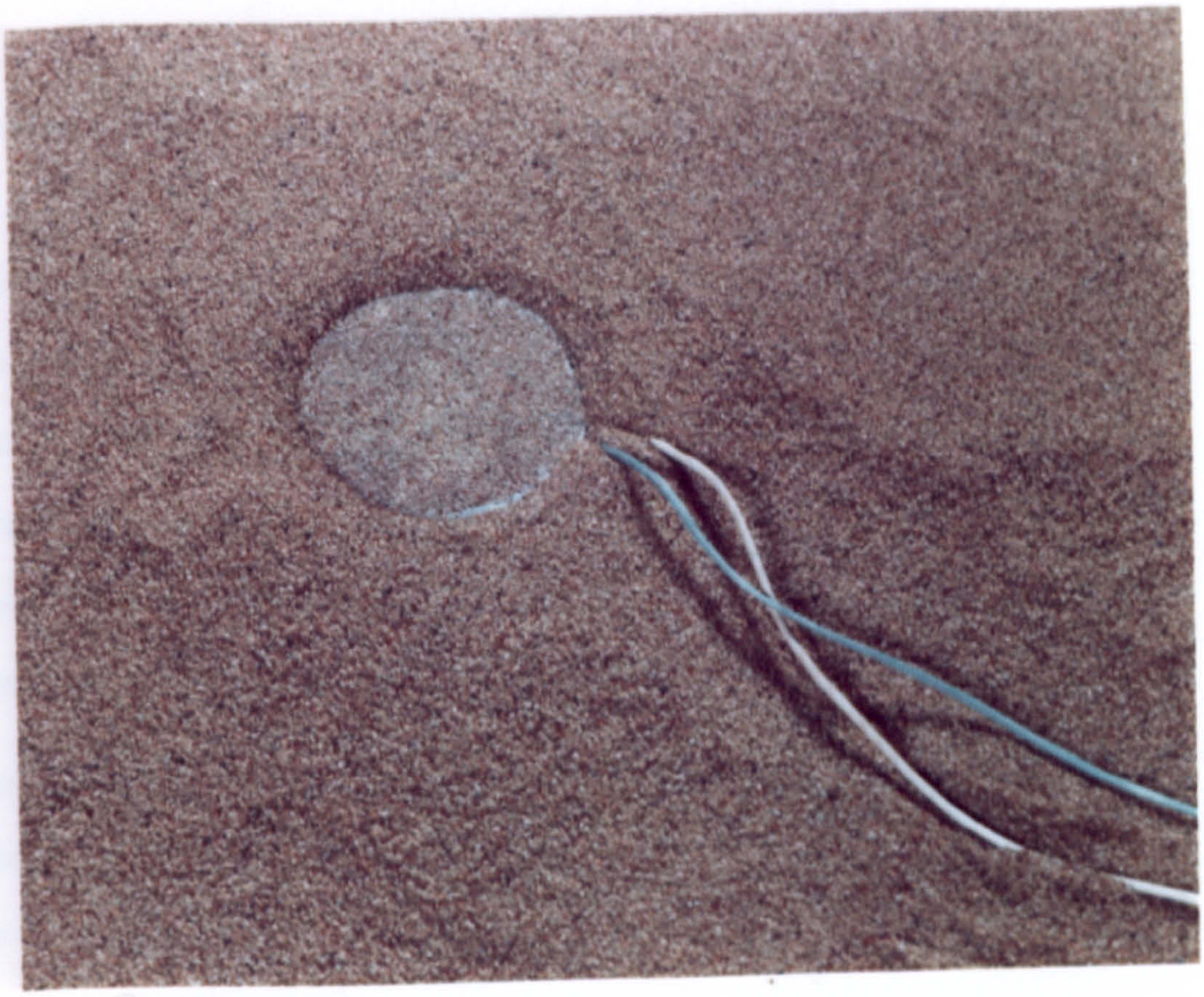

Figure 5.4(a) EMBEDDED CELL PLACED TO MEASURE VERTICAL PRESSURE

Figure 5.4(b) EMBEDDED CELL PLACED TO MEASURE HORIZONTAL PRESSURE

6. Preliminary Tests

The perspex silo shown in Figure 4.5 was used for preliminary tests to identify the probable pressure distribution and indicate the critical positions of pressure measurement in the large scale test model. The silo plan size was 500mm by 500mm. The vertical sided section was 500mm deep and the hopper was 500mm deep. The ratio of the silo wall length to pressure cell diameter was too small to enable an accurate plot of the pressure profile over the wall or across any horizontal section. Therefore, the model only permitted observation of general trends in the pressure distribution.

Pressure normal to the silo walls was measured at the positions shown in Figure 6.1. The silo was filled by distributed filling with grade 16/30 Leighton Buzzard sand. Figure 6.2 shows the mean pressures from five tests in which the cells were placed symmetrically about the vertical centreline at 365 mm. above the outlet. Figure 6.3 shows horizontal pressure at the wall of the bin, 650 mm. above the outlet. There is a sharp pressure drop from the stiff corners of the silo to the deformed central section of the wall. The ratio of horizontal to vertical pressure, K, at the centre of the wall appears to be less than K_a. This puzzling observation is discussed in Chapter 8.

The positions of measurement of vertical pressure are shown in Figure 6.1 and the mean pressures from five tests are shown in Figure 6.4. However, the tests indicated that the vertical pressure is a maximum somewhere between the corners and the centre of the silo and a minimum close to the centre of the deformed wall. It is difficult to draw conclusions about the distribution of vertical pressure since the variation between successive tests was as high as the variation between cells placed in different positions for a single test.

The tests showed that there can be a significant pressure gradient across a horizontal section. Pressure is lower at the centre of the silo wall than at the corners. It is also evident that vertical pressure is not constant over a horizontal cross section. The results show that a complete picture of the stress state of the stored material can only be achieved if pressure is measured at regular spacings throughout the silo.

Cells placed in the large scale model should be positioned at a reduced spacing in the vicinity of the corners to ensure that an accurate profile of the pressure gradient is obtained.

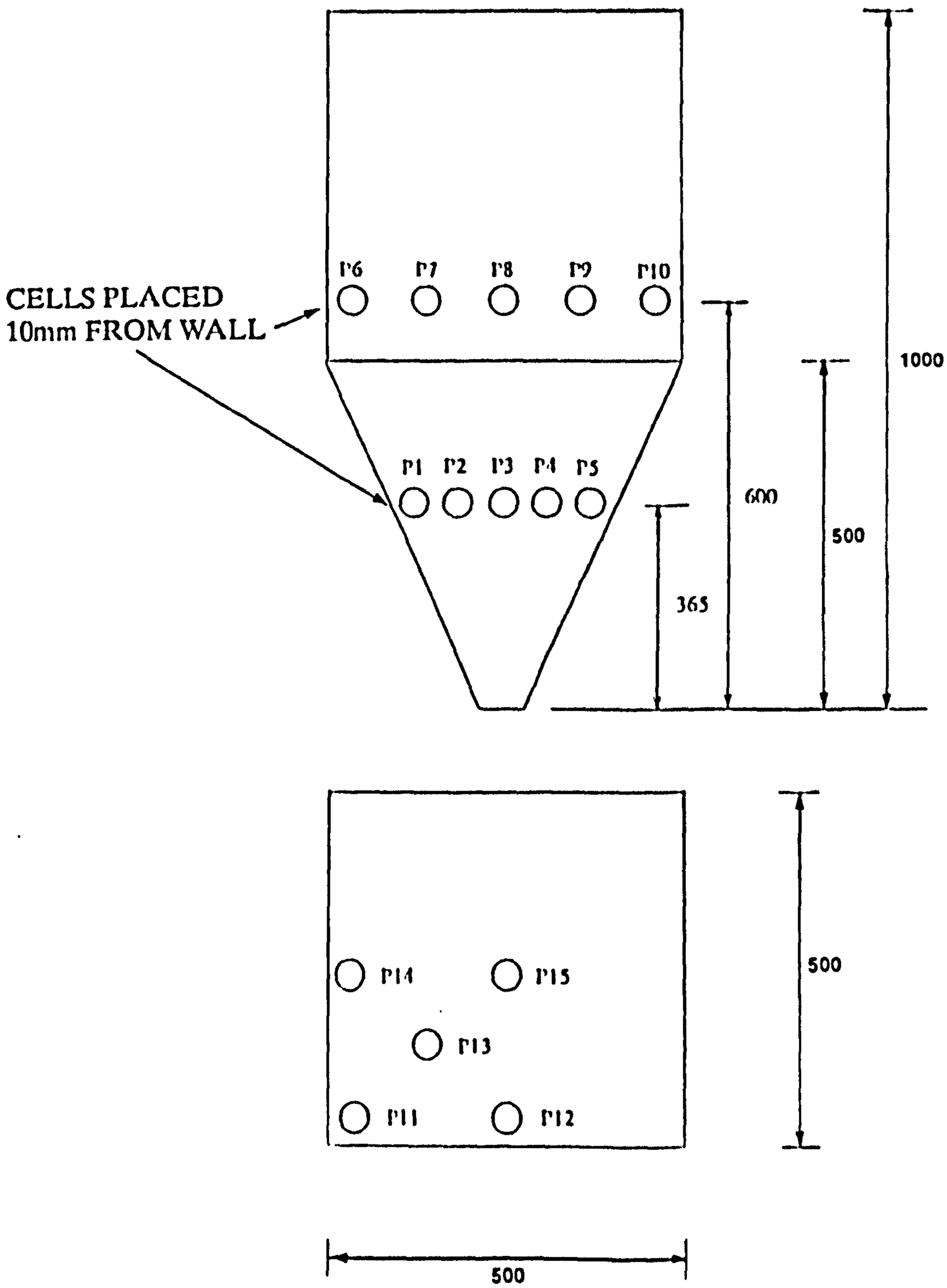

Figure 6.1 POSITIONS OF EMBEDDED CELLS IN THE PERSPEX SILO

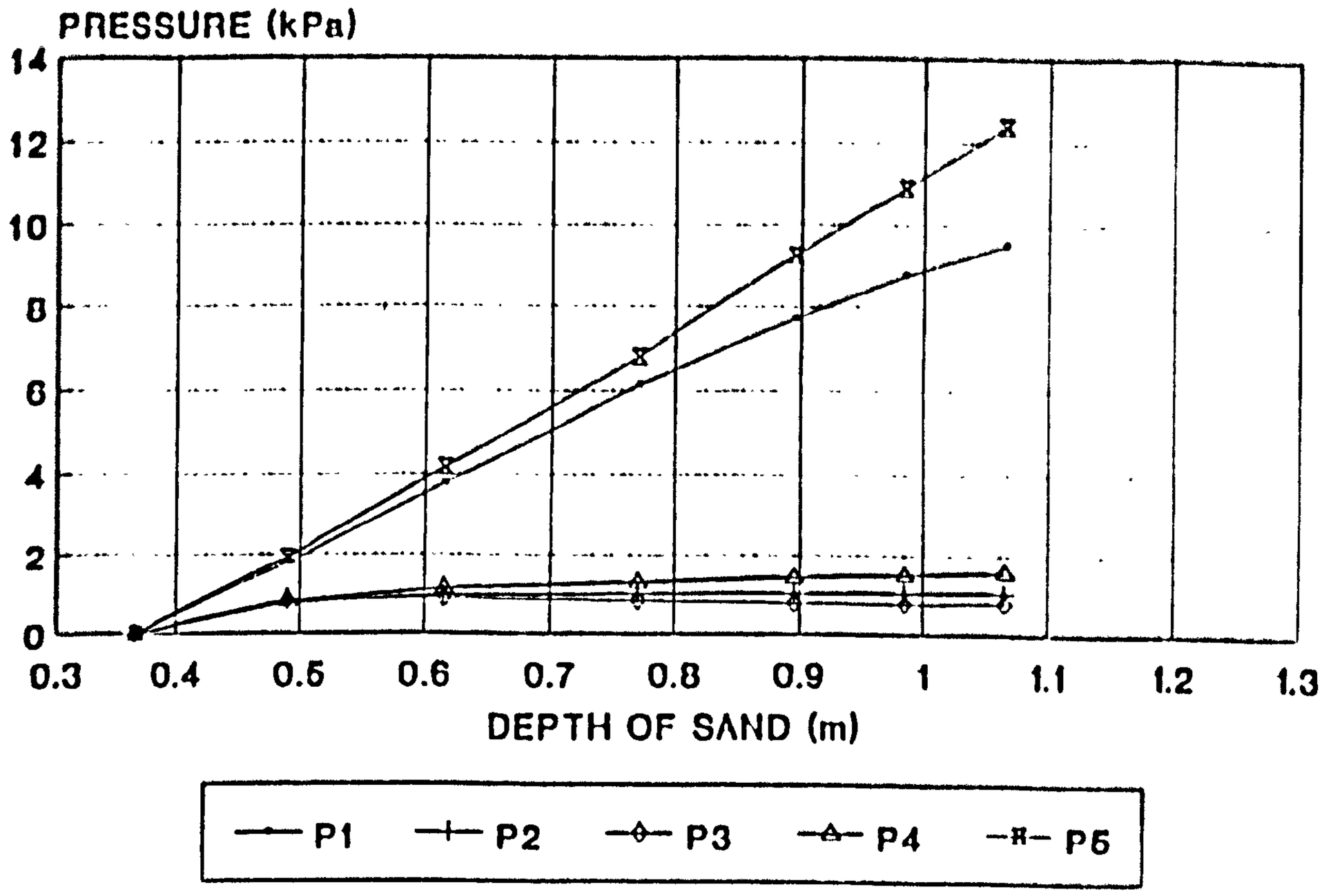

Figure 6.2 PRESSURE NORMAL TO THE HOPPER WALL

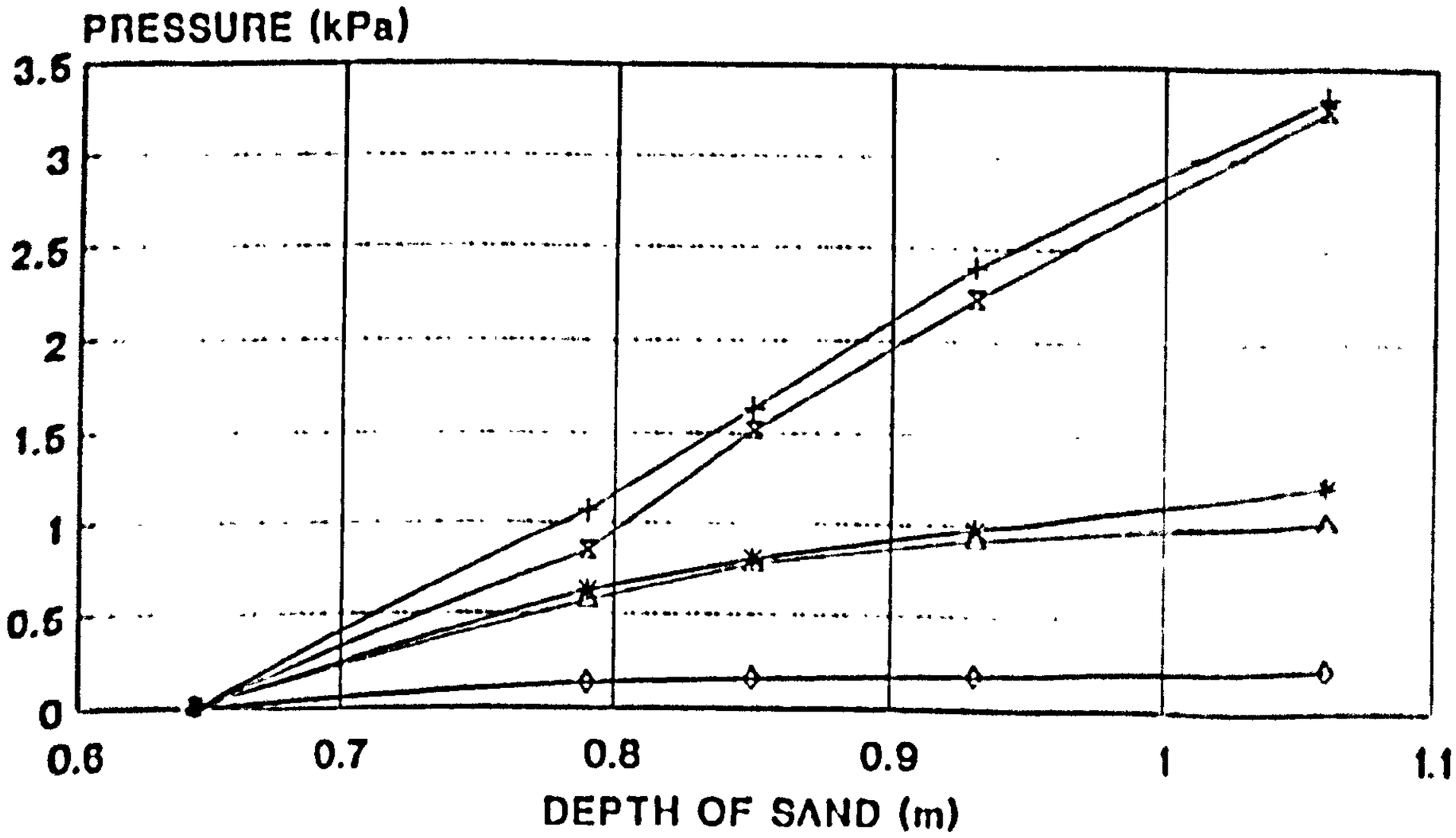

Figure 6.3 PRESSURE NORMAL TO THE BIN WALL

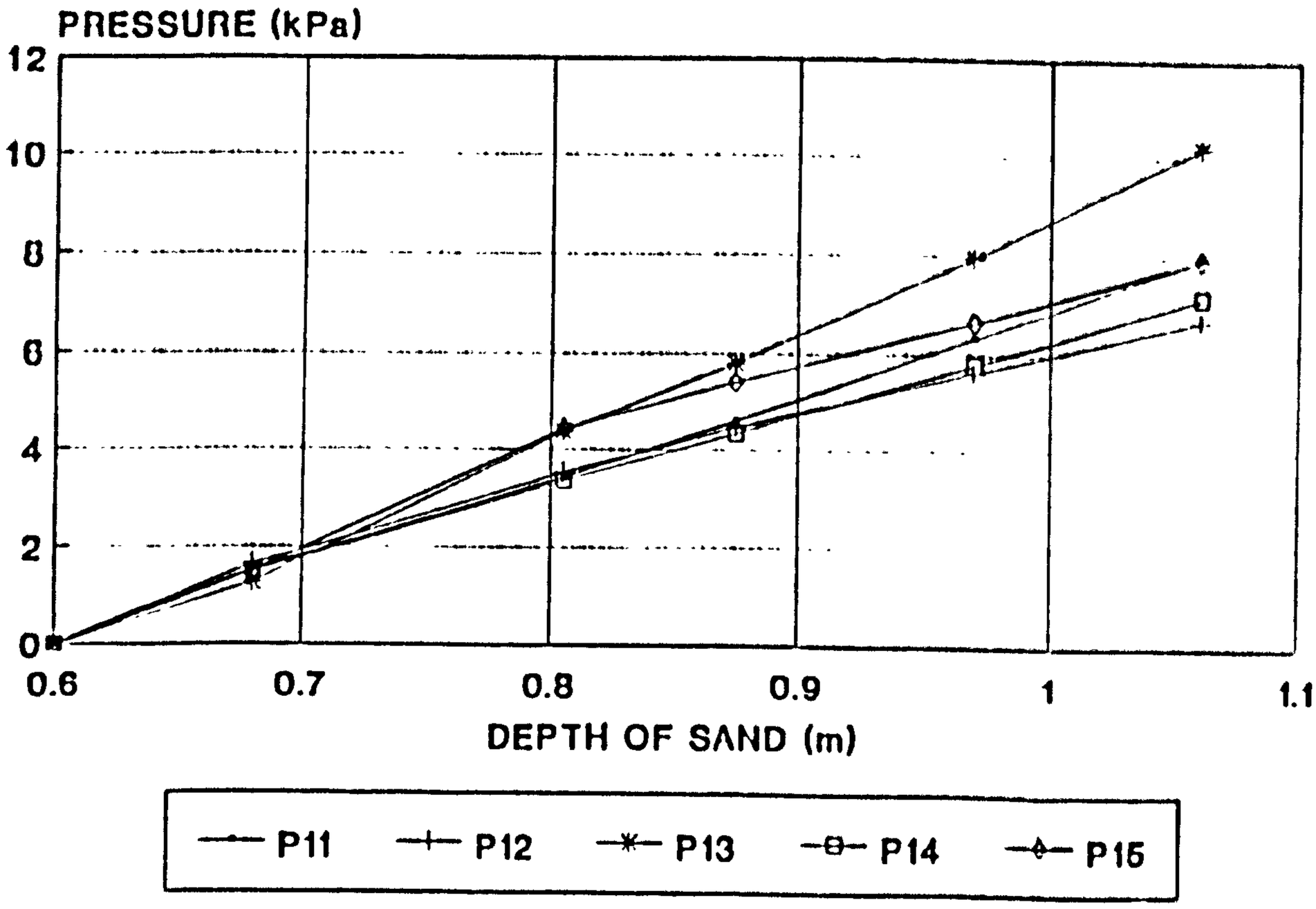

Figure 6.4 VERTICAL PRESSURE IN THE PERSPEX MODEL

7. Test Procedure

The large scale silo model was filled in height intervals of 250 mm. The discharge holes in the filler box were blocked whilst the box was filled from the bucket elevator. The surface of sand in the filler box was levelled carefully with a shovel. It was important that the level of sand in the filler box was controlled since this determined the level of sand in the silo. Deviations from a level surface in the silo were corrected from the filler box. The box was marked to indicate the level of sand required to fill the silo by 250mm. When the required level was reached, the bucket elevator was halted and the stops removed from the filler box holes rapidly and in a random order. On completion of discharge from the filler box measurements in the silo were taken. The stops were then replaced and the filler box refilled. The process was repeated until the silo was filled.

Measurements of pressure, deformation and strain were recorded at intervals of constant depth during filling and constant time during discharge. Embedded pressure cells were used to record the pressure at six positions within the sand during each test. Each test was repeated five times. Pressure cells were rotated between tests so that a cell did not occupy any position for more than one test. The installation and positioning of the embedded cells are described below.

The average time taken to fill the silo was three and a half hours. The time intervals between increments of load were kept constant except when the embedded cells were installed. Placement of the cells required the complete emptying of the filler box and its removal from over the top of the silo. This facilitated the lowering of a cage into the model from which the cells could be placed into the sand. Measurements were taken immediately after the completion of discharge from the filler box.

Discharge of the silo was continuous and took approximately thirty five minutes. Measurements were taken at intervals of one minute. Some tests were conducted with shorter intervals between measurements but rapid pressure fluctuations were not noticeable and so more frequent measurements were not necessary.

7.1. Embedded cell placement

Embedded cells were placed in many positions at different orientations to determine the stored material stress state throughout the silo. The actual positions varied from the intended positions because of difficulties in controlling the level of the stored material. The topography was measured on three separate occasions during a single test after completion of discharge from the filler box. A Dumpy level was used and the surface level was found to vary by up to plus or minus 75mm. from the intended level. Further inaccuracies were anticipated due to differences in the cell position in relation to the cell wall from the intended position. Five random checks of the cell position were carried out and the cells were found to be situated within 10mm. of the intended position. The tests to determine the pressure were repeated five times for each position of measurement and so any errors due to inaccurate positioning were reduced in the presentation of the mean results.

Cells were positioned to determine the distribution of pressure normal to the wall and the distribution of vertical and horizontal pressure over horizontal cross sections at five different depths. The measurements showed a steep pressure gradient across horizontal sections close to the wall and so at two levels, 750mm. above the transition and 500mm. above the outlet, the horizontal spacing between cells was reduced to investigate the rate of decrease in pressure from the corner. Cells near the corner were placed so that the cell face was approximately 10 mm. from one wall and the edge was approximately 10mm. from the corner.

Cells placed to measure pressure normal to the wall were no further than 25mm. from the wall. A gap was always left between the cell and the wall to ensure that the cell was completely surrounded by sand. Bransby [112] showed that any difference between the pressure at 25mm. from the wall and the pressure at the wall is negligible.

8. Presentation and Discussion of the Test Results

In Chapter 5 it was concluded that reasonable results from the pressure cells are only possible if they are the mean of a large sample of data. The results from the preliminary tests described in Chapters 5 and 6 were studied and it was concluded that five separate tests would be sufficient to ensure the accuracy of the mean data from each point of measurement. In total, data for the mean pressure and standard deviation were collected from eighty five positions. The test procedure and the laboratory air temperature and humidity were controlled throughout the test series.

The results of strain, deformation and pressure measurements are presented in two forms. The mean results are plotted against the depth (distance from the silo outlet to the surface of the stored material) during filling. In addition horizontal and vertical elevations show the mean values of all the measurements for a single load case. (Sand at one, two or three metres above the outlet.)

Measurements were recorded at intervals of one minute during discharge of each test. Photographs were taken from above the silo at the same intervals during one randomly selected test so that the instrumentation measurements could be related to the sand level.

8.1. Strain Results

A full set of strain readings from a single test are given in Appendix B. This section includes a discussion of only some of the results. It includes strain gauges placed to ensure that loads on the silo walls were symmetrical during each test and also a check on the consistency of strain readings over the entire test period.

8.1.1. Symmetry Check

The positions of strain measurement are shown in Figure 8.1. Figures 8.2 to 8.6 enable a comparison of the increase of strain during filling on the four walls of the silo at points $S4$, $S7$, $S12$, and $S15$. Each graph shows the strain/depth relationship for four walls at a single position. The walls are differentiated by their orientation. They are labelled North, South, West or East. Both horizontal and vertical strains are compared. The good correlation between the results for each position suggests that the magnitude and distribution of pressure is similar on every wall. Any deviation from the mean strain for the four walls was random (it was not repeatable between similar tests) and so it is possible that the pressure deviations are also random. The results indicate that the silo loading is symmetric and that measurements are only necessary on one half of one wall.

8.1.2. Consistency Between Successive Tests

A direct comparison of pressure measurements recorded at the beginning of the test series with those at the end is only possible if variation of the environmental conditions and the test procedure is minimised. To check that the test conditions remained constant for the entire test period, the horizontal and vertical strains were measured at positions $S4$, $S7$, $S12$, $S15$, $S16$ and $S20$ during filling. The results of every fifteenth test are shown in Figures 8.7 to 8.17 (only the results from gauges measuring significant strain are shown). The variation for the tests conducted over the four month period was not higher than that for tests conducted over a period of a week. It can therefore be concluded that the length of the test period has not had any detrimental effect on the quality of the measured data.

8.2. Wall Deformation

Wall deformation was measured at the positions shown in Figure 8.18. Figure 8.19a shows the mean deformation measured normal to the wall with the silo filled. The deformation at each of the points of measurement is plotted against the depth of stored material during filling in Figures 8.20 to 8.26. Positive deformation is outwards.

The gradients of the plots of wall deformation at points in the upper section of the bin (*D* 12, *D* 13, *D* 22, and *D* 23, Figures 8.23 and 8.26) are gentle in the initial stages of filling. After the surface of the sand has passed the level of the measurement points, the wall deforms at an increased rate. It was shown in Figure 2.3 that a wall deformation of 0.001 times the wall height at the top of the wall might be sufficient to mobilise the active state of pressure. Figure 8.19d shows a vertical section through the centre of the wall when the silo is full. It is apparent that the deformation in the bottom half of the bin is sufficient to mobilise the active state of pressure in the stored material away from the corners. Deformation near the top of the walls of the bin is less than that in the centre of the wall and so the distribution of pressure may not be linear with depth as assumed by Rankine. It is more likely that the pressure distribution down the centre of the wall will resemble that of a wall which deforms by linear translation, as illustrated in Figure 2.6.

Horizontal sections through the wall of the full silo are shown in Figures 8.19b and 8.19c. If the arching hypothesis discussed in Chapter 2 is correct, the variable wall deformation generates horizontal arches. It is evident that the deformation of the wall may be sufficient to mobilise the full shear strength of the stored material and maximise a horizontal redistribution of pressure from the centre of the wall to the corners.

Figures 8.20 and 8.21 show the increase of wall deformation at selected points in the hopper during filling. It is evident that the ring beam at the hopper/bin transition limits deformation of the upper boundary of the hopper wall. This probably prevents the stored material in the upper half of the hopper attaining the full plastic state. Figure 8.19d shows a vertical section through the hopper wall. The

deformed profile is similar to the anchored sheet pile wall shown in Figure 2.8. It suggests that a vertical arch might form behind the hopper in the manner described in Chapter 2.

Horizontal deformation of the corners is partly due to in-plane stretching of the walls (membrane action). However, the deformation measured at points 'D16' and 'D20' cannot be entirely attributed to in-plane strain. The transducer was positioned 50mm. from the corner and so some bending deformation is included. Figure 8.19c shows plots of wall deformation over a horizontal section. If the curve representing wall deformation when the silo is full is continued to the corner, the displacement at the corner can be estimated; it is 0.21mm. This is still too great to be entirely attributed to in-plane strain of the adjacent wall and so there is possibly some error of the displacement measurements. This error may be due to rigid body movement of the silo or movement of the transducer support frame. The accuracy of all the displacement data was checked and the error was found to be negligible at all the measurement points except those in the corners. The accuracy check is discussed in Chapter 9.

8.3. Pressure Measurement - Wall Cells

8.3.1. Consistency of results

Although a change in the wall pressure distribution from one test to the next affects the wall stresses, it is not possible to monitor the consistency of the pressure distribution from the strain gauge results. This is because the wall stresses and hence strain gauge readings may not be sensitive to quite large changes in the pressure distribution near the corners. Therefore, the consistency of the wall pressures between tests was established from the wall cells.

Pressure measurements were recorded by the wall cells for every test. The positions of measurement are shown in Figure 8.27. The pressures measured normal to the wall during filling for the first twenty tests are shown in Figures 8.28 to 8.31. The standard deviation and mean for each cell at three metres of sand are presented in Table 8.1.

Position	Mean	S.D.
A	6.55	1.61
B	4.37	0.70
C	9.66	0.89
D	1.28	0.43

TABLE 8.1 - Mean Pressures (kPa), Standard Deviations and Coefficients of Variation for the Wall Cells with the Silo Full

The results are widely scattered. This is particularly evident from cells 'A' and 'D' which were fixed into the walls at points of maximum wall deformation. There was no evidence of long term trends and so the scatter is attributable to differences between individual tests. Some error is due to differences in the surface level of the stored material. At great depths this will lead to only a small error and so a

more probable cause of variation was the different particle structure created after discharge from the filler box. When the pressure recorded by a cell was in excess of the mean at low levels of sand, the cell continued to record pressures higher than the mean and with a similar error for the entire test. This suggests that pressure variation is due to the manner of particle packing. The sand is not isotropic and homogeneous and so the initial stress field is influenced by the lodgement of particles after fall from the filler box. It is different for each test. The variation from the mean will be constant for a test because the initial stress field influences the stress field throughout the test. The differences did not show up in the strain gauge readings because the pressures at points 'A' and 'D' were very small in comparison to the pressures at the same level near to the corners. Because the pressure normal to the wall at the centre of the wall span is relatively small, a significant difference in pressure at the centre of the wall has only a negligible effect upon the wall stresses.

8.3.2. Pressure Distribution

There are too few wall cells to draw detailed conclusions about the pressure distribution but they do give some insight into the effect of wall flexibility on wall pressure. A comparison of Figures 8.19 and 8.28 to 8.31 shows that low pressures at points 'A' and 'D' correspond to areas of large wall deformation. The lowest wall deformation transpires at point 'C' and this coincides with the highest pressure. At point 'A' the increase in pressure diminishes with increasing depth of sand in the silo. The same reduction in the rate of increase of pressure during filling is apparent at point 'B', but to a lesser extent. At point 'C' the rate of increase of pressure during filling remains virtually constant.

The transfer of pressure to the wall via friction slows the rate of increase of pressure during filling but it does not account for all of the reduction at cells 'A' and 'D'. The sharp decline in the increase in pressure at areas of high wall deformation and the linearity of the pressure/depth curve at cell 'C' suggests that there is a transfer of pressure from the deformed centre of the wall to the stiff corners.

The pressure at point 'B' is low in comparison to that at point 'C' and yet the wall deformation is also small. This is due to a seperate arching phenomenon which will be called ring beam arching and is discussed in detail below.

8.3.3. Coefficient of wall friction

The shear stress at the interface of the stored material and silo wall was measured by each of the wall cells (in the manner described in Section 5.3.3.1.) and divided by the normal pressure results to determine the coefficient of wall friction during filling. The friction coefficient for Leighton Buzzard sand sliding on steel plate was found in the Direct Shear Box. Since there is some uncertainty as to the accuracy of the shear box tests for the calculation of an in-situ angle of friction, it was necessary to ascertain the value in the silo. Measurements were taken to establish the fully mobilised coefficient of friction and also the head of sand required to mobilise the full coefficient.

The face of the wall cells was machined during the cell manufacture. An accurate measurement of wall friction is only possible if the surface roughness of the face of the cell is the same as the roughness of the silo wall. The wall roughness was measured using a microscope and a paint was selected to give the cell face the same surface texture.

The Mean and Standard Deviation for the first twenty tests are presented in Table 8.1 for each of the cells with the silo full. The Standard Deviation for the measurements from cell 'A' was larger than that for the others cells. The friction pressure measured by cell 'A' was liable to extensive drift (probably due to cell error) and so the results were treated with scepticism. The results of Cells 'B' and 'C' were sensitive to drift for the first half metre of filling, after which they stabilised at a constant coefficient for the remainder of the test. It is difficult to determine the exact head of stored material required to mobilise the full coefficient of friction due to the sensitivity of the cells caused by drift in the early stages of loading but it can be concluded that it is less than 0.5m.

The coefficient of friction for cell 'D' is considerably lower than for the other cells. Vertical pressure at the wall is very low at this point and so it is possible that the stored material consolidation is not sufficient to mobilise the full coefficient of friction.

Since a stable coefficient of friction was achieved at cells 'B' and 'C' for every test it is reasonable to take the average of the results for these two cells as representative of the fully mobilised coefficient of friction throughout the silo. The average value is 0.708 whereas the comparative value obtained from the shear box tests was 0.65. The inaccuracy of the shear box results has been discussed above. For all further calculations, a value of 0.7 has been used.

8.4. Pressure Measurements - Embedded Cells

Tests were conducted to investigate the magnitude and distribution of horizontal and vertical pressure in the bin and hopper and pressure normal to the inclined wall of the hopper. The different orientations of the cells are shown in Figure 8.32a. The first tests determined the pressure distribution normal to the bin wall (Position 1) and normal to the hopper wall (Position 6). These were followed by measurements of horizontal pressure parallel to the wall (Position 2), horizontal pressure at forty five degrees to the wall (Position 3) and vertical pressure adjacent to the wall (Position 4). The determination of the total stress state required inclined pressure measurements in two directions but this was not possible due to the cell calibration problems discussed in Chapter 5.

The cell positions and directions of measurement are shown in Figure 8.32b. Each measurement point is labelled with two letters and a number to indicate its position within the silo and the direction of measurement. A key is given in Table 8.2.

Symbol	Description
	Symbols referring to the location of the cell
W I	Cell place adjacent to the wall Cell placed internally (away from the wall)
	Symbols referring to the direction of measurement
N P H V	Pressure measured normal to the wall Pressure measured parallel to the wall Horizontal pressure measurement (direction usually indicated on diagram) Vertical pressure measurement

TABLE 8.2 - Key to embedded cell positions

An example of the data recorded from a single position is given in Figure 8.33. It shows the increase in pressure during filling for five tests and the mean for position *WN*3. For simplicity of presentation, the remaining data is presented in a condensed form. Only the mean pressure distribution for five tests is given for each position of measurement. Tables 8.3 to 8.7 present the mean and standard deviations for each position when the silo is full.

Position	Mean	S.D.	C.o.V.	Position	Mean	S.D.	C.o.V.
WN1	28.2	2.05	0.07	WN2	8.9	2.2	0.25
WN3	3.7	.41	0.11	WN4	14.4	3.2	0.22
WN5	25.7	0.8	0.03	WN6	49.5	5.2	0.11
WN7	37.9	4.8	0.13	WN8	20.9	4.4	0.21
WN9	9.4	1.4	0.15	WN10	10.3	0.8	0.07
WN11	15.0	0.7	0.04	WN12	22.0	2.4	1.09
WN13	17.8	1.9	0.11	WN14	36.7	2.1	0.06
WN15	6.6	0.9	0.14	WN16	2.4	0.5	0.21
WN17	1.2	0.5	0.42	WN18	1.2	0.5	0.43
WN19	7.4	1.0	0.14	WN20	2.3	0.4	0.17
WN21	2.4	0.5	0.21	WN22	1.7	0.7	0.41
WN23	8.0	0.4	0.05	WN24	20.8	0.9	0.04
WN25	20.4	2.1	0.1	WN26	6.1	1.4	0.23
WN27	11.7			WN28	4.2	0.3	0.07
WN29	7.1	0.6	0.08	WN30	8.1	1.1	0.14

TABLE 8.3 - Mean Pressures (kPa), Standard Deviations (kPa) and Coefficient of Variation for Embedded Cells placed to measure pressure normal to the wall with the silo full

Position	Mean	S.D.	C.o.V.	Position	Mean	S.D.	C.o.V.
IH1	5.3	0.5	0.09	IH2	6.4	0.6	0.09
IH3	12.0	0.9	0.07	IH4	11.9	1.4	0.12
IH5	10.9	0.8	0.07	IH6	11.3	1.2	0.11
IH7	11.1	1.6	0.15	IH8	8.6	1.1	0.13
IH9	5.5	0.9	0.17	IH10	5.2	1.2	0.23
IH11	7.7	0.6	0.08	IH12	7.1	1.4	0.19

TABLE 8.4 - Mean Pressures (kPa), Standard Deviations (kPa) and Coefficient of Variation for Embedded Cells placed to measure horizontal pressure away from the wall with the silo full

Position	Mean	S.D.	C.o.V.	Position	Mean	S.D.	C.o.V.
WP1	6.1	0.9	0.15	WP2	13.4	1.6	0.12
WP3	10.5	2.1	0.2	WP4	9.4	1.9	0.2
WP5	3.7	0.5	0.14	WP6	5.2	0.7	0.14
WP7	8.6	0.9	0.10	WP8	9.8	3.1	0.32

TABLE 8.5 - Mean Pressures (kPa), Standard Deviations (kPa) and Coefficient of Variation for Embedded Cells placed to measure horizontal pressure parallel to the wall with the silo full

Position	Mean	S.D.	C.o.V.	Position	Mean	S.D.	C.o.V.
IH1	7.9	0.9	0.12	IH2	7.1	0.4	0.06
IH3	9.0	0.7	0.07	IH4	2.5	1.1	0.44
IH5	2.7	0.8	0.29	IH6	21.7	1.8	0.08

TABLE 8.6 - Mean Pressures (kPa), Standard Deviations (kPa) and Coefficient of Variation for Embedded Cells placed to measure horizontal pressure at 45° to the wall with the silo full

Position	Mean	S.D.	C.o.V.	Position	Mean	S.D.	C.o.V.
IV1	55.2	4.9	0.09	WV2	38.4	5.1	0.13
WV3	43.9	5.1	0.12	IV4	47.9	3.8	0.08
WV5	19.5	4.3	0.22	WV6	43.9	4.9	0.11
IV7	38.3	10.8	0.28	WV8	11.3	2.6	0.23
WV9	20.8	5.2	0.25	IV10	36.4	4.7	0.13
IV11	29.8	6.7	0.22	IV12	33.6	2.0	0.06
WV13	31.2	4.4	0.14	WV14	36.5	3.4	0.09
WV15	12.6	2.0	0.16	IV16	21.2	4.1	0.19
IV17	27.9	5.2	0.19	IV18	33.9	2.7	0.08
WV19	16.0	4.0	0.25	WV20	17.2	4.6	0.27
WV21	28.2	3.4	0.12				

TABLE 8.7 - Mean Pressures (kPa), Standard Deviations (kPa) and Coefficient of Variation for Embedded Cells placed to measure vertical pressure with the silo full

The actual pressures were calculated using equation 5.1 and with constants A = 0.83 and B = 0 to compensate for placement errors.

8.4.1. Pressures Measured Normal to the Wall - Positions 1 and 6

The computed pressures normal to the wall when the silo is filled to 1.0, 2.0 and 3.0 metres above the outlet are presented in Figures 8.34 to 8.36. The mean pressures from five tests are shown for each position of measurement in Figures 8.39 to 8.46. A comparison of the wall deflections (Figure 8.19) and the wall pressures (Figure 8.36) shows that the maximum wall pressures coincide with areas of low wall deformation at the corners, the outlet and the ring beam and low pressures coincide with areas of high deformation at the wall centres. The increase in pressure during filling at points across a horizontal plane at 1.6 metres above the outlet (points *WN*24, *WN*30, *WN*29, *WN*28, *WN*20) are plotted in Figures 8.44 to 8.46. A horizontal section of the pressure distribution at the silo wall is shown in Figure 8.38. It shows the pressure distributions for the silo filled to 2.0 and 3.0 metres above the outlet. The distribution for the silo filled to 2.0 metres above the outlet shows only a small variation of pressure across the horizontal section. When the surface level has reached 3.0 metres above the outlet there is a steep pressure gradient across the wall. At 3.0m of sand and 40mm from the corner, the pressure is 17kPa. At 150mm from the corner it has decreased to 7kPa. It continues to decrease to a minimum of 2kPa at the centre line of the wall.

A similar pressure reduction is apparent in the hopper. Figure 8.37 is a horizontal section of pressure normal to the wall at 500mm above the hopper outlet. The pressure is shown for the silo filled to 1.0, 2.0 and 3.0 metres above the outlet. The decrease from the corner is not as sharp as in the bin due to the higher stiffness of the hopper wall.

The pressures at the points *WN*3, *WN*16, *WN*17, *WN*18' along a vertical centreline of the bin and hopper walls are close to their maximum values at 0.5m. head of sand above the gauge positions. A comparison of pressure at these positions and pressure at points *WN*16, *WN*20, *WN*29, *WN*30 and *WN*24 on a horizontal plane shows that the head of sand required to achieve the maximum pressure may increase with distance from the vertical centreline of the wall. In the corners of the silo at points *WN*6, *WN*7, *WN*8, *WN*24, *WN*25 and *WN*26, after an initial non-linear response, the pressure increases almost linearly with depth for the duration of filling.

Some pressure difference between the corners and the centre of the wall is because the sand in the non-deforming corners is in an elastic at-rest state of pressure and sand in the centre of the wall is in a plastic active state of pressure. The steep pressure gradient shown in Figures 8.37 and 8.38 cannot be attributed entirely to the difference between elastic and plastic stress states. It is likely that the wall deformation mobilises shear stresses in the stored material and generates a pressure transfer (horizontal arch) from the centre of the wall to the corners. The theory of arching was described in Chapter 2 and the arching behind the model silo wall is described in detail in Chapter 11.

An indication of the depth of stored material required to induce sufficient wall deformation and shear strength within the stored material to mobilise the horizontal arch redistribution can be gained from Figures 8.39to 8.42. At a horizontal section 500 mm. above the outlet and with the sand level at 750 mm. above the outlet the pressure at the corner of the silo is 4.0 kPa. and the pressure in the centre is 2.4 kPa. The variation can be attributed to a combination of the difference between the elastic and plastic stress states existing at the corners and centre of the wall respectively, in addition to an arching pressure redistribution. As the sand level increases, the pressure in the centre of the wall increases slowly at a nearly constant rate to a maximum of 4.4 kPa at the end of filling. Meanwhile the pressure at the corner increases rapidly and nearly linearly throughout the filling period to a final value of 45.5 kPa. The significant change in the gradient of the pressure increase in the centre of the wall (when the sand level is 250mm. above the point of measurement) marks the point where the arching phenomenon starts to dominate the pressure distribution.

The steep pressure gradient across the wall was observed at every level of measurement other than at the ring beam between the hopper and bin. Figure 8.36 shows that the pressure at this level is constant over most of the wall but there is a sharp pressure drop in the corner and an increase close to the corner. There are at least two phenomena that could lead to this pressure drop and they are discussed in turn.

1. A local arch forms within the stored material over the corner. In section 8.2 it was stated that the ring beam deforms inwards during filling. Deformation is a minimum at the corners and increases towards the centre of the ring beam. The inwards deformation of two perpendicular walls and the resulting compression of the stored material may lead to an arch or 'bridge' formation of dense material over the corner. This arch will be called the ring beam arch and its effect is to relieve pressure from the corner and increase it at some distance towards the centre of the wall. This ring beam arch formation is described in detail in Chapter 11.

2. The pressure drop may be due the effect of a vertical arch in the hopper. The arch 'bridges' the centre of the wall and increases the pressure at the ring beam and at the outlet. The steep gradient of the pressure versus head of sand curve at points *WN* 1 and *WN* 5 (Figure 8.39) suggests that some pressure may be redistributed from the centre of the hopper wall to stiff parts above and below as well as to the edges of the wall. If this is the case it is probable that the corners of the silo at the ring beam level will be unaffected by the pressure increase at the ring beam level due to the geometry of the hopper wall. An arch will have most affect over its shortest span and this is from the hopper outlet to the centre of the ring beam or from the corners of the hopper wall between the outlet and the ring beam. The effect is progressively less from the centre of the ring beam to the corners of the ring beam.

8.4.2. Other Horizontal Pressure Measurements

8.4.2.1. Horizontal pressures parallel and at 45° to the wall - Positions 2 and 3

The positions of measurement of pressure parallel to the wall (Position 2, Figure 32a) are shown in Figure 8.51 and the positions of measurement at 45° to the wall (Position 3, Figure 32a) are shown in Figure 8.56. The following discussion refers to principal stress directions and wall slope close to the wall and on a horizontal plane. Because of symmetry shear stress at the centre of the wall must be zero. The minimum principal stress aligns with the direction of maximum wall deformation and is normal to the wall and hence the intermediate principal stress is parallel to the wall. This is confirmed by the pressure measurements. The results of cells placed to measure horizontal pressure parallel to the wall at different levels are shown in Figures 8.49 to 8.51. In the centre of the wall (*WP* 1 and *WP* 5), the pressure parallel to the wall is almost double the pressure normal to the wall. Figure 8.57 shows the results from cells placed at 45° to the wall. At position *WH* 4, the pressure is equal to half the sum of the pressures normal to and parallel to the wall. (*WP* 3 and *WN* 16)

Between the corner and centre of the wall (positions *WP* 7 and *WP* 8), the parallel pressure approaches that of pressure normal to the wall. At these points the wall slope produces shear stresses in the sand and the major principal stress direction rotates towards a plane at 45° to the wall. At the corner both the wall slope and the wall deformation are zero and the stored material is restrained in all horizontal directions. The horizontal pressure is the same in all directions.

Pressure parallel to the wall is less than normal pressure at the level of the bin and hopper transition. Wall deformation at the transition is very small and so it was expected that the pressure would be similar in every direction. The difference may be due to the position of the cells. Cells placed to measure normal pressure were situated below the ring beam whereas cells placed to measure pressure parallel to the wall were positioned above the ring beam.

8.4.2.2. Horizontal pressure away from the wall - Positions 1 and 3

The positions of pressure measurement away from the walls are shown in Figures 8.48 and 8.56. Horizontal pressure was measured at four points at three levels away from the wall of the silo (*III*1 to *III*12). Figure 8.51 shows that pressure rises steadily from a minimum at the centre of the wall to a maximum in the centre of the silo. Because of symmetry, pressure normal to perpendicular walls along the diagonals should be equal and so it was measured normal to one wall only (*III*2, *III*6, *III*10).

A comparison of the results for pressure measured normal and parallel to the wall (Figure 8.51) with those for pressure at 45° to the wall (Figure 8.57) allows some conclusions to be made about the stress state on a horizontal plane through the stored material. The directions of the minor principal stresses at points along the centrelines of the silo (positions *III*1, *III*3, *III*9, *III*11) only deviates a little from the normal to the wall. This is because the wall slope at the centre of the wall is zero and so the shear stress on planes perpendicular to the wall in the stored material behind the centre of the wall are also zero. Some rotation of the direction of the principal stresses may have occured due to the influence of the deformation of the two walls adjoining the wall being considered. The principal stresses at cells *III*2 and *III*10 are at an angle of 45° to the wall. The stress state at these points is influenced in equal amounts by the deformation of two walls.

At the transition, there was only a negligible variation of horizontal pressure within the stored material. This was expected because the wall deformation is very small due to the influence of the stiff ring beam and so the stored material is close to the elastic at-rest state of equilibrium. Shear stresses on a horizontal plane are very small as is the two dimension Mohr's circle representing stresses on the plane.

8.4.2.3. Horizontal pressure next to the hopper wall - Position 5

Pressure cells were placed in the positions shown in Figure 8.59 They were initially placed to measure horizontal pressure adjacent to the hopper wall to determine the direction and magnitude of the major and minor principal stresses. The calibration factors 'A' and 'B' from equation 5.1 were not determined for the embedded cells placed to measure pressure normal to the hopper wall, and so the principal stresses cannot be calculated.

The horizontal pressure data are useful for confirmation of the conclusions reached from the cells placed to measure pressure normal to the wall. Figure 8.60 shows that there is a considerable difference in pressure between points *WH*4 at the centre of the transition and *WH*1 at the centre of the hopper wall when the silo is full and hence confirms the inclined cell data.

8.5. Vertical pressure - Position 4

Vertical pressure was measured at six levels in the silo at the positions shown in Figure 8.61. A typical example of the measurements recorded at a single position (*IV*11) is shown in Figure 8.62. There appears to be one rogue set of data which is probably due to the cell placement technique. It is possible that the rogue data show an actual deviation in pressure and so it was incorporated in the calculations of the mean pressure and standard deviation.

The distribution of vertical pressure on a horizontal section is shown for different depths in Figures 8.63 to 8.65. The vertical pressure close to the wall follows a similar trend to the horizontal pressure. It is maximum in the vicinity of stiff areas such as the corners, and minimum near the points of maximum wall deformation. Figures 8.66 to 8.72 show the mean of the increase in pressure for five tests during filling. Pressure at points *WV*2, *WV*5, *WV*8, *WV*19 at the centre of the bin and hopper walls continues to increase throughout the test but at a somewhat lower rate than pressure at points *WV*3,

*WV*6, *WV*9 and *WV*21 at the corners. Some reduction in the rate of pressure increase during filling was expected due to the effect of wall friction but this would be constant across the wall. It is evident therefore, that vertical pressure in the vicinity of the wall is re-distributed and is probably influenced by horizontal arching. (Both horizontal and vertical pressure on a horizontal plane are redistributed from the centre of the wall towards the corners.) Point *WV*20, which is situated between the bin wall centre and corner, does not feel a significantly higher pressure than point *WV*19 in the centre of the wall. This indicates that the arch is effective over at least half the wall span.

An indication of the depth of stored material required to mobilise a redistribution of vertical pressure is given in Figures 8.63 to 8.65. Figure 8.63 shows pressure at different levels in the hopper when the surface of the sand is at 1.0m above the outlet. There is little evidence of arching at low depths. Vertical pressure is nearly constant at every level except in the bottom of the hopper. At 250mm. above the outlet some variation is noticeable. Figure 8.67 shows the increase of vertical pressure with filling for point *WV*5 in the centre of the hopper wall. The gradient is nearly constant for the first 750mm. of filling but starts to decrease significantly from this point throughout the filling period.

Pressure away from the wall increases with increasing distance from the wall. Figure 8.65 shows that a peak pressure occurs approximately half way between the wall and the corner of the bin. Pressure in the centre of the silo is greater than the pressure in the vicinity of the centre of the wall. In the hopper, vertical pressure was only measured at three points at each level. Measurements were not conducted to determine the pressure between the hopper wall and the centre of the silo. It may rise from a minimum at the centre of the wall to a peak at some distance between the centre of the wall and the centre of the silo or it may simply rise to a peak at the centre.

Vertical pressure was measured at the bottom of the hopper and found to be significantly less than the vertical pressure 200mm. above. This suggests that there is a Janssen arch in the lower half of the hopper. Additional vertical pressure is carried by wall friction and vertical pressure near the outlet is reduced.

With the exception of the corners, there is only a little variation in vertical pressure at the level of the ring beam. In the vicinity of the corners pressure drops sharply in line with the horizontal pressure measurements. A possible explanation was given in Section 8.4.1. when it was suggested that a local arch (ring beam arch) forms over the corner relieving pressure from the corner and increasing it towards the centre of the wall.

8.6. Discharge results

8.6.1. Flow channel size

Observation of the stored material from above the silo suggested that the flow mode was 'funnel flow' (Figure 8.73). Pressure cells were placed in the positions shown in Figure 8.61. Cells placed in the centre of the silo fell into the flow channel at the start of discharge. Cells placed 500mm away from the centre, remained in place until the surface of the sand dropped to their level. This indicates that the flow channel was less than one metre wide throughout the silo.

8.6.2. Wall cell and deformation results

Figure 8.74a shows the wall cell measurements during discharge for a single test at points 'A' to 'D' (Figure 8.27). The results shown are from one typical test only. Readings were taken at intervals of one minute. Two other tests were conducted with readings at a shorter interval but none of the rapid fluctuations evident in the results of some other workers (discussed in Section 2.2.2.1) was noticed.

The pressure at cell 'A' rose 2kPa during the first thirty minutes of discharge. This was followed by a steep rise over the next three minutes to a maximum pressure which coincided with a sand level equal

to 1.125m. above the level of the cell. It was fifty per cent higher than the maximum filling pressure. A rapid decrease was evident over the next four minutes and the pressure dropped almost linearly to zero. A similar phenomenon was seen at cell 'D'. The pressure started to increase when the sand level was at 0.6m. above the cell. It rose to approximately one hundred per cent above the maximum filling pressure at a level of 0.3m. above the cell. At cells 'B' and 'C', the pressure decreased steadily from the start of discharge until the sand reached a level of 0.6m. above the cell. This was followed by an increase until the sand was 0.3m. above the cell. The maximum pressure measured at cell 'B' during discharge was ten per cent higher than the maximum filling pressure whereas the maximum discharge pressure at cell 'C' was forty per cent less than the maximum filling pressure.

The pressure fluctuations described above are attributed to wall flexibility. They may be caused by two separate phenomena.

1. A partial break down of the arches formed during filling occurs during discharge. The consolidation pressure at any point in the stored material is probably reduced throughout the discharge period. A corresponding reduction in the shear strength may result in a breakdown of the horizontal arch. Pressure in the corner would decrease and pressure in the centre of the wall would increase as a result.

2. The rapid pressure rise in the latter stages of discharge is due to inward deformation of the wall. Figure 8.76 shows the wall deformation at position *D* 10 (Figure 8.18) during discharge. For the first fifteen minutes the wall deformation is less than 0.2mm. The rate of inwards deformation increases from this point and is nearly linear for ten minutes before the level of sand reaches the level of *D* 10. Comparison with the wall cell pressure measurements (Figure 8.73) shows that the sharp inwards deformation corresponds to the rapid pressure increase and suggests that the stored material moves towards a passive plastic stress state during discharge.

8.6.3. Embedded cells

Figure 8.74b shows the discharge pressures measured by the embedded cells placed in front of the wall cells. At point 'A', the pressure increases for the first thirty minutes of discharge. This is in agreement with the wall cell at point 'A'. However, the sharp increase in pressure measured by the wall cell shortly before the end of discharge was not recorded by the embedded cell. At point 'D' a small increase in pressure was measured just before the surface of the stored material passed the embedded cell. The increase was negligible in comparison with that measured by the wall cell at the same position. Pressure measured at points 'B' and 'C' decreased at a nearly constant rate until a period of between five and twelve minutes before the sand surface passed the cell level. From this point, the pressure remained constant until it dropped sharply to zero. The period of constant pressure coincided with the pressure increase measured by the wall cells at the same positions.

The results show that the embedded cells may exhibit the same pressure trends that were measured by the wall cells. However, the embedded cells placed a small distance from the wall are not sensitive to the sharp pressure increases measured by the wall cells during discharge. Reasons for the difference are unknown.

8.6.4. Vertical pressure

Figure 8.75 shows the vertical pressure at different points in the silo. The positions of measurement are shown in Figure 8.61. Vertical pressure in the centre of the silo (*IV*4) falls to zero immediately after the start of discharge. Away from the centre, the pressure cells measured a small increase, possibly due to friction applied to the boundary of the stationary mass from the flowing contents. As the contents in the channel flow, they exert a vertical force on the edge of the stationary medium. Although greatly reduced, some of this force will also be felt at the wall.

As discharge continues the vertical pressure at any level in the silo decreases at a constant rate to zero when the surface of the material reached the level of the pressure cell.

8.6.5. Strain gauges

Figures 8.77 to 8.80 show the strain gauge results at various positions on the external face of the silo wall. The positions are shown in Figure 8.1. At every position the measured strains decrease throughout the discharge period. The results prove that the high pressures measured by the wall cells during discharge and described in Section 8.6.2 do not generate the high wall stresses. This is because the high pressures occur in a localised region and do not significantly affect the overall behaviour.

The results suggest that discharge does not lead to the worst load case for design. The highest wall stresses were measured when the silo was full. The results from this model suggest that similar silos can be designed for the static pressure case when the silo is full. No additional overpressure factor is required to allow for high discharge pressures.

8.6.6. Wall friction

The coefficient of wall friction was calculated from the walls cells during discharge. The wall friction force declined at a nearly constant rate from the start of discharge. Cells 'B','C' and 'D' exhibit negative friction before the end of discharge. This seems to be due to elasticity within the stored medium. As the head of sand above any point in the bin is reduced, inward deformation of the wall and strain energy recovery generate an upward strain of the stored material and hence negative friction on the wall.

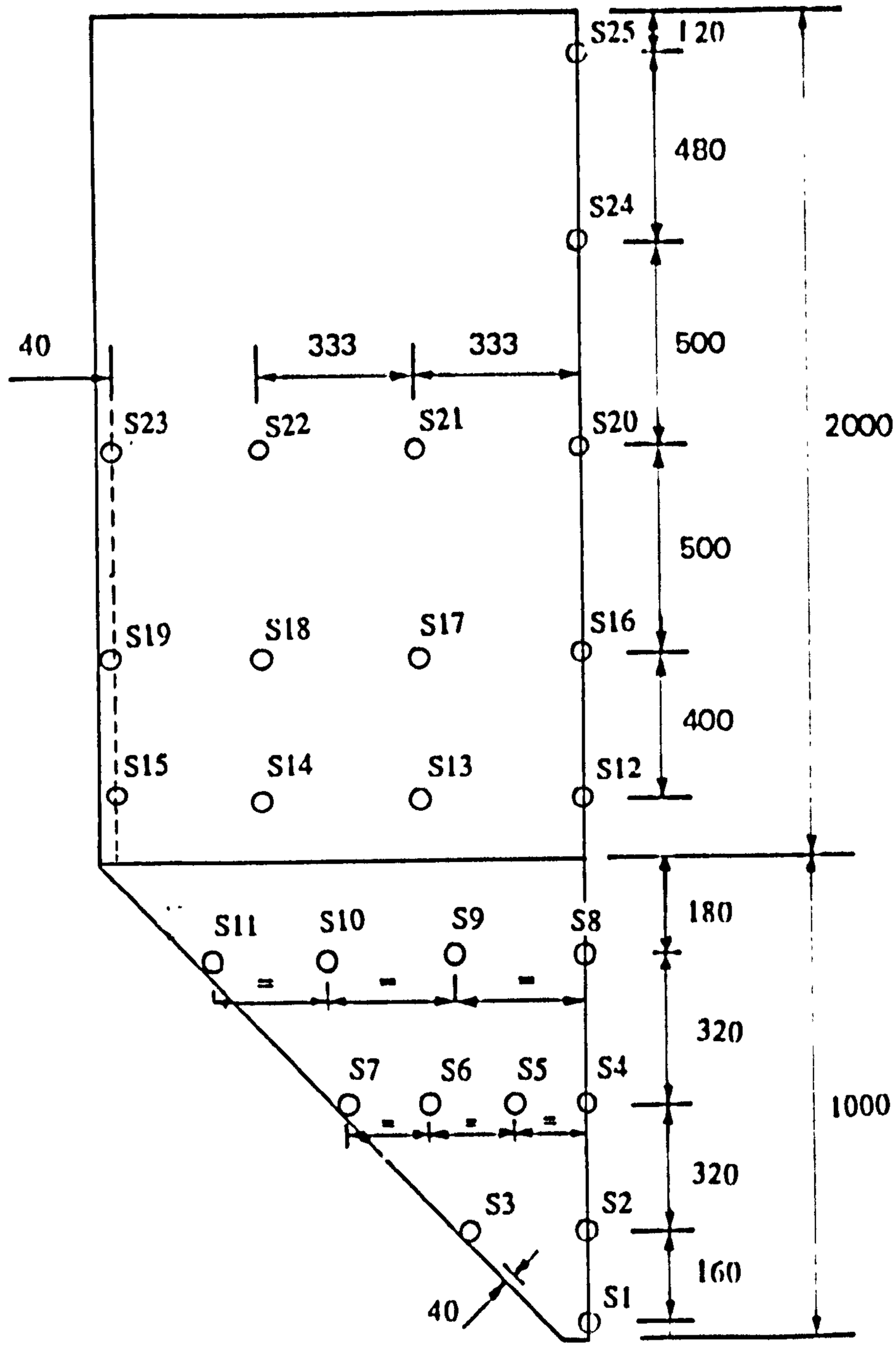

Figure 8.1 POSITIONS OF STRAIN GAUGES (Dimensions in mm)

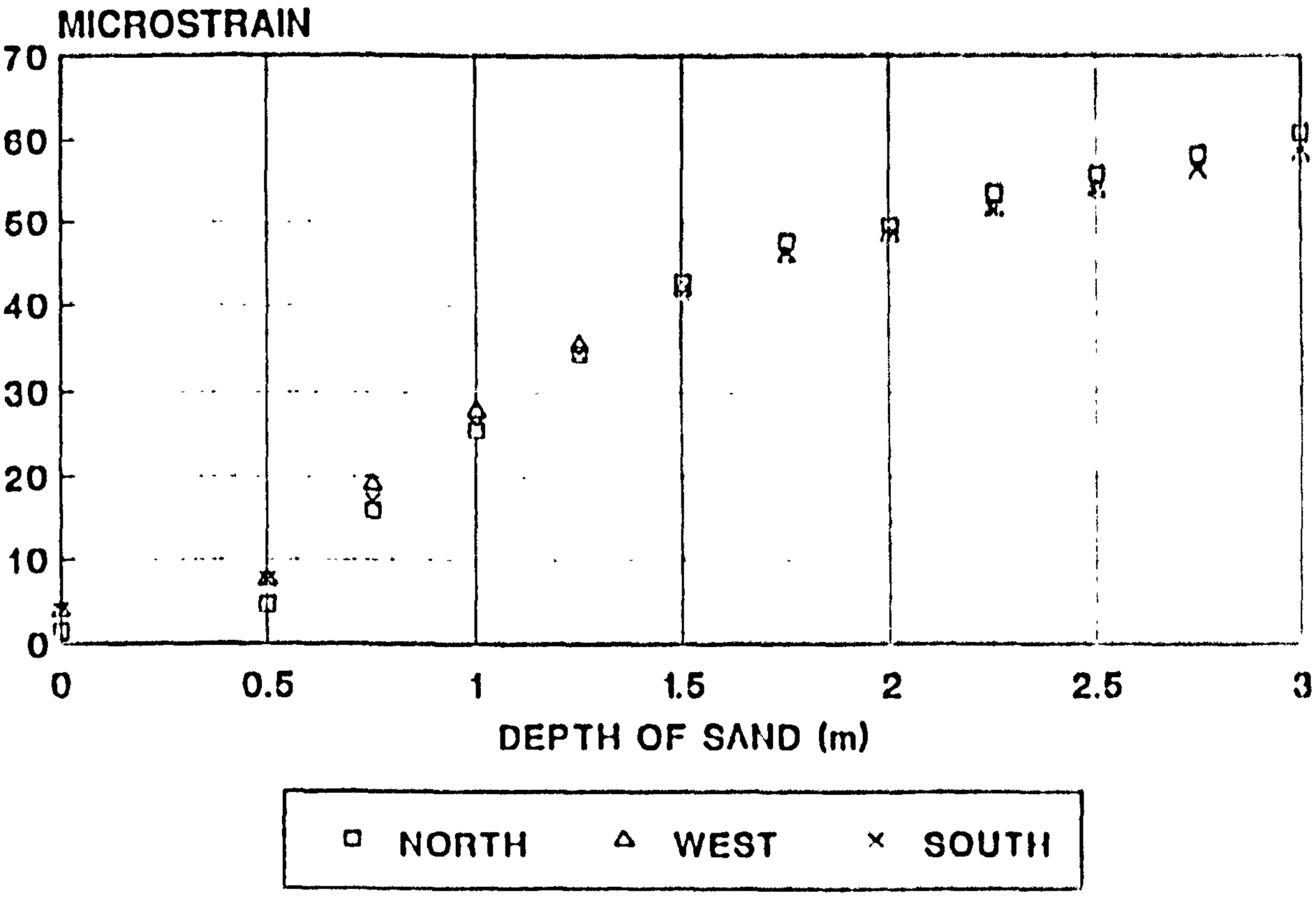

Figure 8.2

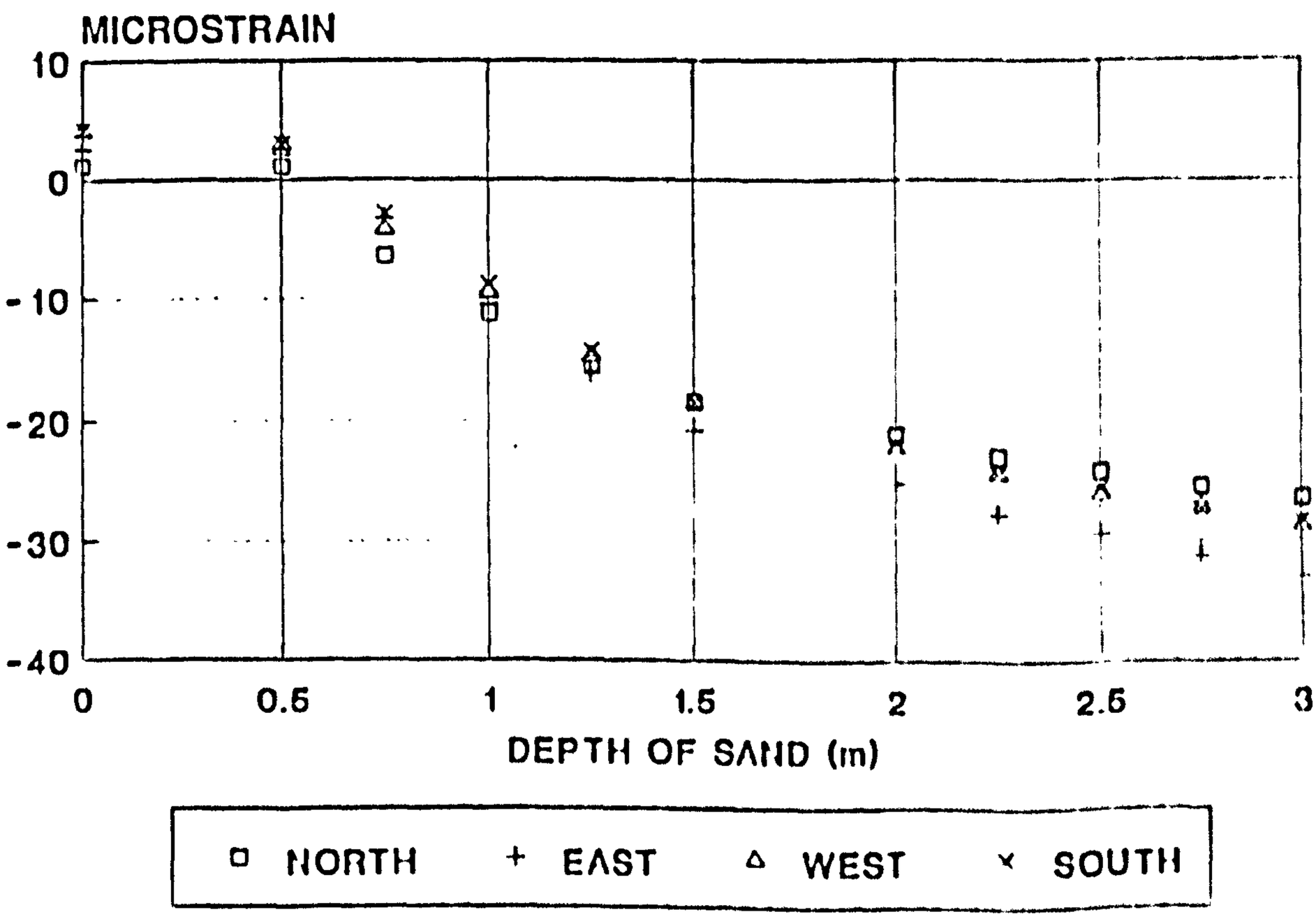

Figure 8.3

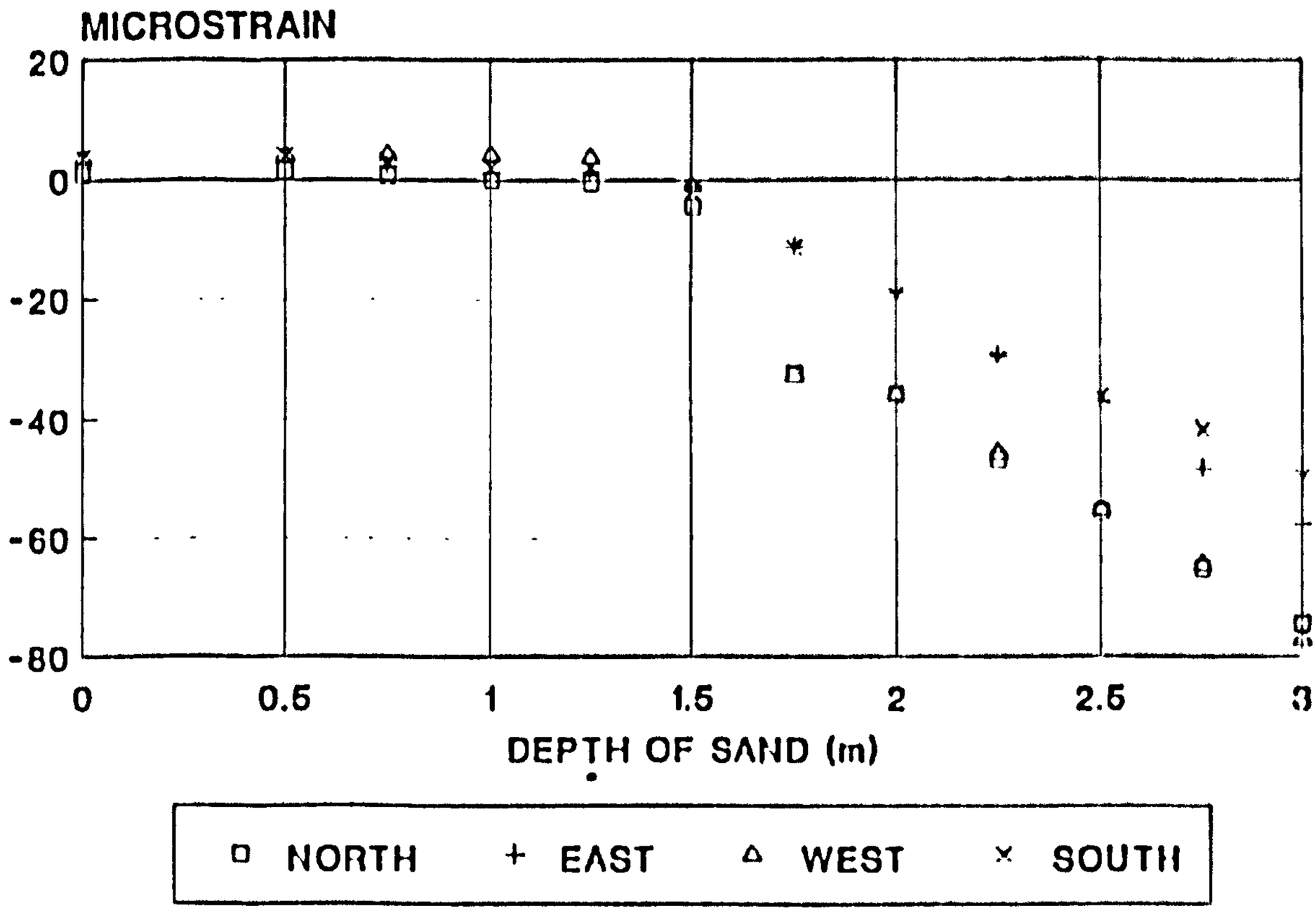
HORIZONTAL STRAIN
SYMMETRY CHECK POSITION 'S12'
MICROSTRAIN
20
0
-20
-40
-60
-80
0
0.5
1
1.5
2
2.5
3
DEPTH OF SAND (m)
NORTH
EAST
WEST
SOUTH

Figure 8.4

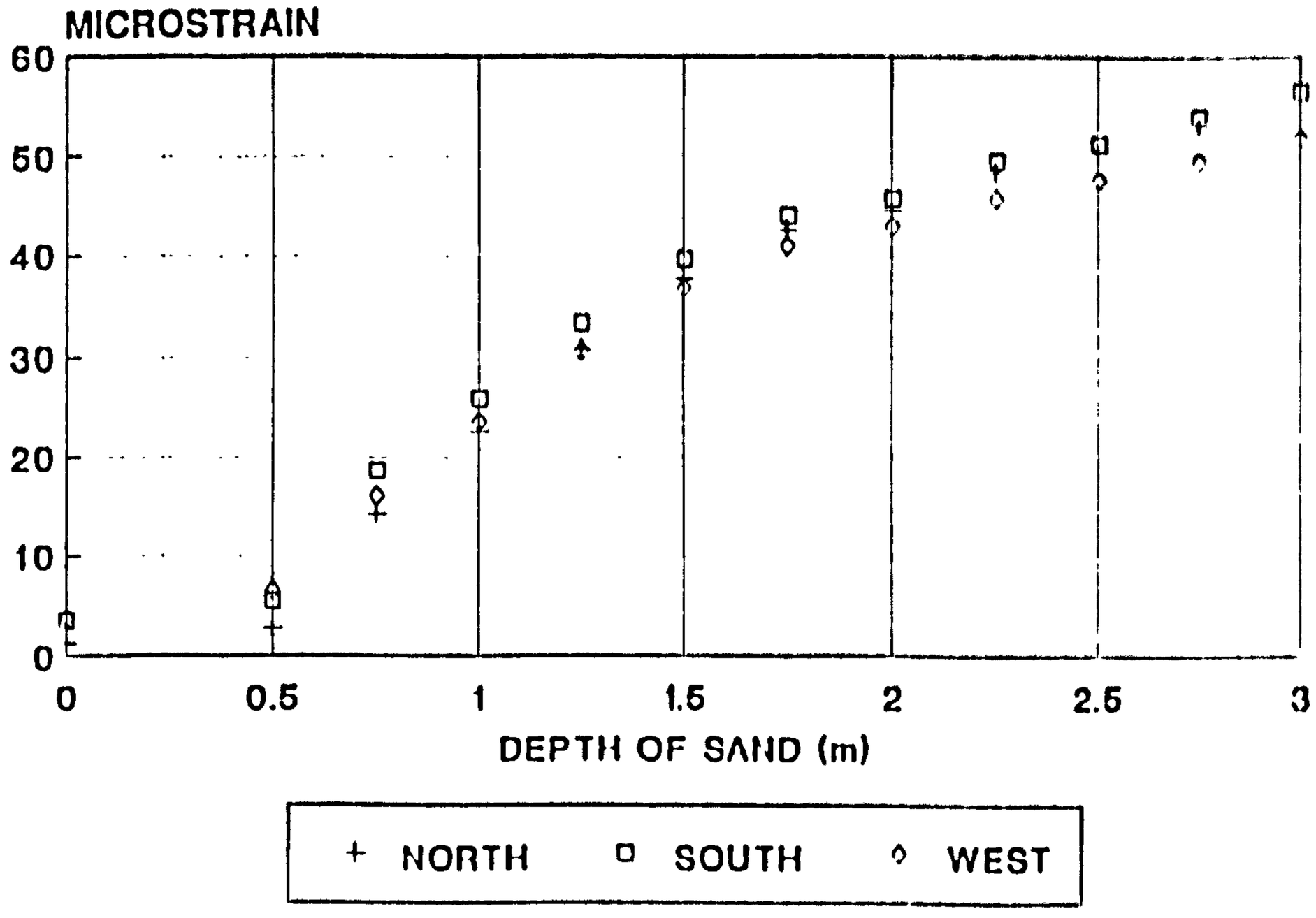

Figure 8.5

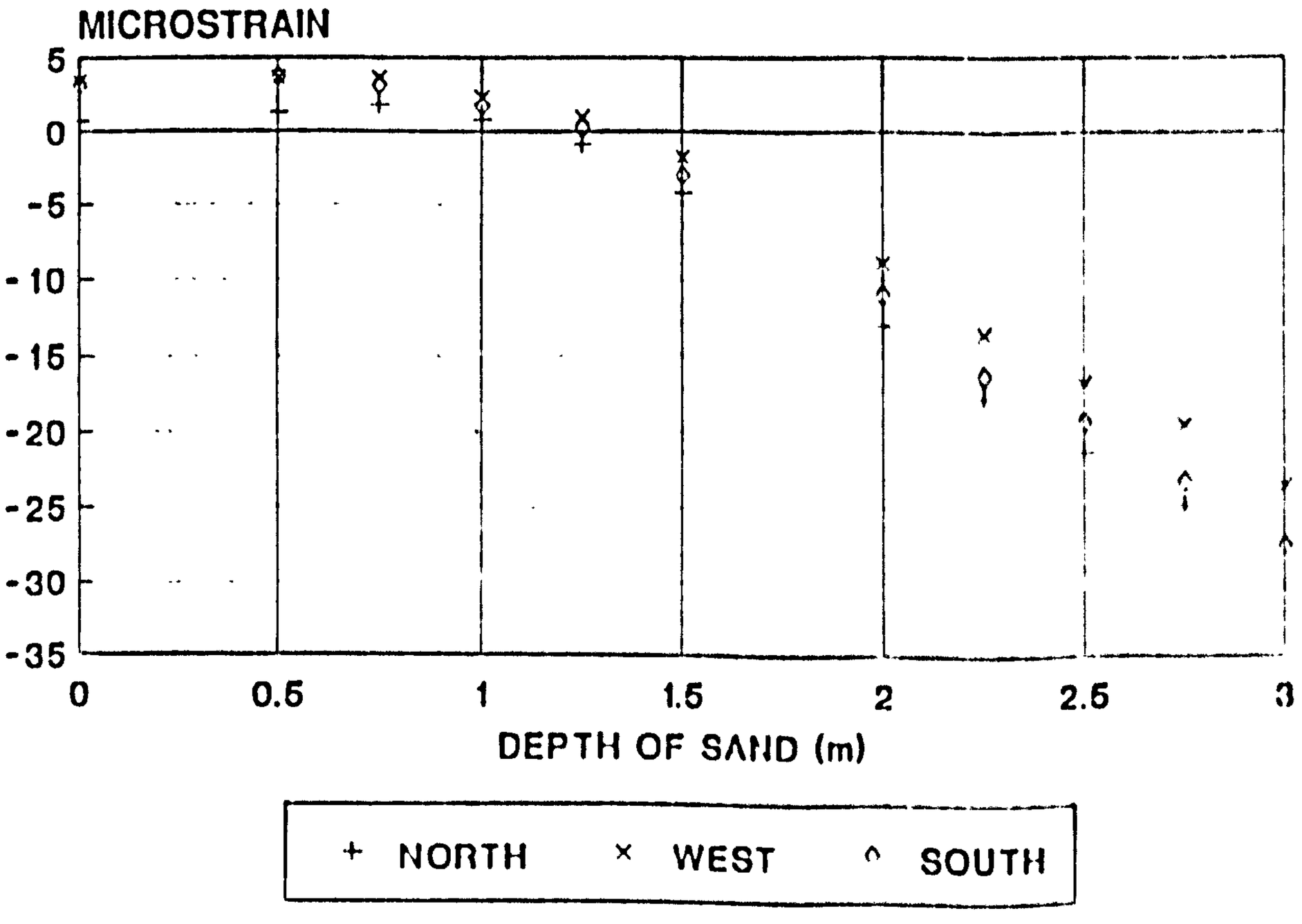

Figure 8.6

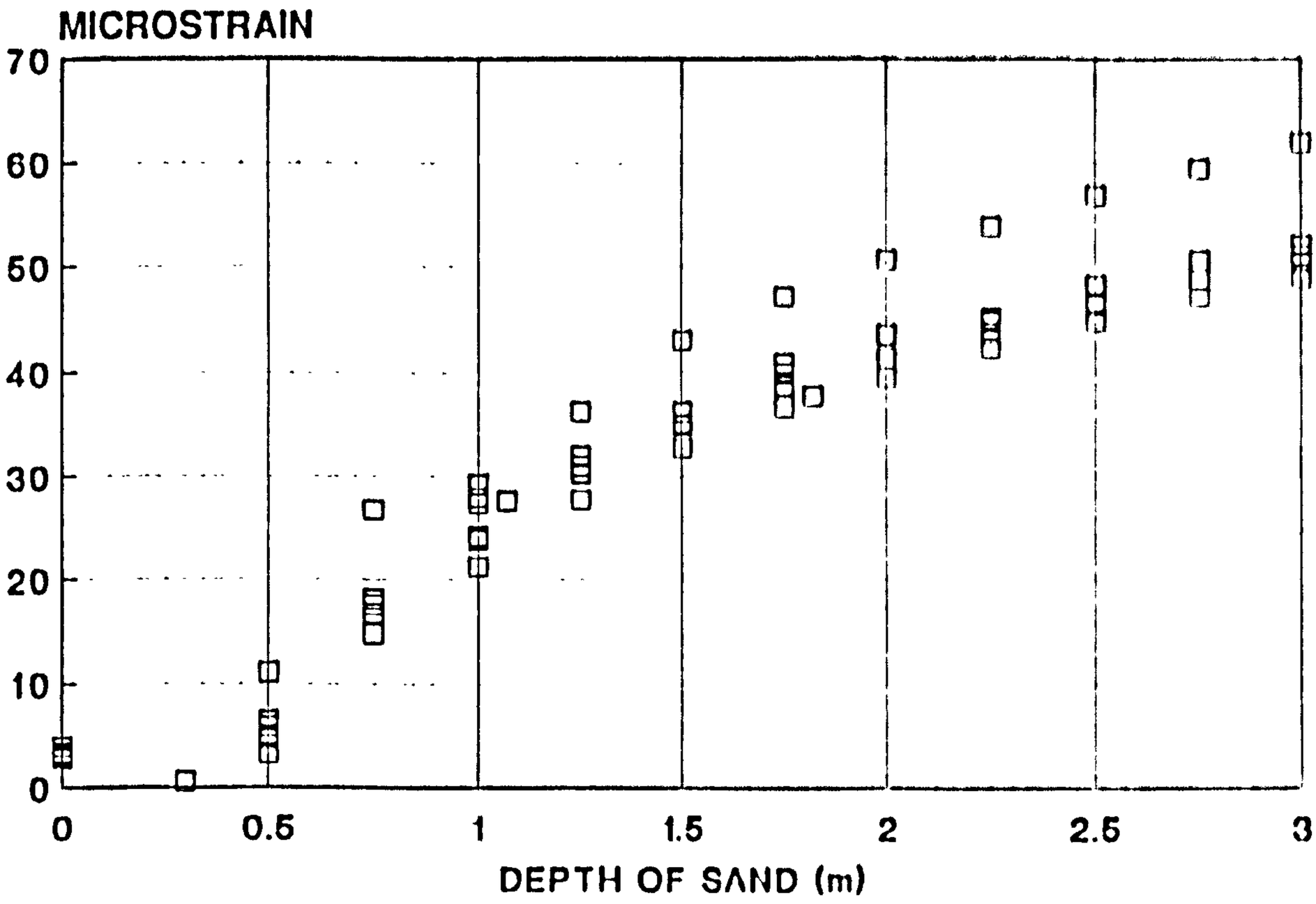

Figure 8.7

Figure 8.8

VERTICAL STRAIN
CONSISTENCY CHECK POSITION 'S12'

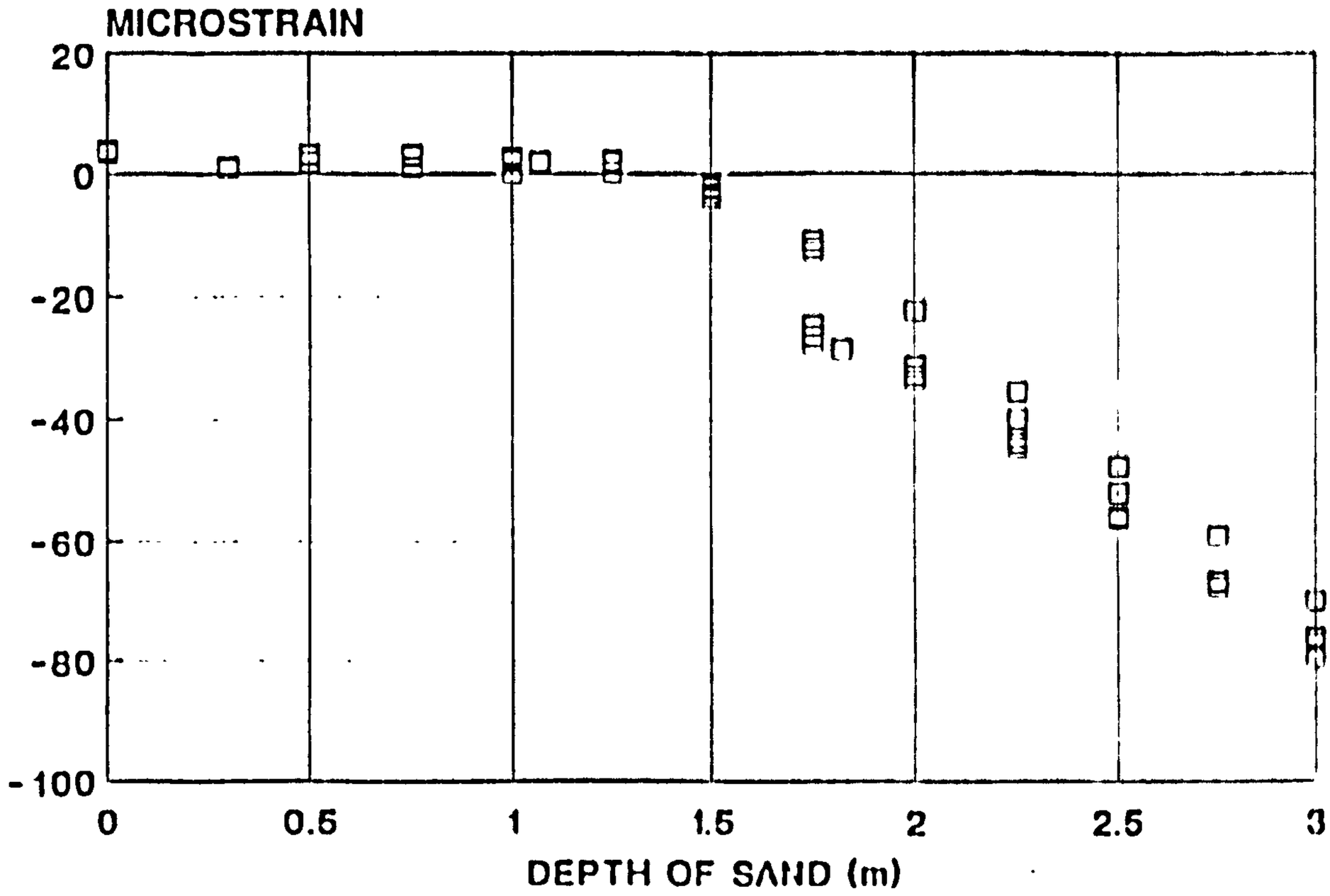

Figure 8.9

VERTICAL STRAIN
CONSISTENCY CHECK POSITION 'S15'

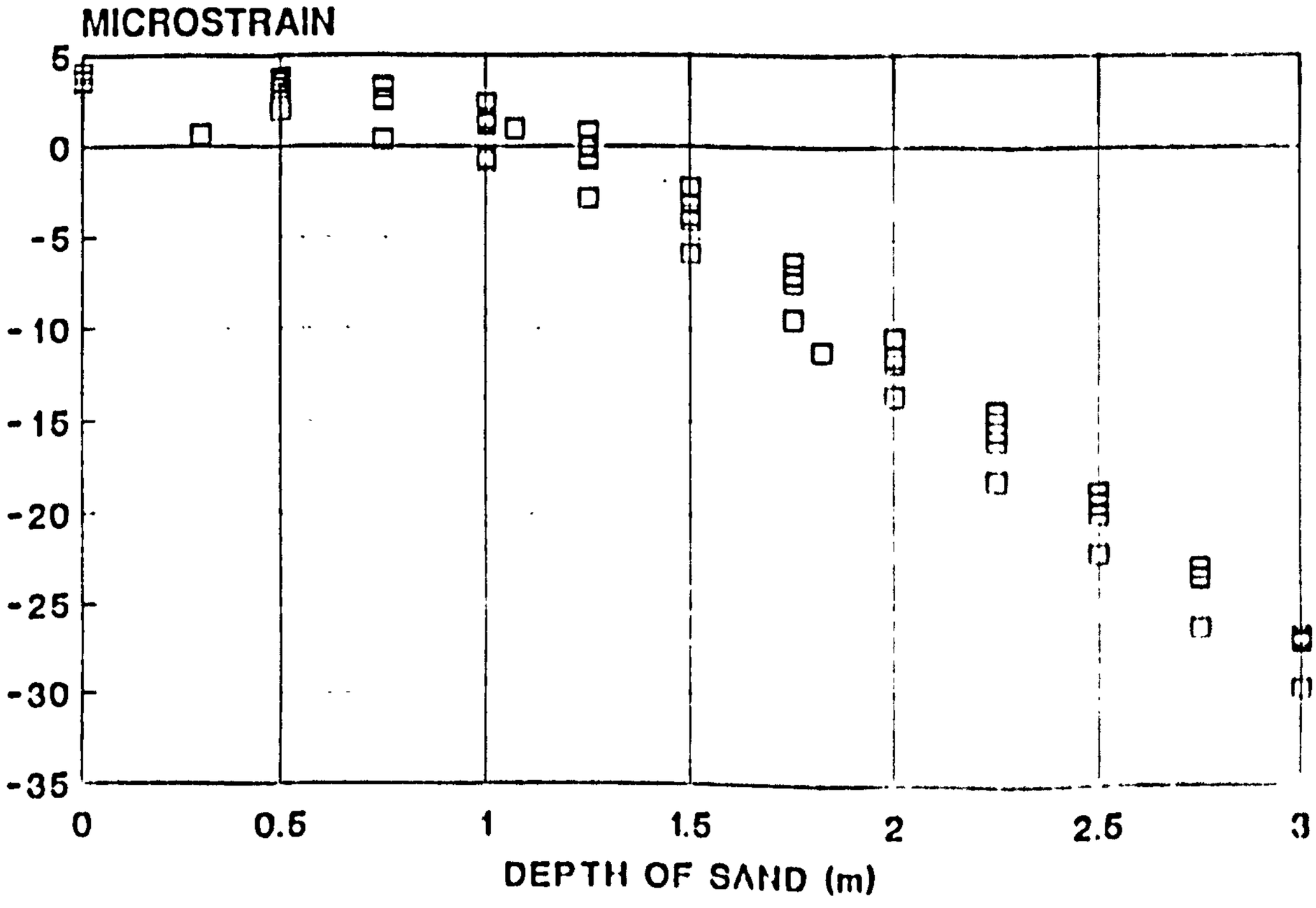

Figure 8.10

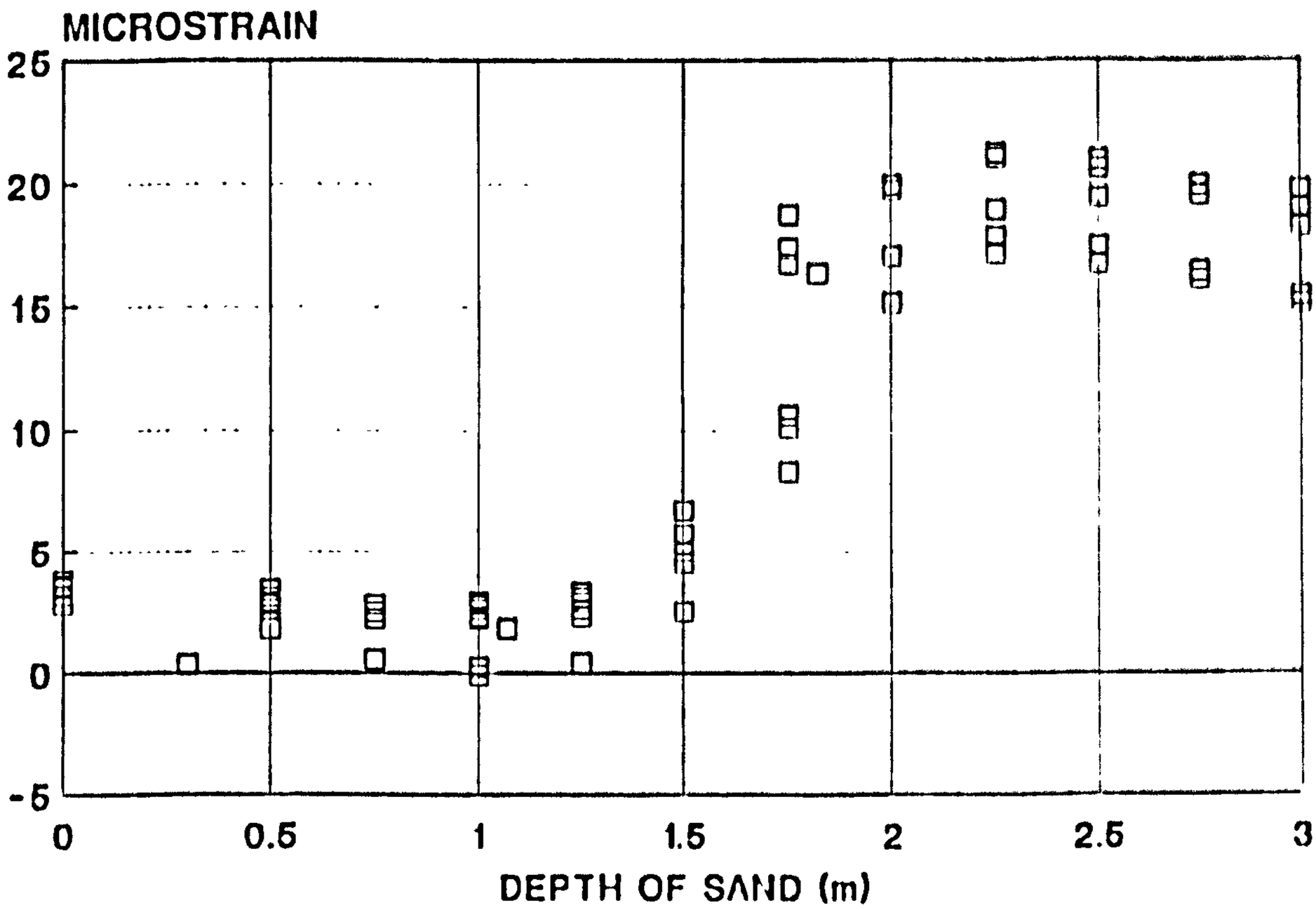

Figure 8.11

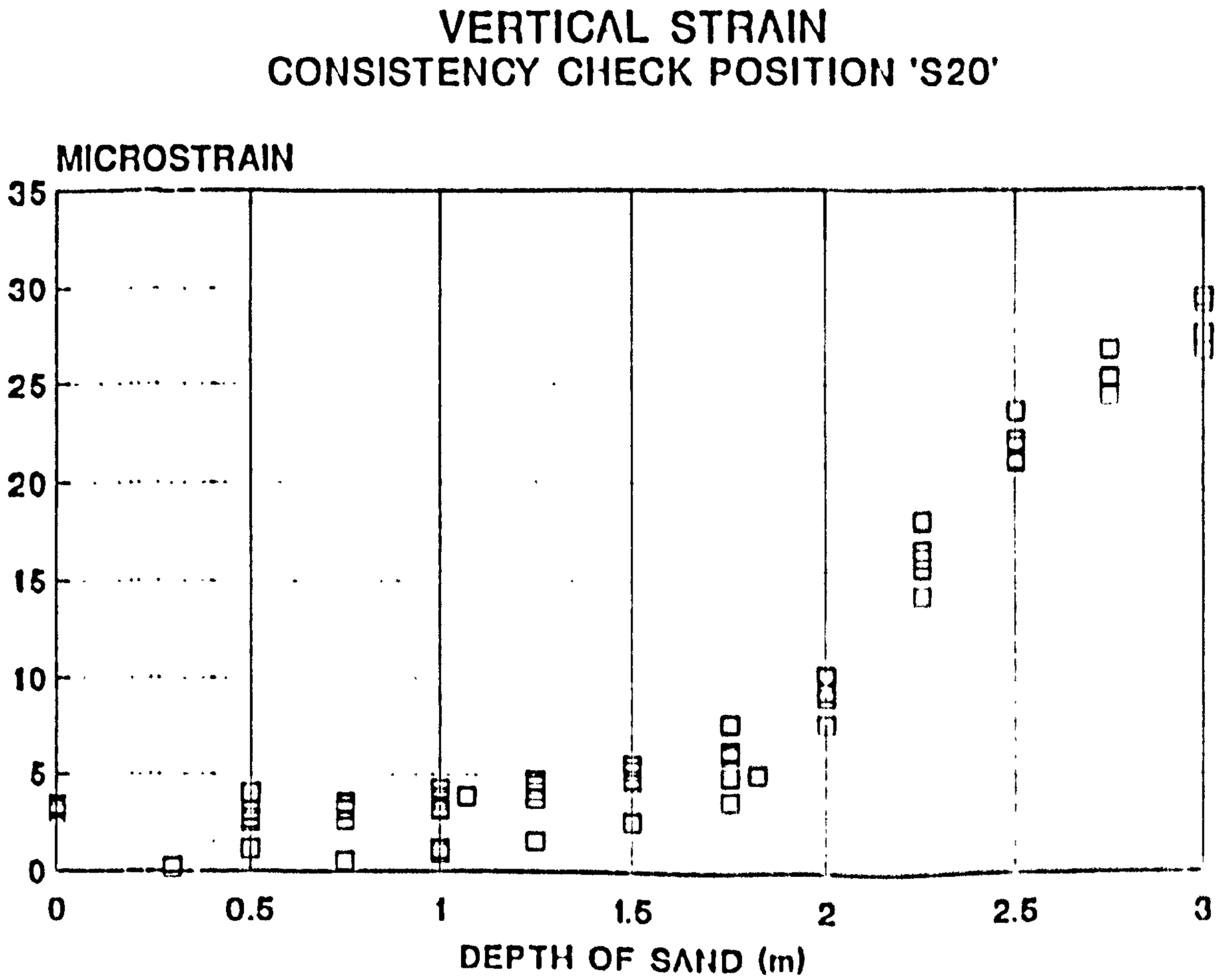

Figure 8.12

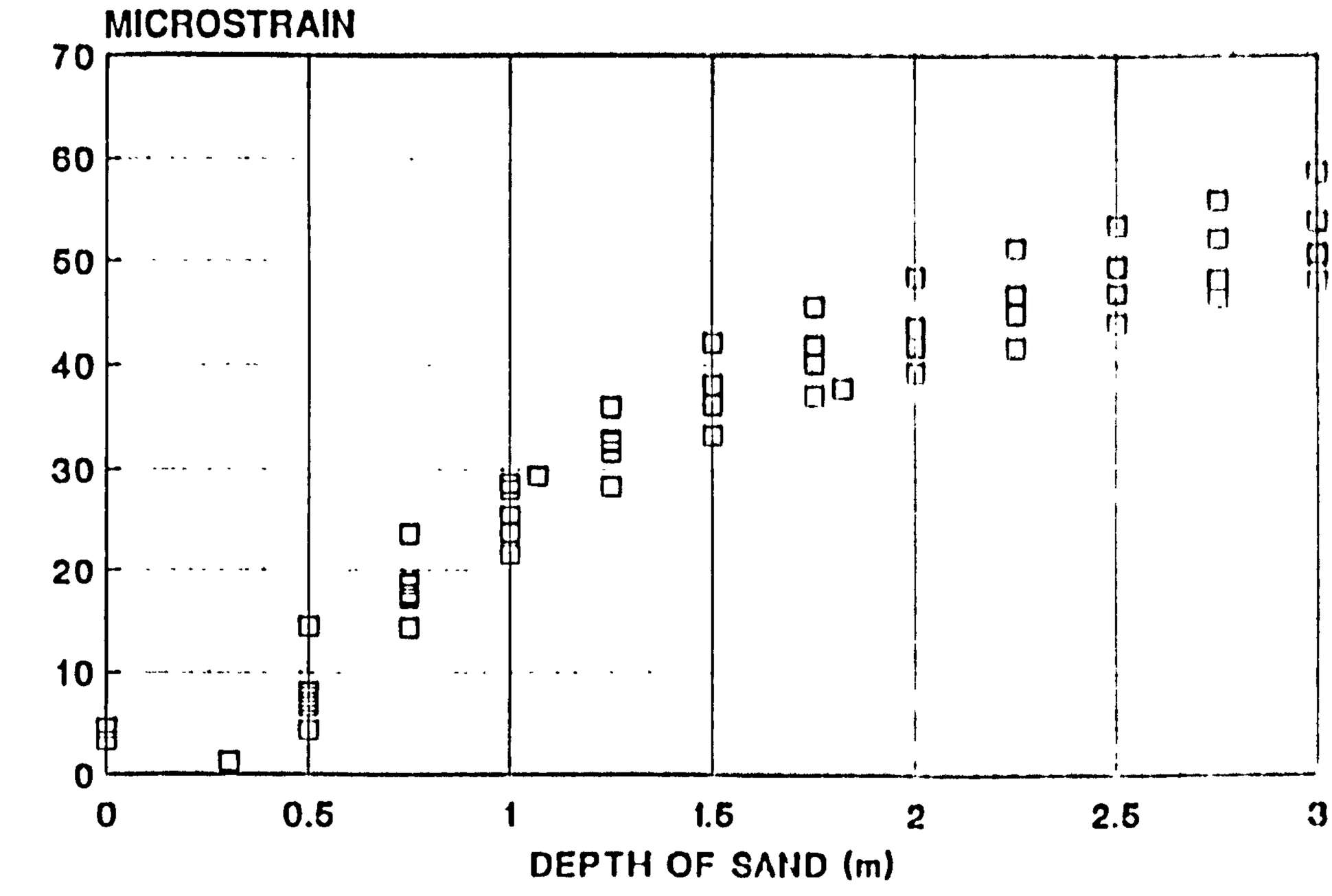

Figure 8.13

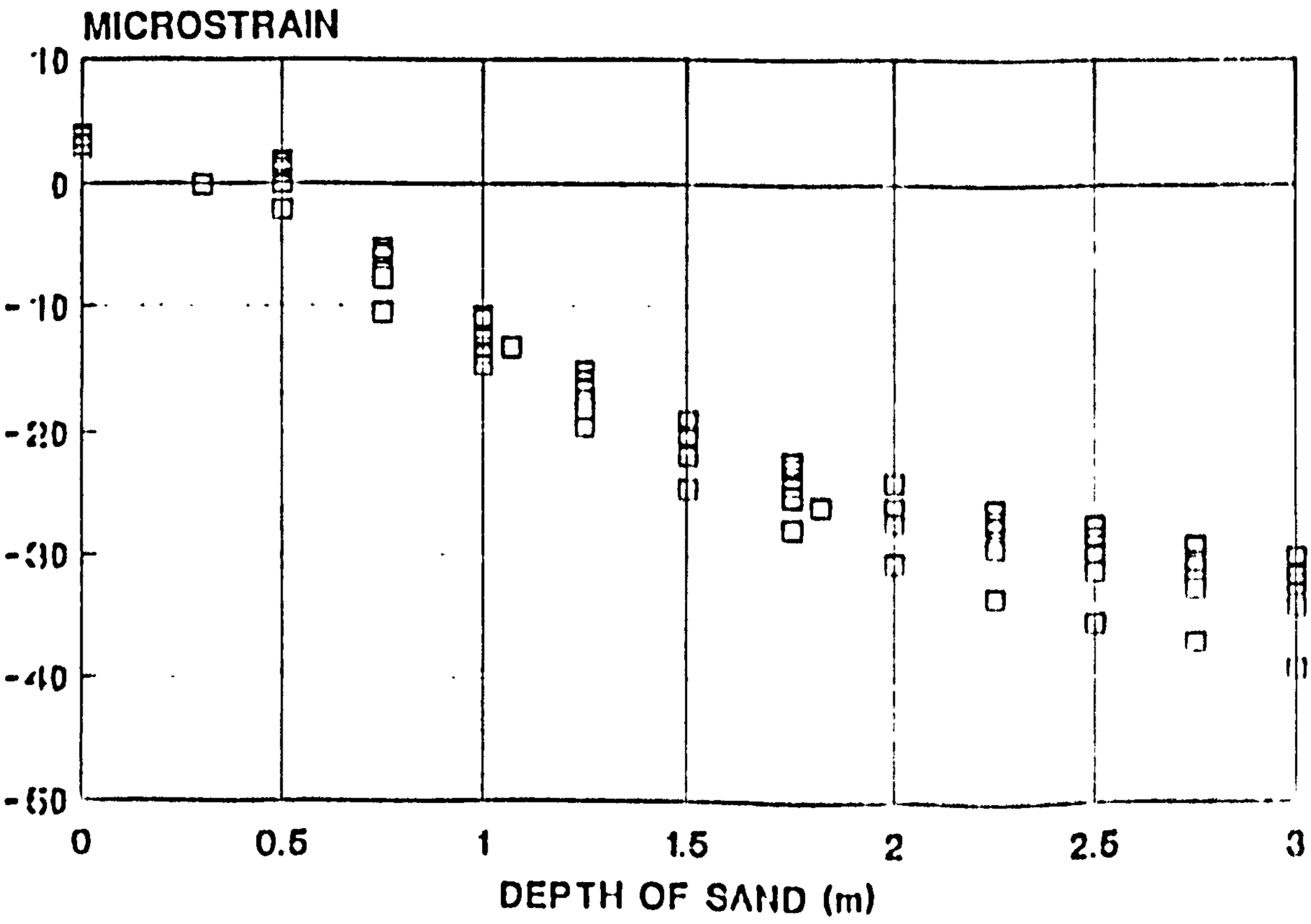

Figure 8.14

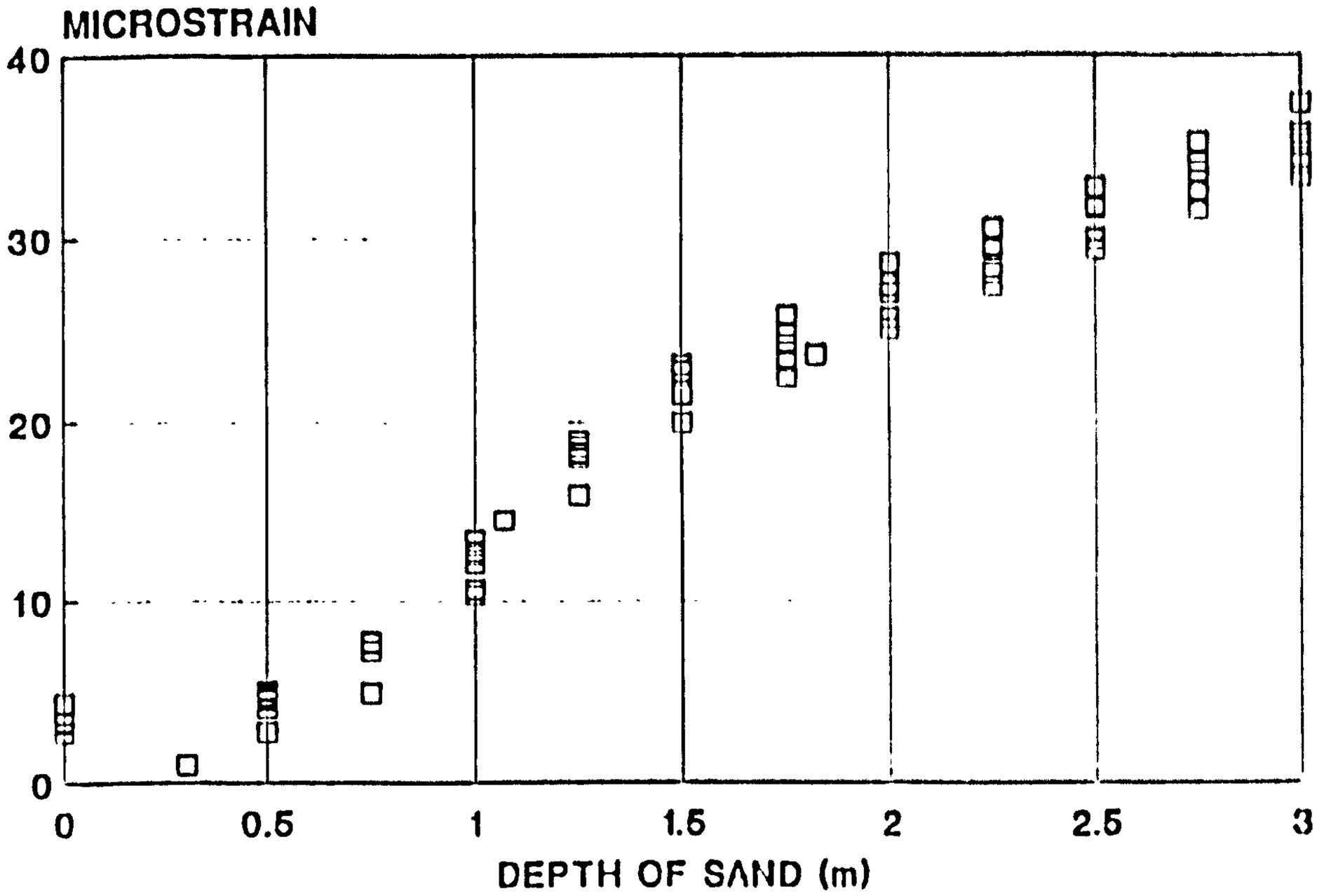

Figure 8.15

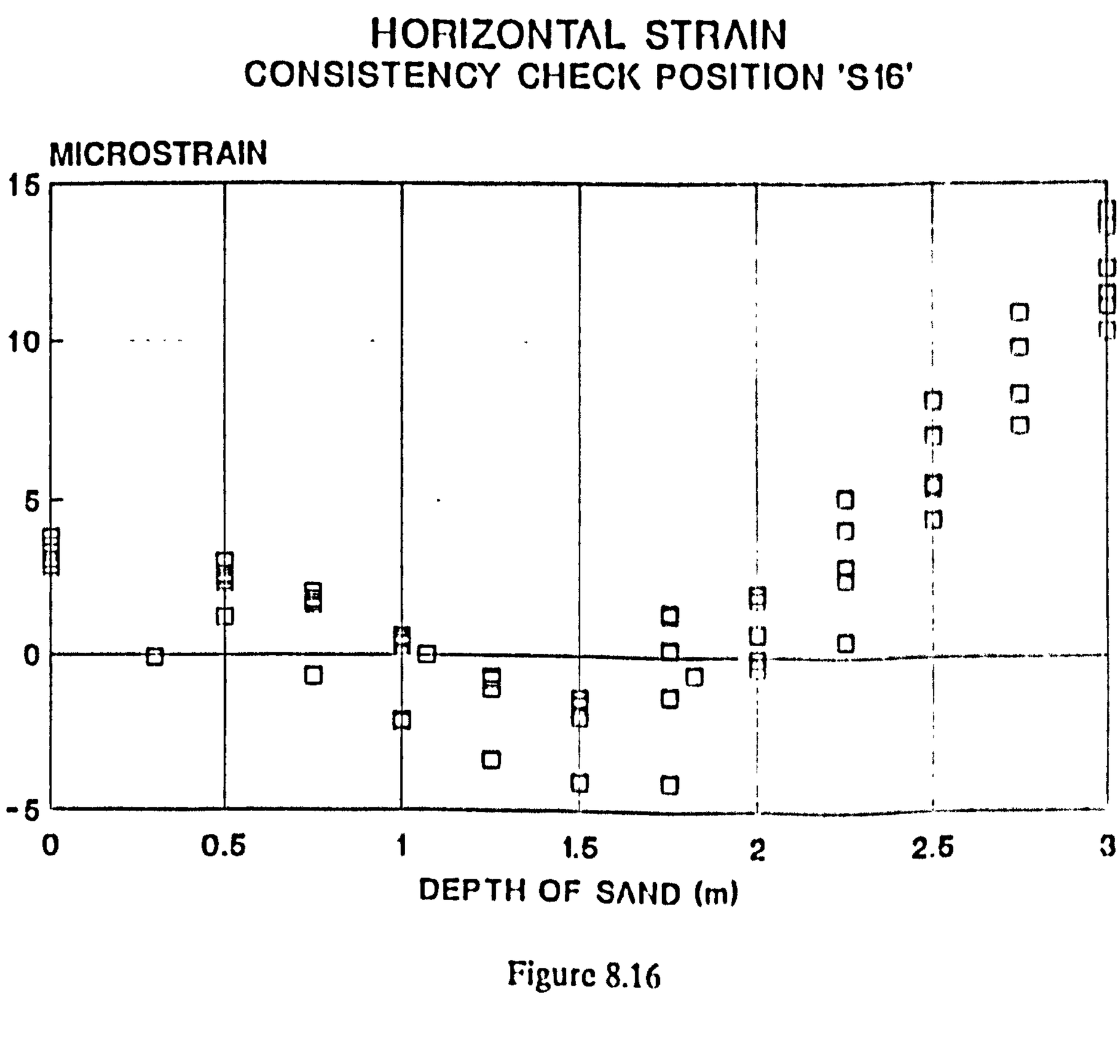

Figure 8.16

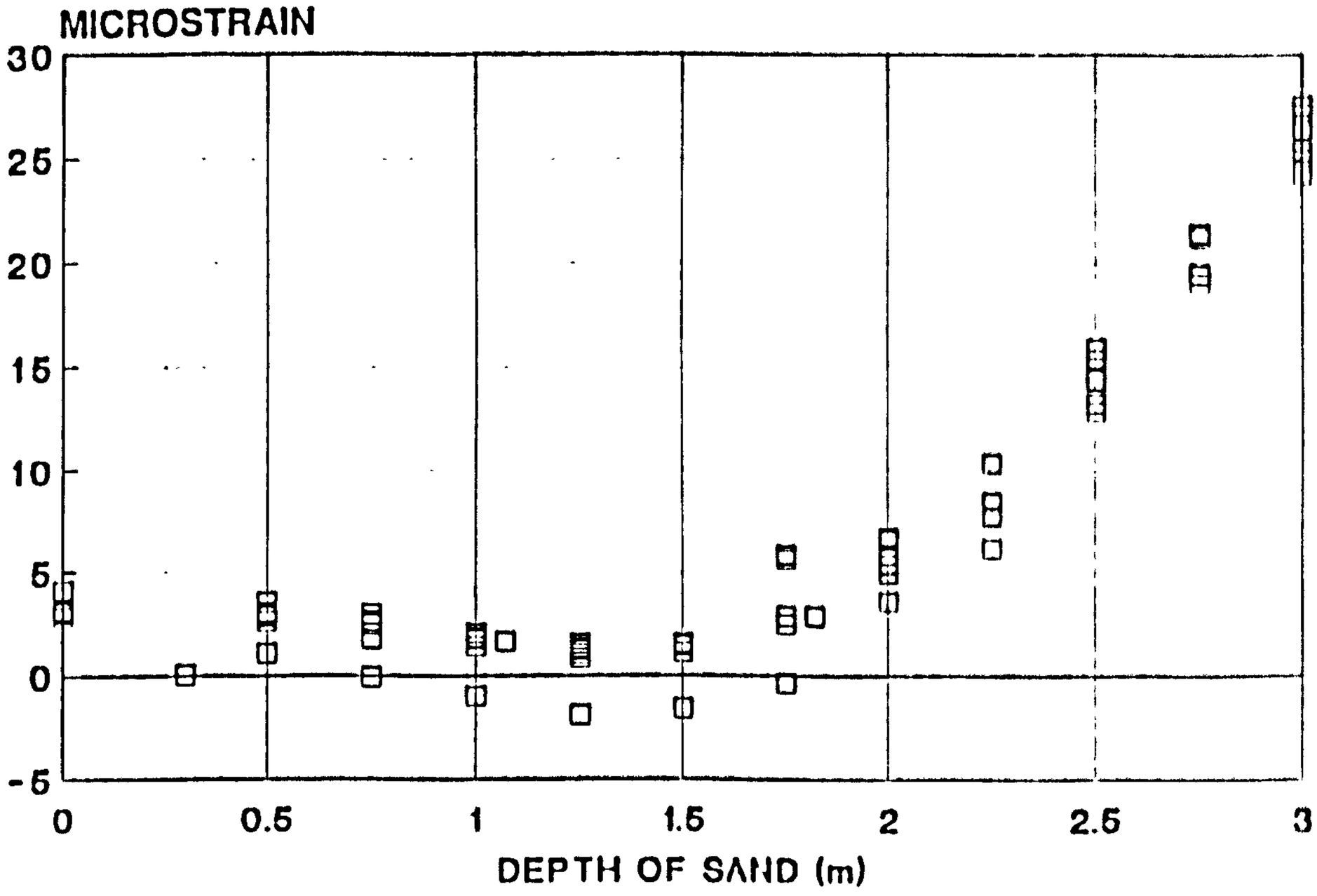
HORIZONTAL STRAIN
CONSISTENCY CHECK POSITION 'S20'
MICROSTRAIN
30
25
20
15
10
5
0
-5
0
0.5
1
1.5
2
2.5
3
DEPTH OF SAND (m)

Figure 8.17

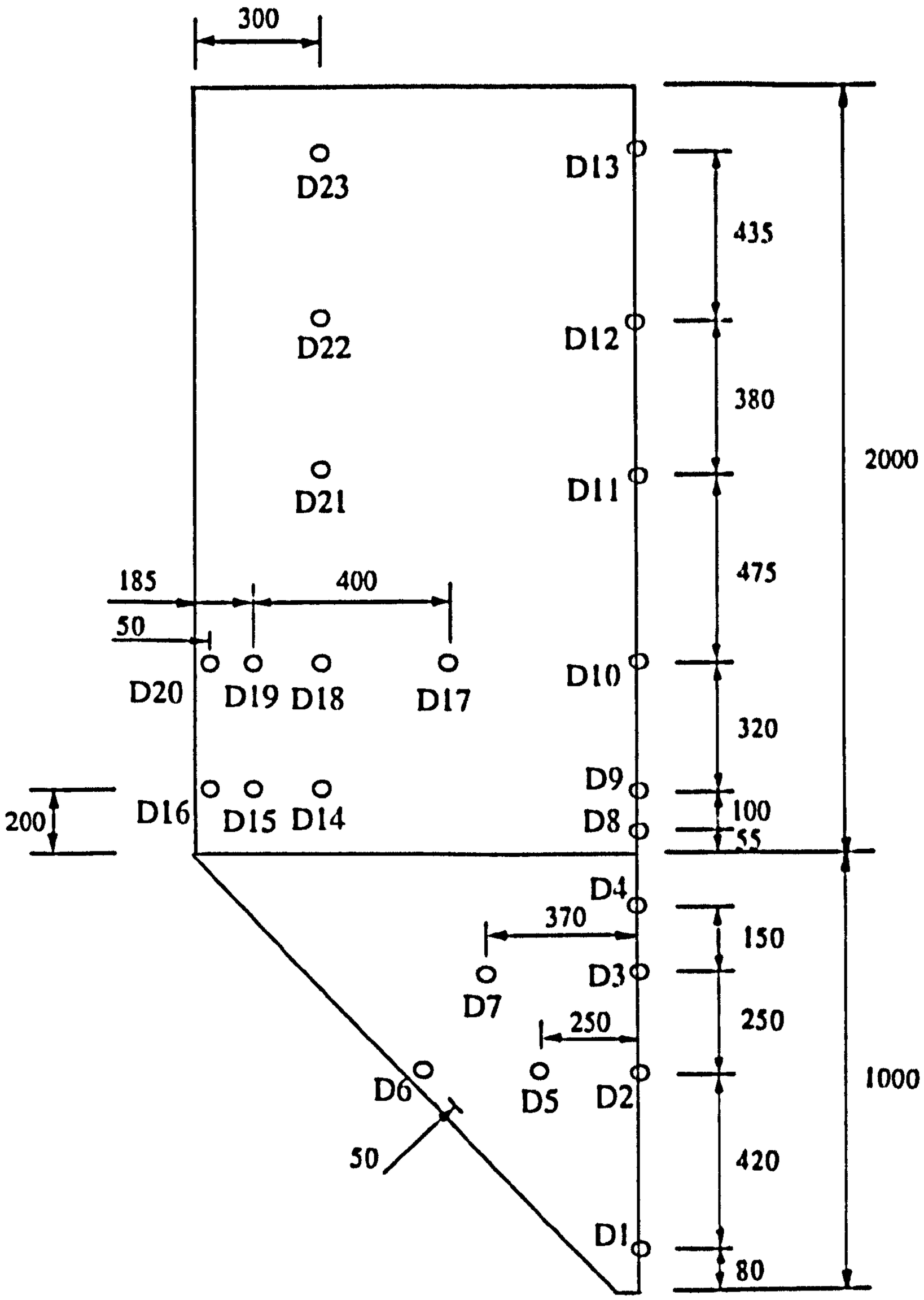

Figure 8.18 POSITIONS OF DIAL GAUGES PLACED TO MEASURE DEFORMATION NORMAL TO THE WALL
(Dimensions in mm)

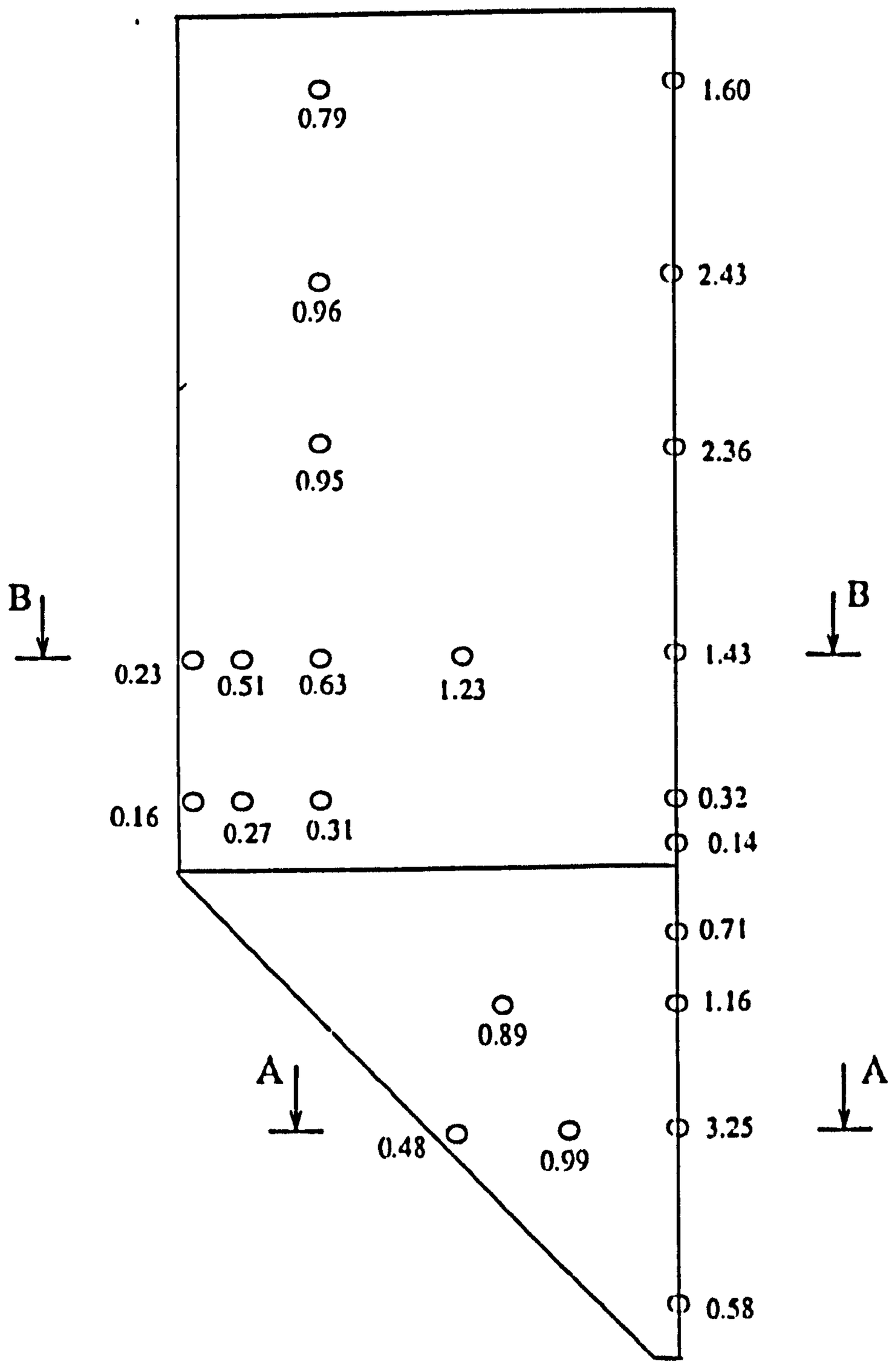

Figure 8.19a DEFORMATION 3.0 m SAND

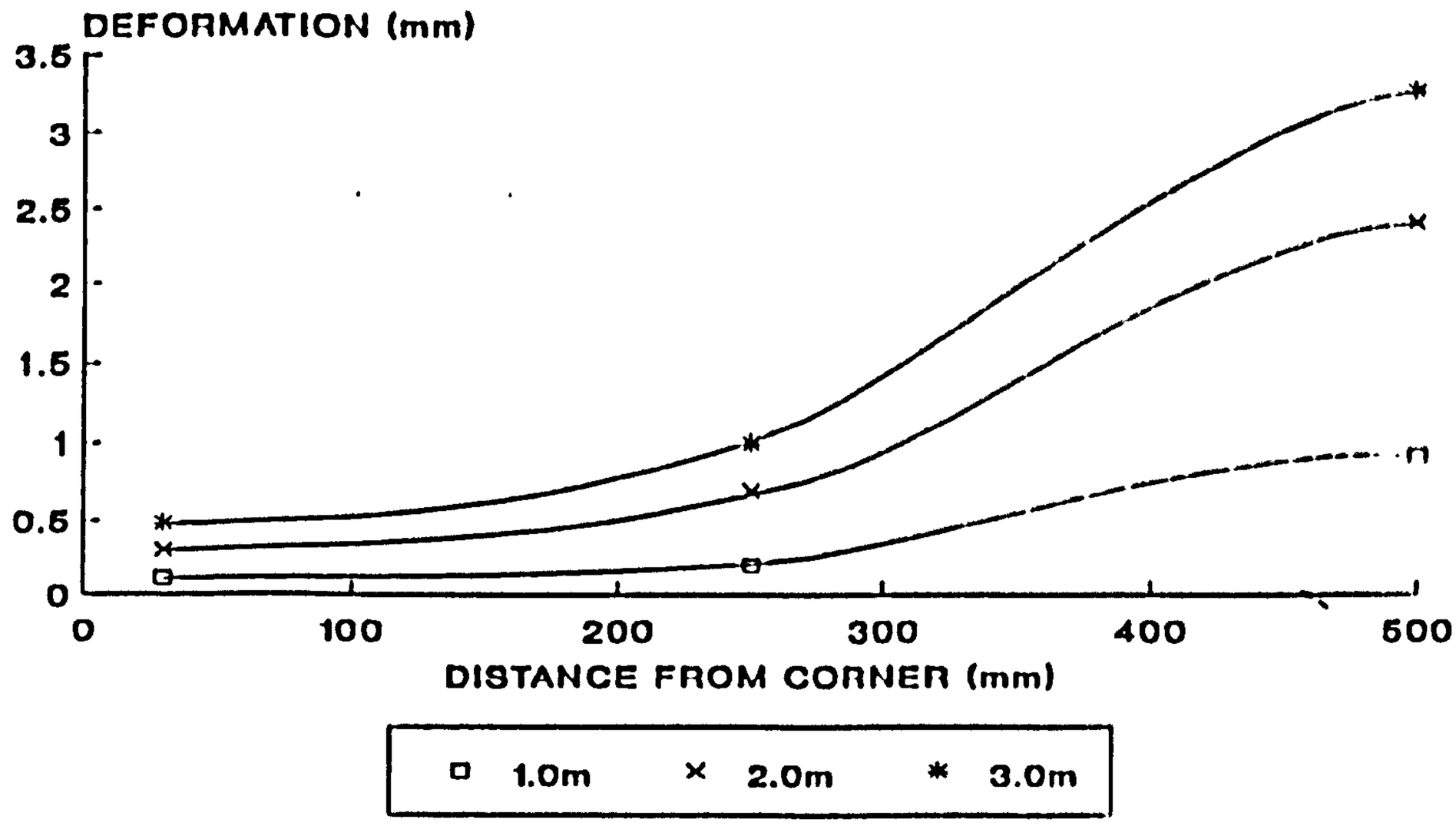

Figure 8.19 b

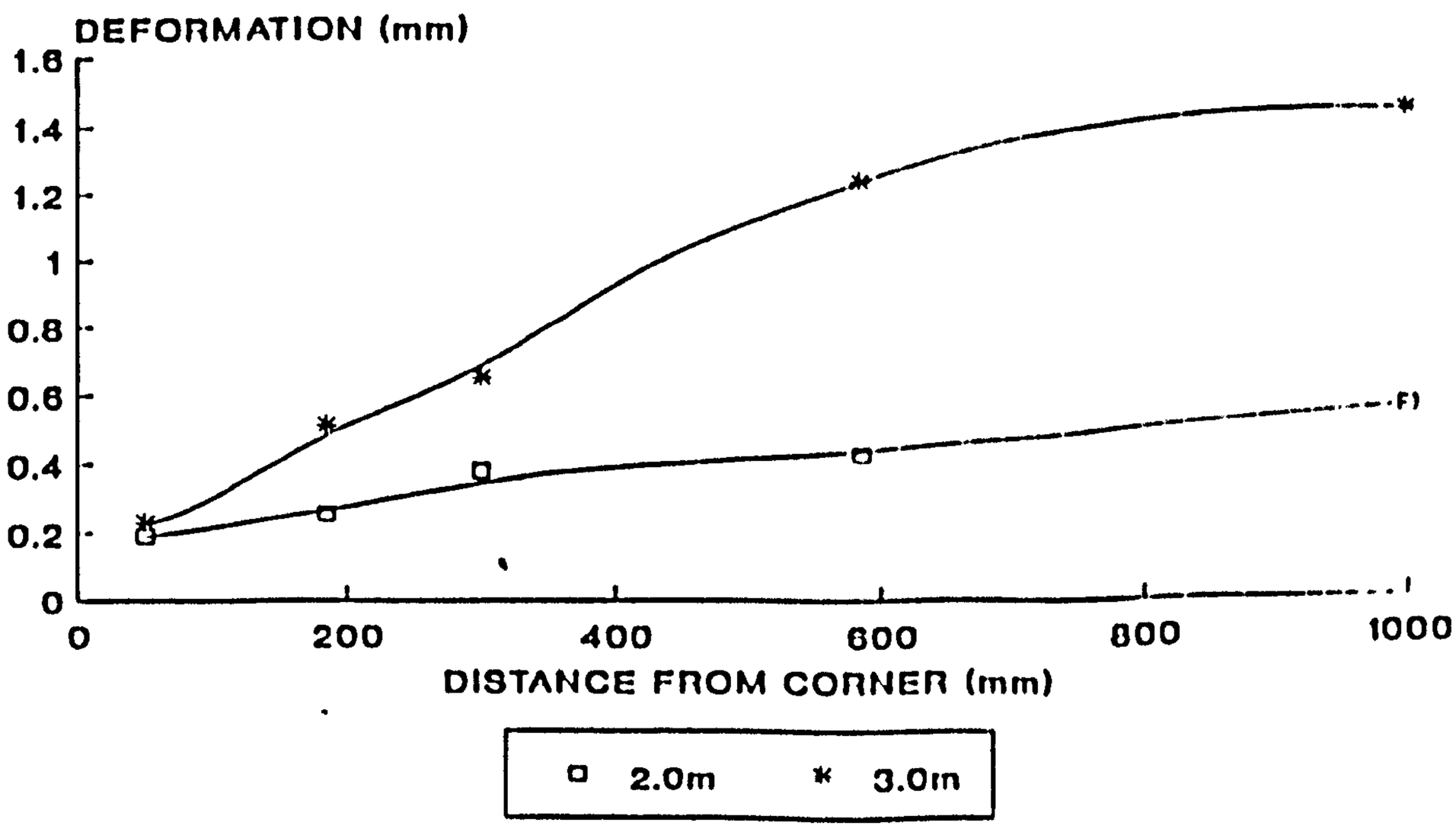

Figure 8.19 c

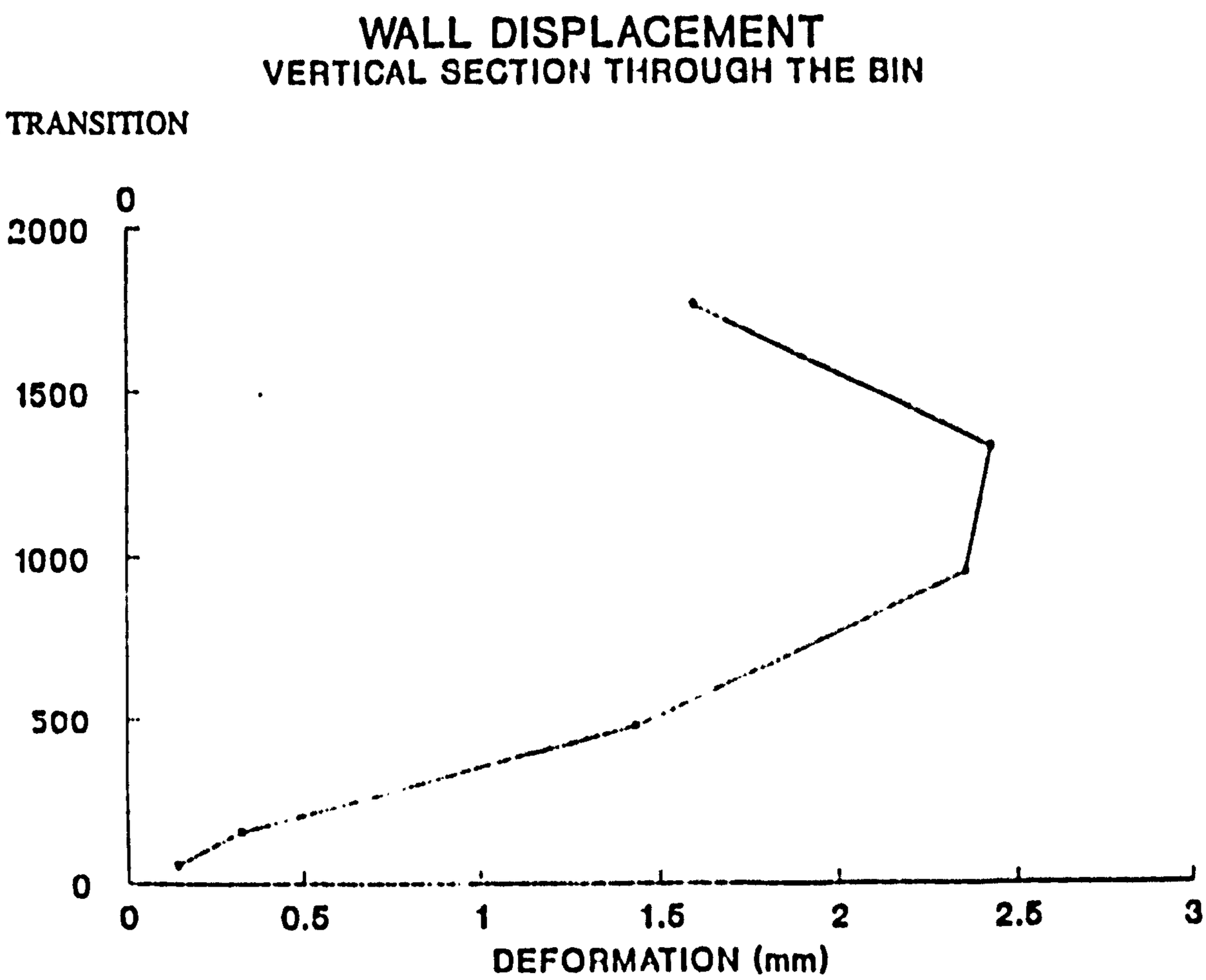
WALL DISPLACEMENT
VERTICAL SECTION THROUGH THE BIN
DISTANCE FROM TRANSITION
(mm)
2000
1500
1000
500
0
0
0.5
1
1.5
2
2.5
3
DEFORMATION (mm)

Figure 8.19d

WALL DEFORMATION

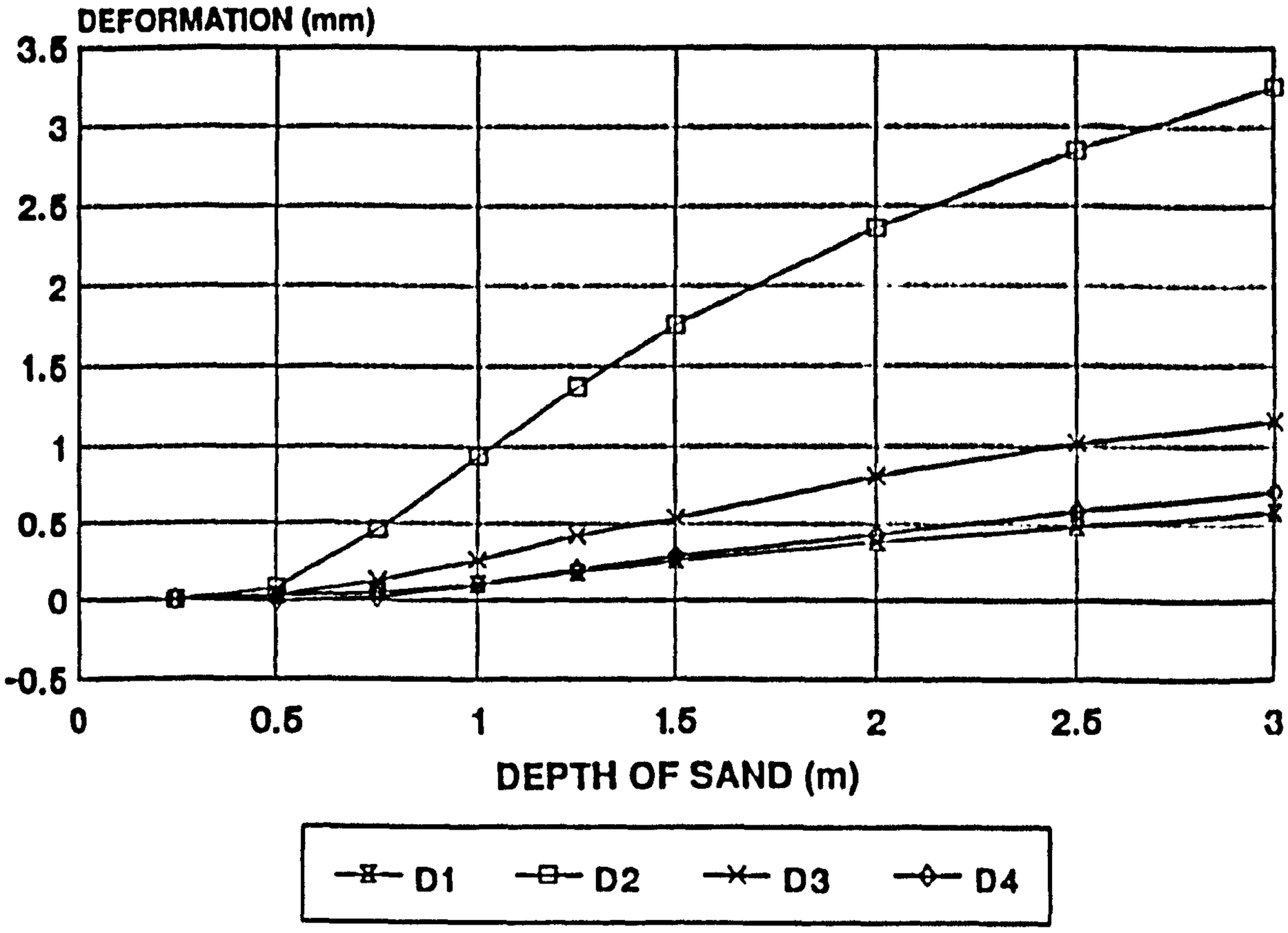

Figure 8.20

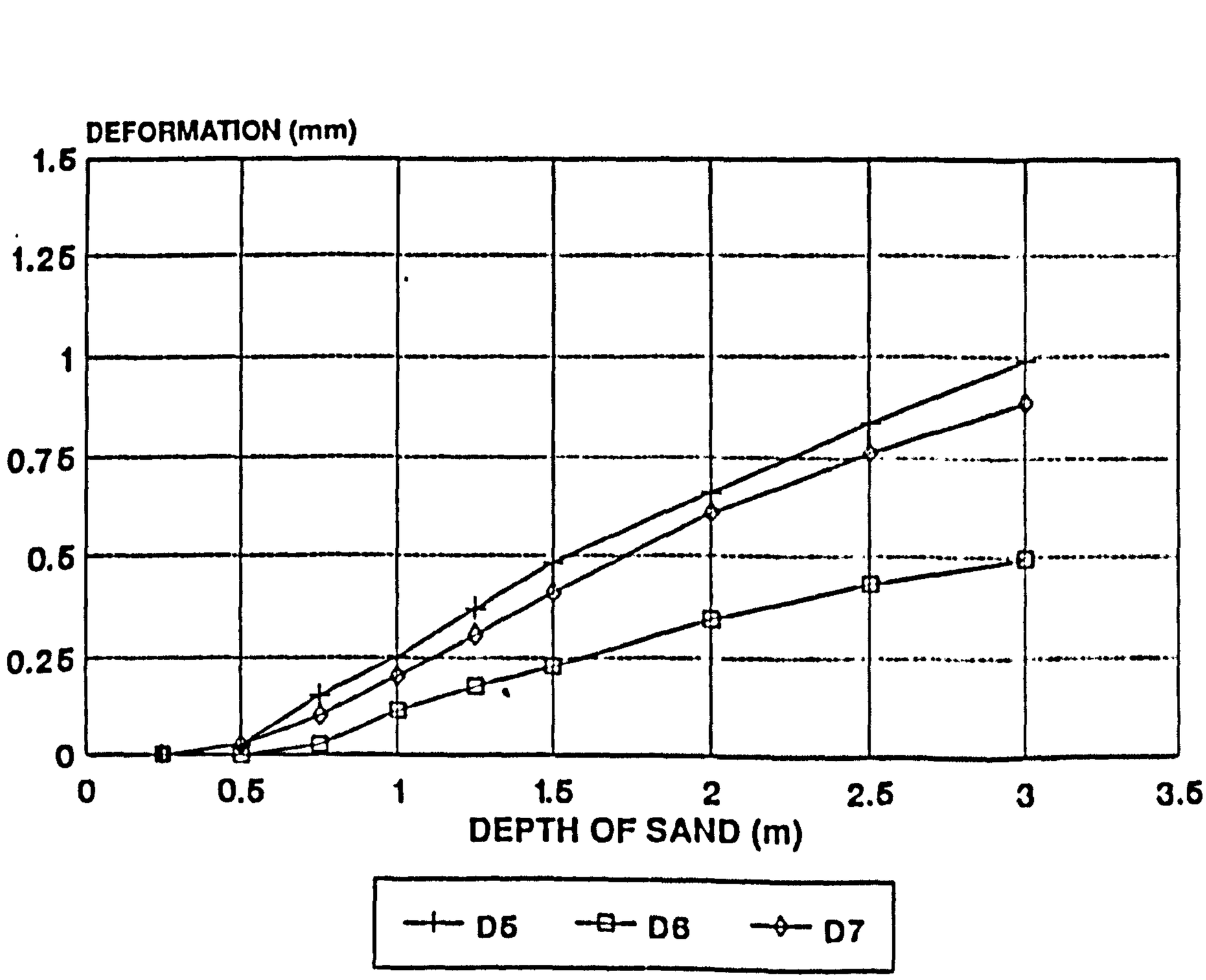

Figure 8.21

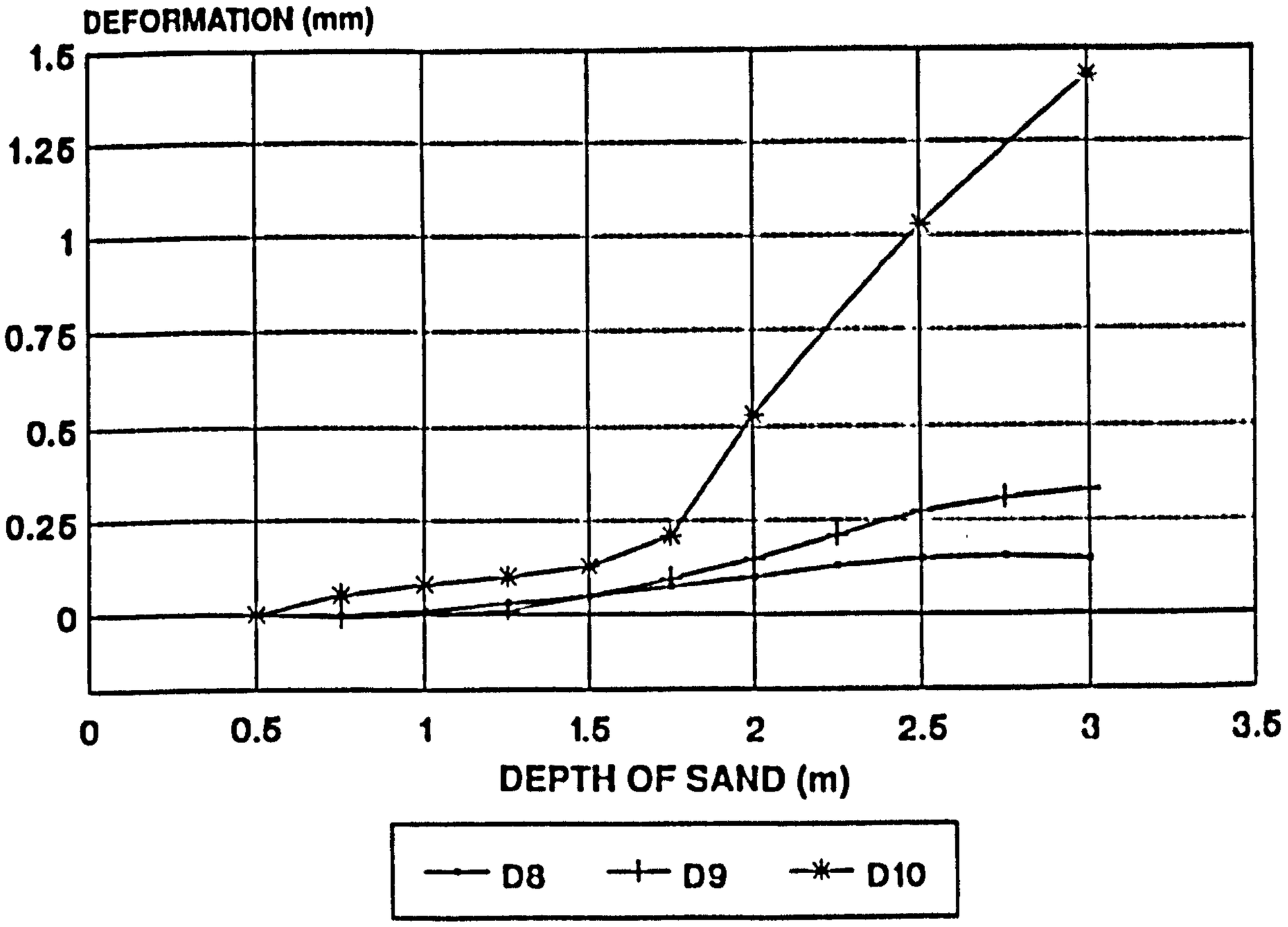

Figure 8.22

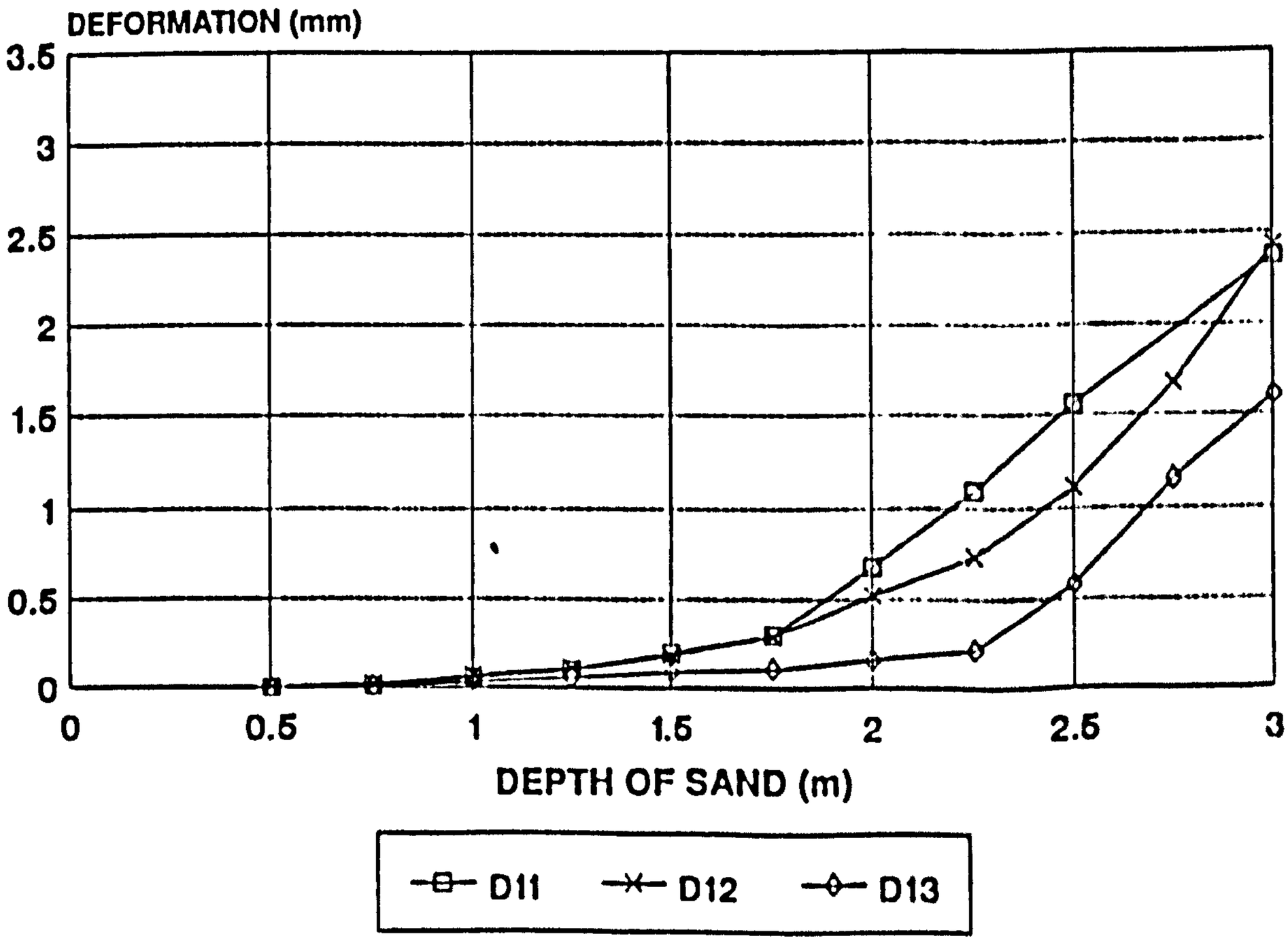

Figure 8.23

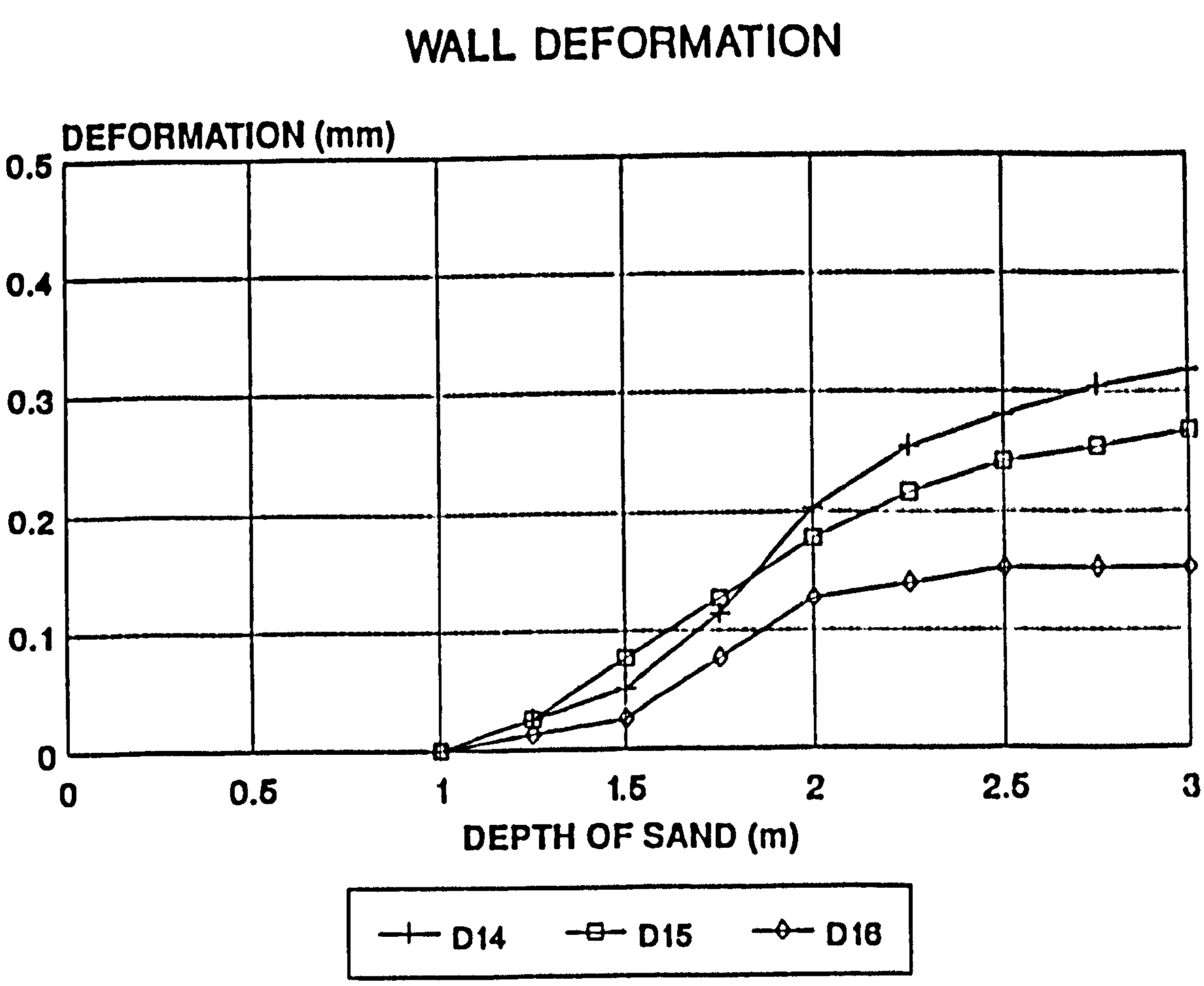

Figure 8.24

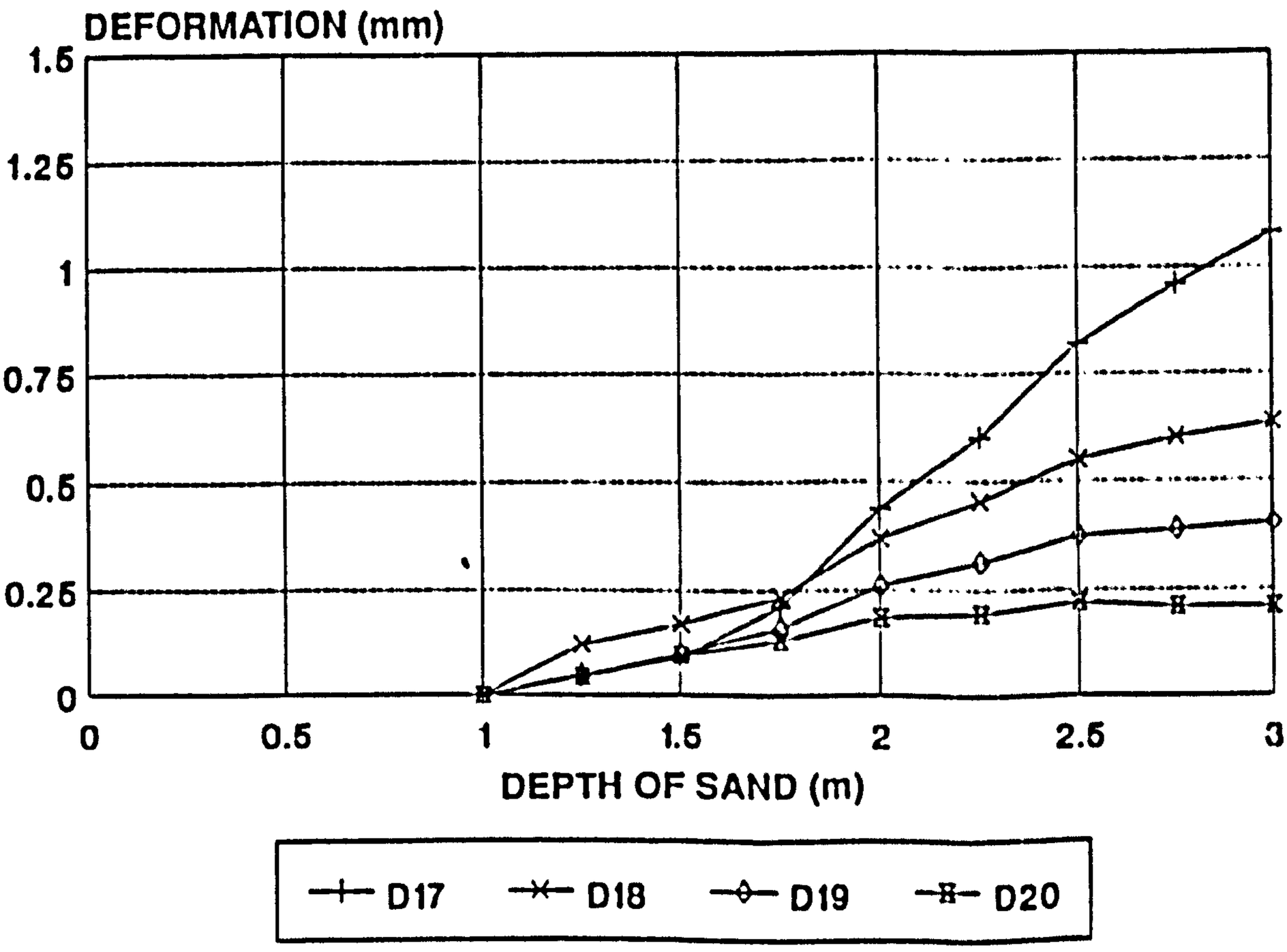

Figure 8.25

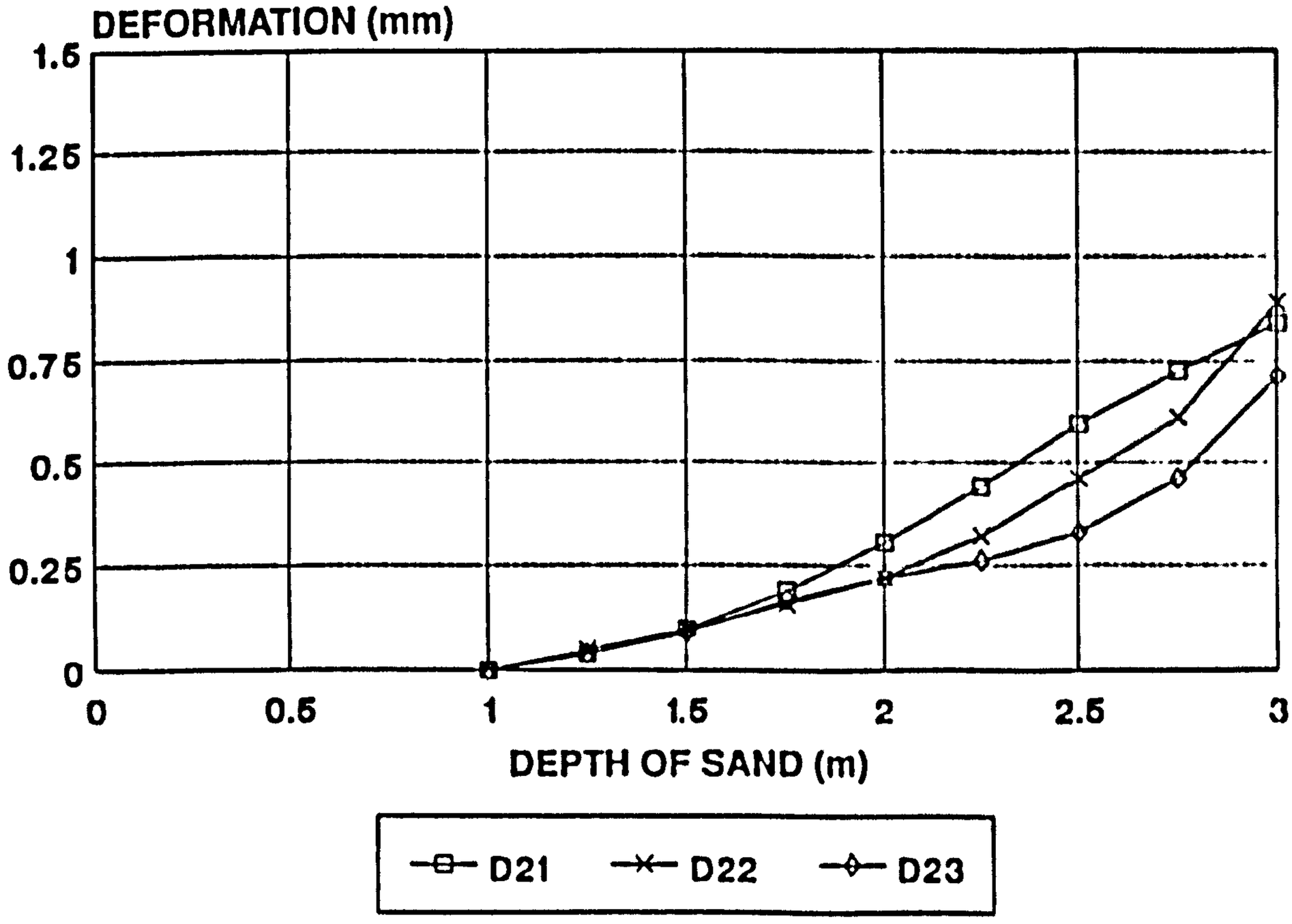
WALL DEFORMATION
DEFORMATION (mm)
1.6
1.25
1
0.75
0.5
0.25
0
0
0.5
1
1.5
2
2.5
3
DEPTH OF SAND (m)
D21
D22
D23

Figure 8.26

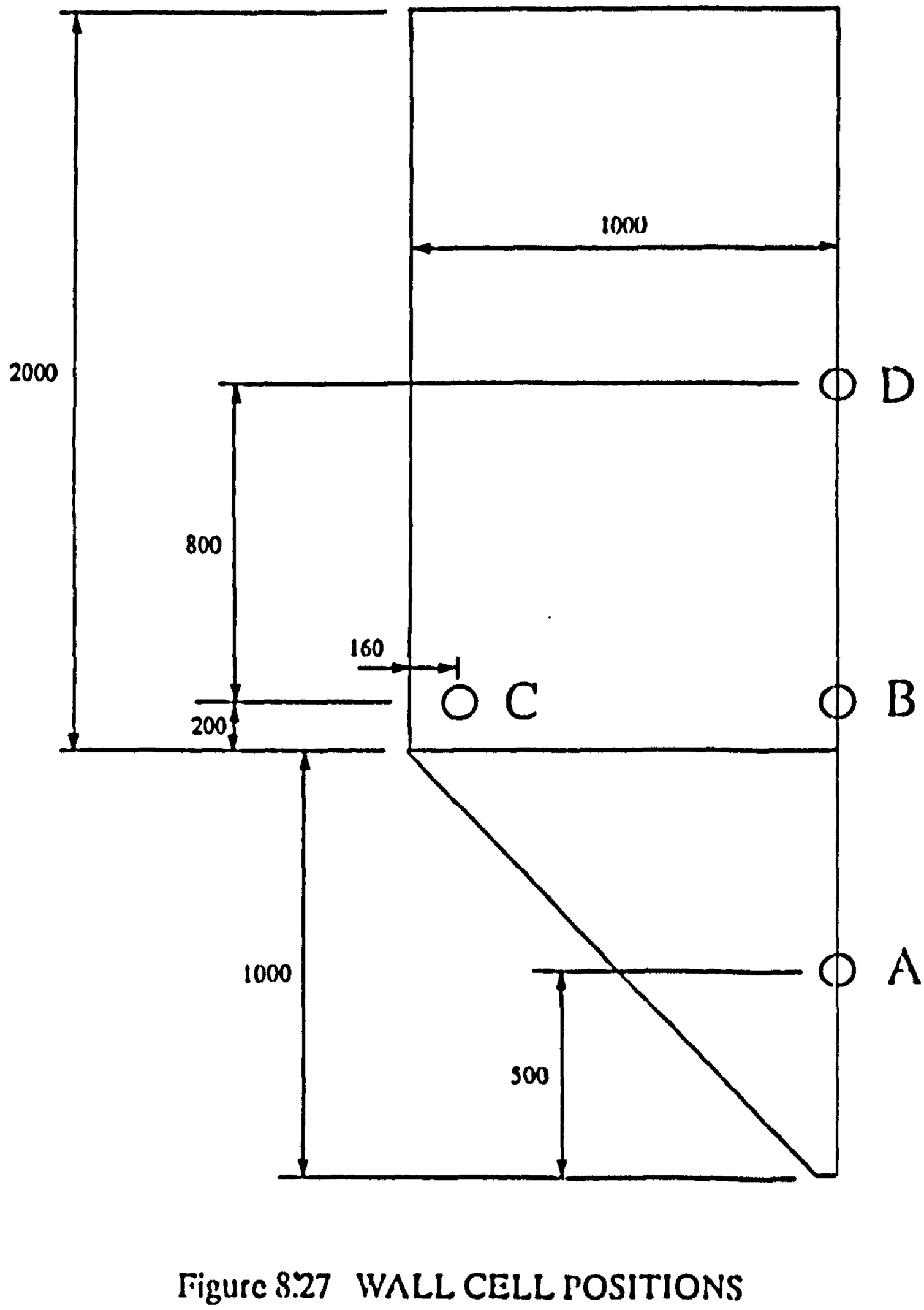

Figure 8.27 WALL CELL POSITIONS
(Dimensions in mm)

WALL CELLS - NORMAL PRESSURE
CELL A

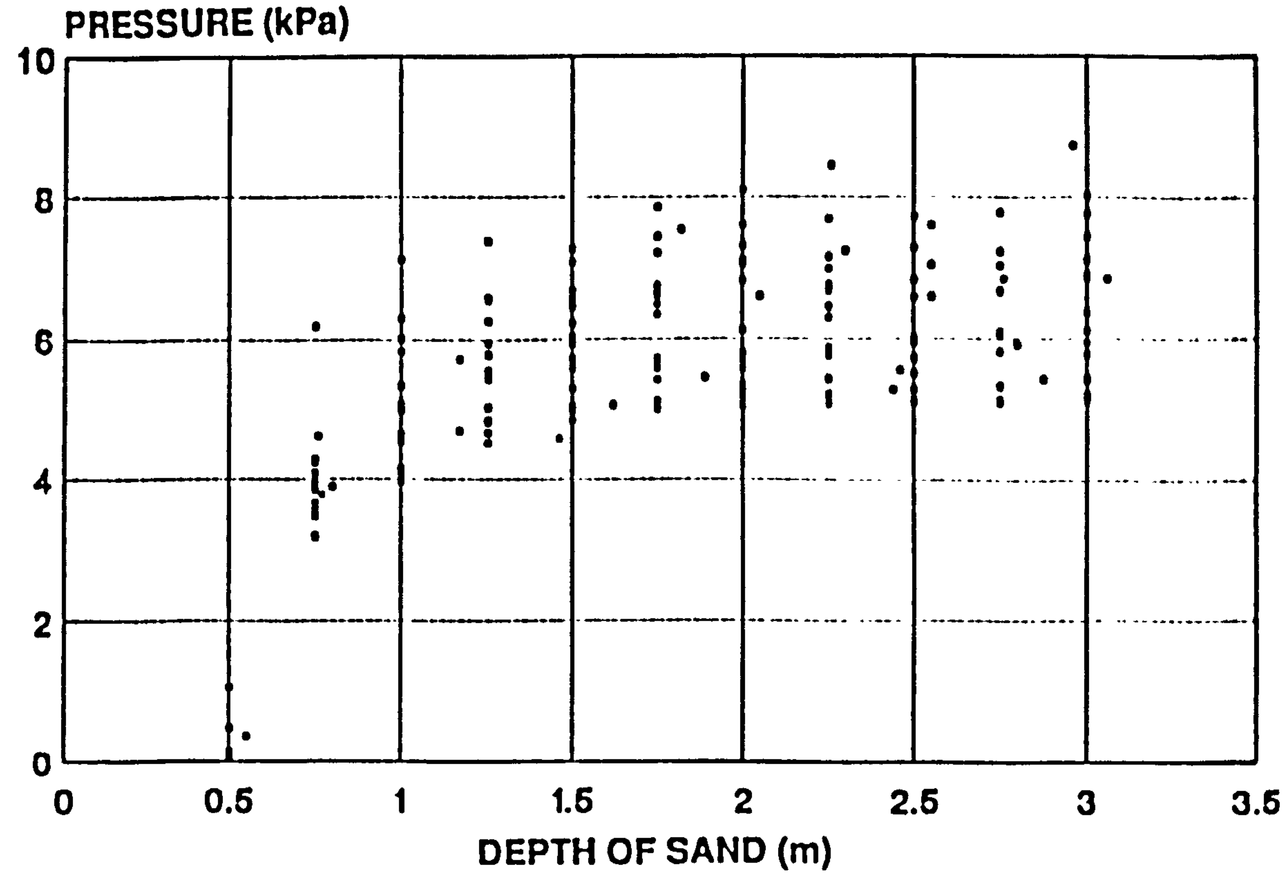

Figure 8.28

CELL B

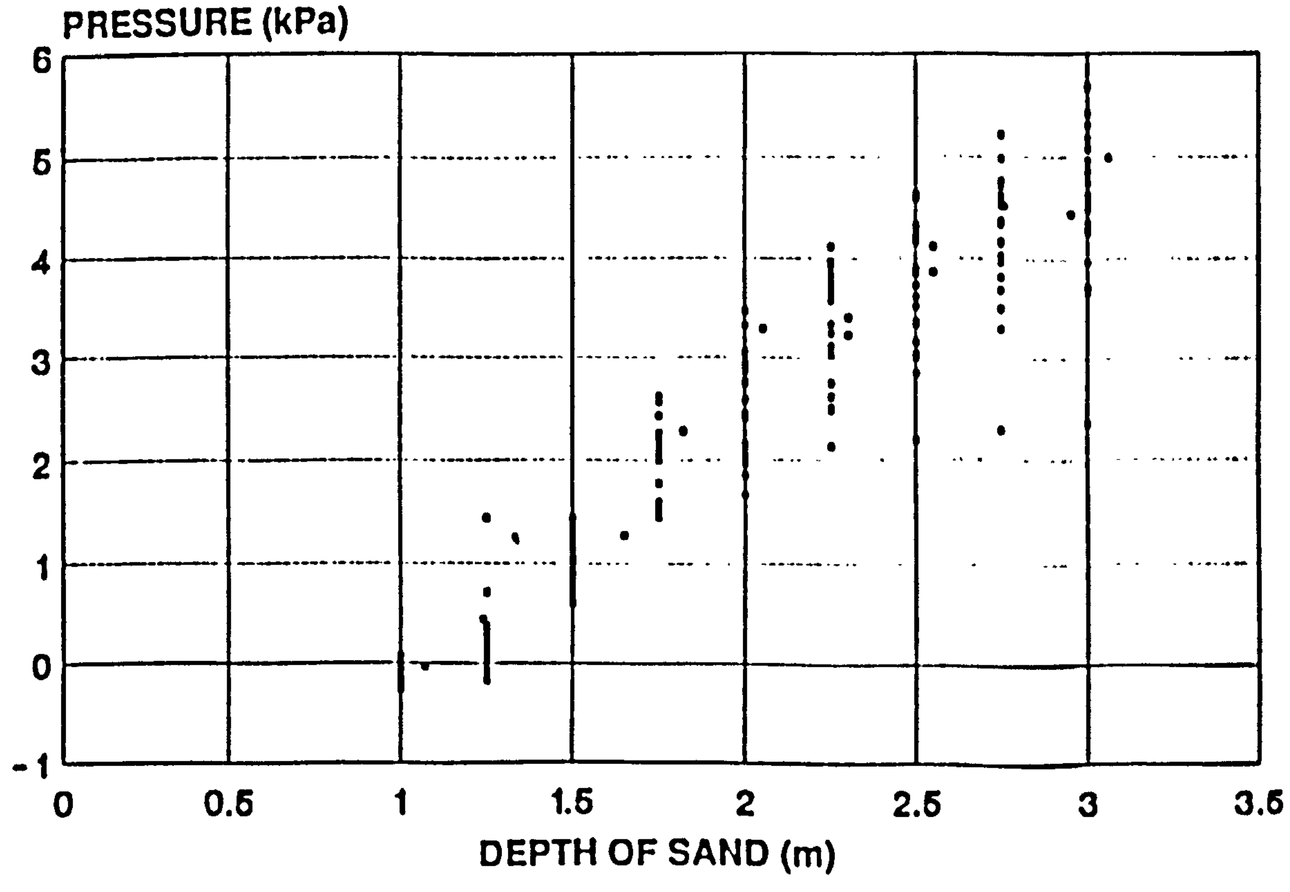

Figure 8.29

WALL CELLS - NORMAL PRESSURE
CELL C

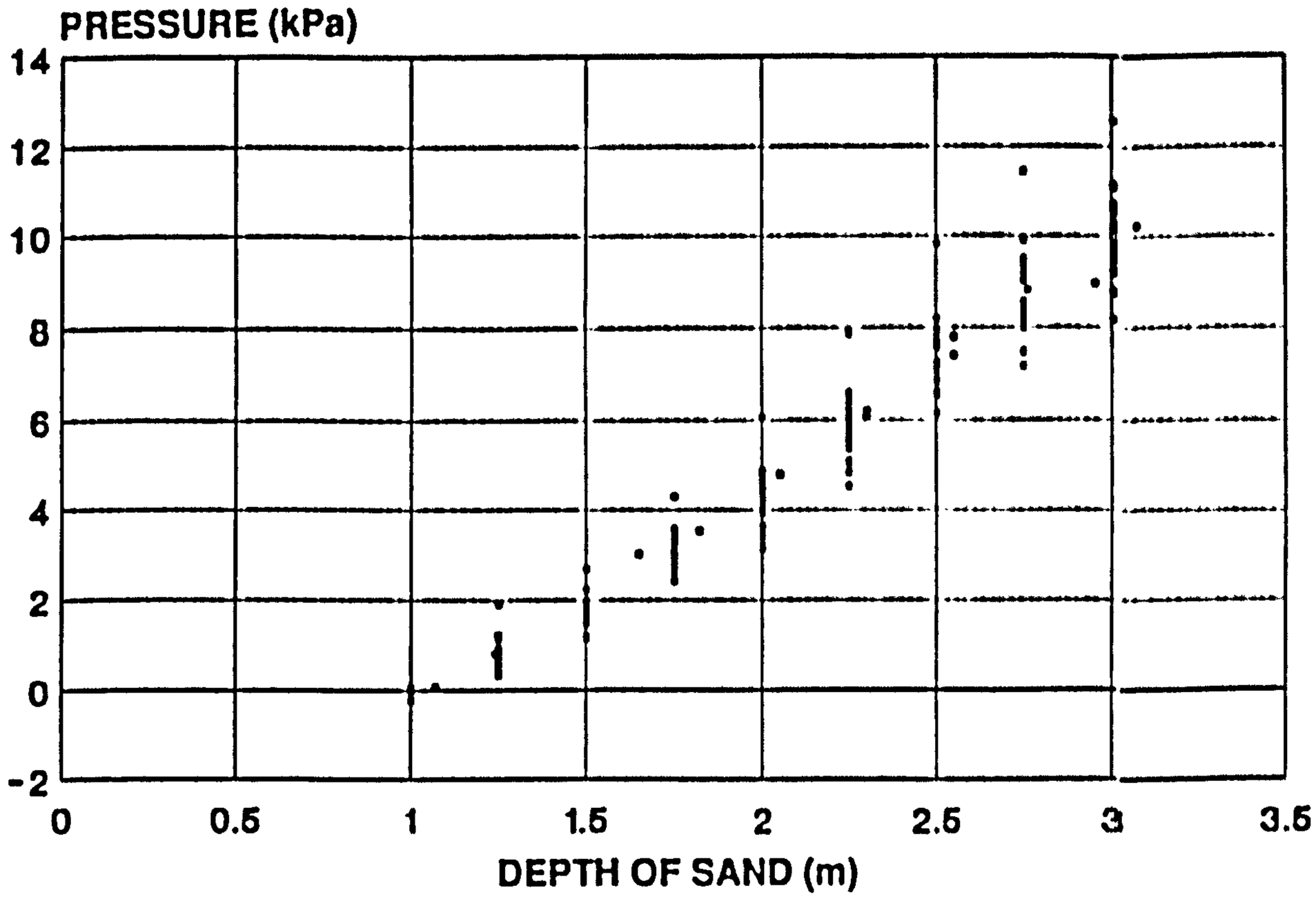

Figure 8.30

CELL D

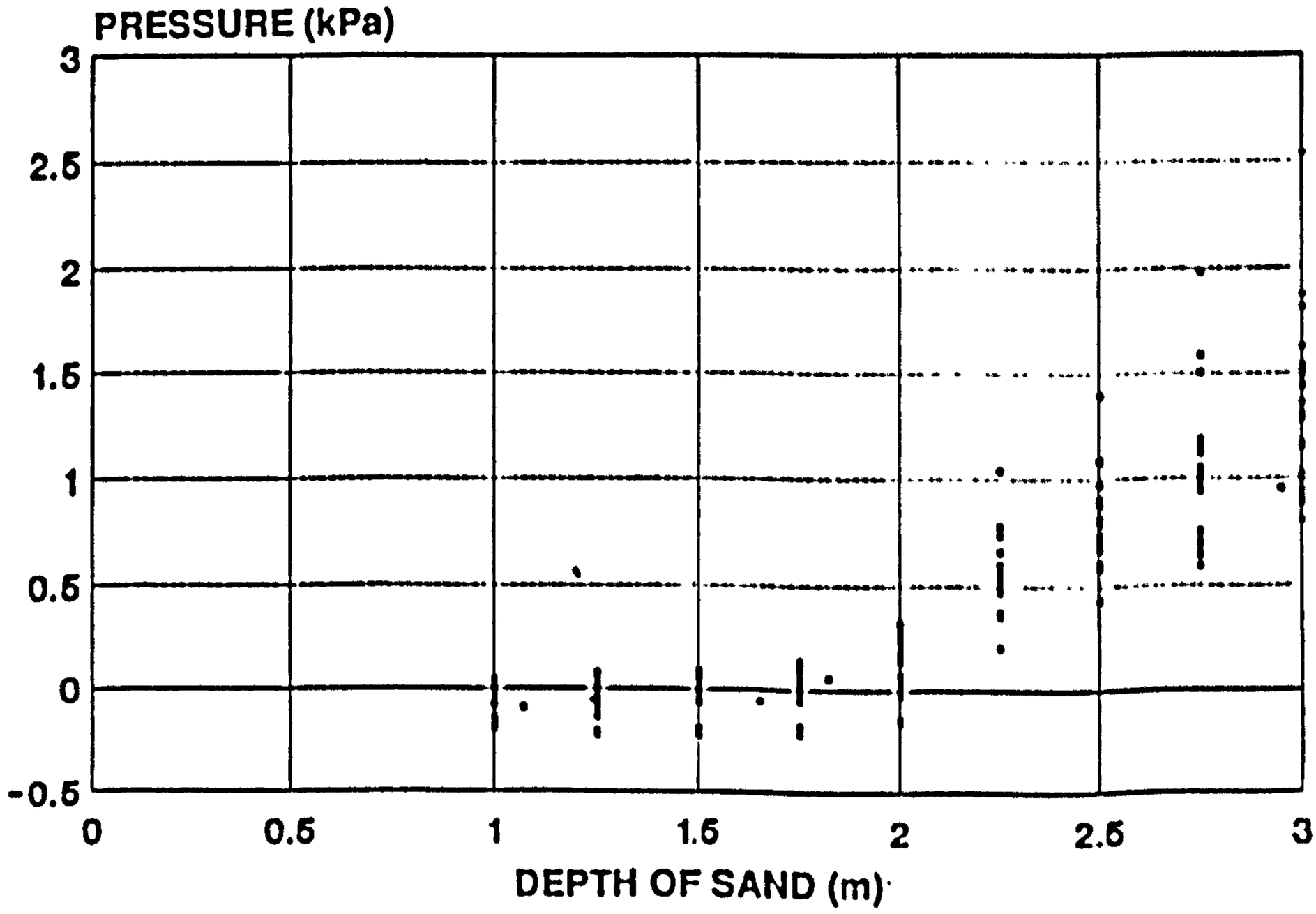

Figure 8.31

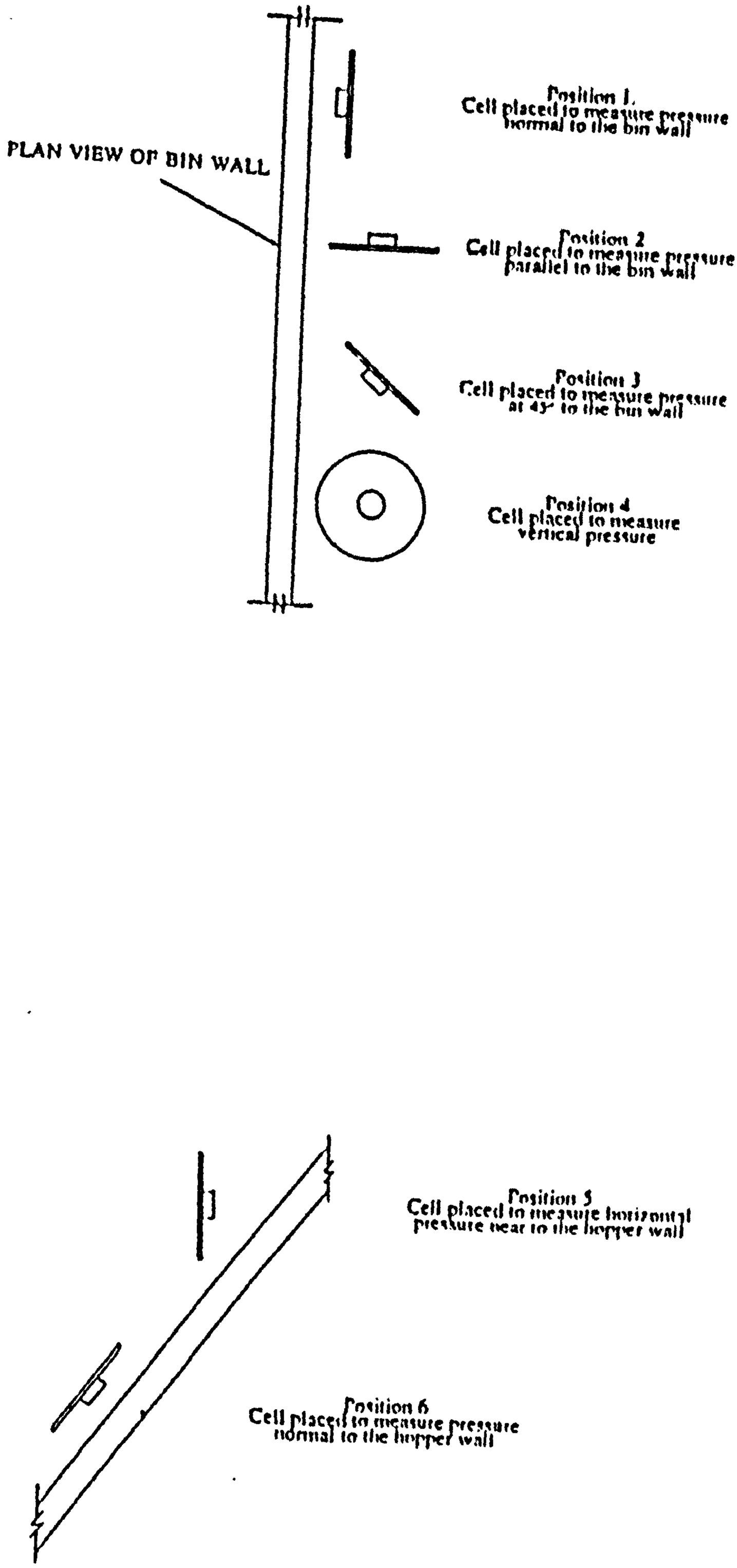

ELEVATION THROUGH THE HOPPER WALL.

Figure 8.32a CELL ORIENTATIONS

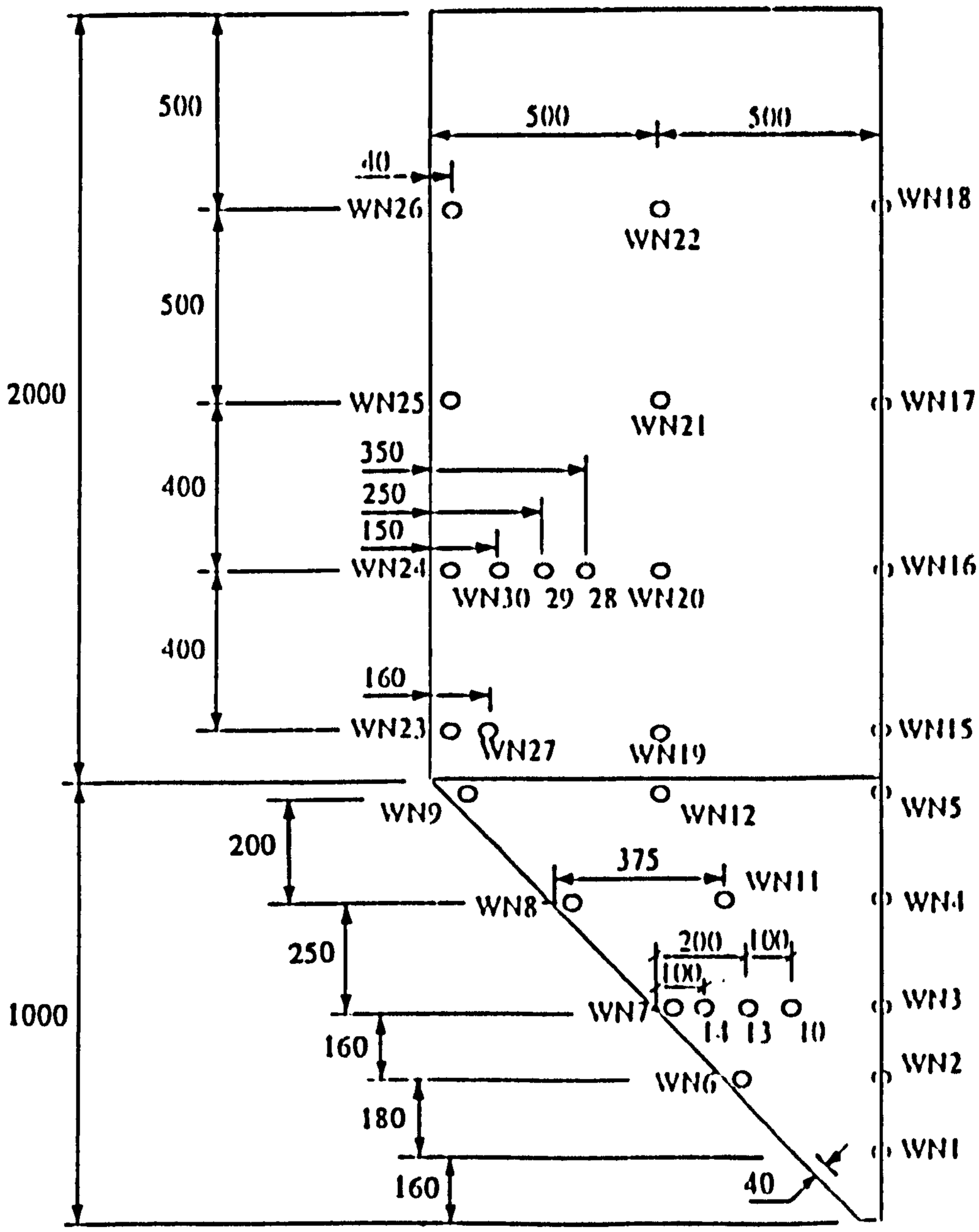

Figure 8.32b POSITIONS OF EMBEDDED CELLS PLACED TO MEASURE PRESSURE NORMAL TO THE WALL
(Dimensions in mm)

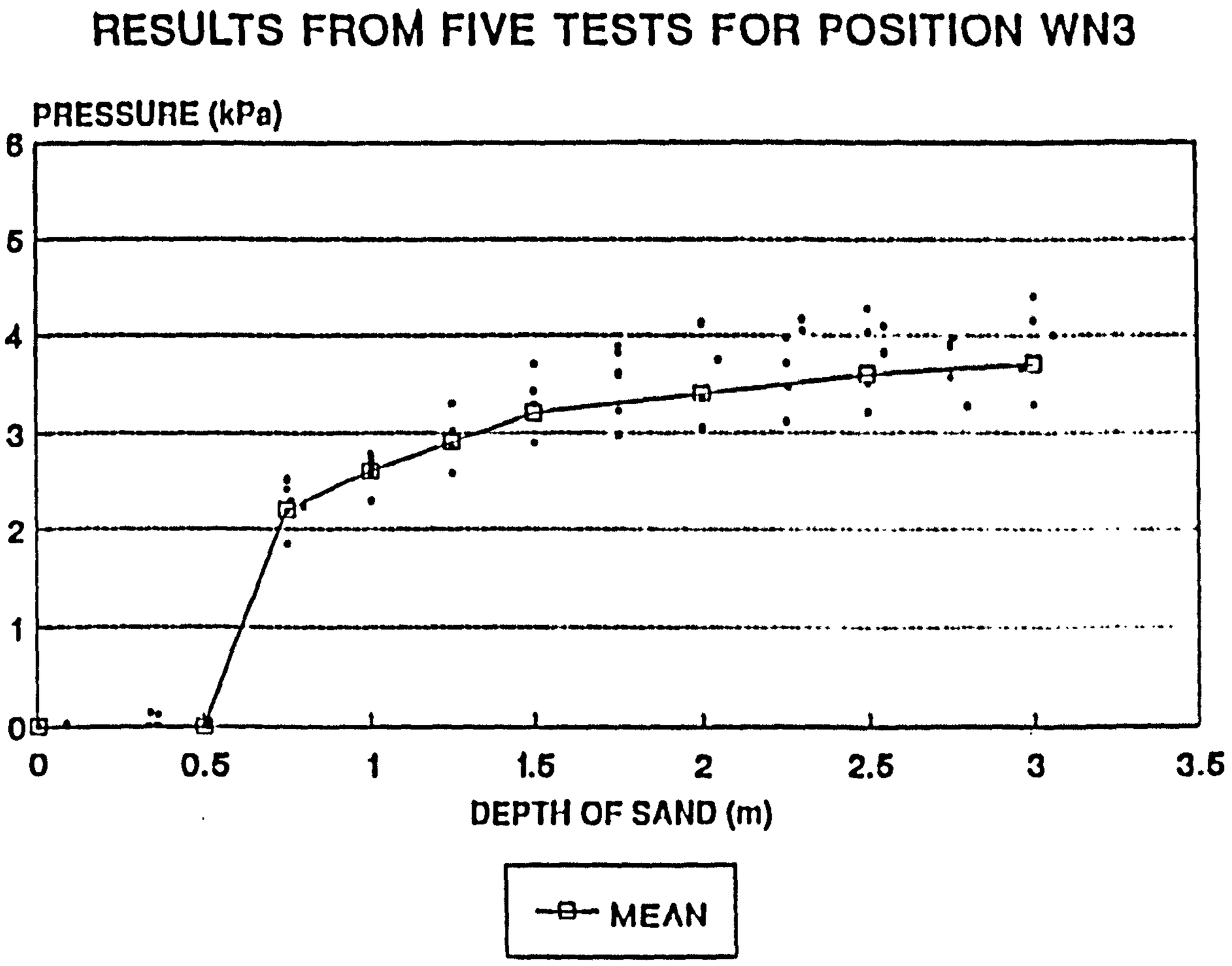
RESULTS FROM FIVE TESTS FOR POSITION WN3
PRESSURE (kPa)
6
5
4
3
2
1
0
0
0.5
1
1.5
2
2.5
3
3.5
DEPTH OF SAND (m)
MEAN

Figure 8.33

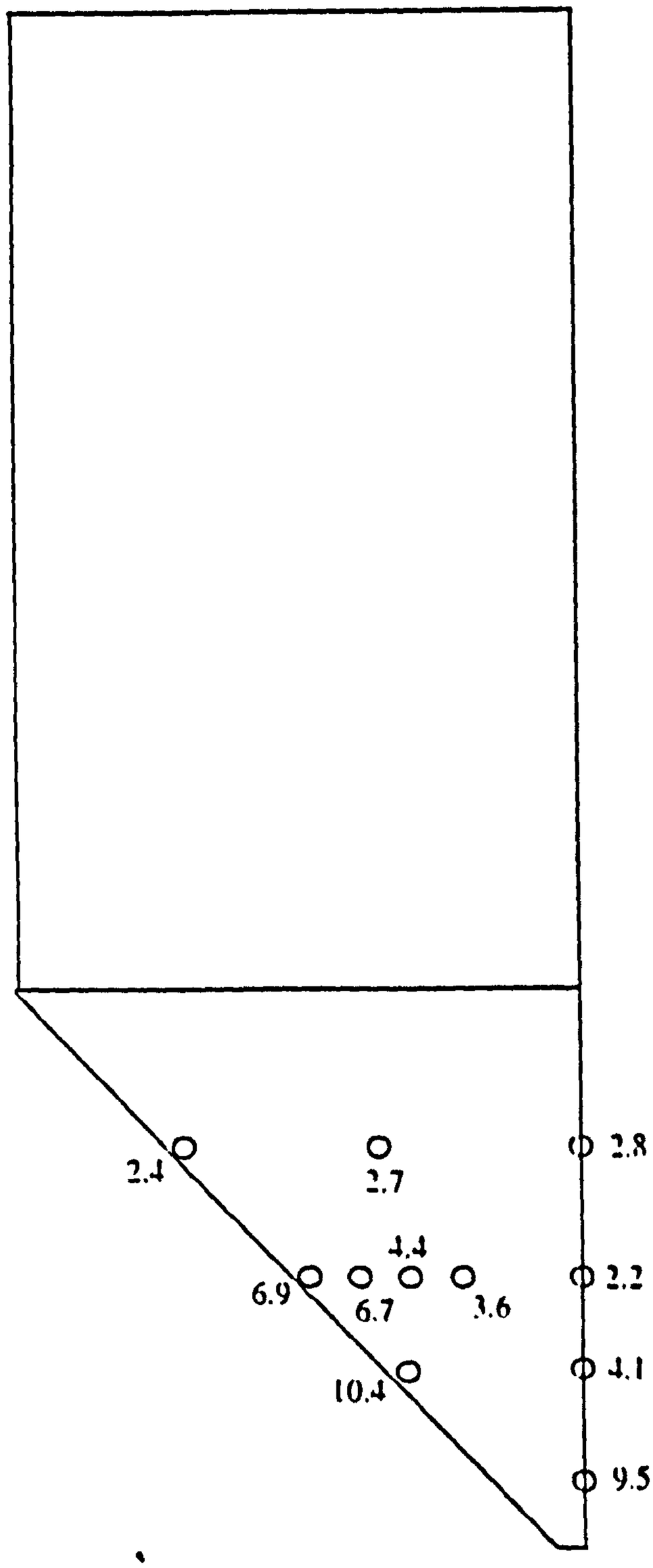

Figure 8.34 PRESSURES NORMAL TO THE WALL (kPa) 1.0 m OF SAND

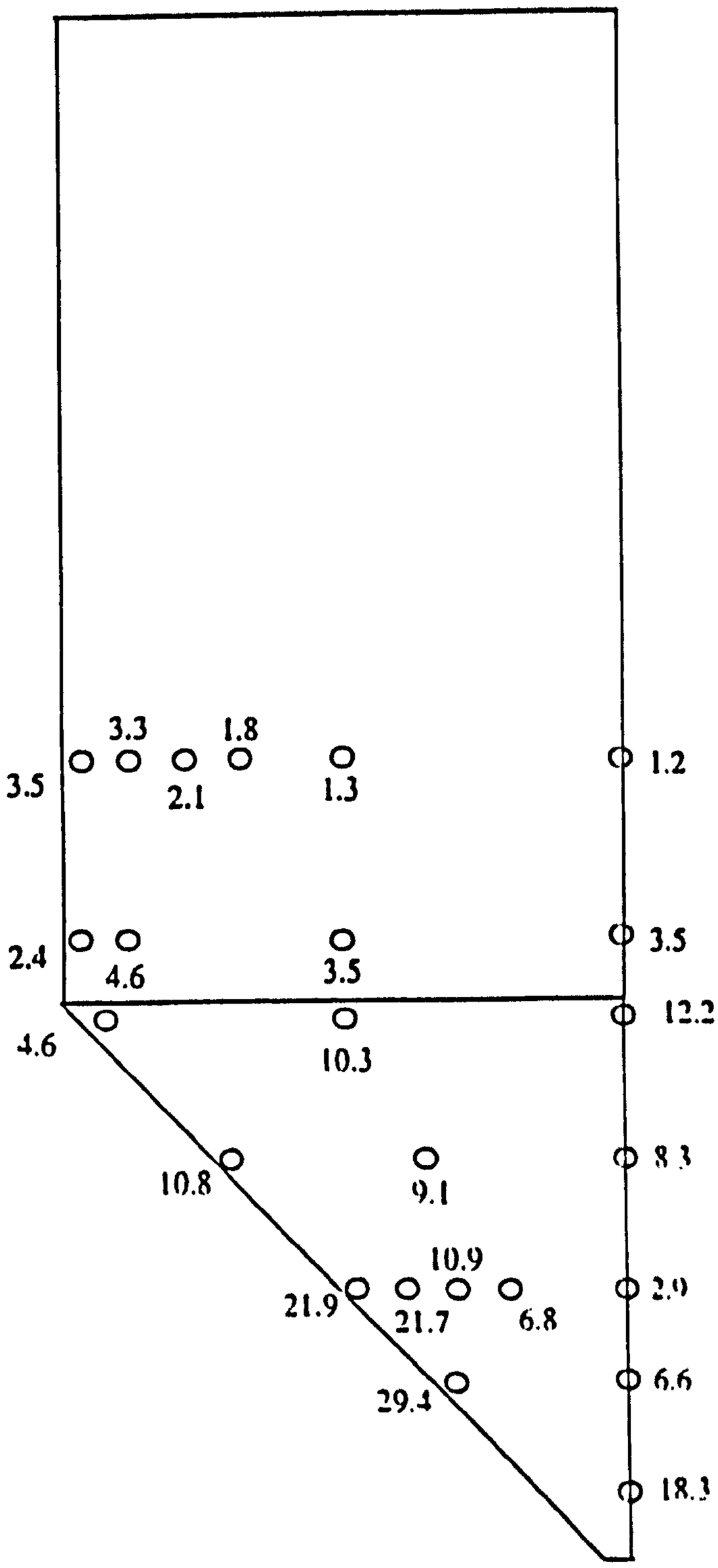

Figure 8.35 PRESSURES NORMAL TO THE WALL (kPa) 2.0 m OF SAND

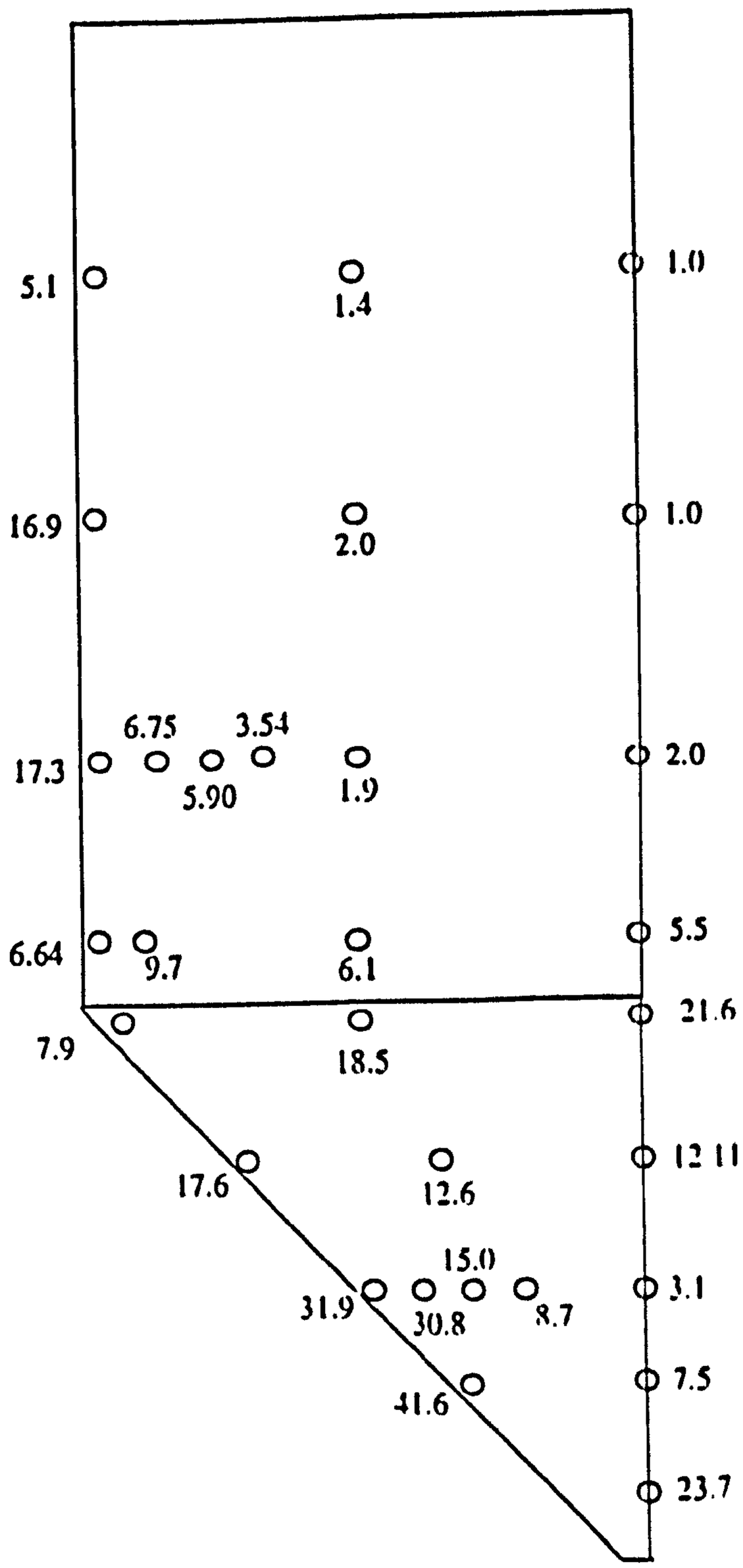

Figure 8.36 PRESSURES NORMAL TO THE WALL (kPa) 3.0 m OF SAND

NORMAL PRESSURE
SECTION A-A 500mm ABOVE THE OUTLET

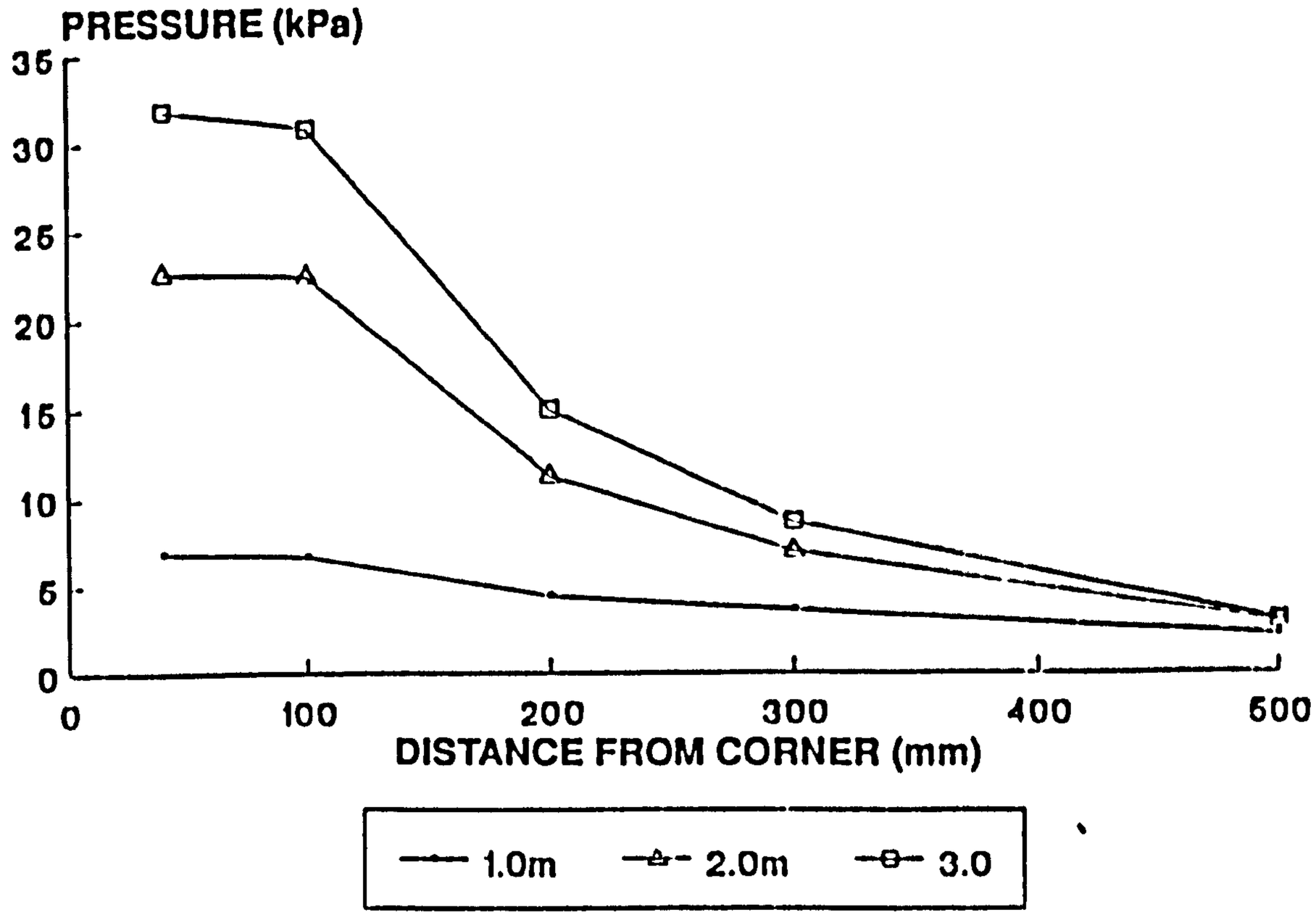

Figure 8.37

NORMAL PRESSURE
SECTION B-B 1600mm ABOVE THE OUTLET

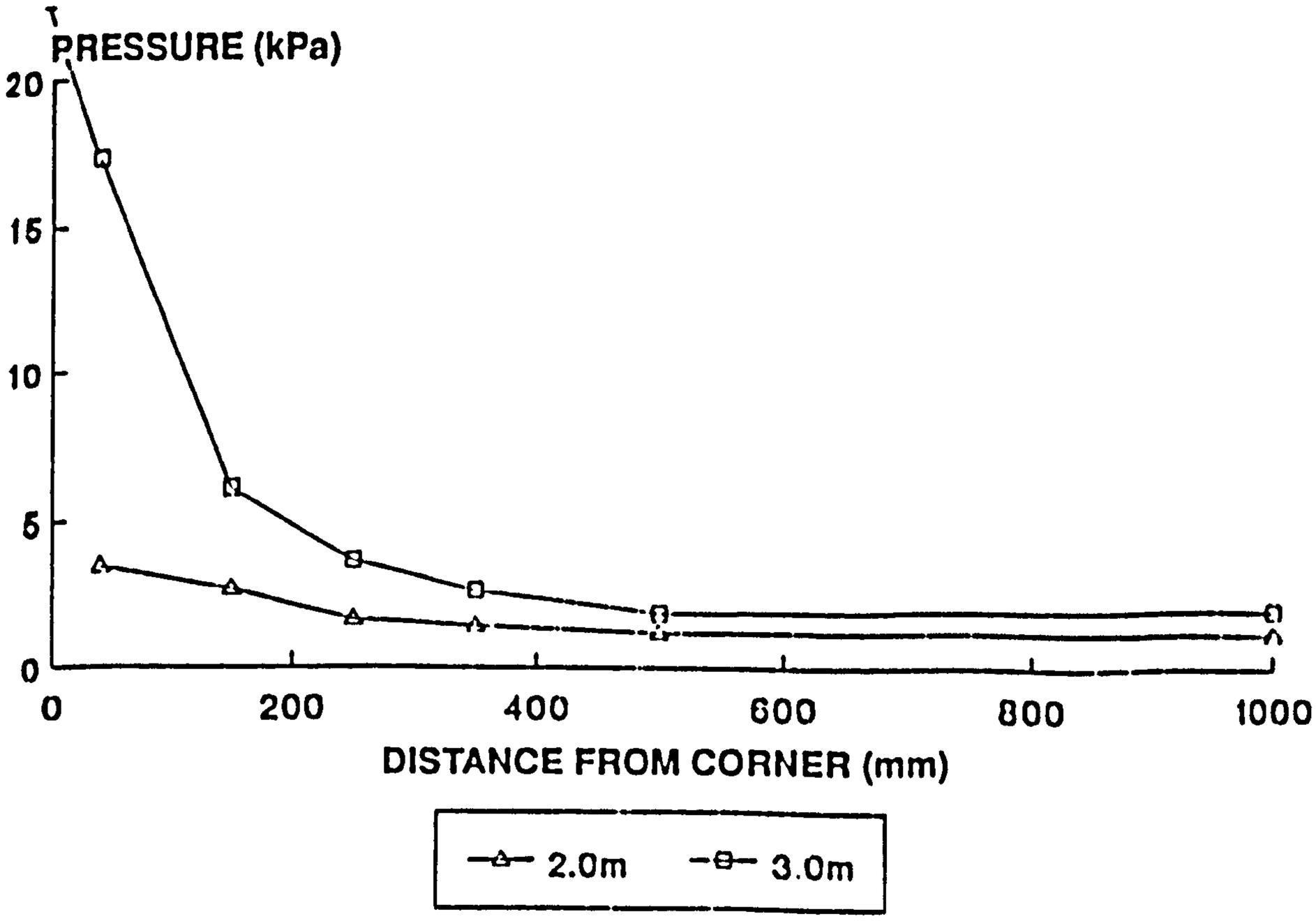

Figure 8.38

PRESSURE NORMAL TO THE WALL

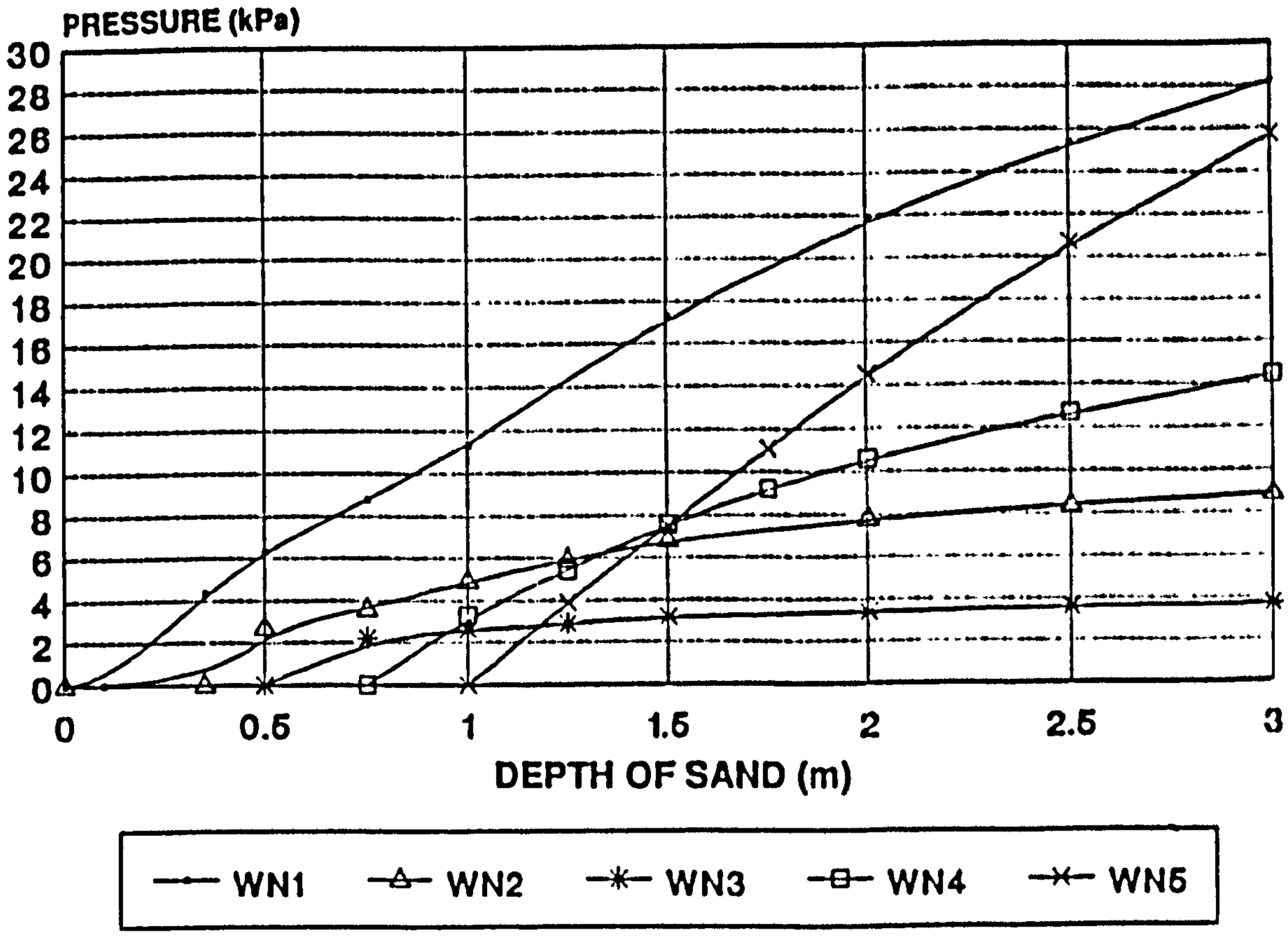

Figure 8.39

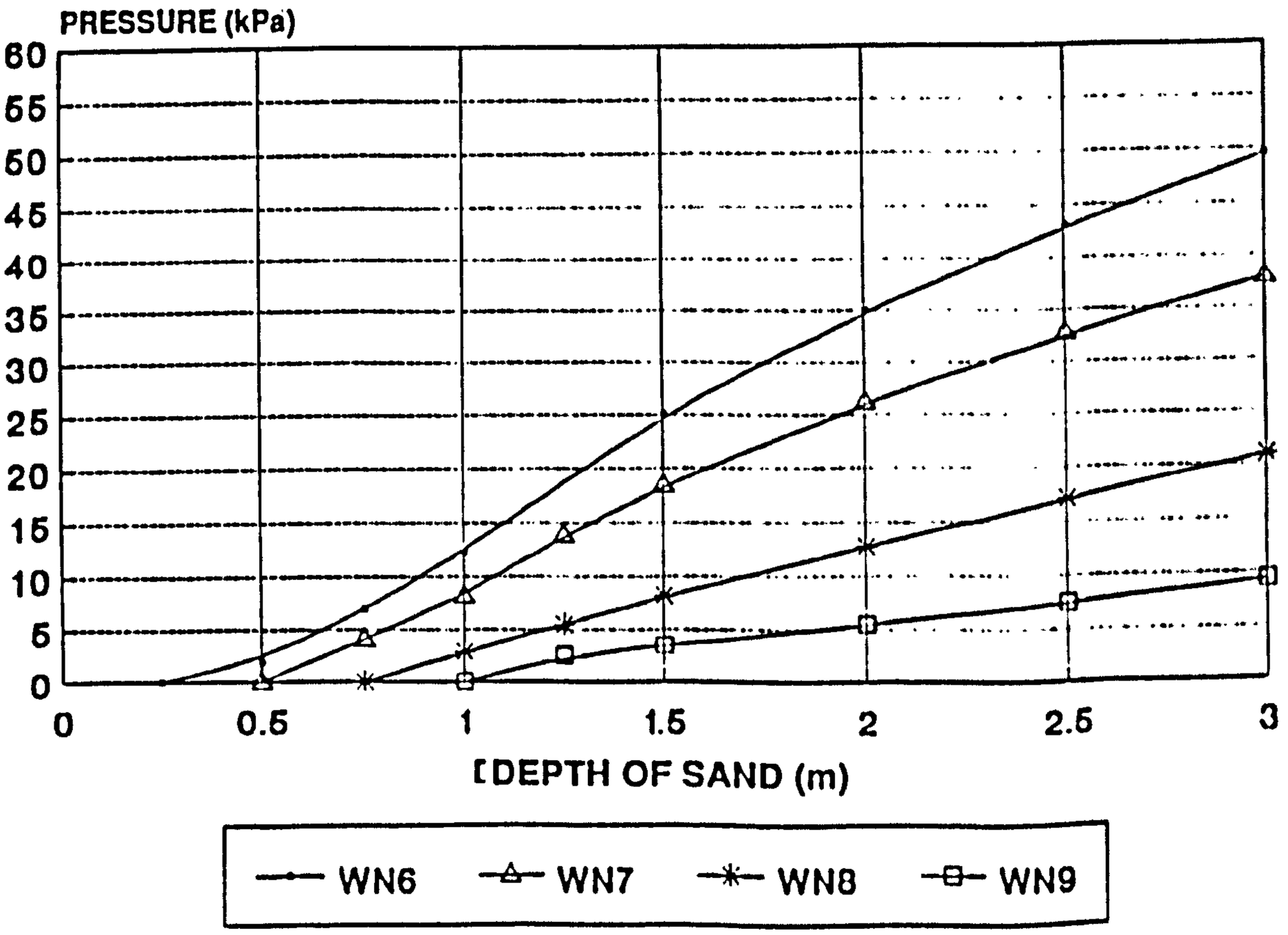

Figure 8.40

PRESSURE NORMAL TO THE WALL

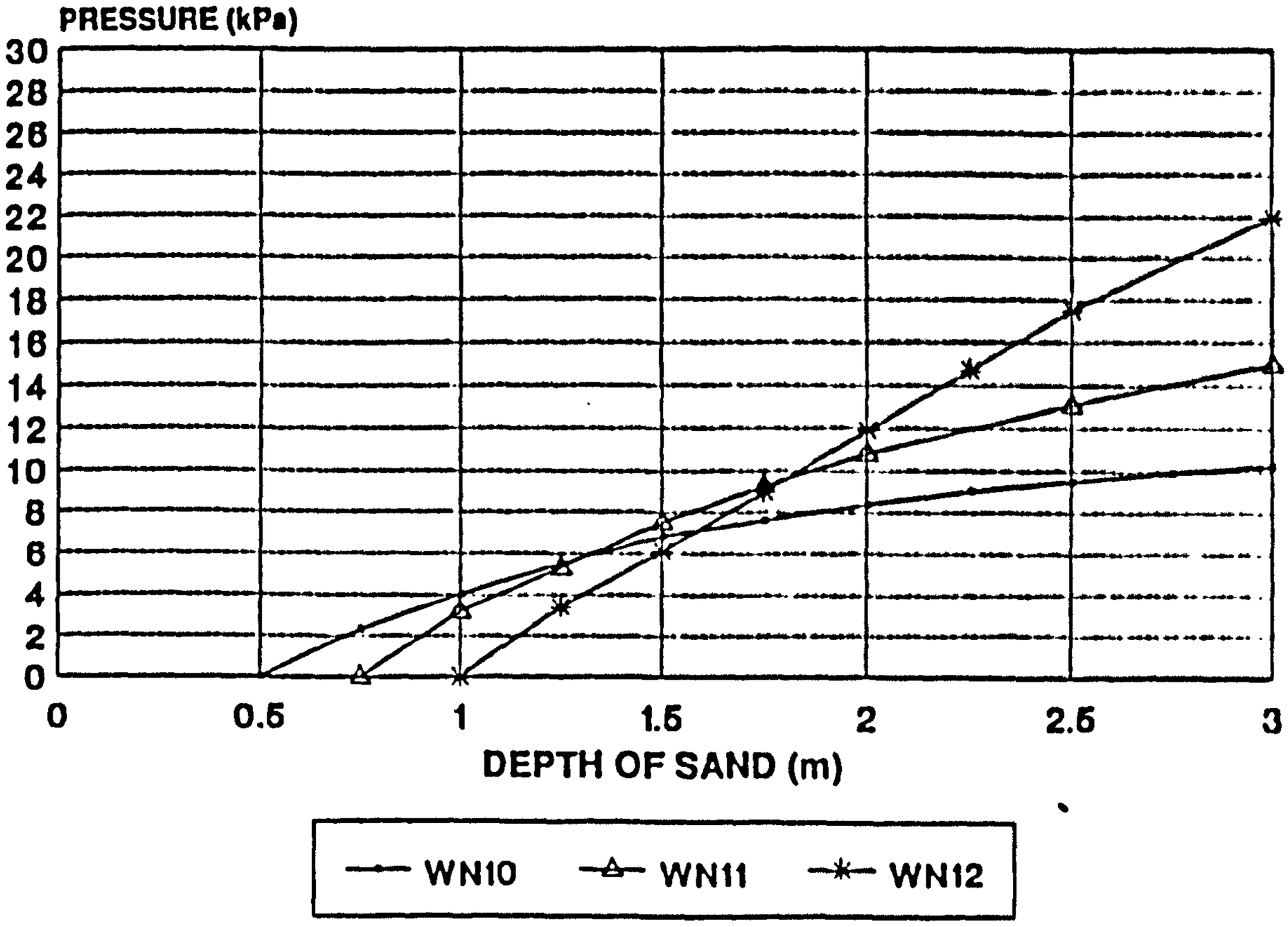

Figure 8.41

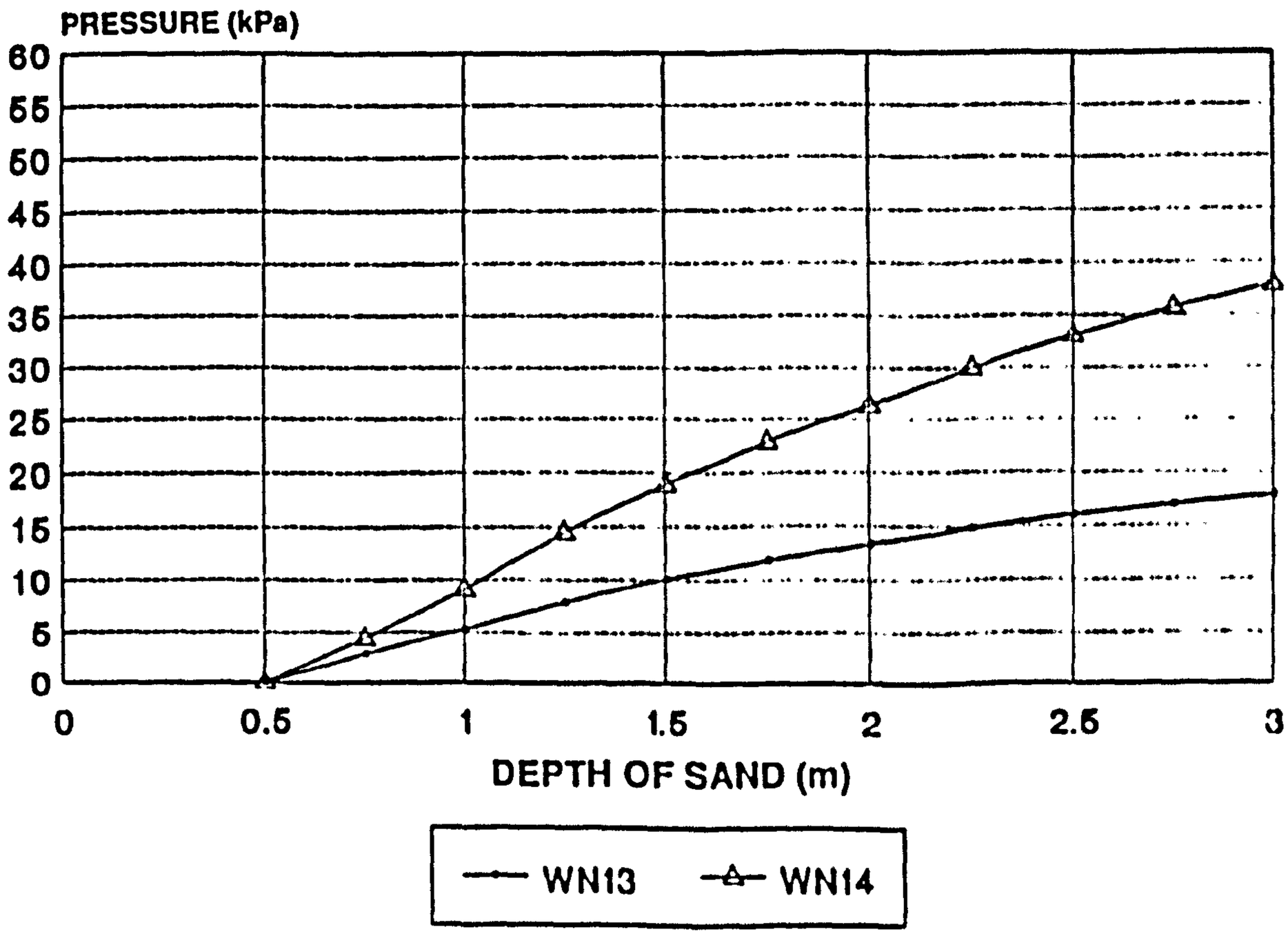

Figure 8.42

PRESSURE NORMAL TO THE WALL

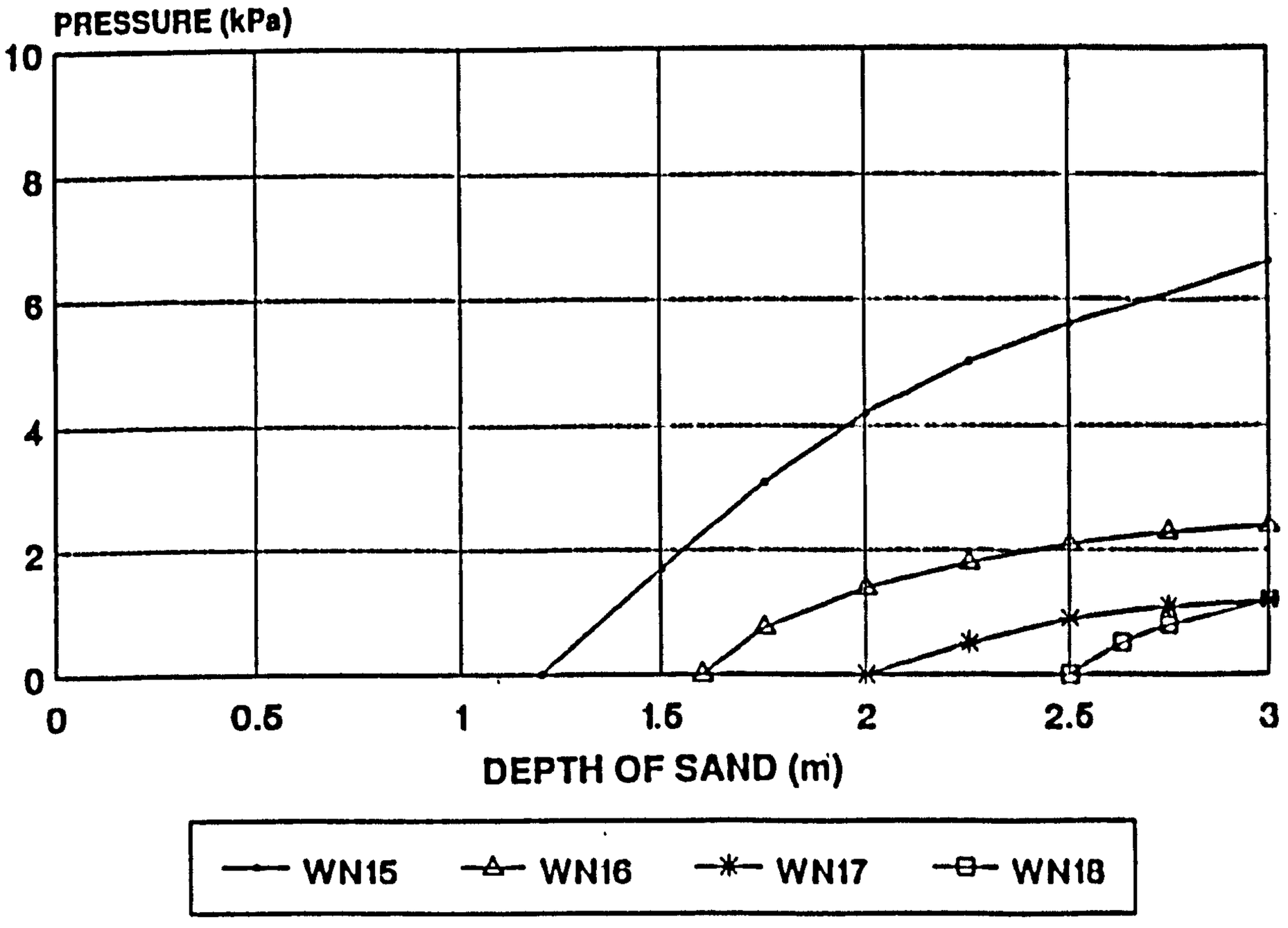

Figure 8.43

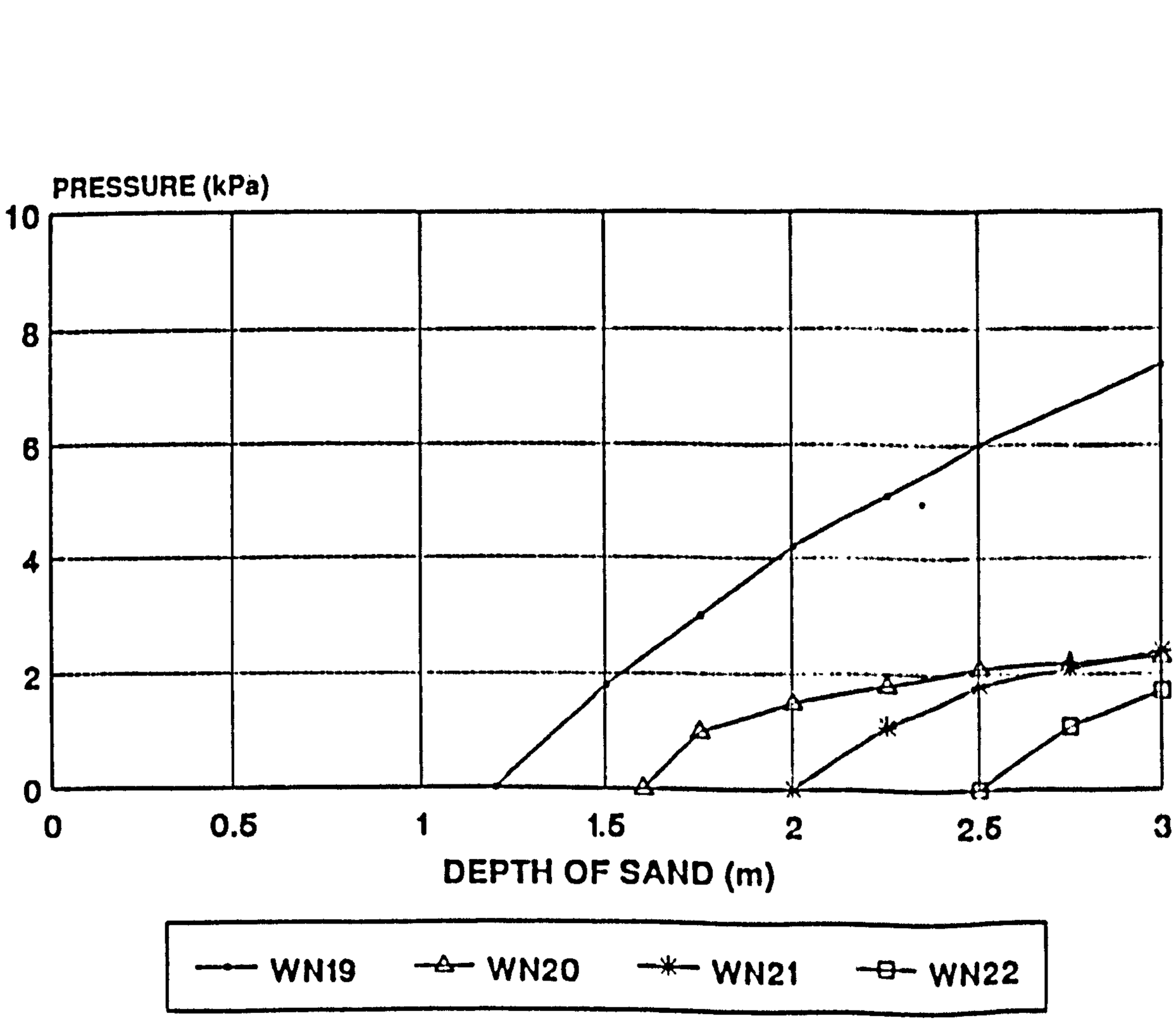

Figure 8.44

PRESSURE NORMAL TO THE WALL

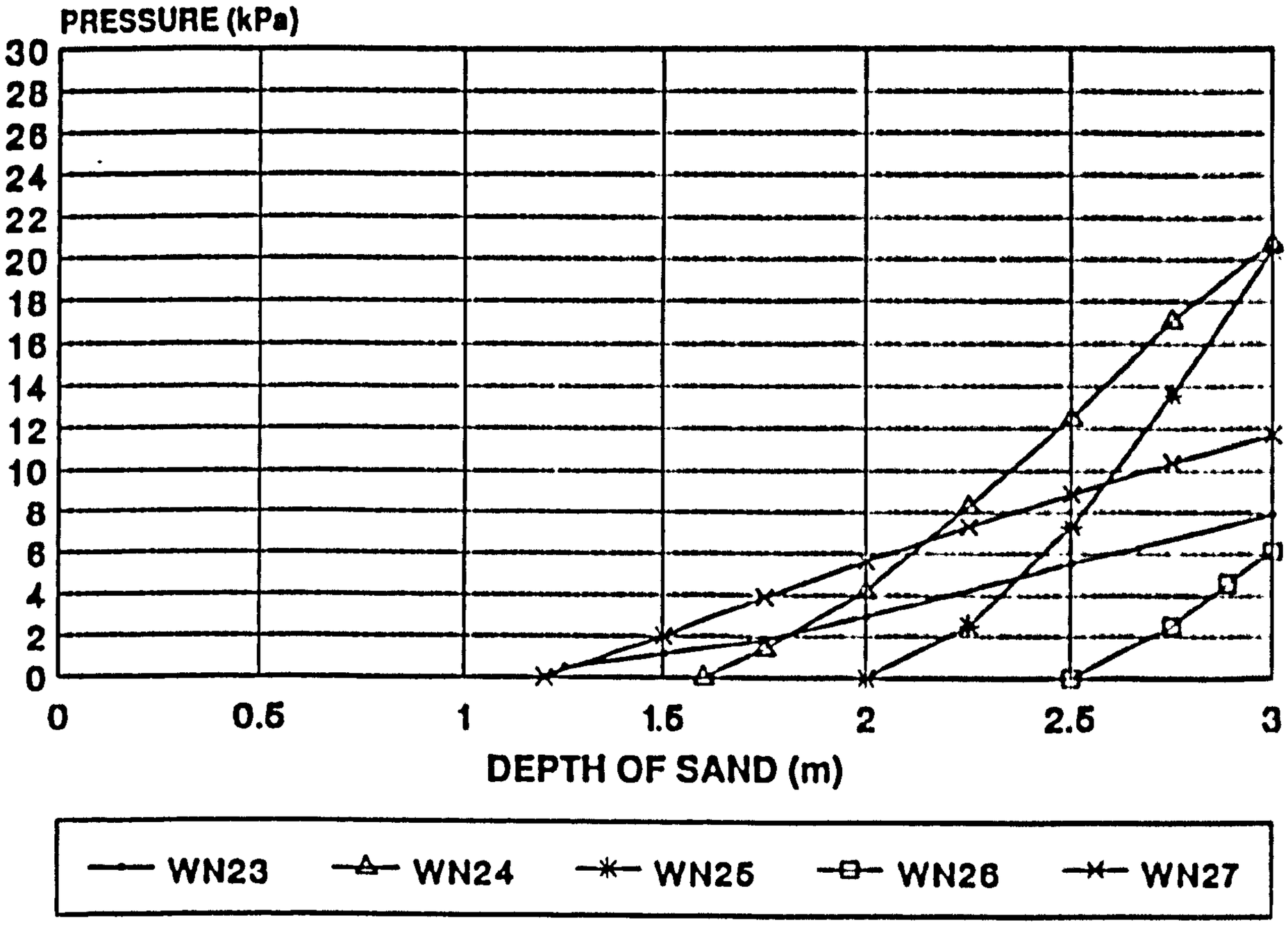

Figure 8.45

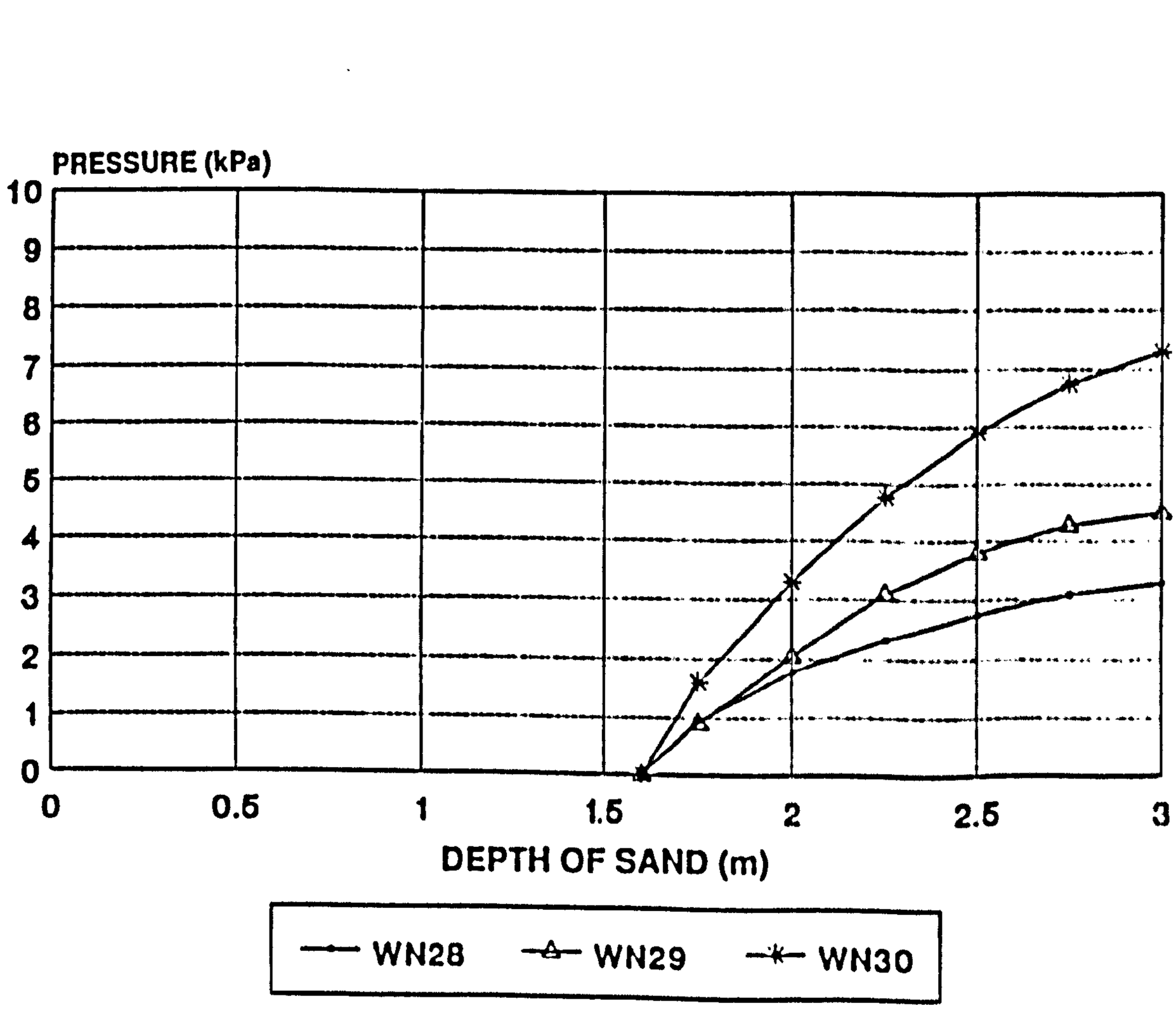

Figure 8.46

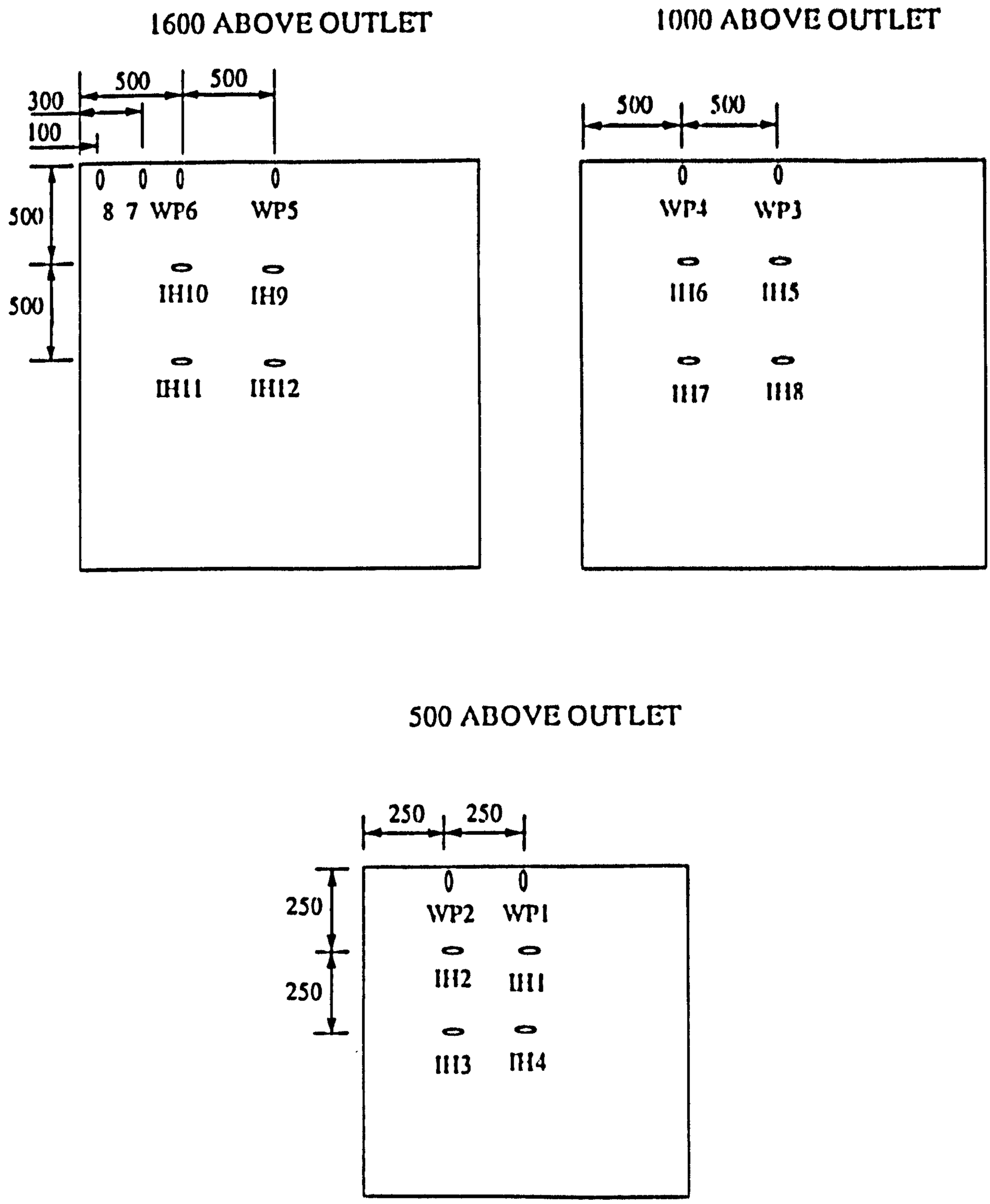

Figure 8.48 POSITIONS OF EMBEDDED CELLS PLACED TO MEASURE HORIZONTAL PRESSURE AWAY FROM THE WALL AND PARALLEL TO THE WALL
(Dimensions in mm)

500 ABOVE OUTLET

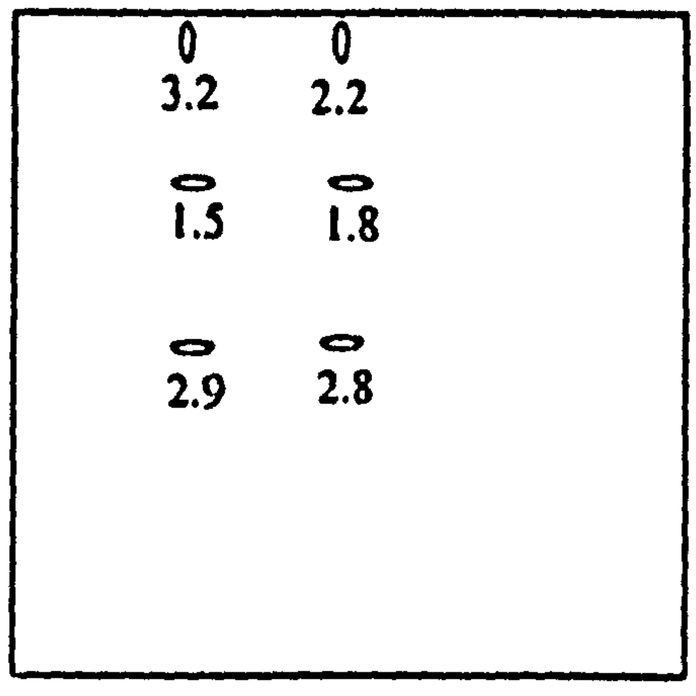

Figure 8.49 HORIZONTAL PRESSURE (kPa) 1.0 m OF SAND

1600 ABOVE OUTLET

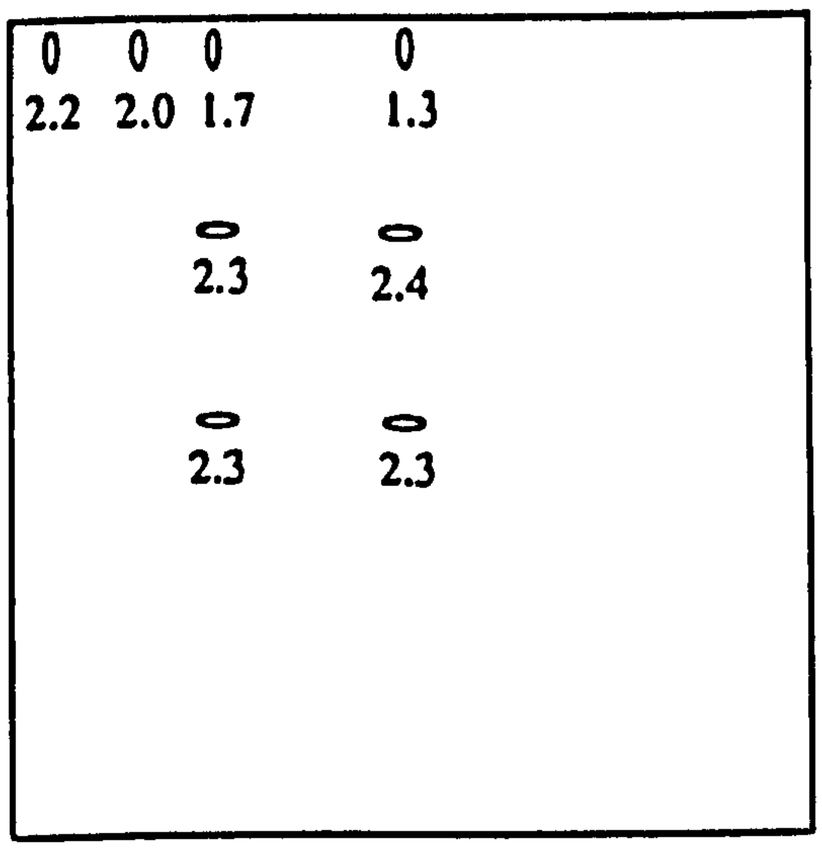

1000 ABOVE OUTLET

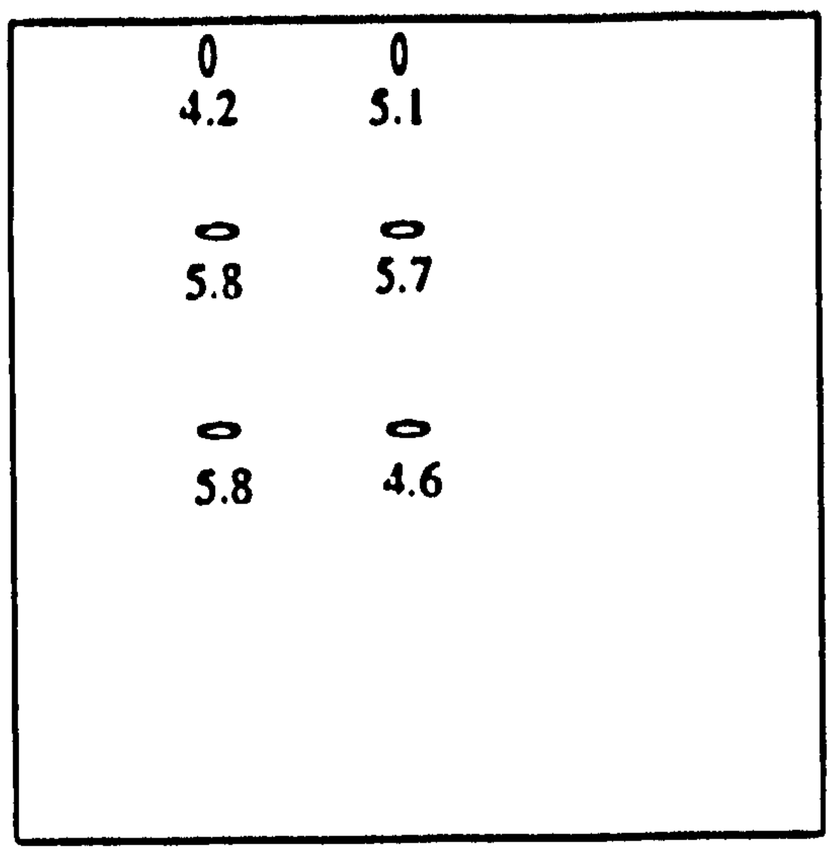

500 ABOVE OUTLET

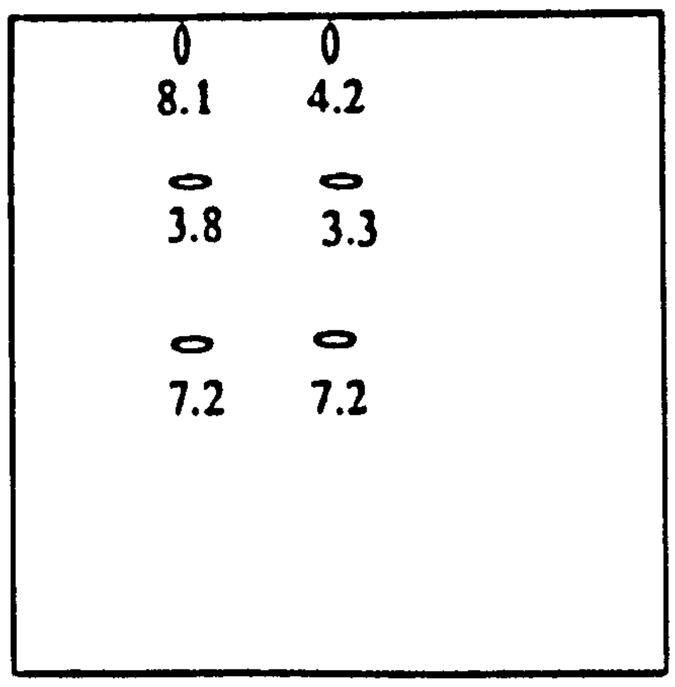

Figure 8.50 HORIZONTAL PRESSURE (kPa) 2.0 m OF SAND

1600 ABOVE OUTLET

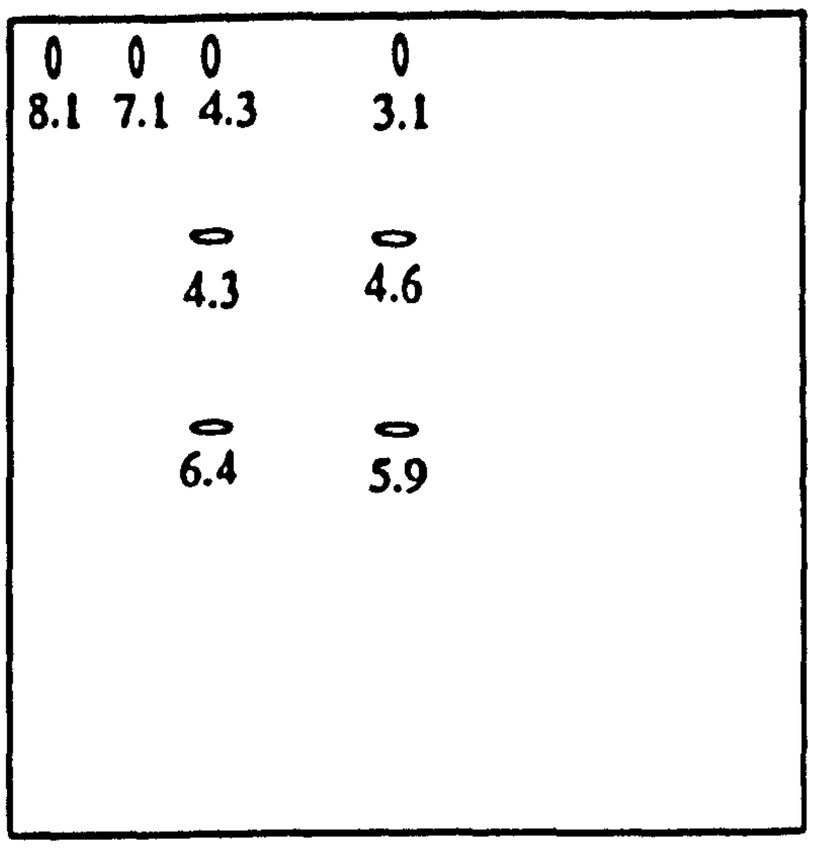

1000 ABOVE OUTLET

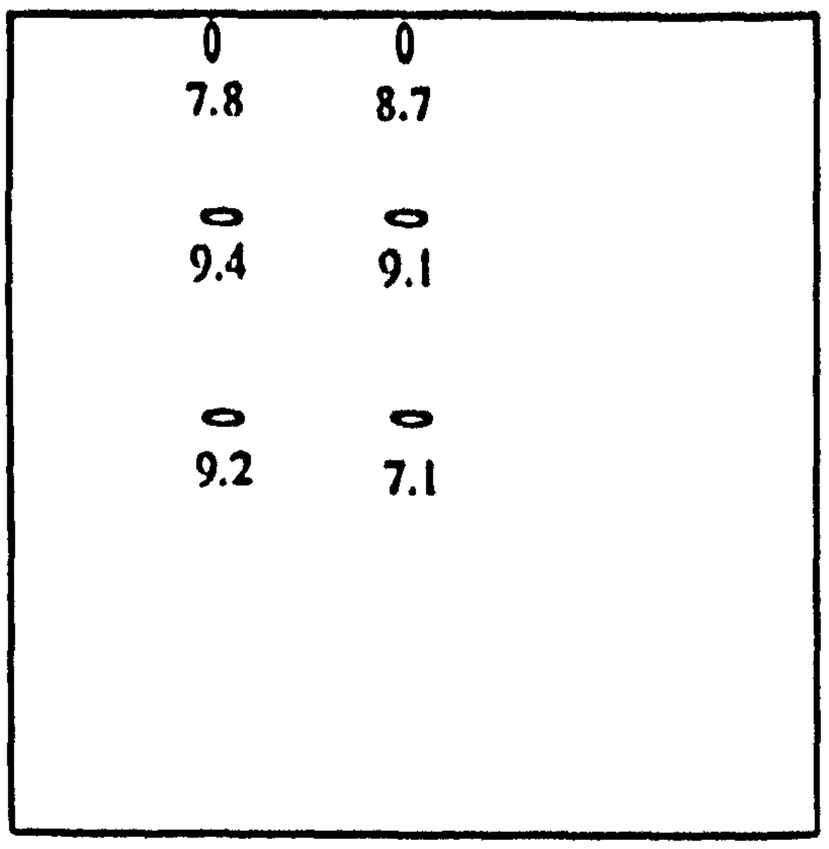

500 ABOVE OUTLET

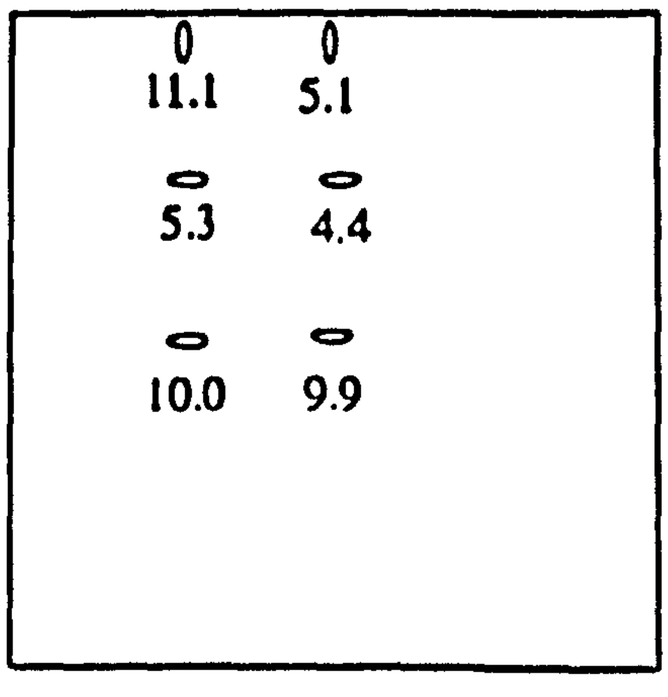

Figure 8.51 HORIZONTAL PRESSURE (kPa) 3.0 m OF SAND

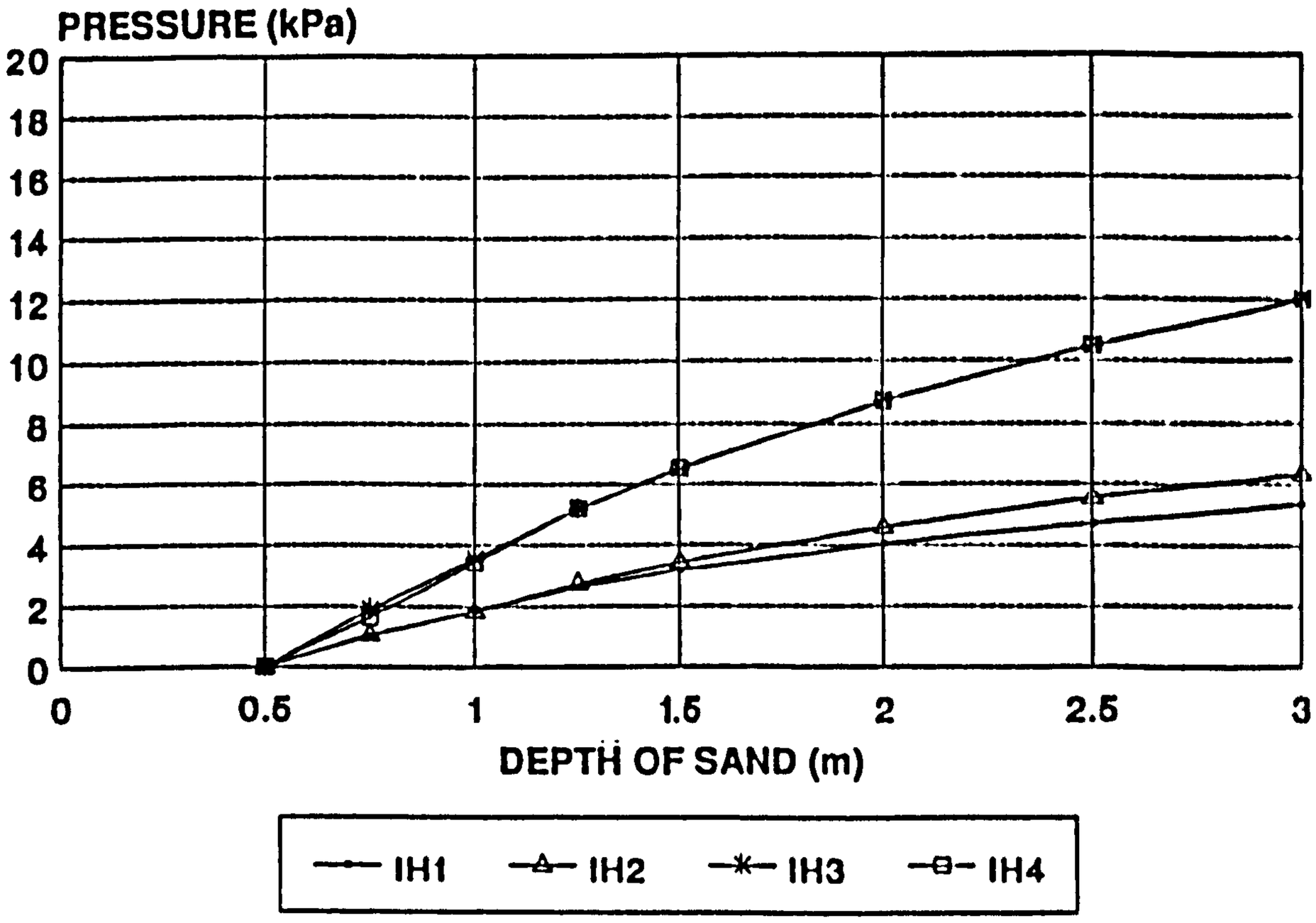

Figure 8.52

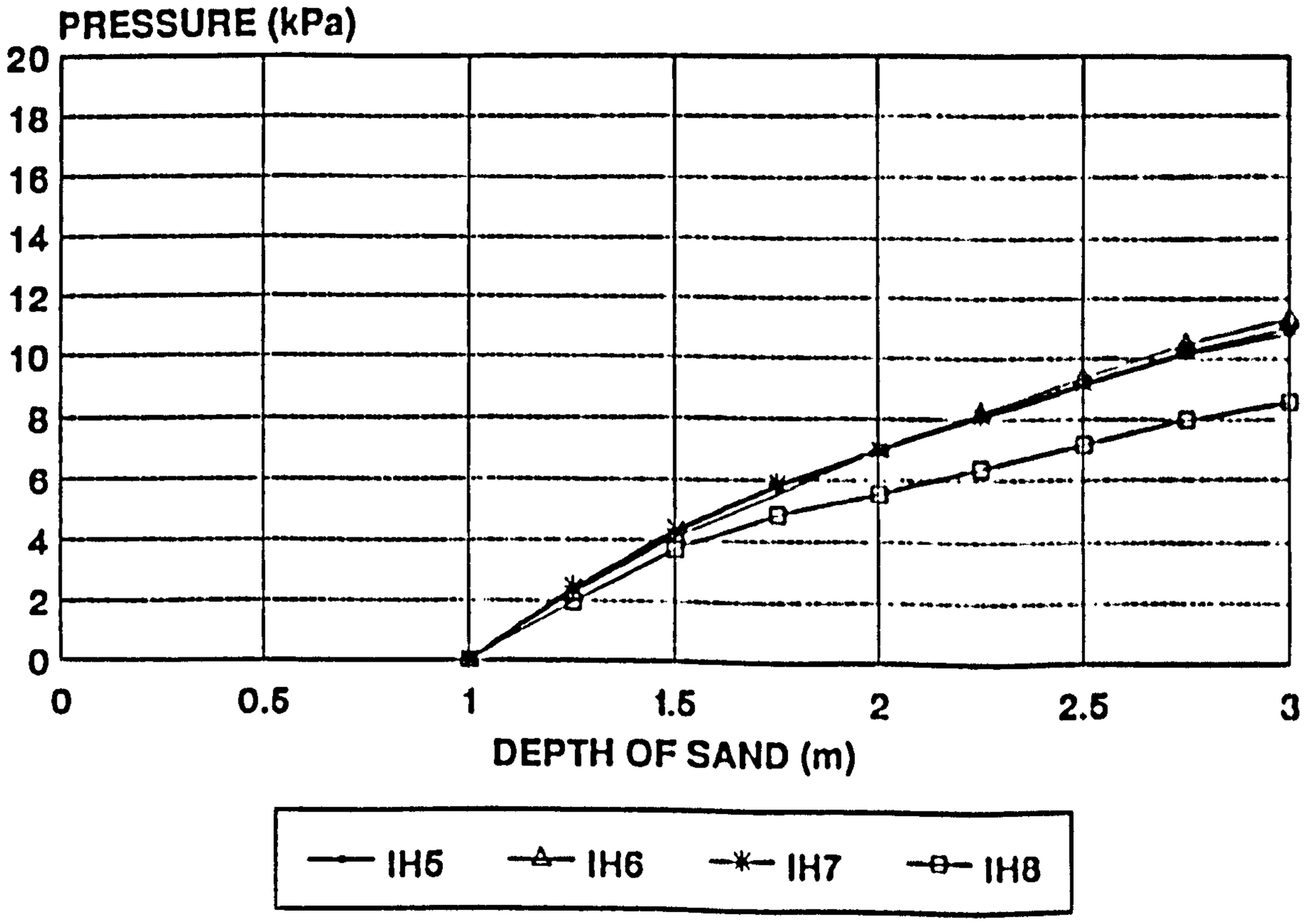

Figure 8.53

HORIZONTAL PRESSURE AWAY FROM THE WALL
1600 mm ABOVE THE OUTLET

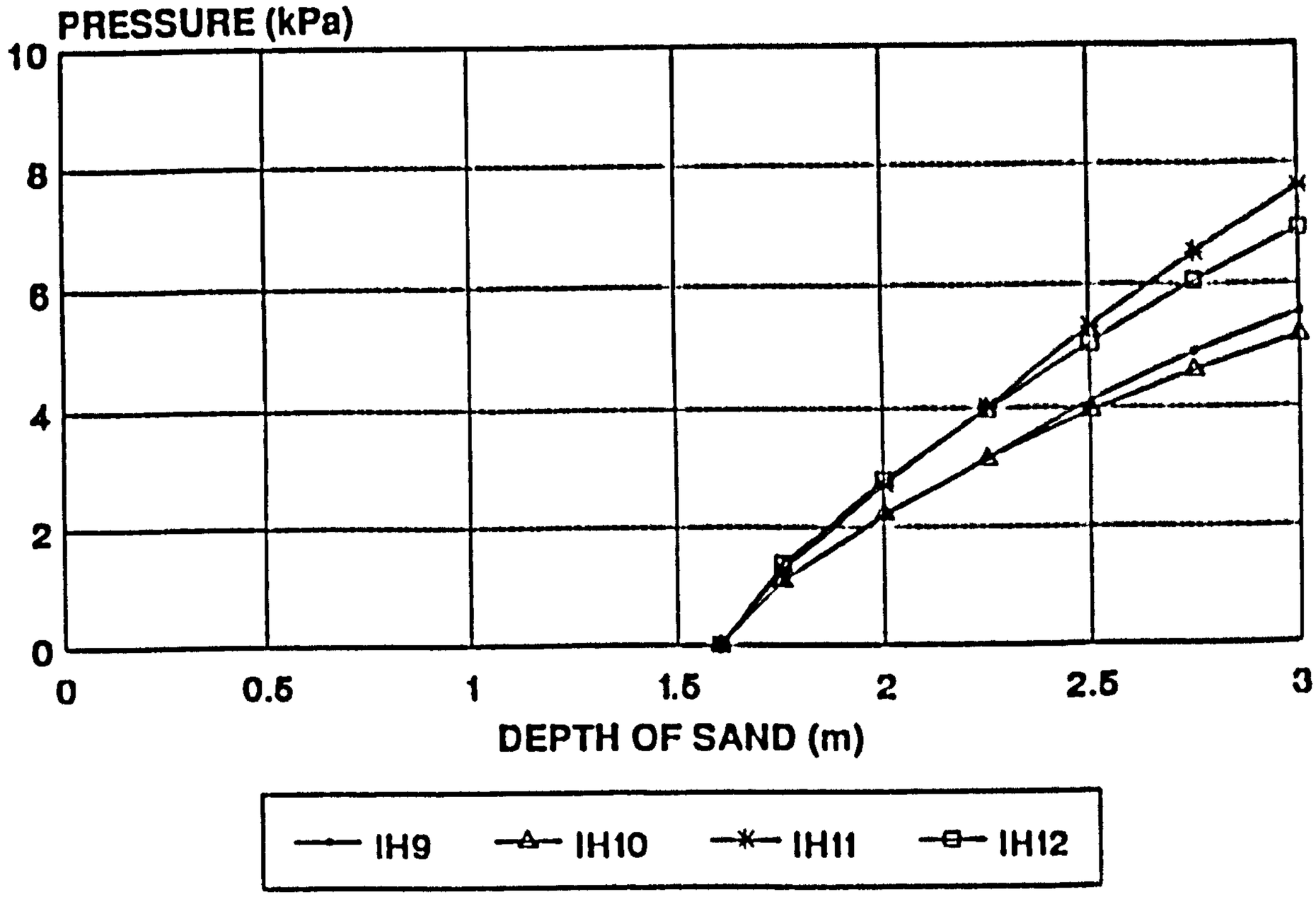

Figure 8.54

PRESSURE PARALLEL TO THE WALL

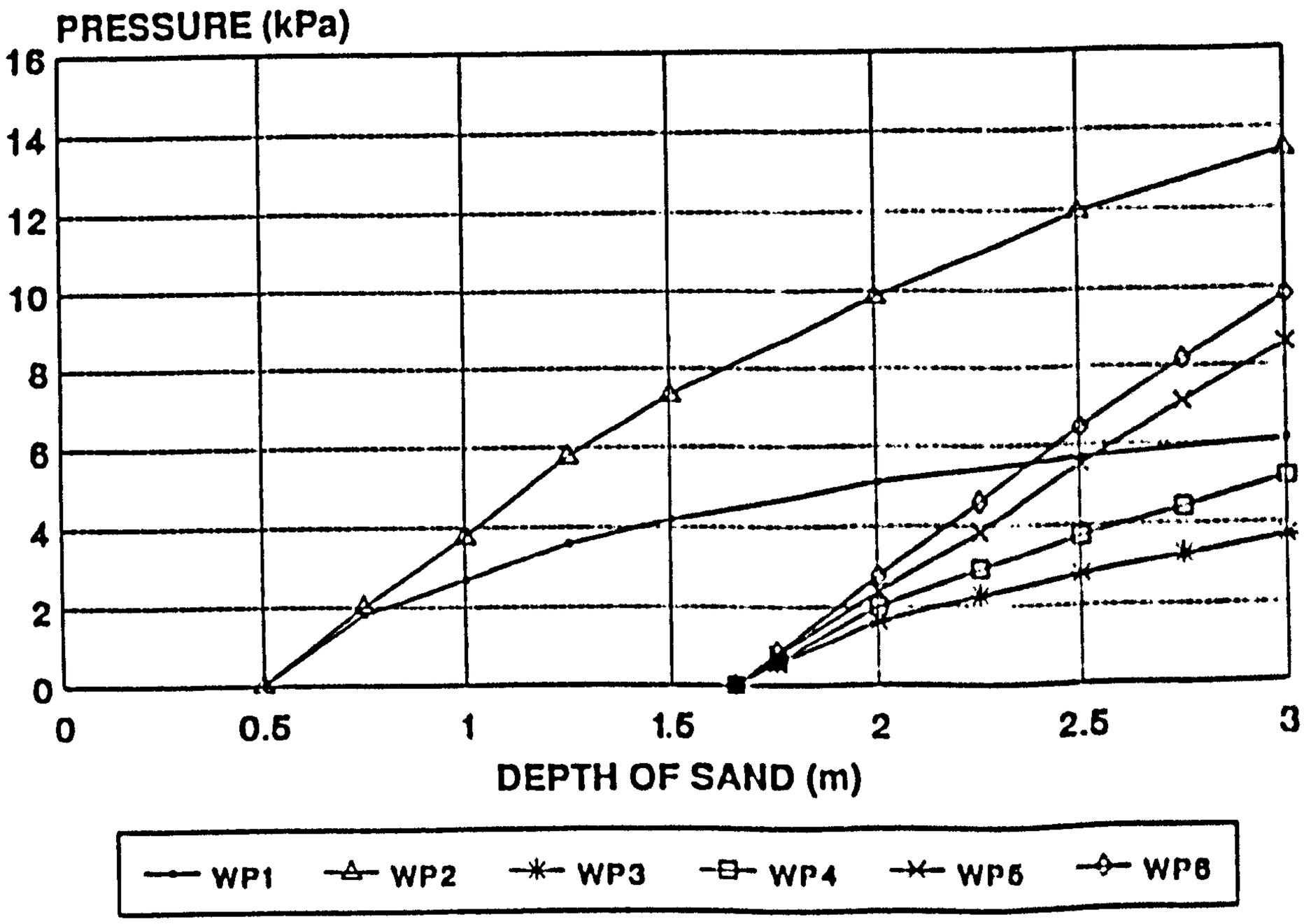

Figure 8.55

1600 ABOVE OUTLET

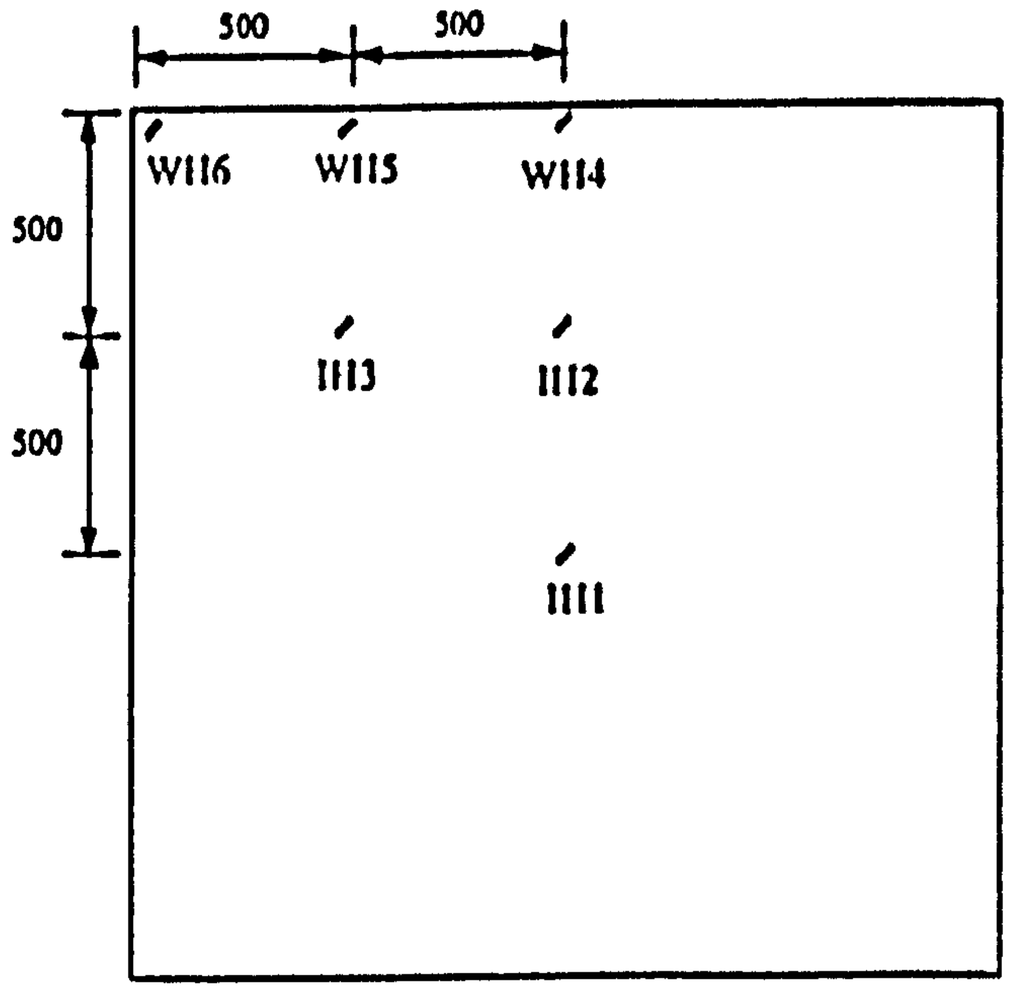

Figure 8.56 POSITIONS OF CELLS PLACED TO MEASURE HORIZONTAL PRESSURE AT 45 DEGREES TO THE WALL (Dimensions in mm)

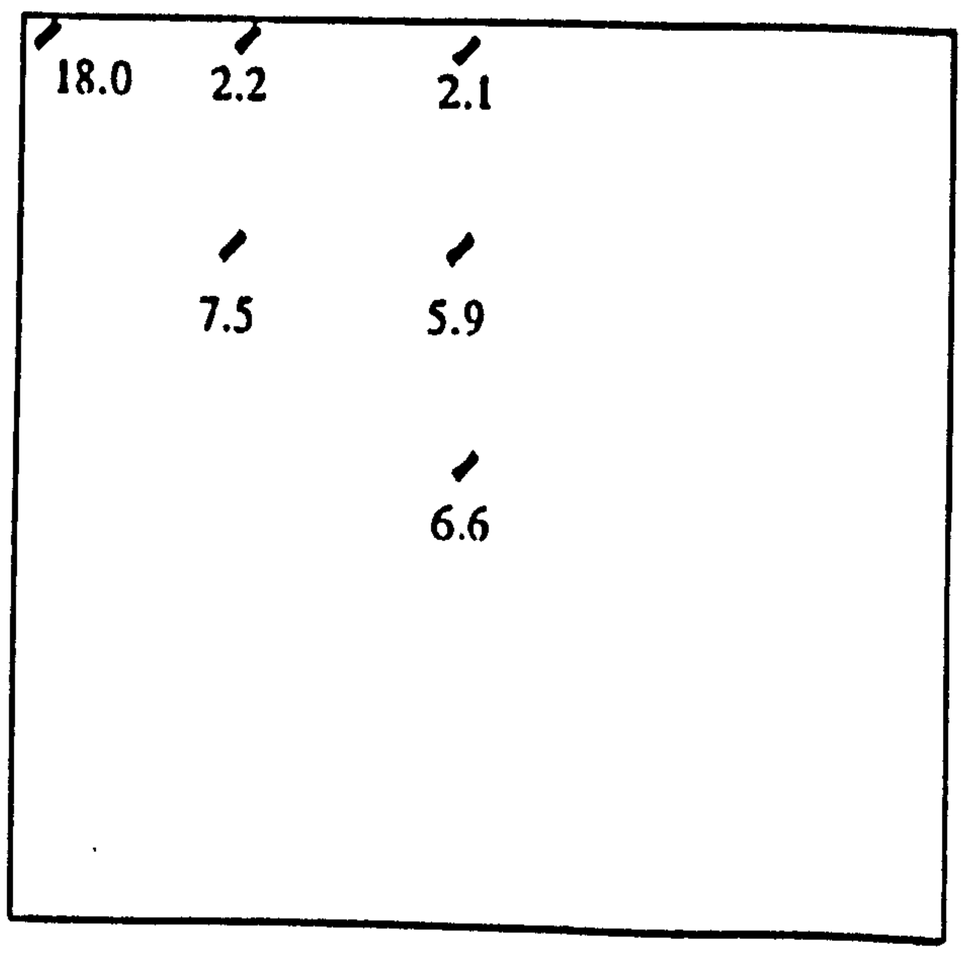

Figure 8.57 HORIZONTAL PRESSURE AT 45 DEGREES TO THE BIN WALL 3.0 m OF SAND

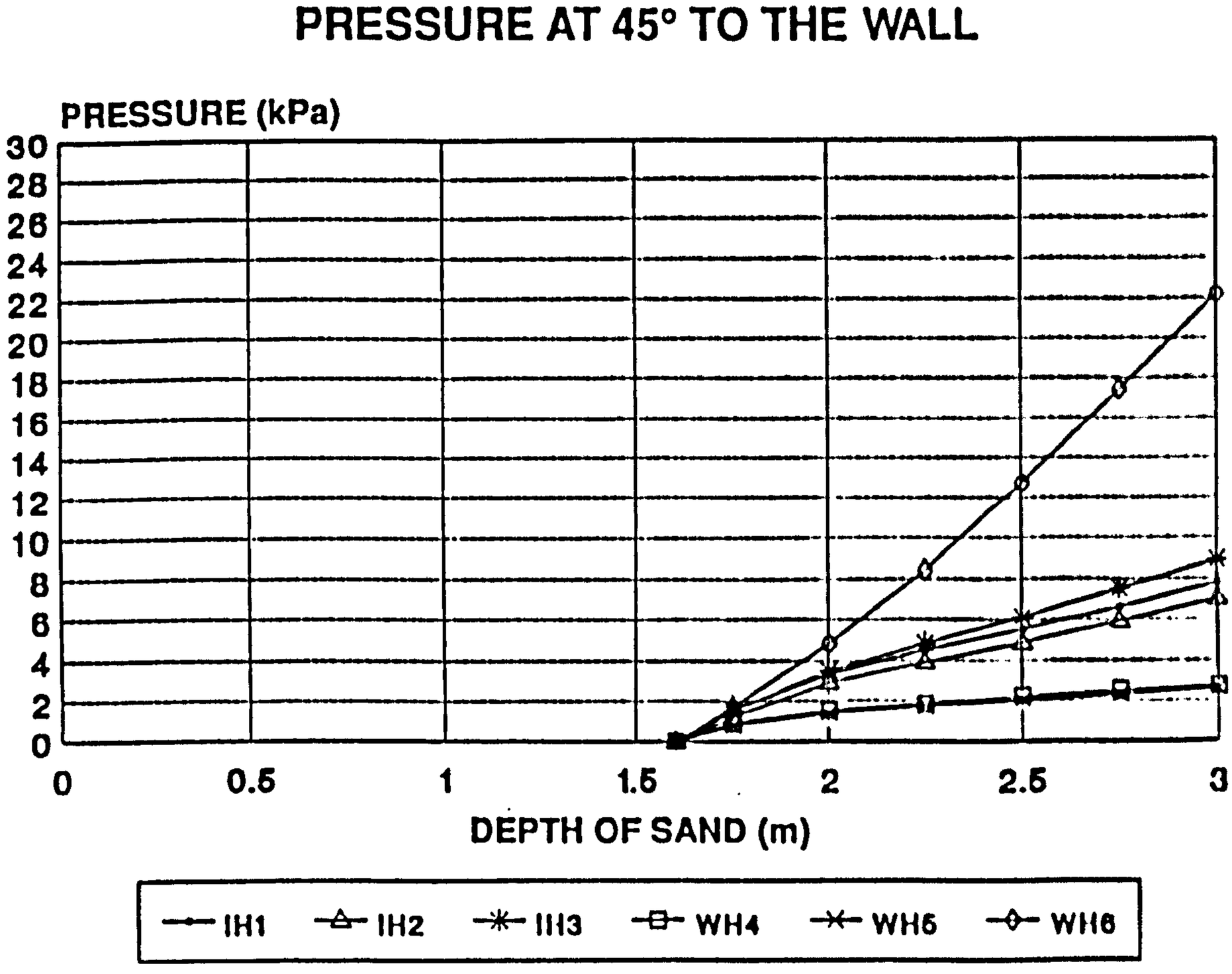
PRESSURE AT 45° TO THE WALL
PRESSURE (kPa)
30
28
26
24
22
20
18
16
14
12
10
8
6
4
2
0
0
0.5
1
1.5
2
2.5
3
DEPTH OF SAND (m)
IH1
IH2
IH3
WH4
WH5
WH6

Figure 8.58

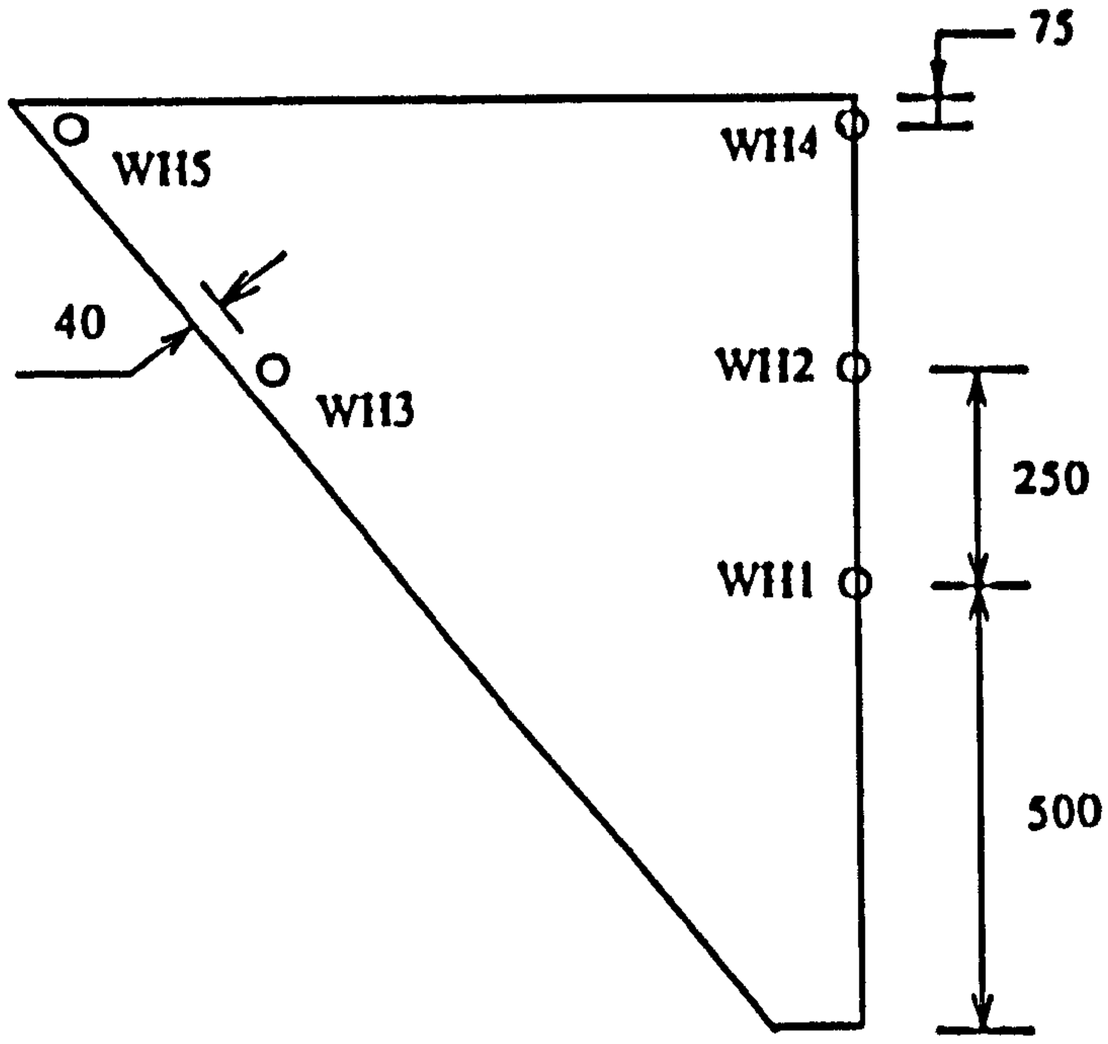

Figure 8.59 POSITIONS OF HORIZONTAL PRESSURE MEASUREMENT IN THE HOPPER

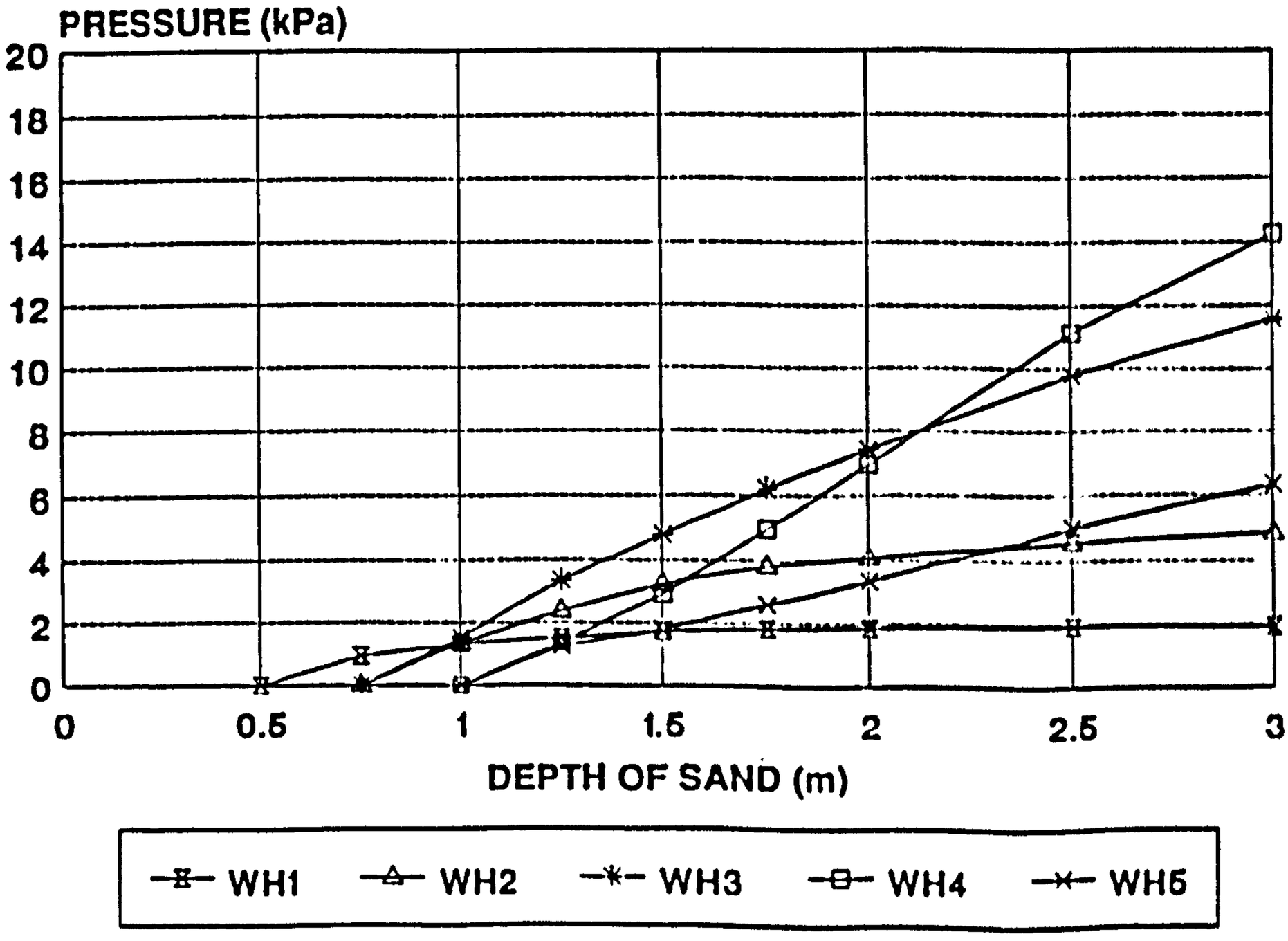

Figure 8.60

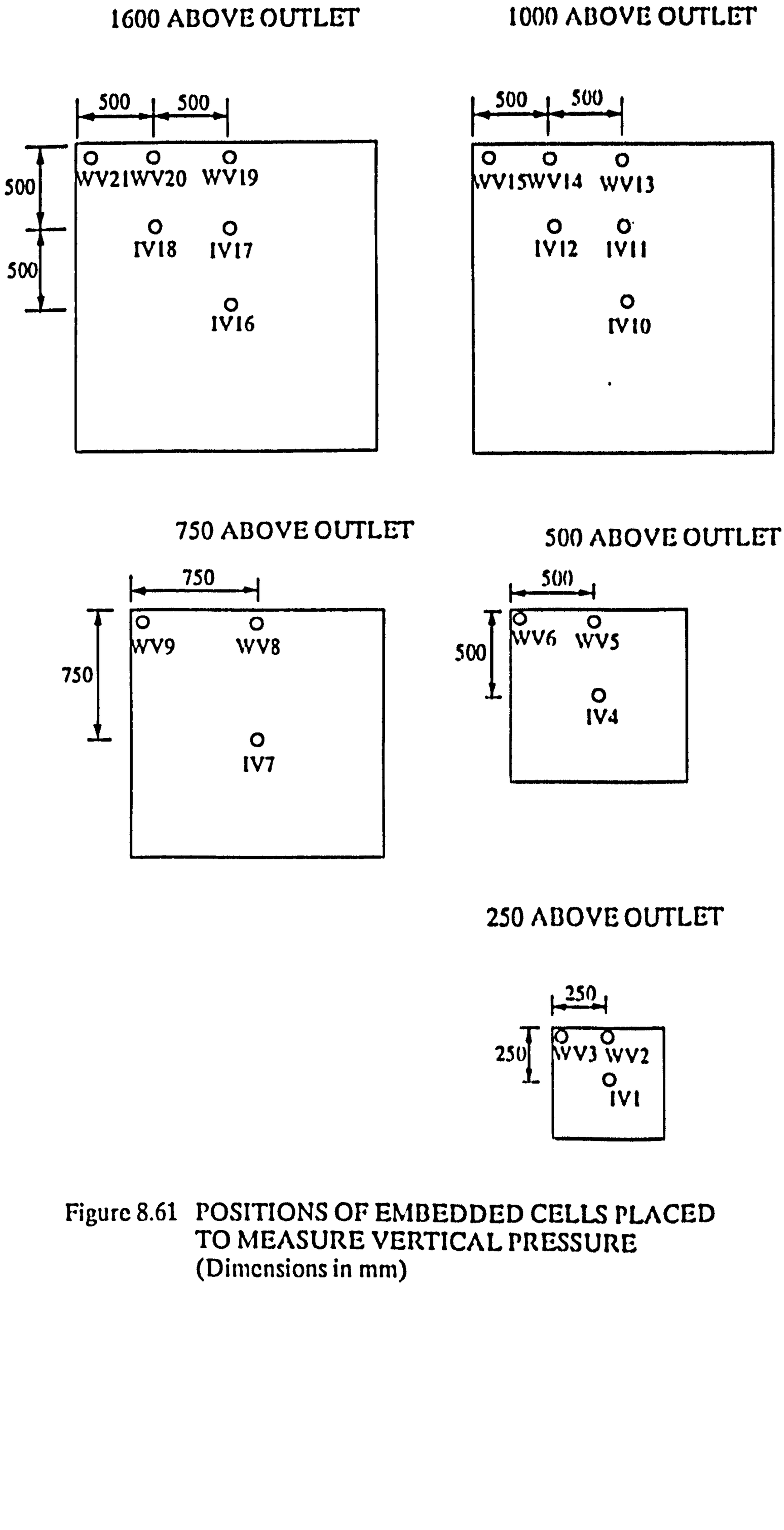

Figure 8.61 POSITIONS OF EMBEDDED CELLS PLACED TO MEASURE VERTICAL PRESSURE
(Dimensions in mm)

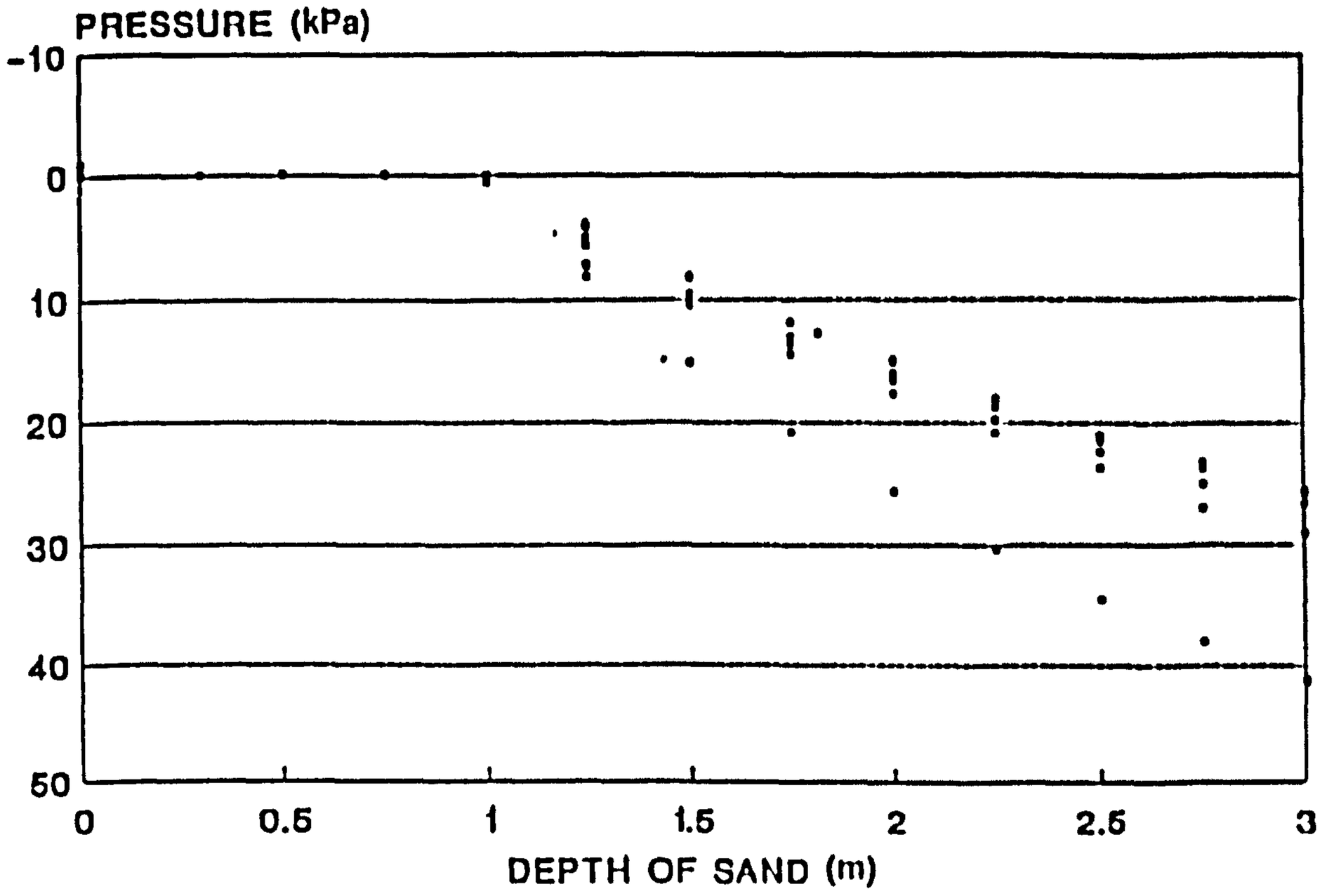

Figure 8.62 .RESULTS FROM FIVE TESTS, POSITION IV11

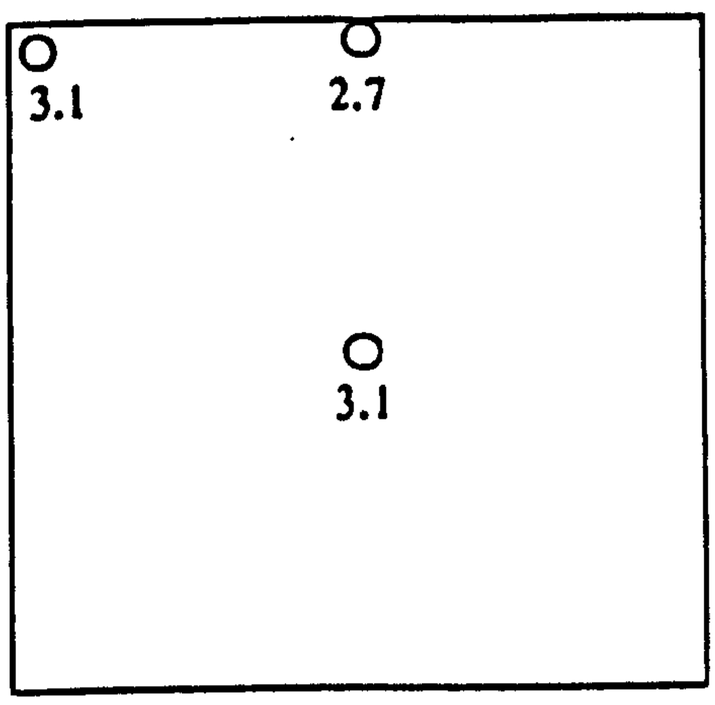

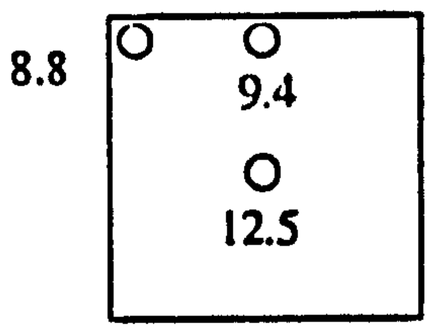

Figure 8.63 VERTICAL PRESSURE (kPa) 1.0 m OF SAND

1000mm ABOVE OUTLET

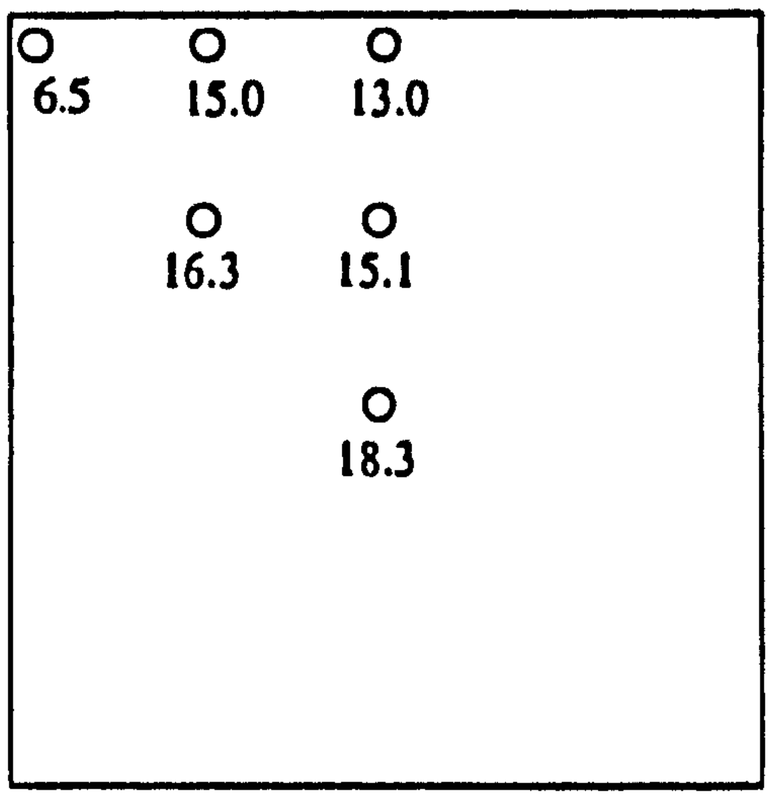

750mm ABOVE OUTLET

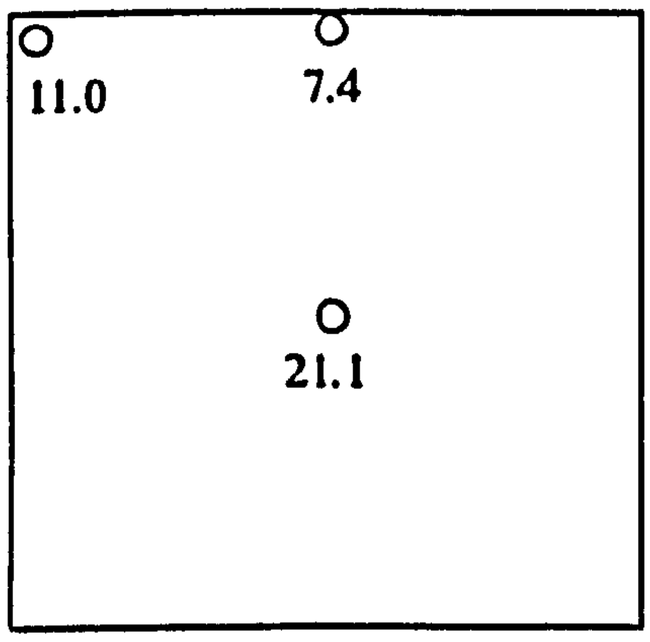

500mm ABOVE OUTLET

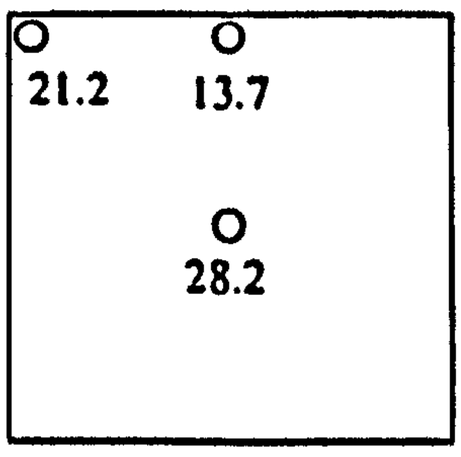

250mm ABOVE OUTLET

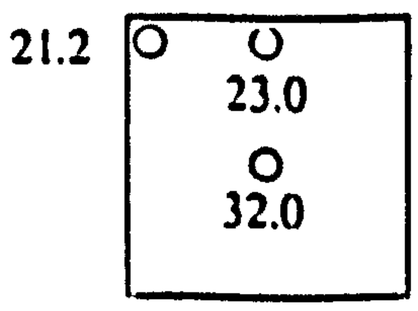

Figure 8.64 VERTICAL PRESSURE (kPa) 2.0 m OF SAND

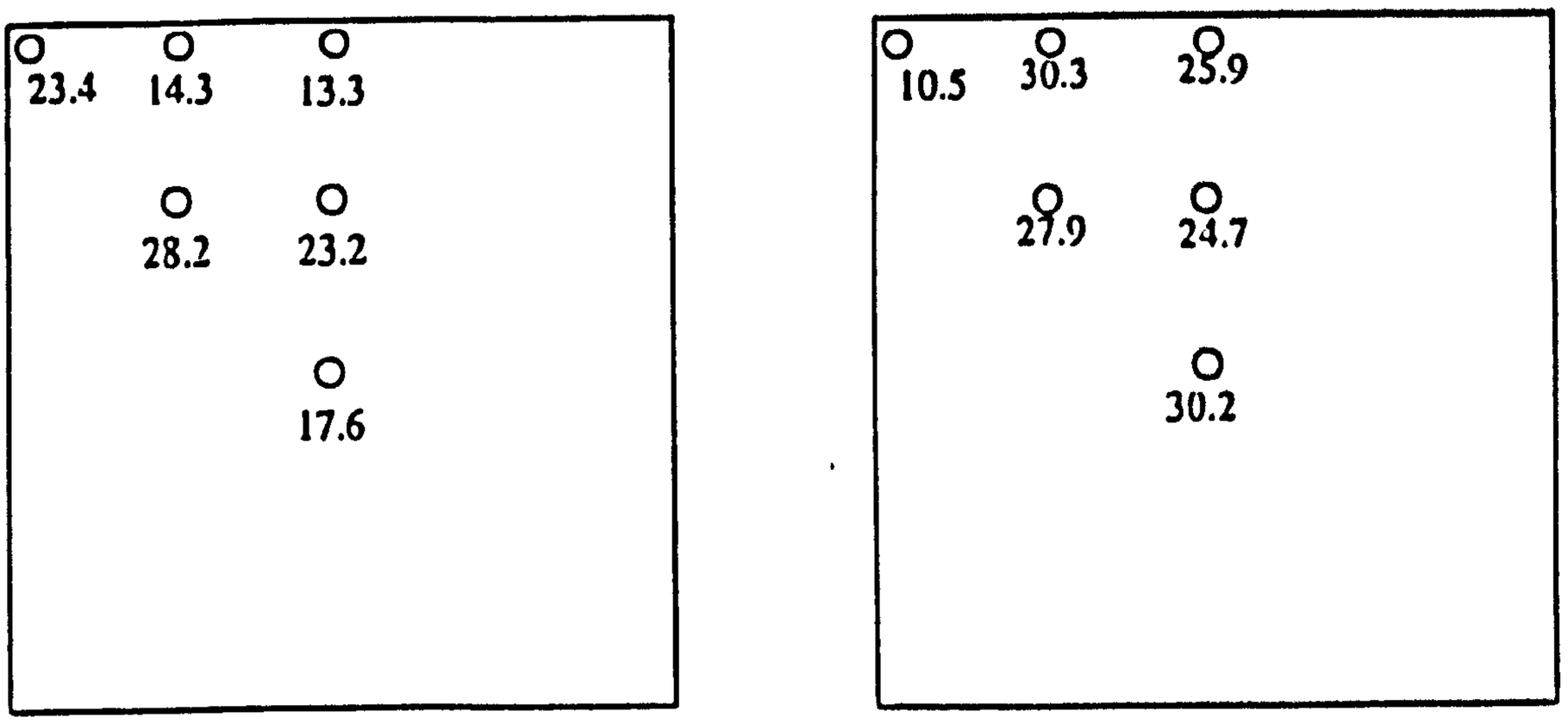

Figure 8.65 VERTICAL PRESSURE (kPa) 3.0 m OF SAND

VERTICAL PRESSURE
250 mm ABOVE THE OUTLET

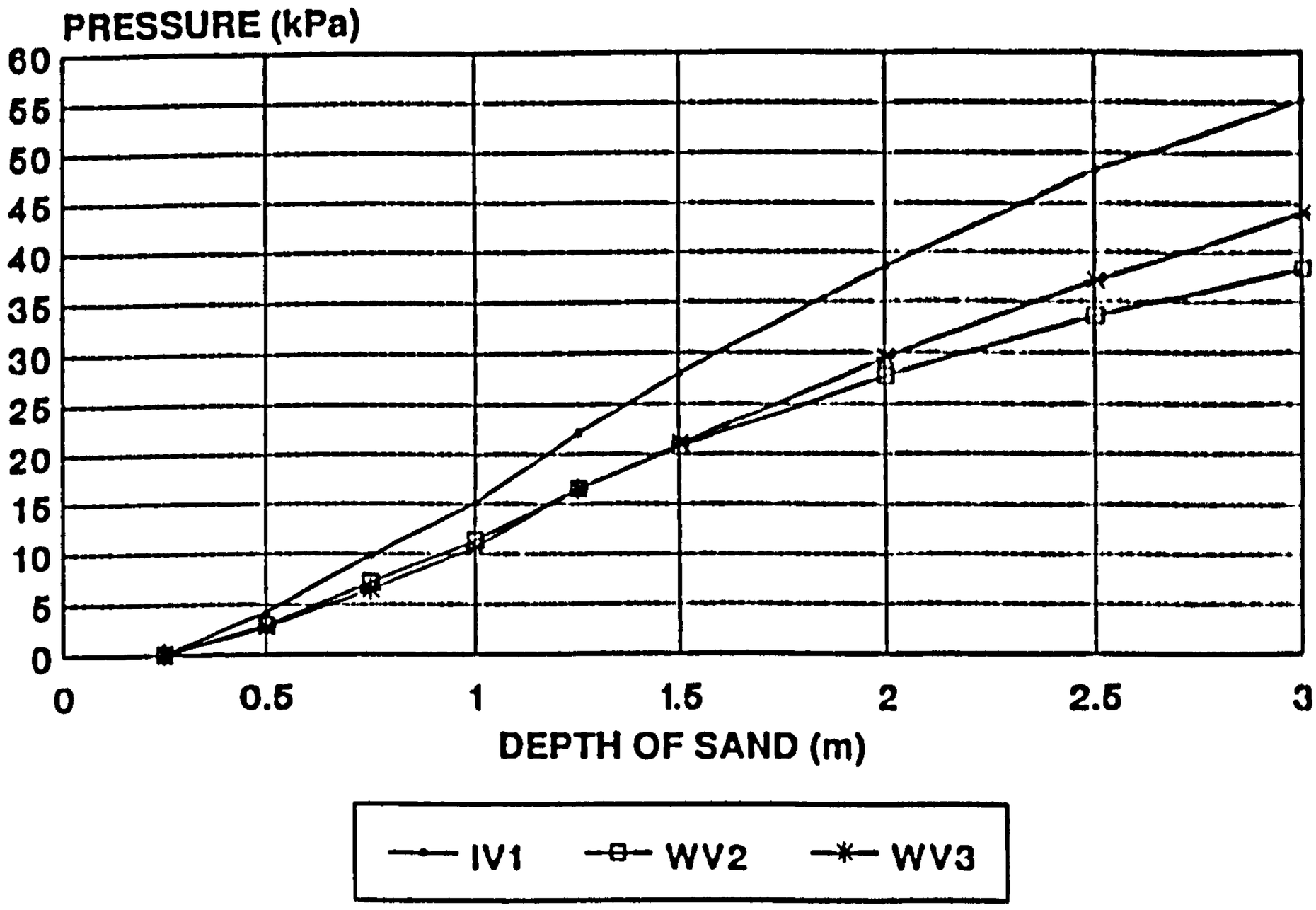

Figure 8.66

VERTICAL PRESSURE
500 mm ABOVE THE OUTLET

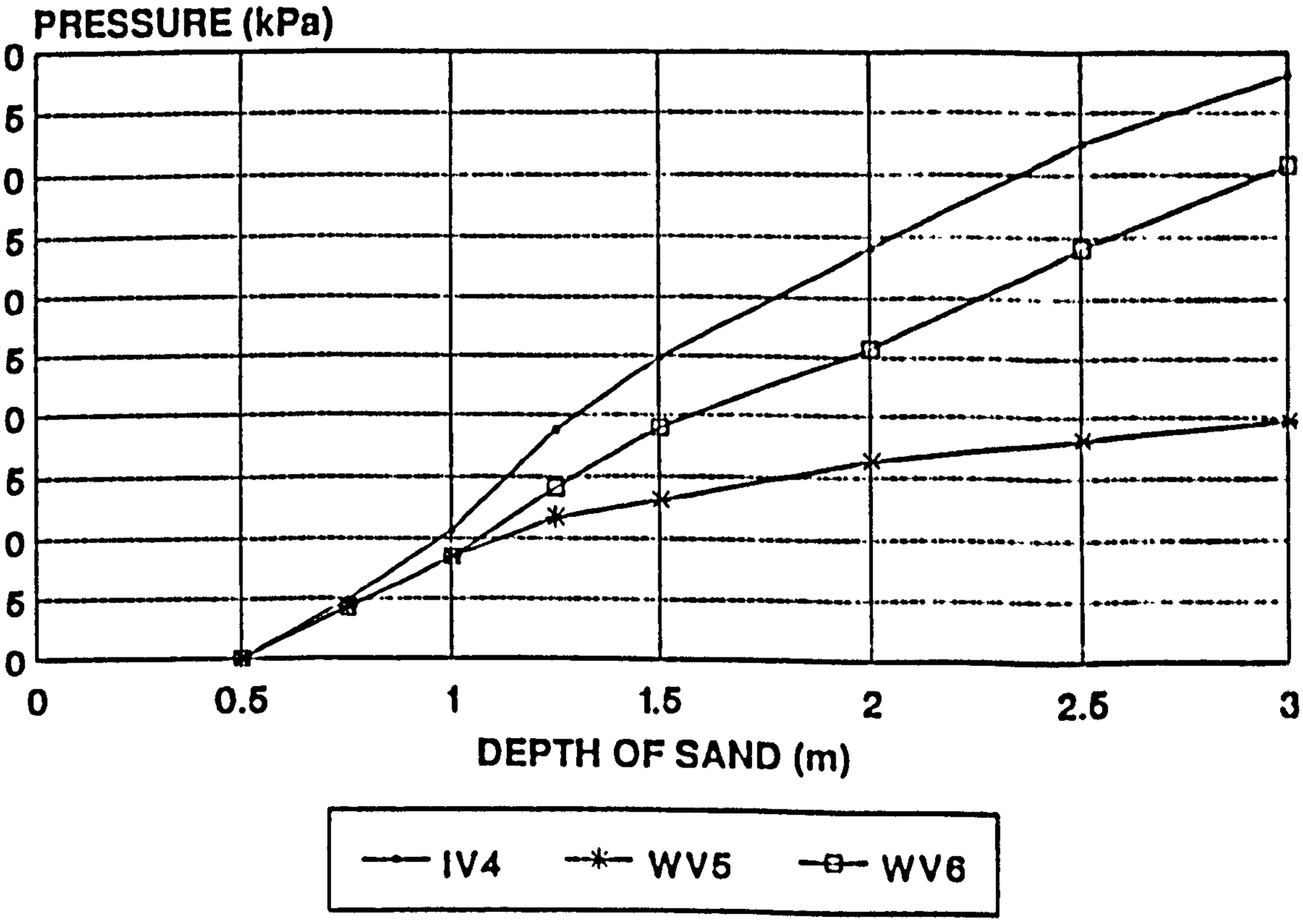

Figure 8.67

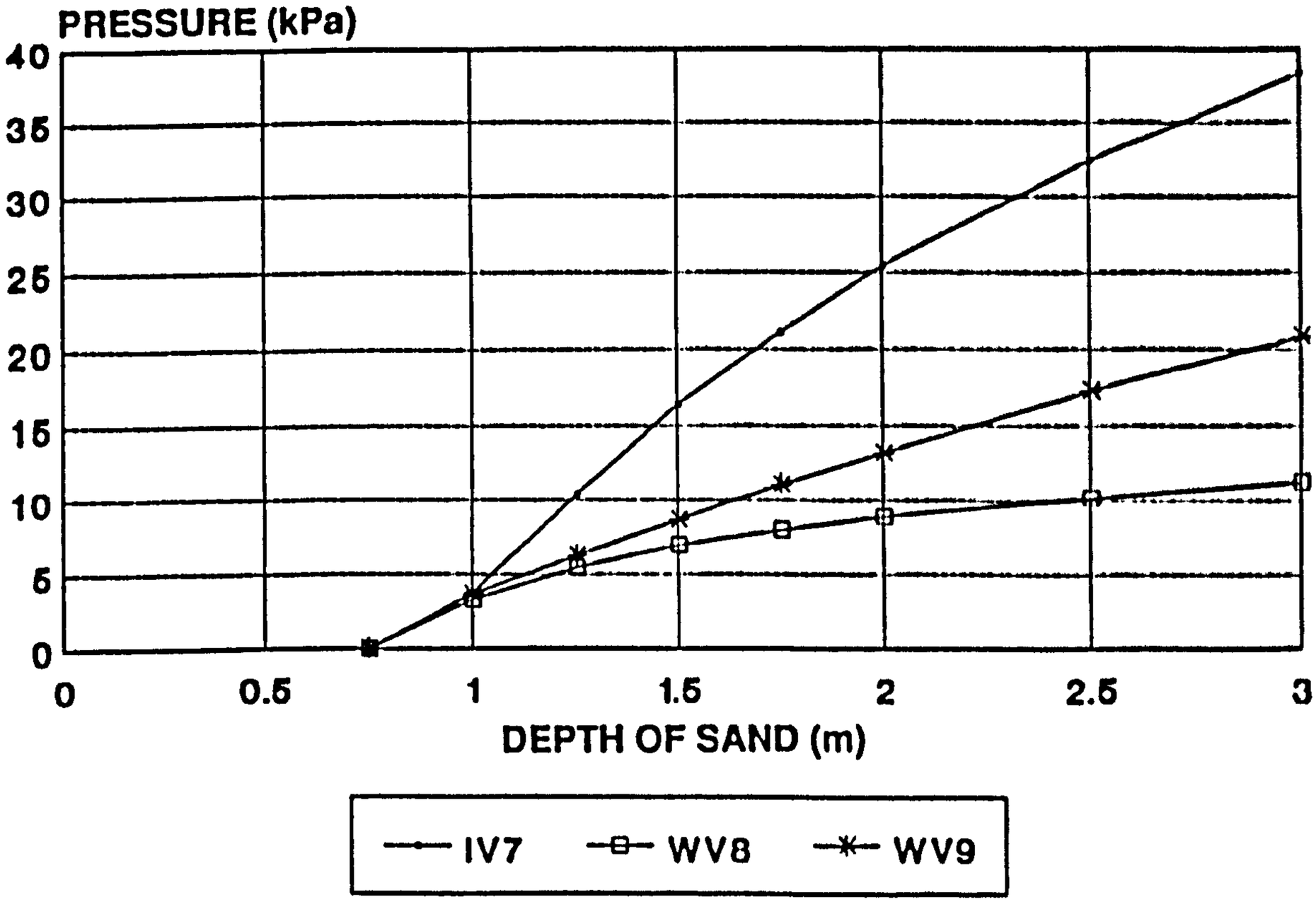

Figure 8.68

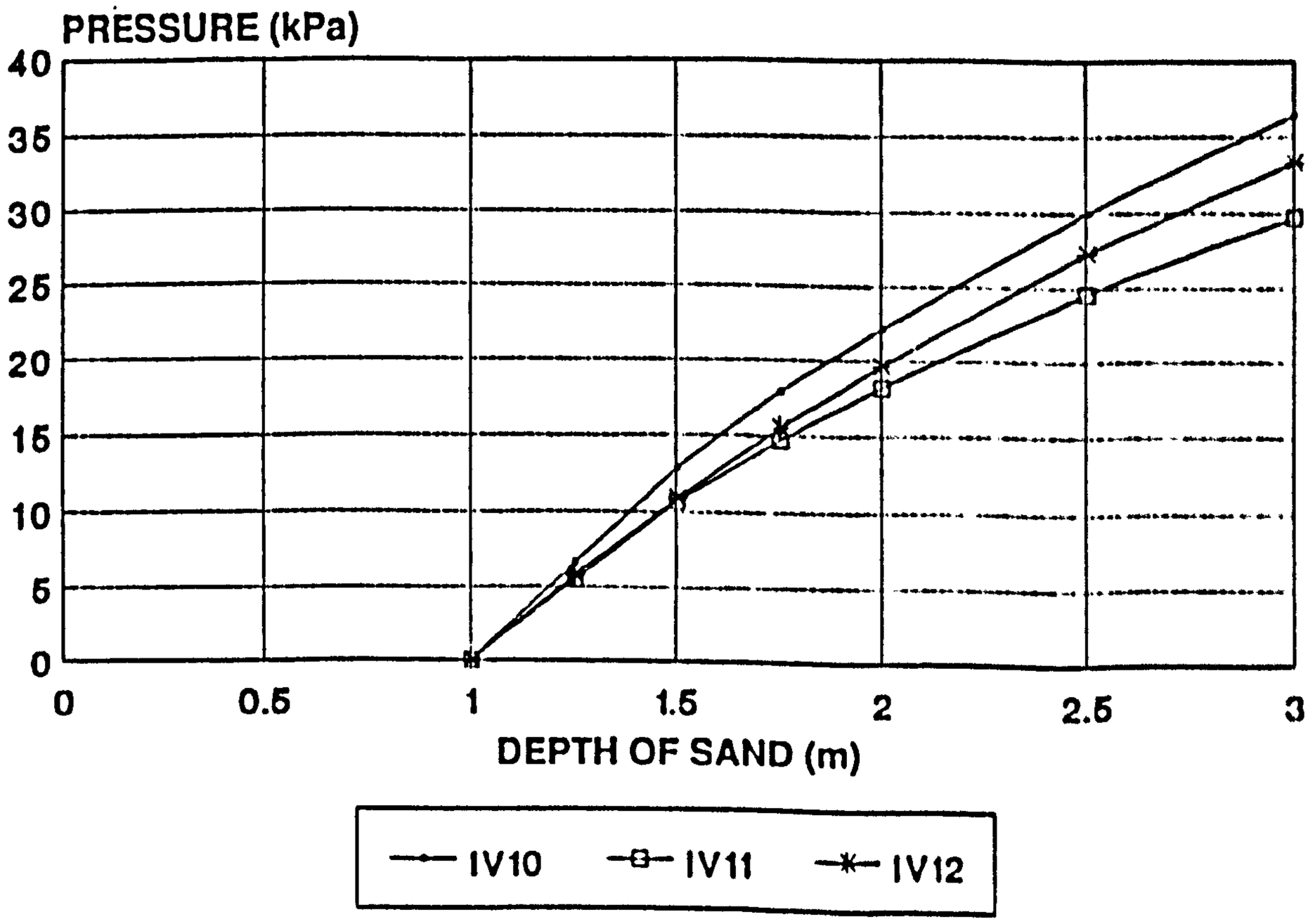

Figure 8.69

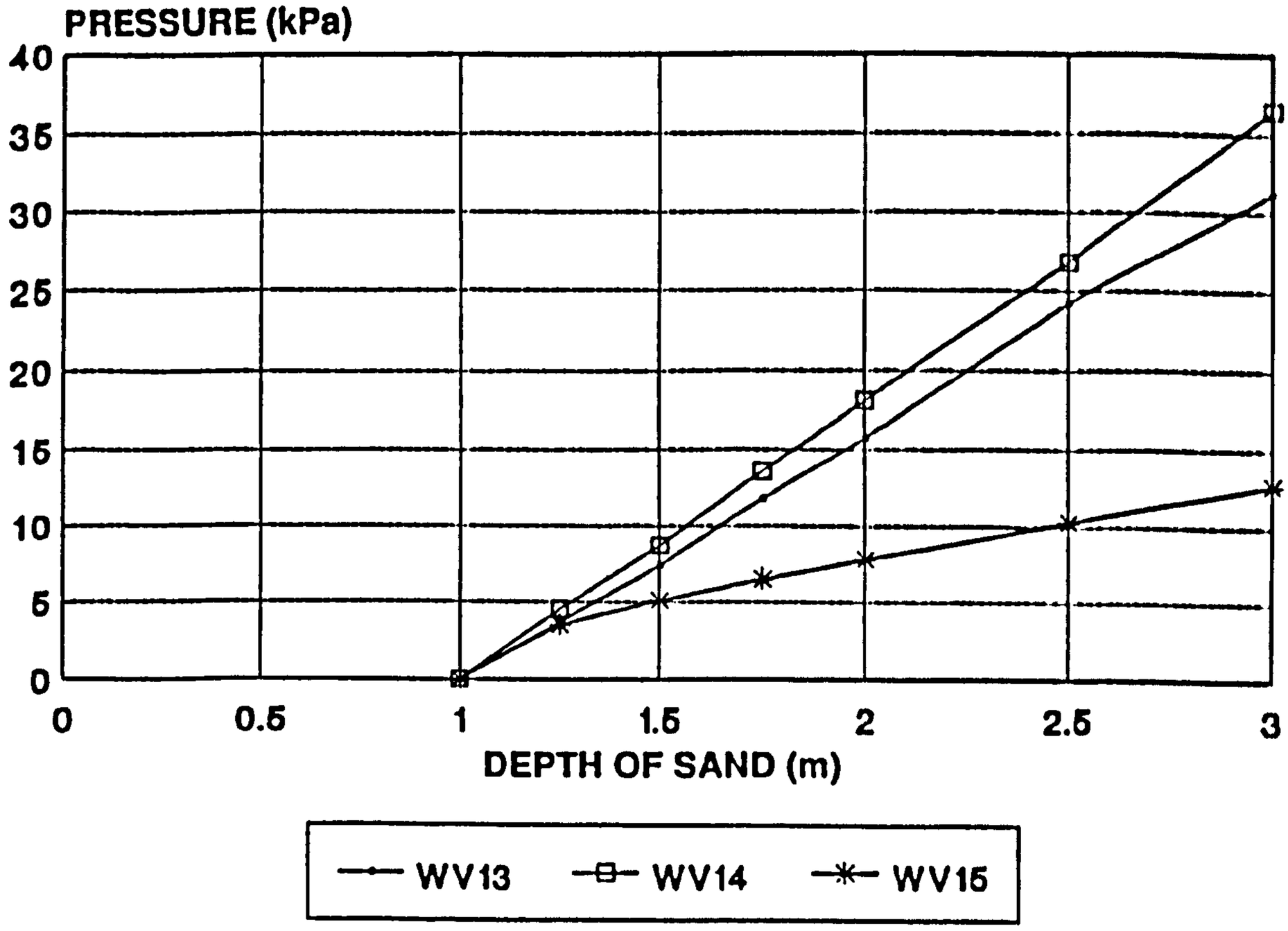

Figure 8.70

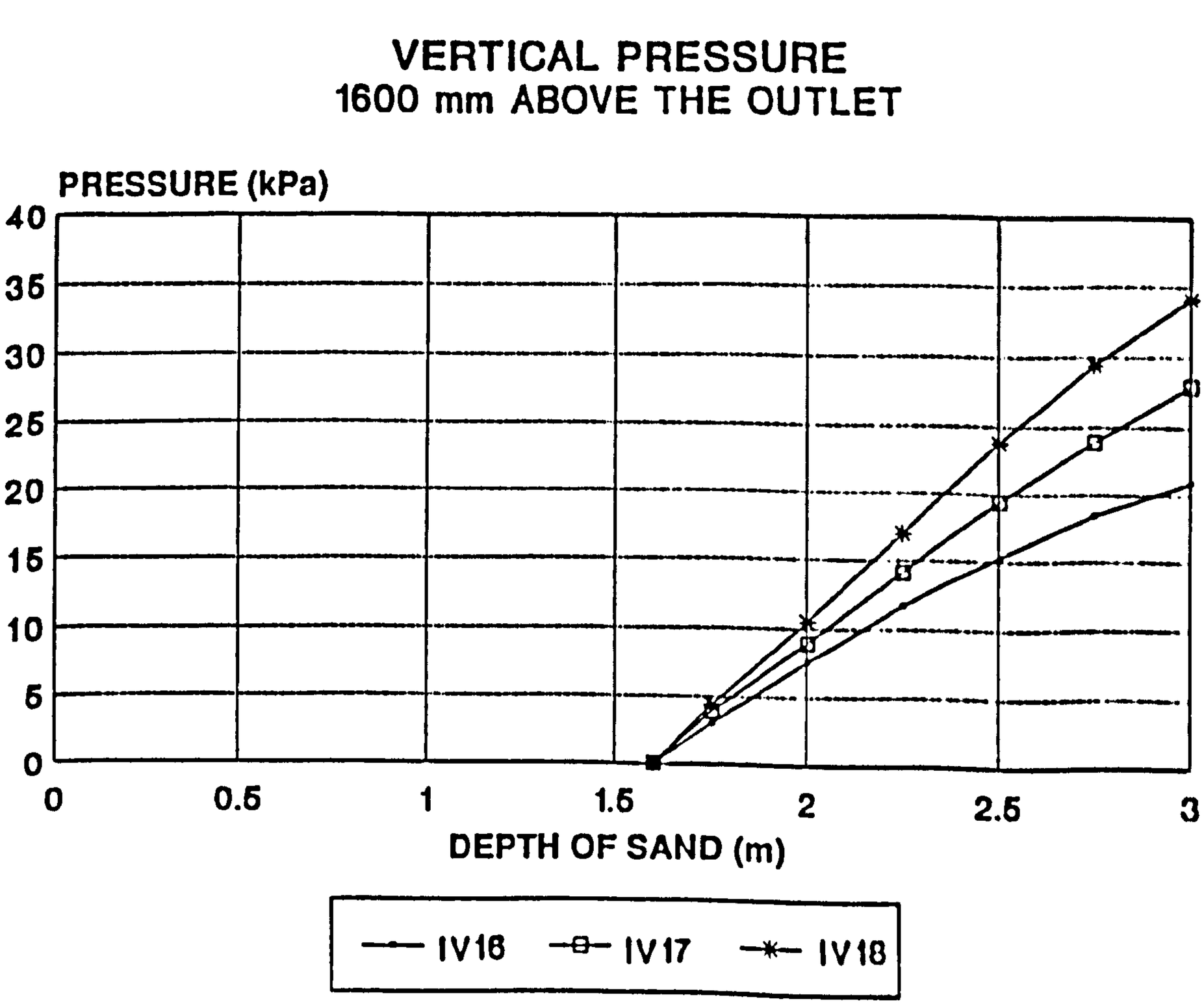

Figure 8.71

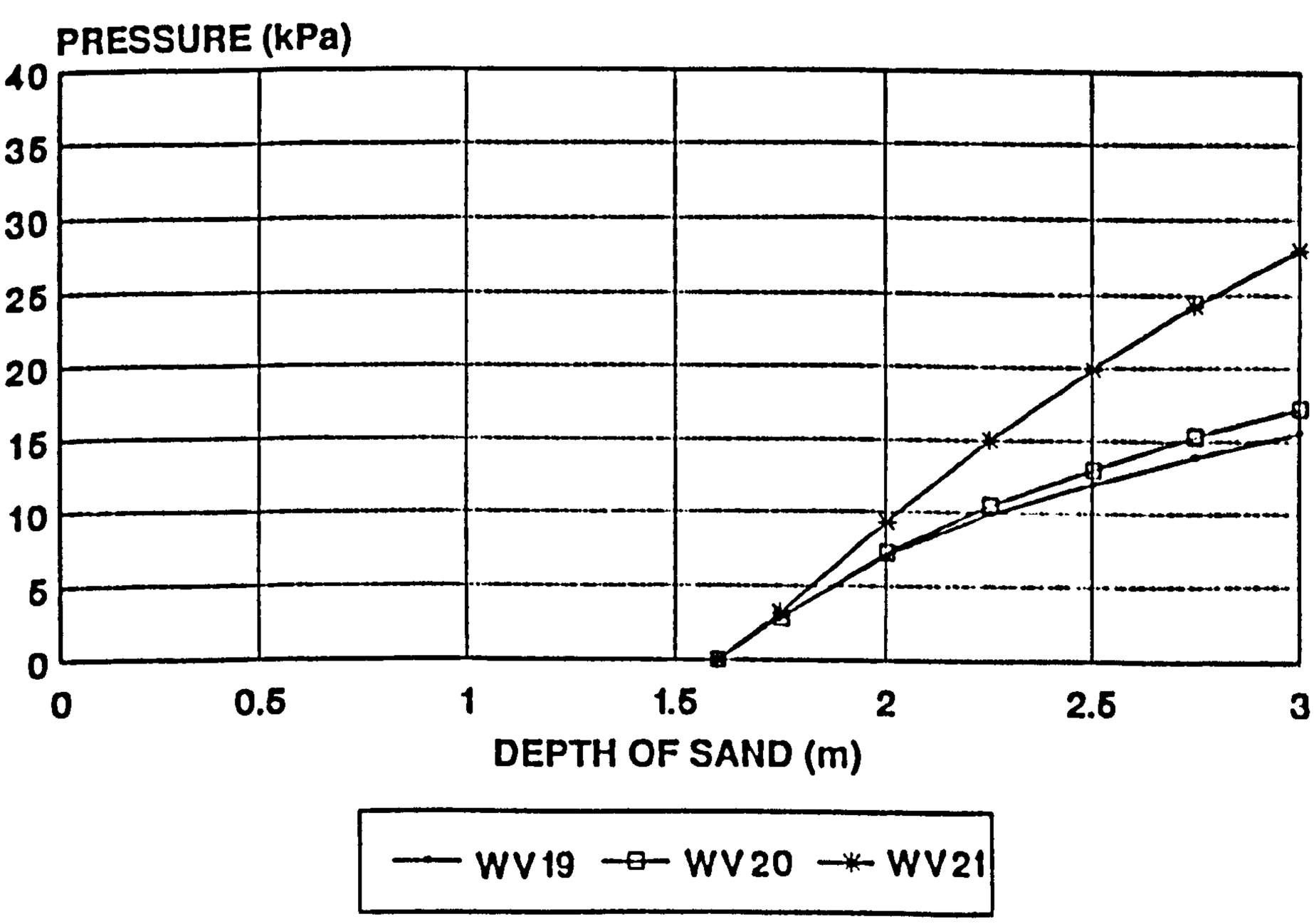
VERTICAL PRESSURE
1600 mm ABOVE THE OUTLET
PRESSURE (kPa)
40
35
30
25
20
15
10
5
0
0
0.5
1
1.5
2
2.5
3
DEPTH OF SAND (m)
WV19
WV20
WV21

Figure 8.72

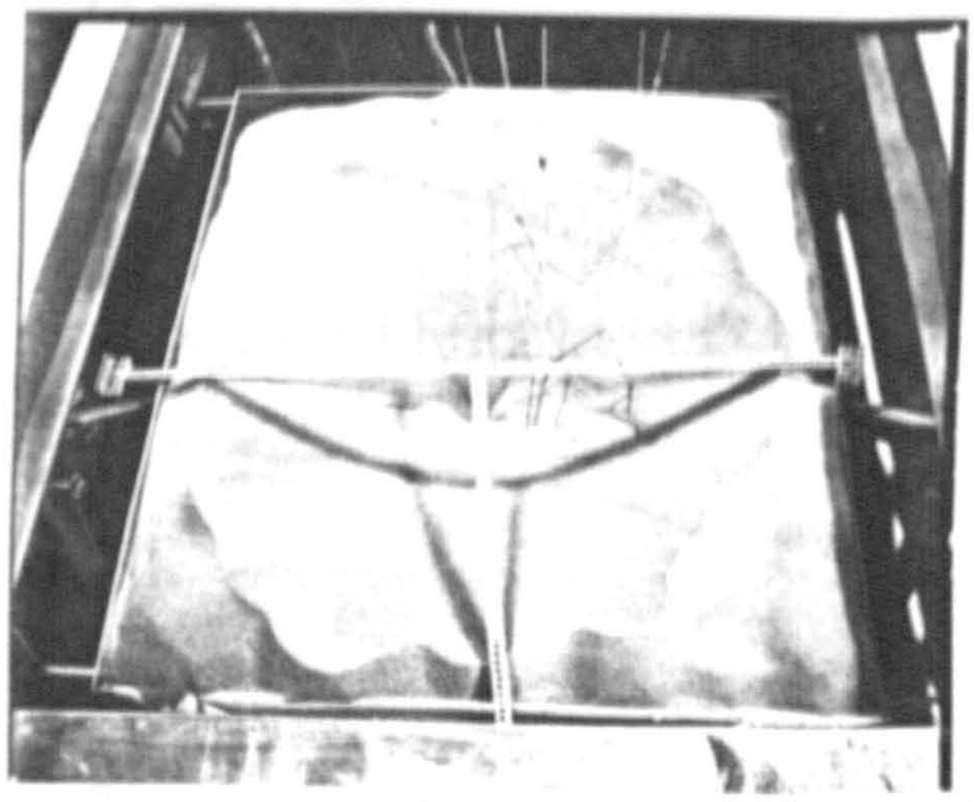

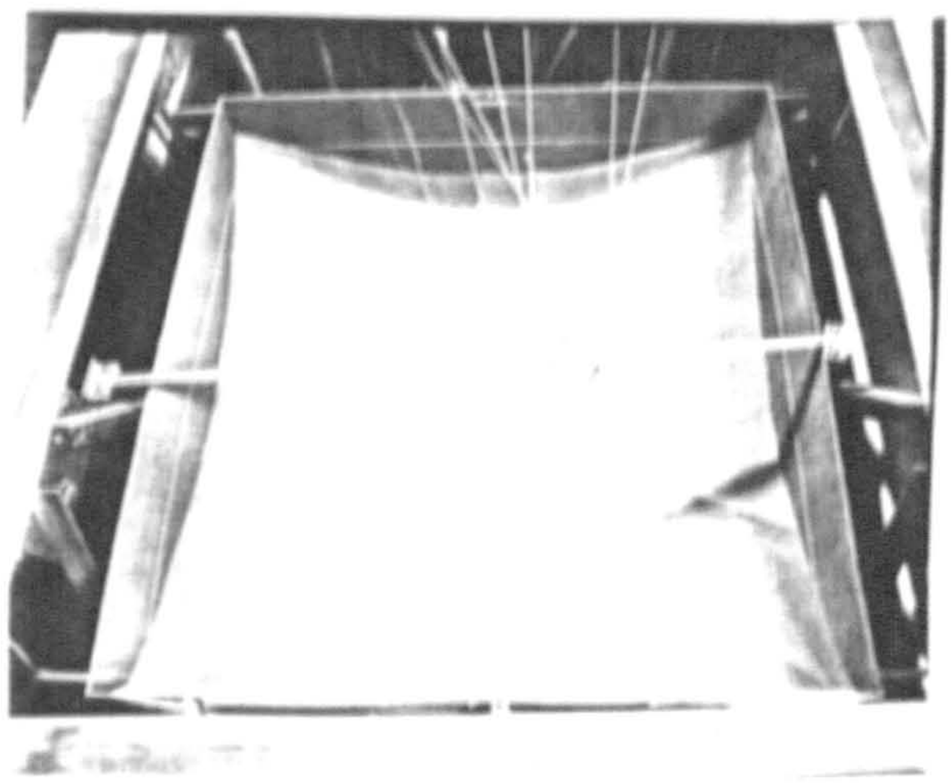

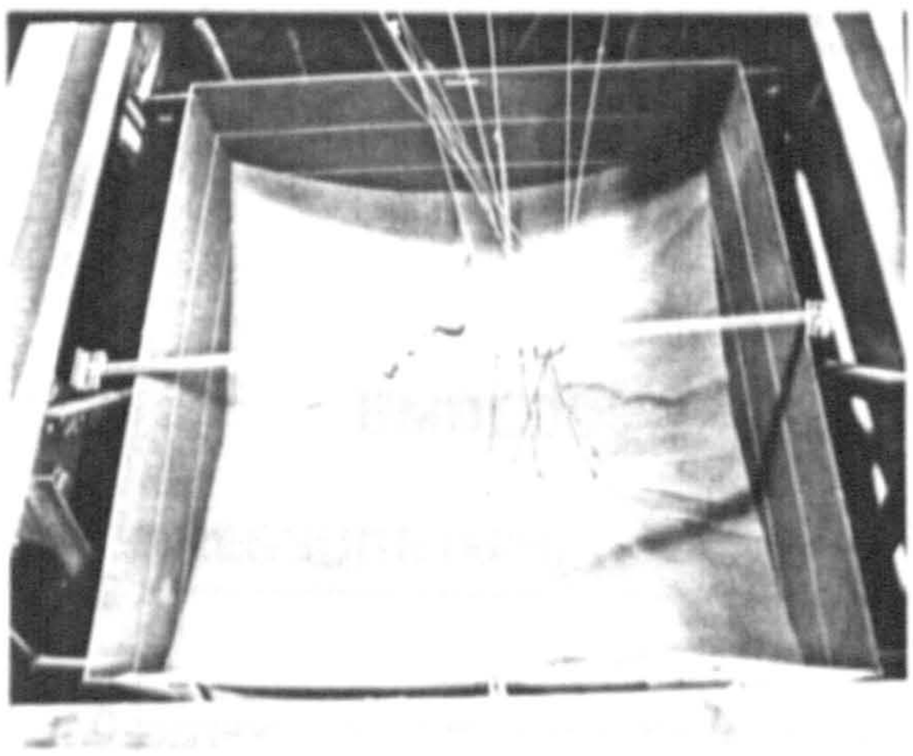

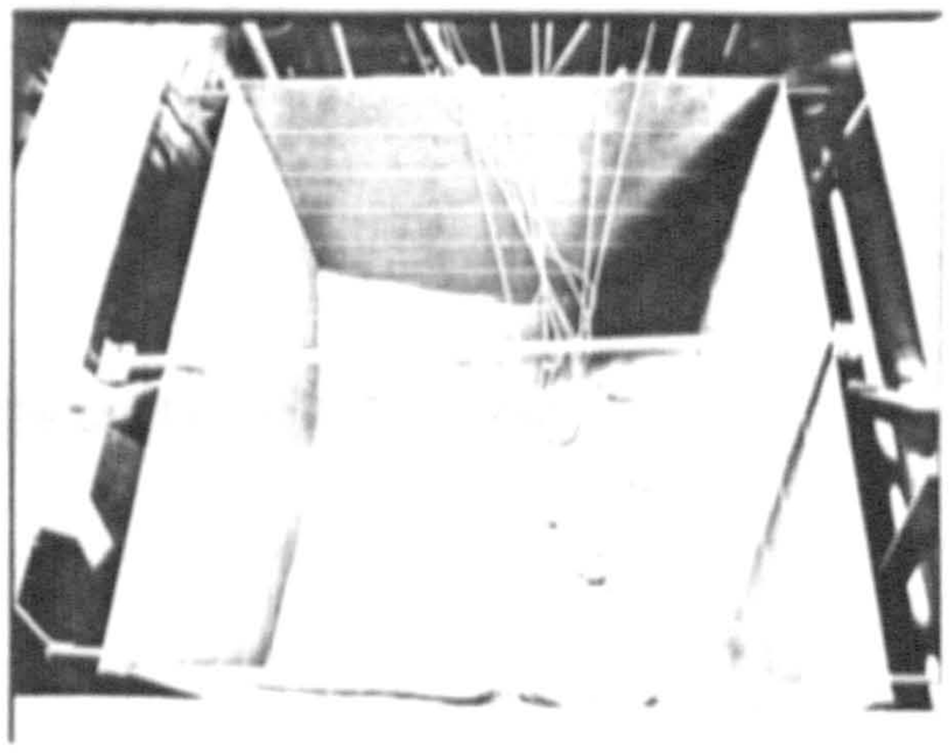

Figure 8.73 SILO DISCHARGING

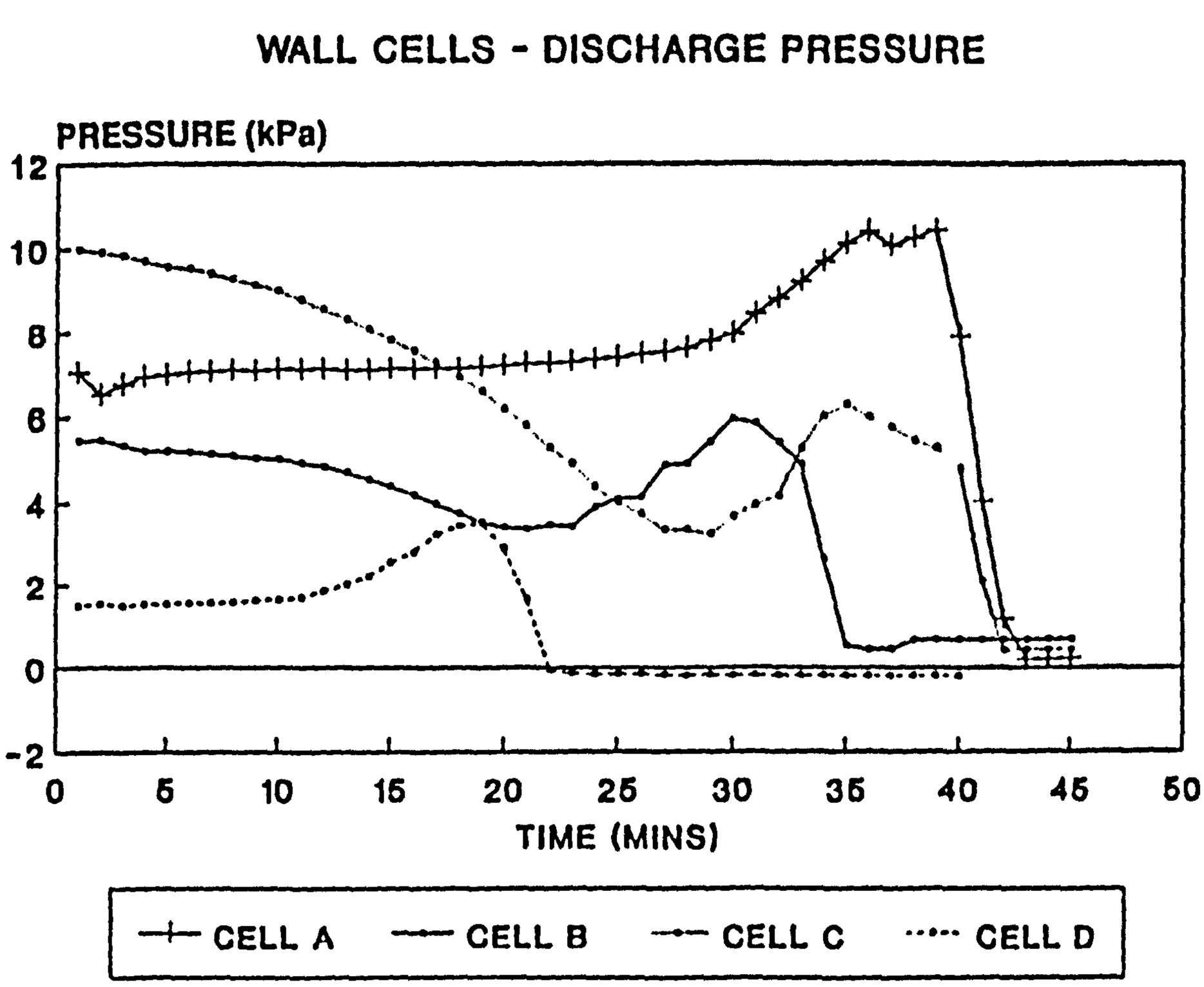

Figure 8.74a

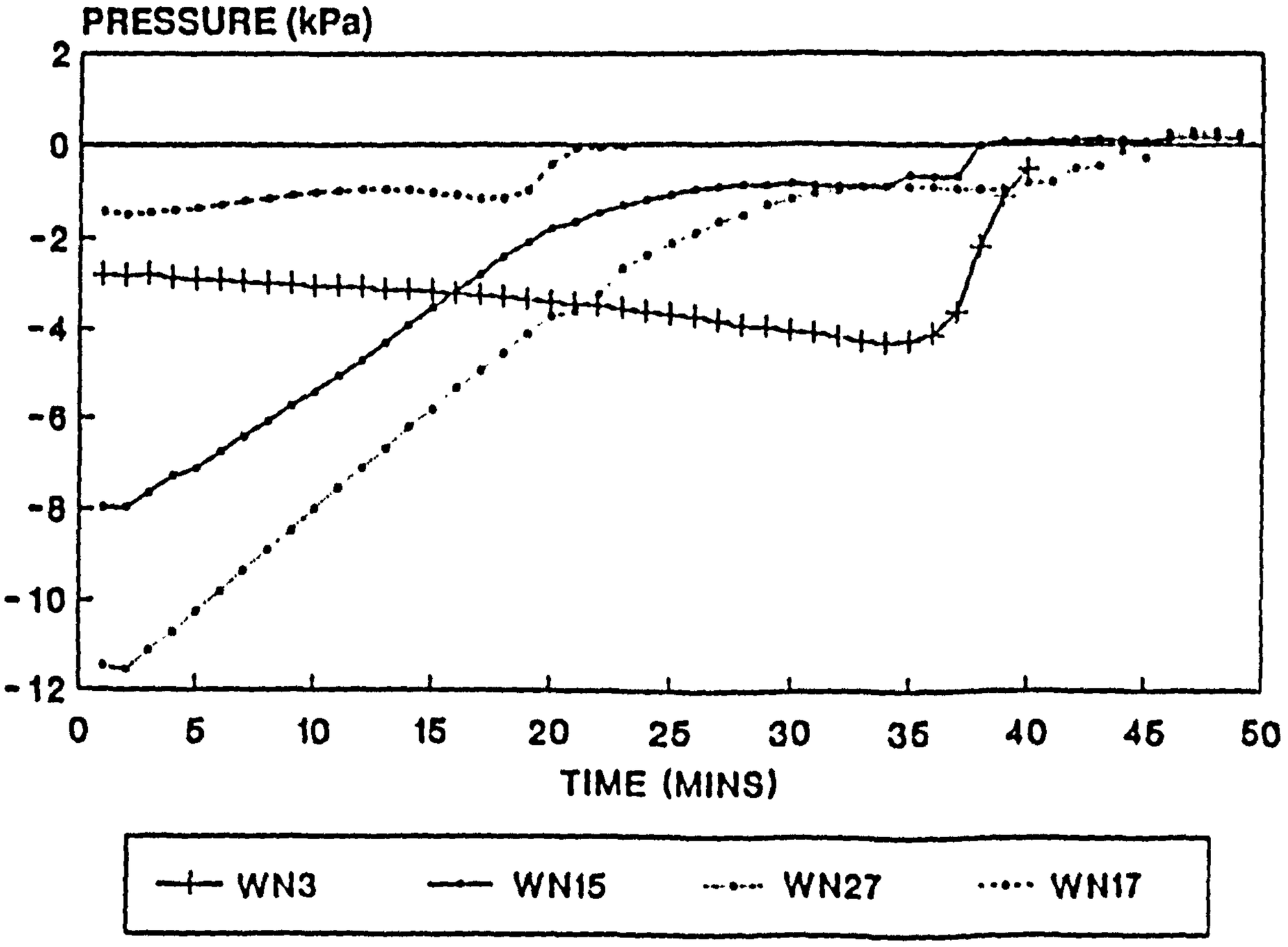

Figure 8.74b

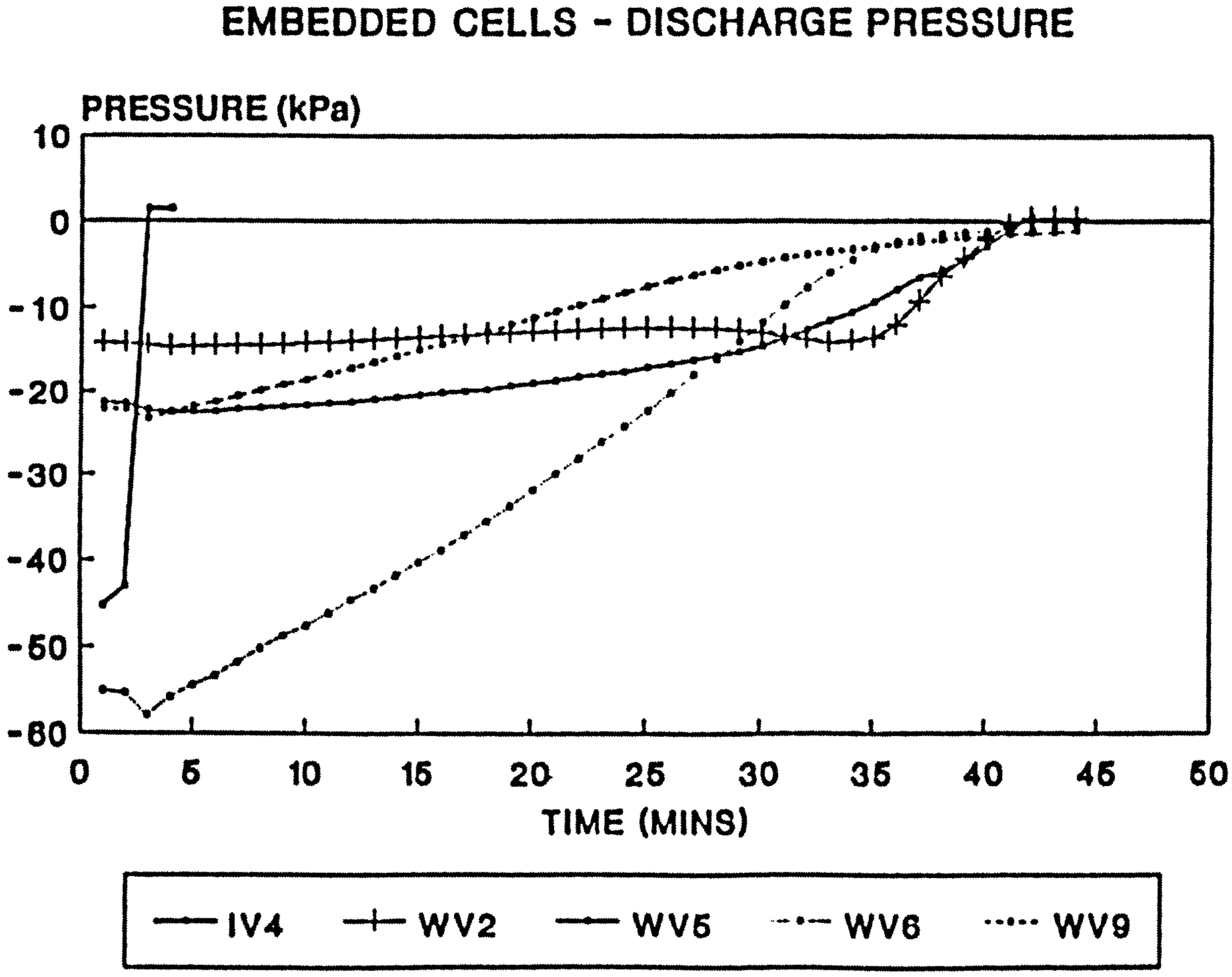
EMBEDDED CELLS - DISCHARGE PRESSURE
PRESSURE (kPa)
10
0
-10
-20
-30
-40
-50
-60
0
5
10
15
20
25
30
35
40
45
50
TIME (MINS)
IV4
WV2
WV5
WV6
WV9

Figure 8.75

WALL DEFORMATION - DISCHARGE

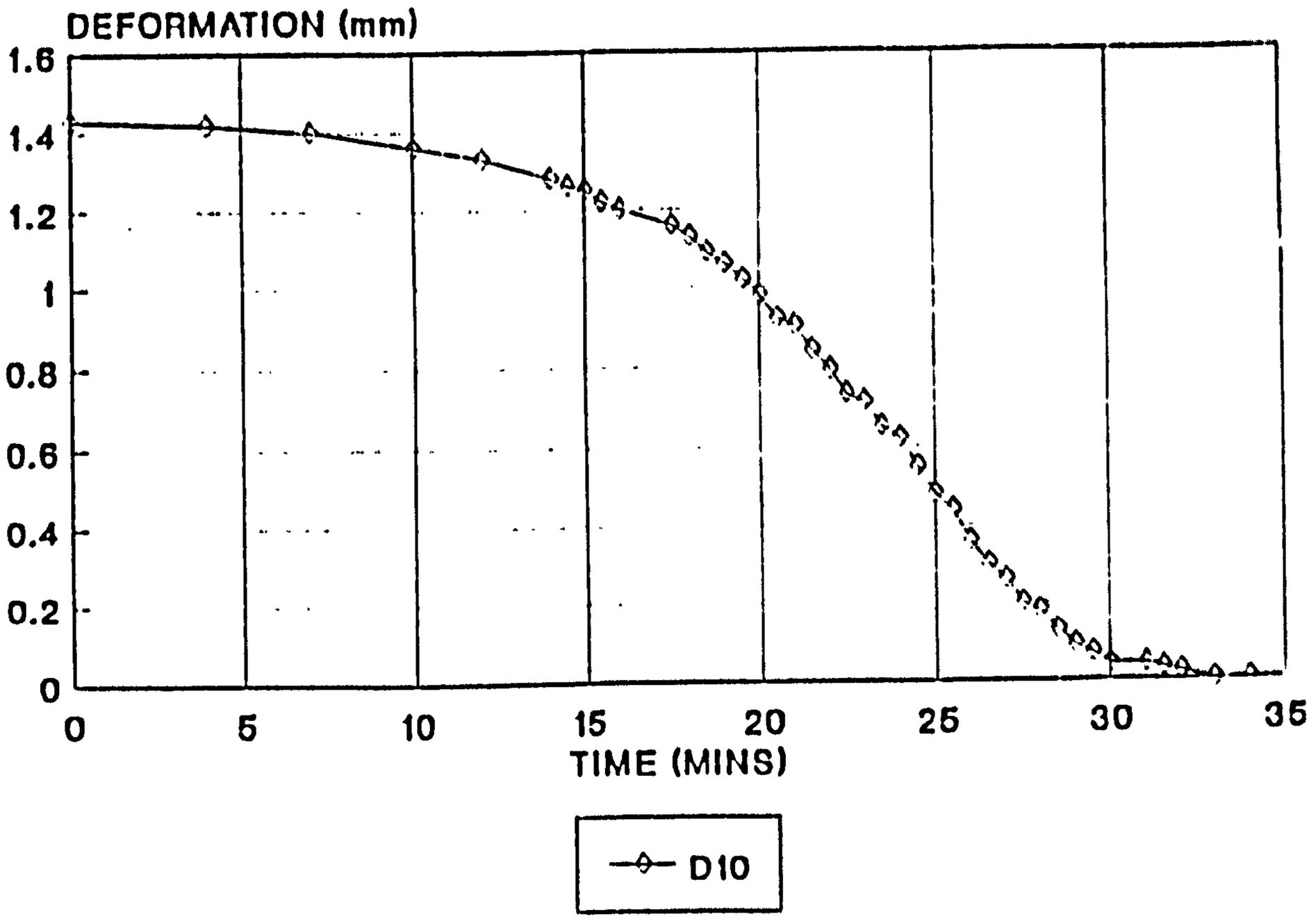

Figure 8.76

HORIZONTAL STRAIN - DISCHARGE

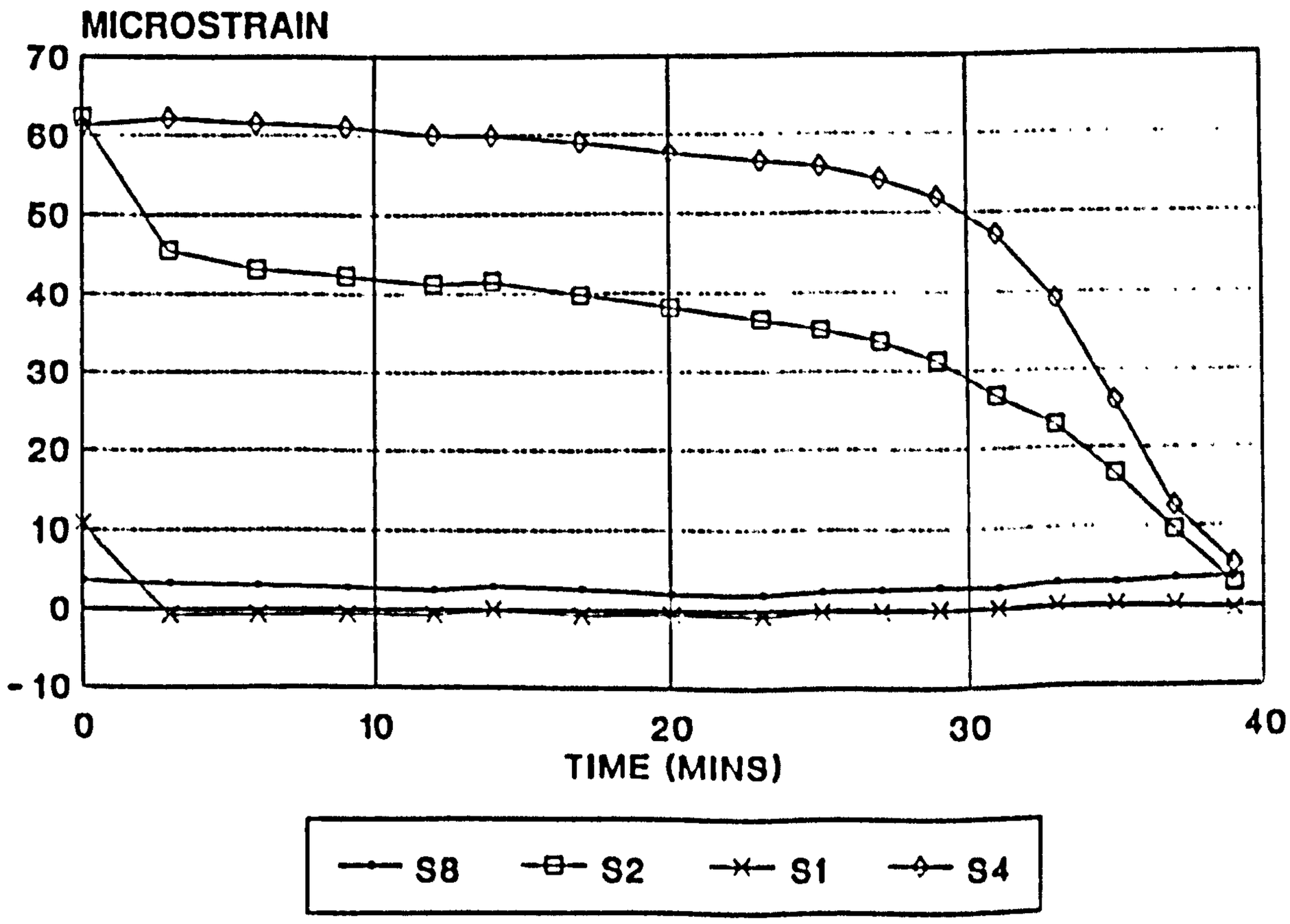

Figure 8.77

HORIZONTAL STRAIN - DISCHARGE

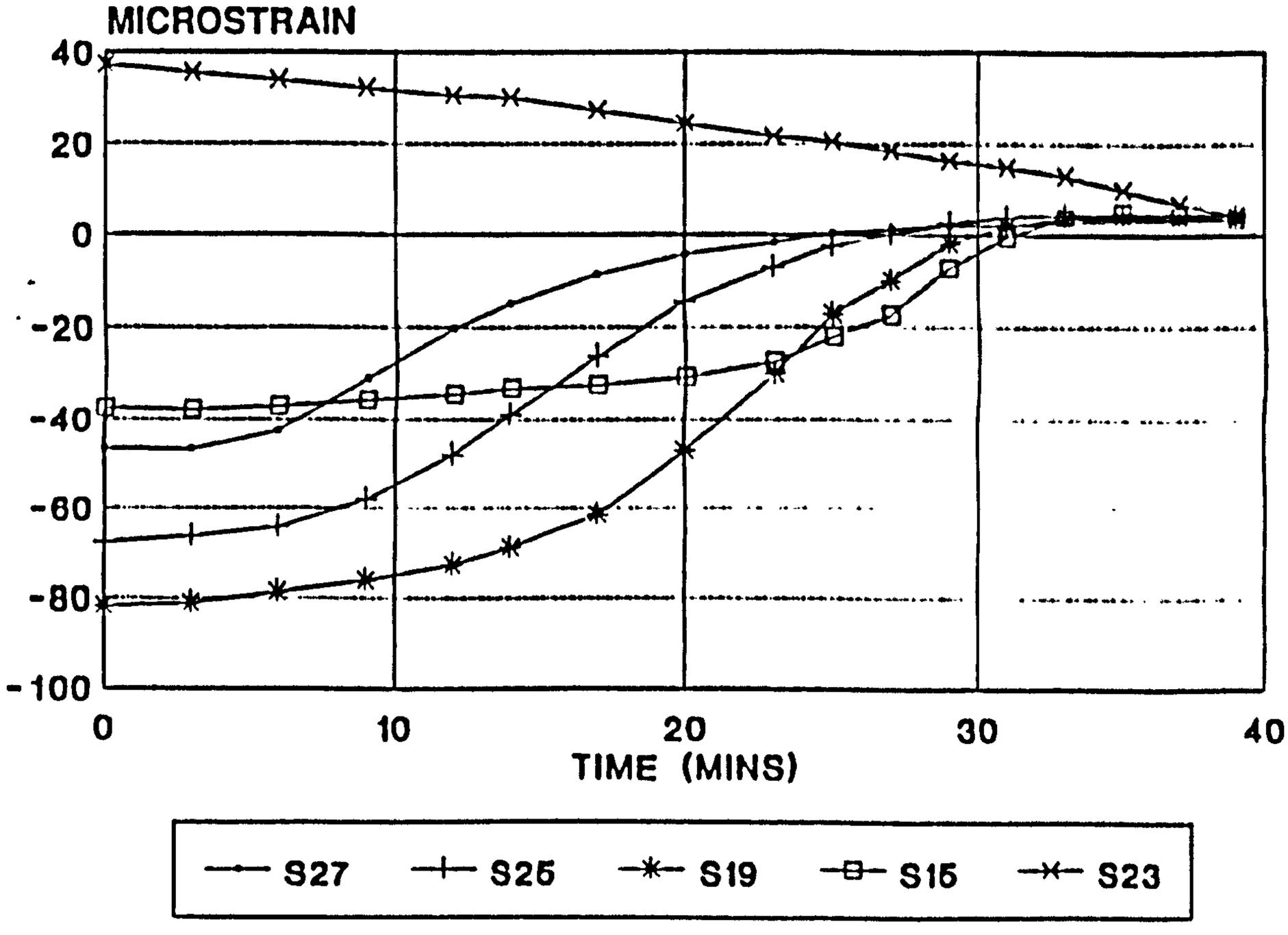

Figure 8.78

HORIZONTAL STRAIN - DISCHARGE

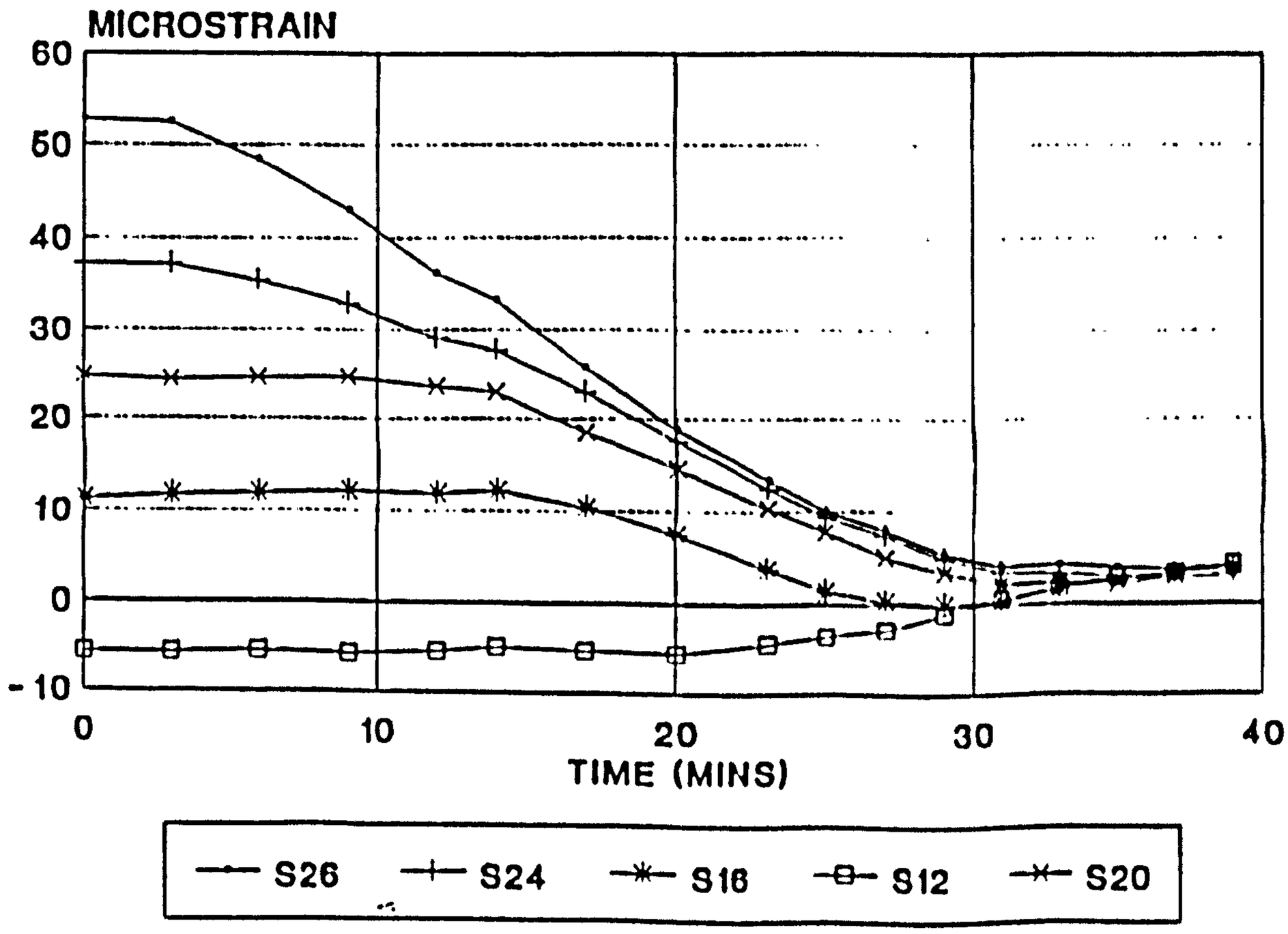

Figure 8.79

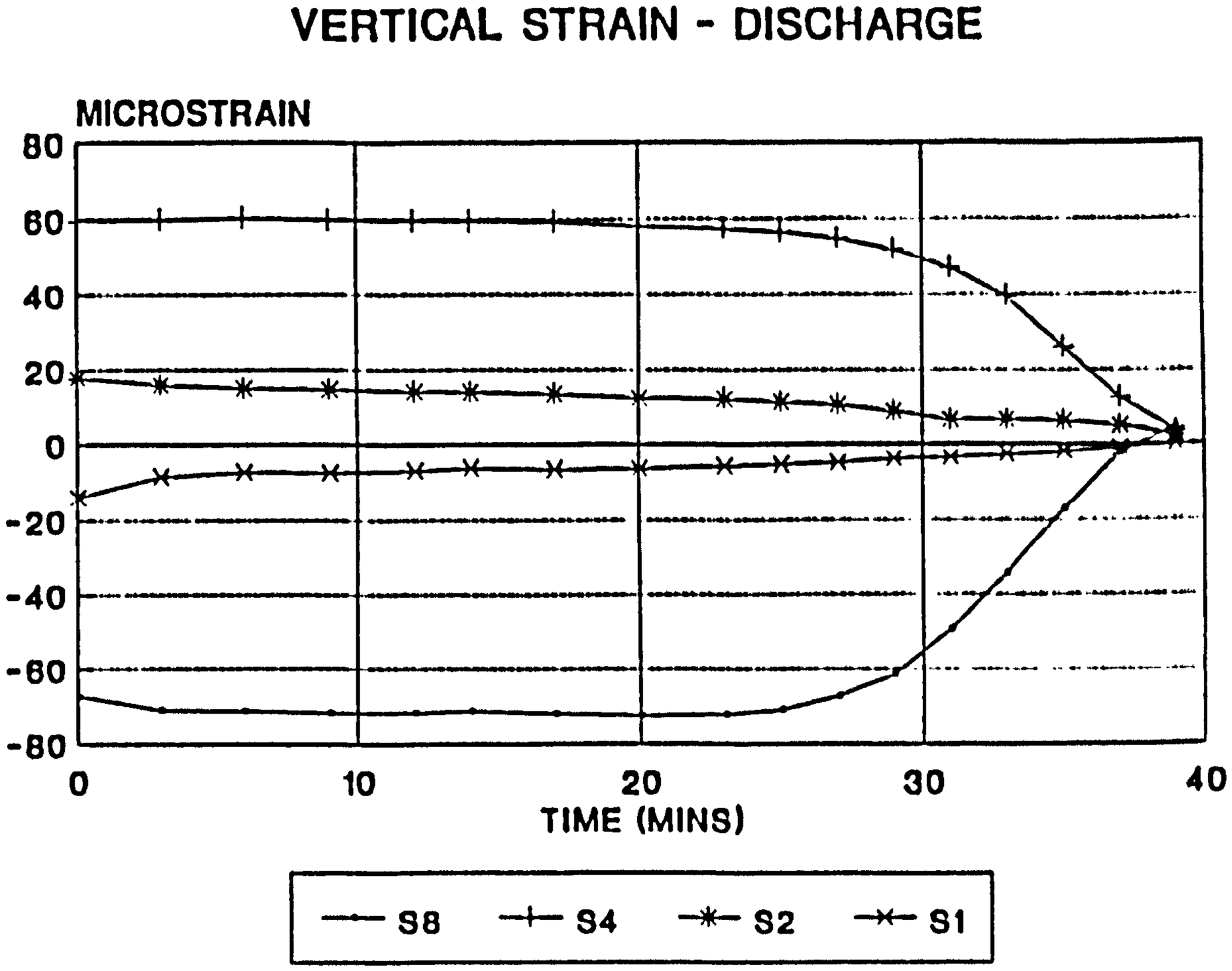

Figure 8.80

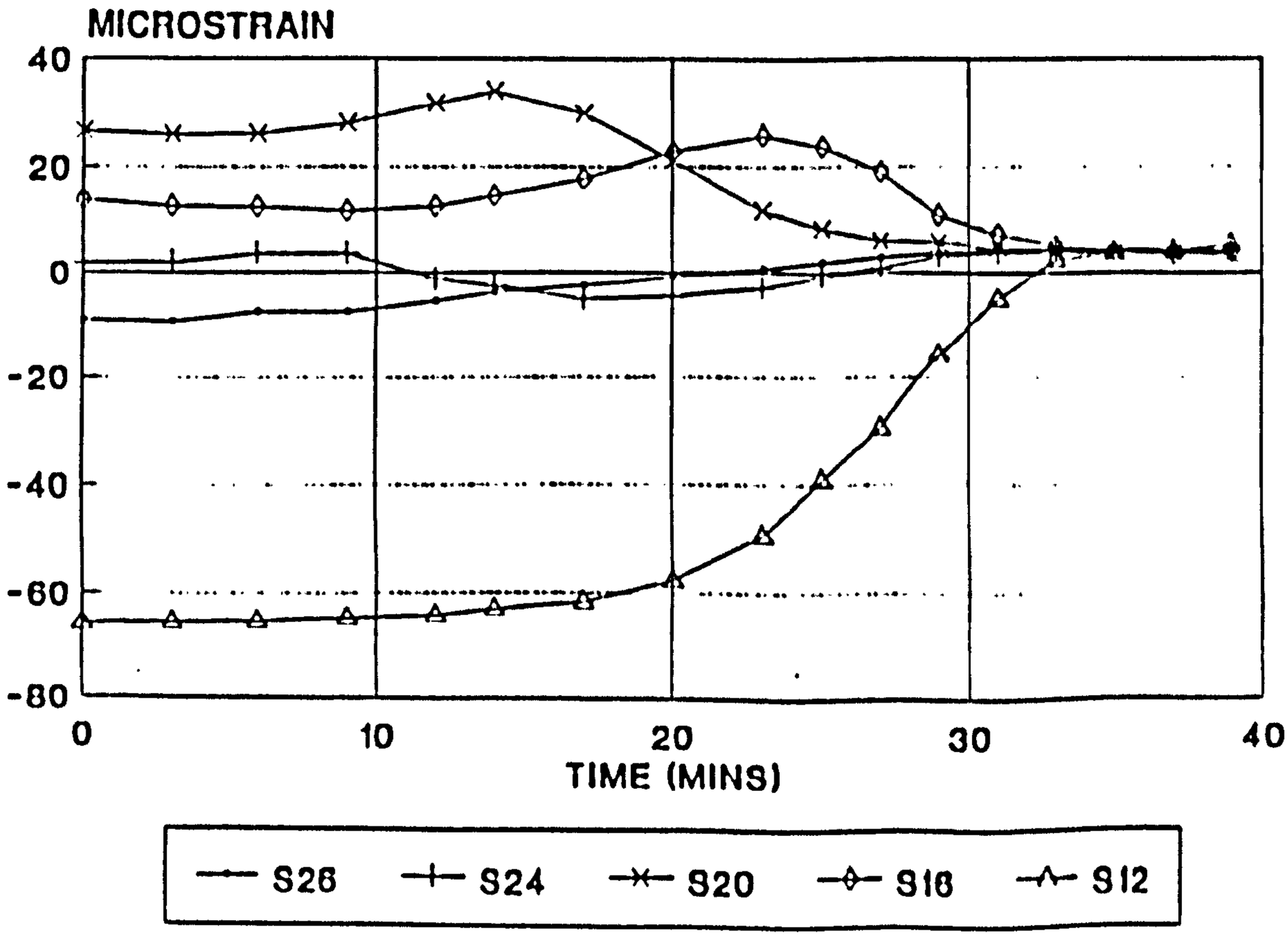

Figure 8.81

9. Checks to determine the accuracy of measured data

Extreme care was taken when selecting, installing and using the instrumentation to ensure that the measured data was accurate. Checks were carried out after testing to confirm the accuracy of the data. It was necessary to check the embedded cell measurements because of their susceptibility to placement error and inaccuracies during calibration; they were checked by investigation of the equilibrium of vertical forces in the silo. Two equilibrium checks were carried out.

a) Vertical equilibrium at the level of the bin and hopper transition with the silo full.

b) Vertical equilibrium of the hopper with the silo full.

The strain gauge results enabled another check on the accuracy of the measured data. The experimental strains were compared with those predicted by a Finite Element analysis incorporating the measured pressure distribution. Good correlation between the two sets of results would suggest that the measured data was accurate.

A final check on the accuracy of the measured data is given in Chapter 11. The Mohr's circles shown in Figure 11.4 illustrate the states of stress of the stored material at different points in the silo. The limiting active state is also shown. The proximity of the Mohr's circles to the limiting active state in areas of large wall deformation gives further confirmation of the accuracy of the pressure measurements.

Concern over the accuracy of the displacement data necessitated a check of its accuracy. This was carried out by a comparison of the displacements predicted by the Finite Element analysis and the measured displacements.

9.1. Equilibrium check at the transition level

The equilibrium of forces was checked at the level of the hopper/bin transition. Vertical pressure was measured at the points shown on plan in Figure 9.1 and pressure was assumed to vary linearly between these points. The sum of the vertical force over one eigth of the transition was determined from numerical integration using Simpsons rule. Since there was only a small variation of pressure at the transition, it is unlikely that the assumption of linearity between measurement points led to a significant error in the summation. The calculated force was multiplied by eight to give the vertical force at the transition. The vertical friction force carried by the wall above the transition was determined in a similar manner. Pressure normal to the wall was measured at the points shown in Figure 9.2, and the sum of the normal pressure distribution acting on half of the wall was again calculated using numerical integration. The spacing between pressure cells was reduced at one level close to the corners to measure the steep pressure gradient. At other levels (except close to the transition) a similar distribution between the measured points was assumed. The coefficient of wall friction was taken from the wall cell results and was 0.7. The friction force for the half wall was calculated from the product of the normal force and the coefficient of friction. Symmetry was assumed and the friction force acting on half of the wall was multiplied by eight to give the sum of the force on all four walls.

The volume and unit weight of the stored material have been assessed. Consideration of the equilibrium of vertical forces leads to

$$\rho V_{bin} = \int_{\frac{-a}{2}}^{\frac{a}{2}} \int_{\frac{-a}{2}}^{\frac{a}{2}} P_v \, dx \, dy + \int_{0}^{h} \int_{\frac{-a}{2}}^{\frac{a}{2}} q \, dx \, dz \qquad (9.2)$$

where x=0 is taken at the centreline of the bin and hopper wall, y=0 is taken at the centreline of the orthogonal bin wall and z=0 is taken at the level of the top of the bin. V_{bin} is the volume of the silo above the transition, ρ is the unit weight of the contents, h is the depth of the bin,

$\int_{\frac{-a}{2}}^{\frac{a}{2}} \int_{\frac{-a}{2}}^{\frac{a}{2}} P_v \, dx \, dy$ is the factored sum of vertical pressure at the transition and $\int_{0}^{h} \int_{\frac{-a}{2}}^{\frac{a}{2}} q \, dx \, dz$ is the sum

of the frictional drag above the transition.

The calculation yields:-

Total weight of the contents = 16.29 * 8 = 130.3 kN

Sum of vertical force at the transition and friction force = 107.7 + 37.9 = 145.6 kN

The measured vertical force and friction force are unfactored. If the measured pressures are multiplied by the calibration constant (0.83) determined in Chapter 5, the sum of the vertical force at the transition and the friction force becomes

89.39 + 31.46 = 120.84

The difference between the measured force and the weight of the contents is within the bounds of an error analysis which considers the deviation in the surface of the contents from that assumed in the volume calculation, variation in material density and wall friction from the measured values, and variation due to the linear interpolation between the results.

9.2. Equilibrium check in the hopper

The total measured vertical force is equal to the vertical components of wall friction and normal pressure over the hopper wall and the surcharge from the bin. This should be equal to the total weight of the contents of the silo.

The calculation yields:-

Sum of the weight of the hopper contents and the surcharge from the bin = 21.0 + (107.7 * 0.83) = 110.39 kN

Sum of the vertical components of normal force and friction force

= 146.5 * 0.83 = 121.6 kN

The difference between the measured force and the weight of the contents is again within the bounds of an error analysis.

9.3. Comparison of experimental and Finite Element wall stress distributions

A further check of the accuracy of the measured pressures was carried out using the strain gauges. The stress distribution calculated from the measured strains was compared with the stress distribution predicted by a Finite Element analysis incorporating the experimentally measured pressure distribution. Good correlation between the two stress distributions confirmed the accuarcy of the measured strains, the Finite Element model and the measured pressures. The accuracy of the strain gauge measurement system reduces the realistic possibilities of differences between the two sets of wall stresses to:

a. Incorrect assumptions in the Finite Element model.

b. Inaccuracies in the measurement of the pressure field.

c. Inaccuracies arising from the interpolation between measurement points for input into the Finite Element model.

Assumptions related to the boundary conditions of the walls ('a') were a possible cause of inaccuracy of the results from the Finite Element analysis. The Finite Element model is described in Appendix A. The Appendix also includes a description of tests that confirmed the accuracy of the Finite Element model by comparison with a Perspex model silo filled with water. Therefore only inaccuracies due to 'b' and 'c' led to significant differences between the experimental and Finite Element stresses.

A small selection of the results are given in Table 9.1. The positions are shown in Figure 8.1.

Position	Experiment	F.E. with measured pressure
S20	$7\,N/mm^2$	$13\,N/mm^2$
S19	$20\,N/mm^2$	$30\,N/mm^2$
S12	$17\,N/mm^2$	$19\,N/mm^2$

TABLE 9.1 - Comparison of wall stresses

The stress distribution predicted by the Finite Element analysis incorporating the measured pressure distribution was similar to the experimental stress distribution. The maximum principal stress was at point $S19$ and was $30\,N/mm^2$ ($10\,N/mm^2$ higher than the equivalent experimental stress). The major cause of discrepency was probably inaccuracies of the pressure distribution applied to the Finite Element model. In particular, the pressure gradients were not modelled accurately because of the large mesh size adopted and the necessity of applying a uniform pressure to each element in the mesh. However, the reasonable correlation between the two stress distributions tends to confirm the accuracy of the embedded cell pressure measurements and the Finite Element model.

9.4. Assessment of the reliability of the displacement results

Before the start of testing it was expected that displacements would be measured to a high degree of accuracy. The transducers were fixed to a rigid and apparently independent frame (Figure 4.2a). The measured displacements at each position showed good agreement for five tests but there was some doubt about the accuracy of the measurements near the corners. They were larger than expected and so

checks were carried out which confirmed that the silo was not rotating as a rigid body. The accuracy of the measured data were checked by comparison with results from a Finite Element analysis. Displacements predicted by the Finite Element model described in Appendix A and incorporating the measured pressure distribution were compared with the experimental displacements. The deformed wall profiles were similar. The Finite Element model predicted a maximum bin wall deformation of 3.9mm between points *D* 11 and *D* 12 (Figure 8.18). This is over fifty per cent greater than the measured deformation at the same point. The maximum bin wall stresses predicted using the same Finite Element model were also in the region of fifty per cent greater than the measured stresses. The difference may be attributed to the interpolation of measured pressures between points of measurement for input into the Finite Element analysis. Finite Element displacements in the corners were considerably smaller than the measured displacements. The measured displacements in the corners are inexplicably large but the data away from the corners agree with the anticipated trends of distribution and magnitude.

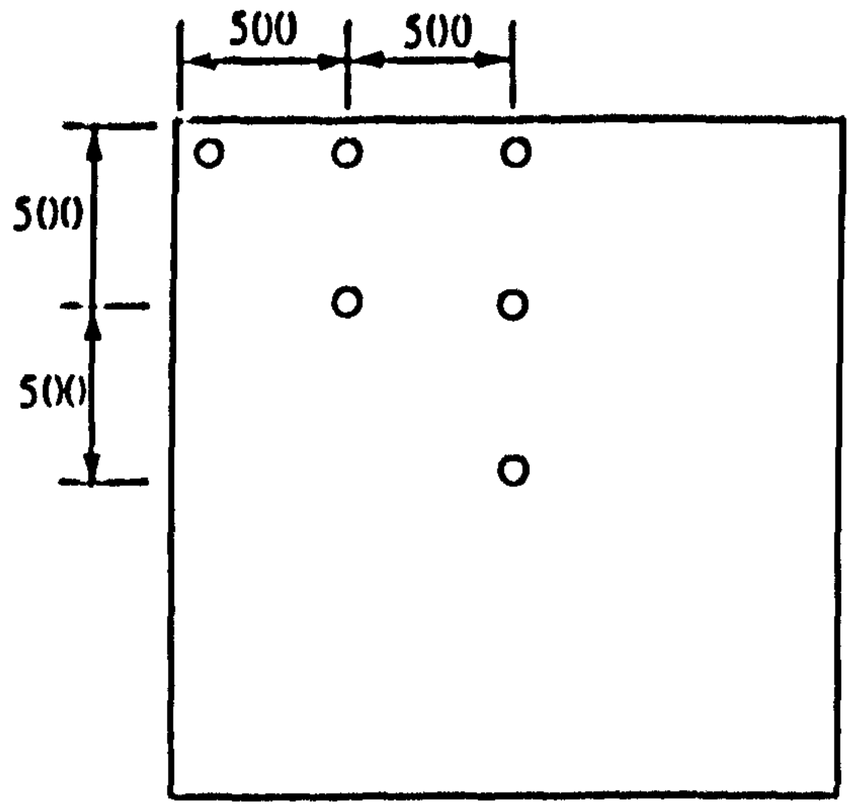

Figure 9.1 VERTICAL PRESSURE MEASUREMENT

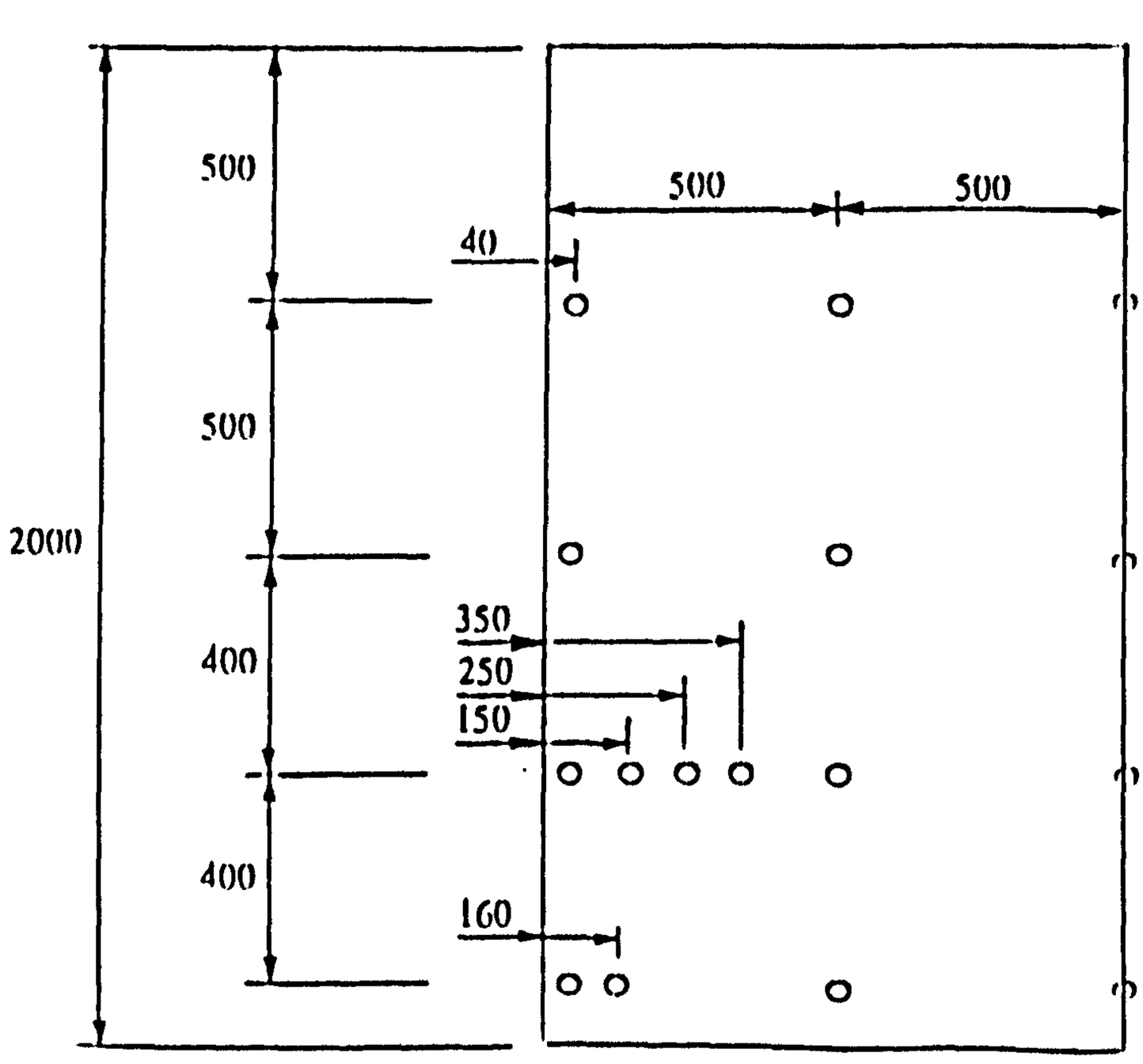

Figure 9.2 HORIZONTAL PRESSURE MEASUREMENT

CELL POSITIONS FOR THE CHECK OF
VERTICAL EQUILIBRIUM

10. Comparison of the experimental results with existing theory

The results of pressure measurements from the model silo (discussed in Section 8.4) show that the pressure at any level on a flexible wall is higher at the corners than in the centre of the wall. In Chapter 3, existing methods of pressure calculation were reviewed and it was found that they did not predict this pressure gradient on a horizontal plane. The gradient is due to a pressure redistribution. In this chapter, the significance of the pressure gradient is investigated by a comparison of the measured pressures and the pressures predicted by existing theories. Finally the measured wall strains are compared with those predicted for a wall under a uniform Janssen pressure distribution to quantify the effect of the true pressure distribution on wall stresses.

10.1. Horizontal pressure in the bin

Figure 10.1 shows the measured pressures normal to the bin wall and pressures calculated from Janssen's formulae for the silo filled with sand. Two values of K, the ratio of horizontal to vertical pressure, are adopted. These were the Jaky coefficient for earth pressure at-rest and the Rankine active coefficient. The two Janssen distributions would be the limiting states of pressure if there were no arching action. Therefore, the comparison gives a good indication of the significance of arching in the silo.

Horizontal arches were evident at any point behind a deformed wall when the level of the surface of the stored material has risen to 0.5 m. above the point of consideration. At point *WN* 16 (Figure 8.32) the measured pressure in the centre of the bin wall is visibly less than the Janssen active pressure when the stored material has risen 0.5 m. The pressure at the corner at the same level (*WN* 24) is more than double the Janssen at-rest value. When the surface of the stored material has risen to a certain point (somewhere between 0.5 m. and 1.2 m. above the wall centre) the rate of increase of pressure in the centre of

the wall has reduced to nearly zero. Therefore pressure in the centre of the wall is progressively less than the Janssen active value as the depth of stored material increases. Pressure at the corner continues to increase rapidly with depth and reaches a value that is more than four times the Janssen at-rest value.

It is not possible for a cohesionless soil to be in a stress state that is less than the limiting active state. Janssen's equation (incorporating Rankines value for K_a) predicts a pressure that is equal to the active state and so the horizontal pressures can only be less than those predicted by Janssen if the vertical pressures are also lower. This is in fact the case, and further discussion is presented in Section 10.2.

At points just above the ring beam, the horizontal pressure at the centre of the wall increases to a value above the Janssen active pressure and the corner pressure decreases towards the Janssen at-rest pressure. At the ring beam level, pressure in the centre of the beam (WH4, Figure 8.59) rises to nearly twice the Janssen at-rest value. This is because the inward deformation of the ring beam generates a move towards the passive pressure state. In addition a ring beam arch forms over the corners and generates a pressure increase in the middle of the beam. In the corners at the ring beam level pressure drops to less than the at-rest value. An arch formation 'bridges' the corner and results in pressure relief at the corner and pressure increase over the remainder of the ring beam. This arch formation is discussed further in Section 11.1.

10.2. Vertical pressure

Figures 10.3 and 10.4 show the measured vertical pressures and the Janssen and hydrostatic distributions. The positions of points for comparison are shown in Figure 10.2. A comparison of the experimental and theoretical pressure distributions indicates the effect of arching and wall friction on vertical pressures. Without any arching the vertical pressure would be closely approximated by the Janssen active pressure in the centre of the wall and the Janssen at-rest pressure in the corners. In the centre of the silo the effect of wall friction is reduced (as described in Section 2.1.1.) and so the vertical pressure

should be equal or close to the hydrostatic pressure. Figure 10.4 indicates that there is an extensive pressure transfer at the wall due to arching. Measured vertical pressures are considerably lower than the Janssen active pressure in areas of high wall deformation. In the corners they are equal to the hydrostatic distribution.

It is evident that more load is relieved from the central section of the wall than is imposed on the corners. Therefore, to maintain vertical equilibrium load must be increased away from the walls. Figure 8.65 shows that there is evidence of such an increase between the corner and the centre of the silo (point *IV*18, Figure 8.61) where the measured pressure is greater than the hydrostatic pressure. The pressure increase at this point and the reduced gradient of the pressure increase at the corner indicates the existence of a Terzaghi arch. This was arch described in Chapter 2. In the silo, it reduces vertical pressure near the wall and increases friction on the wall and vertical pressure at some distance from the wall (point IV18). It is described in Section 11.1.

At the centre of the silo the measured pressure follows the hydrostatic distribution from the top of the silo to a point at 250 mm. above the outlet. This suggests that the wall friction and arching have a negligible effect on pressure in the silo centre. The low pressure measured near the outlet suggests that wall friction affects pressure over the entire cross section at this level. The reduced distance between the walls leads to a local Janssen arch formation that is similar to arching between the walls of a deep silo (Janssen's theory).

The measured vertical pressure in the corners at the ring beam level is less than half the Janssen at-rest value. This follows a similar trend to the horizontal pressure and was discussed in Section 8.4.1.

10.3. Pressure normal to the hopper wall

In Chapter 3 it was stated that there is a wide variation between the existing theories for hopper pressure calculation. The accuracy of the theories for predicting the pressure on a rigid wall is in dispute.

Therefore, it is not possible to determine accurately the extent of arching from a comparison of experiment and theory. The comparison does lead to some conclusions concerning the hopper pressure measurements and the accuracy of the existing methods of pressure calculation on flexible hopper walls.

Figure 10.5 shows a comparison between the Jenike and Walker theories and the experimental results for the hopper filled to the level of the transition ring beam. The distribution of the mean pressure with depth is close to linear. This suggests that there is insufficient consolidation force to develop the shear strength to support a vertical arch (an arch which redistributes pressure from the middle of the wall and increase it at the ring beam and hopper outlet). Therefore, the theoretical predictions of Jenike and Walker, for a hopper without surcharge from the contents of a bin appear to give a reasonable estimation of the mean wall pressure if the true value of wall friction is known.

A comparison of the Walker, Jenike and experimental pressures in the hopper when the silo is full is given in Figure 10.6. Horizontal arching reduces the pressure in the centre of the silo to less than a quarter of the lowest theoretical prediction. Pressure at the corner half way up the silo is three times the highest theoretical prediction.

The mean horizontal pressure (determined by the integration of pressure over a horizontal slice divided by the width of that slice) is no longer linear with depth. It is a maximum at the transition and at the outlet. This suggests that vertical arches relieve pressure from the mid-height of the hopper and increase pressure at the ring beam and the outlet. The measured pressure in the centre of the hopper wall is less than the theoretical values. This suggests that a horizontal arch has formed and redistributed pressure from the centre to the edges. Neither theory incorporates any of the effects of wall flexibility and so they do not give an accurate prediction of the wall pressure. Walker's theory overestimates the mean wall pressures as predicted in Section 3.2.2. Jenike's theory gives a reasonable prediction of the mean experimental wall pressure from just above the outlet to the ring beam. The integral of wall pressure over a horizontal slice using Jenike's theory leads to slightly higher values than those obtained from the experiment. Both distributions were calculated to maintain vertical equilibrium of the hopper but the Jenike distribution incorporated a theoretical surcharge from the bin contents which

was greater than the measured surcharge.

10.4. Ratio of horizontal to vertical pressure

Figures 10.8 to 10.10 show the ratio of horizontal to vertical pressure ($\frac{\sigma_h}{\sigma_v}$) plotted against depth of material for different points in the silo when the silo is full. The positions are shown in Figure 10.7 and labelled as K1 to K9 respectively. The experimentally measured ratios are compared with Jaky's coefficient for earth pressure at-rest and the Rankine active coefficient. The measured values are not necessarily principal stresses and so the comparison is not of theoretical and experimental values of the ratio 'K' as defined in the notation but is of theoretical and experimental ratios of horizontal to vertical pressure.

In the centre of the silo K is equal to the at-rest value. This suggests that the stored material in the centre is not affected by wall deformation and it is in an elastic state of equilibrium. In the corners the stored material is also in an elastic state of equilibrium but the effects of Terzaghi arching result in a ratio of K that is much higher than the at-rest ratio. This is because horizontal and vertical pressures are redistributed from the centre of the silo to the corner. Both pressures are increased by a similar magnitude and so the ratio of horizontal to vertical pressure is increased.

Away from the corners and close to the deformed wall the sand is in a plastic active state of equilibrium. Figure 10.8 shows that the stress ratio at position $K2$ is less than the active ratio. The active ratio is a lower bound. The discrepancy suggests that there is an error in either the theoretical or the experimental ratio. The theoretical value of K_a may be incorrect due to an inaccurate angle of internal friction. In Chapter 3 problems of recreating the stored material stress state in the shear box were discussed. It was concluded that the angle of internal friction was dependent upon the stress path to failure of the stored material and that it could vary in the model silo. A second source of error is the embedded pressure cells. The discussion in Chapter 5 highlighted the problems of obtaining accurate data and showed that the small discrepancy between the measured and theoretical ratios of K_a could be

attributed to measuring errors. Despite these sources of error, the discrepancy between the experimental and theoretical ratios is small and so it is reasonable to conclude that the material near the wall is an active state of plastic equilibrium.

10.5. Wall stresses

The incorporation of the arched pressure distribution into design results in a lower wall stress than an analysis that incorporates an existing theoretical pressure distribution. It follows that economies in the structure of non-circular flexible silos are possible if the true pressure distribution is used. The incorporation of the true pressure distribution is only important if the economies are sufficient to justify any additional computation. This section discusses the results of a study to determine the effect of a non-uniform pressure distribution on the wall stress of the silo test model. It indicates the possible economies arising from the inclusion of a non-uniform pressure in the silo design.

The stress distribution in a flexible wall subjected to a uniform pressure distribution (pressure does not vary on a horizontal plane) was compared with the stress distribution in the same wall subjected to a true pressure distribution. It was not feasible to impose a uniform distribution on the model silo wall and so the experimental wall stresses were compared with wall stresses predicted using a Finite Element model. The Finite Element model described in Appendix B was used. The accuracy of the model was discussed investigated in Chapters 4 and 9 and the stress results correlated well with experimental results from the steel and perspex silos. The Janssen pressure distribution incorporated the stored material properties given in Chapter 5 (Table 4.3). The Rankine active value was selected for the ratio of horizontal to vertical pressure to give the lower theoretical pressure distribution and hence the lowest wall stresses.

The highest wall stresses in the experimental model were close to the centre of the walls, near to the corners and near to the ring beam. The highest experimental principal stress in the bin wall was at point *S* 19, Figure 8.1. It was 20 N/mm^2 and was at an orientation close to the horizontal axis. The principal

stresses along the vertical centreline of the wall did not rise above 8 N/mm^2 except at the bottom of the wall close to the ring beam. Here the maximum measured stress was at point $S12$ (Figure 8.1) and it was 17 N/mm^2.

The stresses predicted by the Finite Element analysis with the Janssen pressure distribution were very different to those from the non-uniform pressure distribution. The maximum stresses were significantly higher in the uniform pressure model. The highest principal stress was 50 N/mm^2 close to the centre of the wall at point $S20$, Figure 8.1. This was more than five times the experimental stress at the same position. The stress at point $S19$ at the corner of the silo was 23 N/mm^2, this was similar to the experimental result.

To summarise, the stress distribution arising from the uniform pressure was very different to that from the non-uniform pressure. In addition the maxximum wall stresses were significantly greater in the wall of the model with the uniform pressure. The difference may justify the development of new theories for pressure calculation in flexible silos.

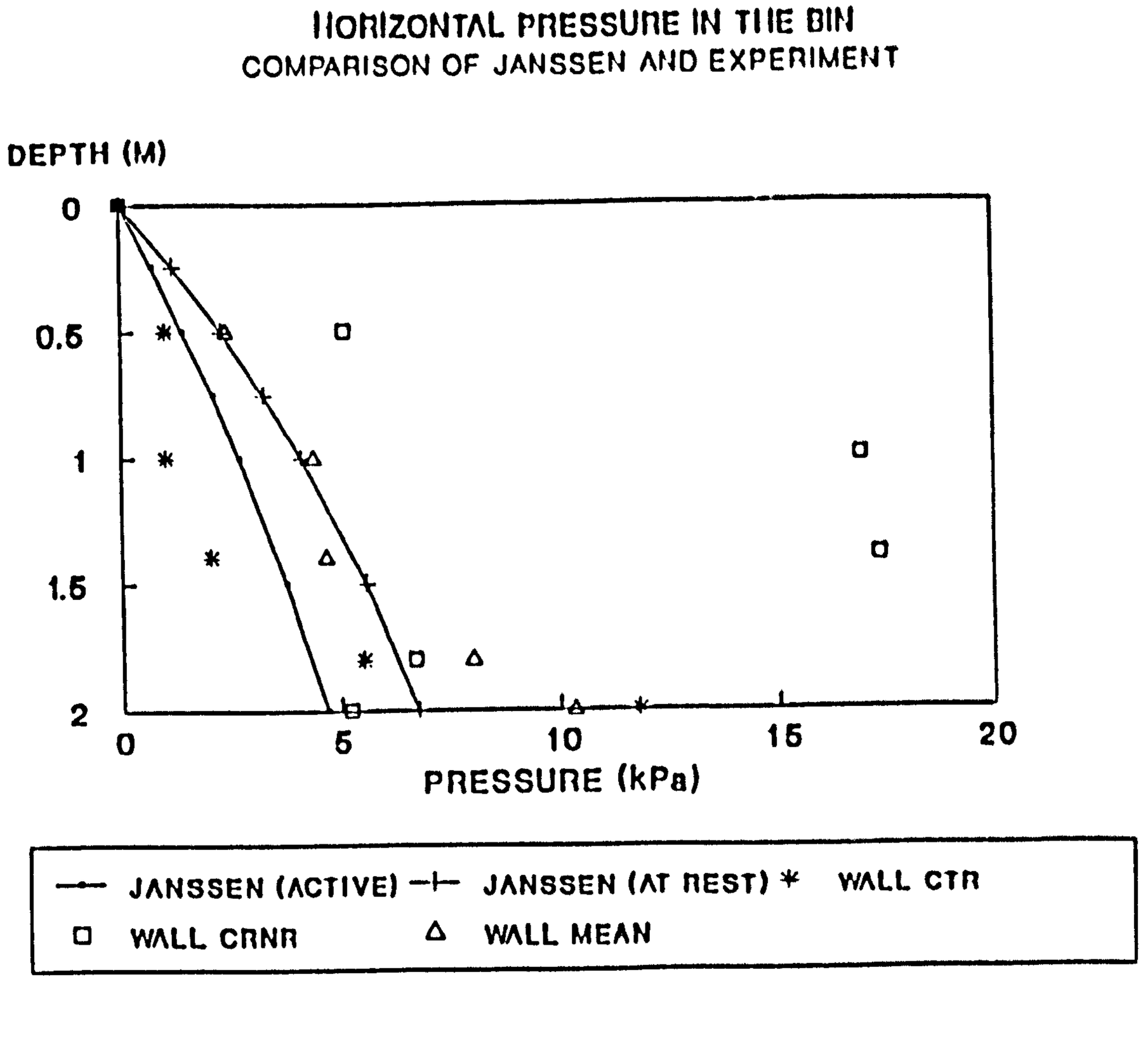

Figure 10.1

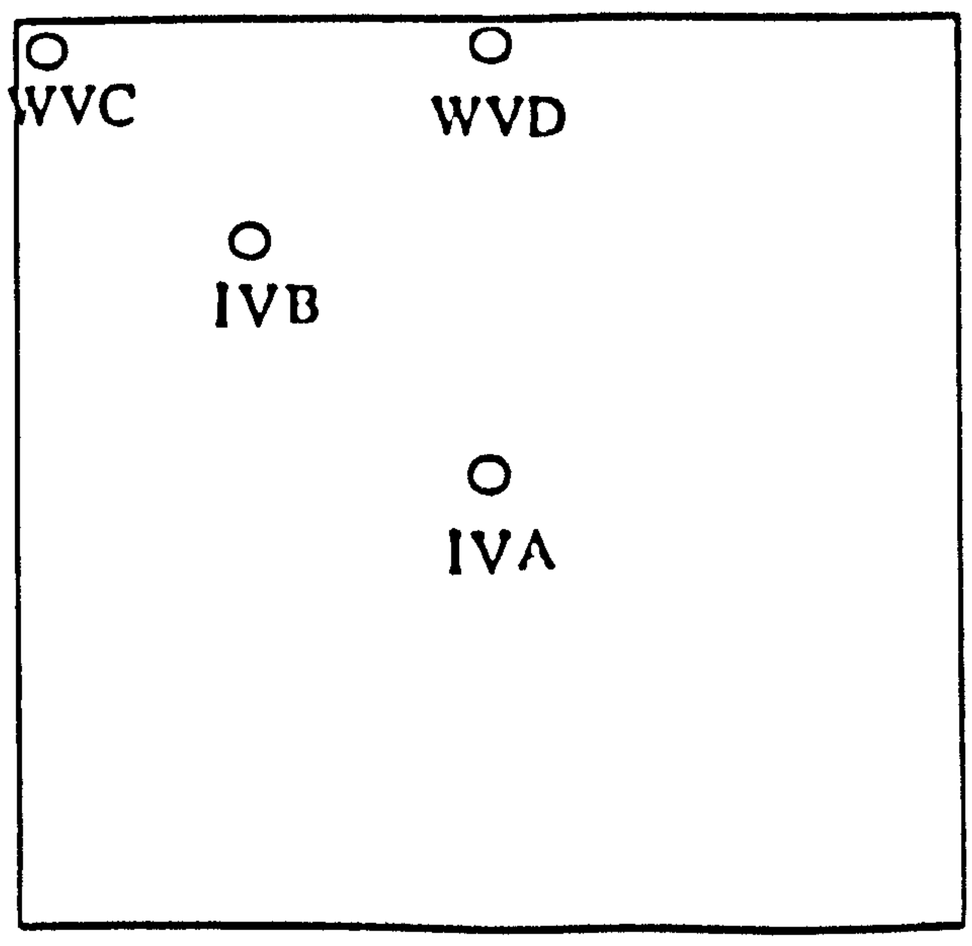

Figure 10.2 KEY TO CELL POSITIONS FOR THE COMPARISON OF EXPERIMENTAL AND THEORETICAL PRESSURE

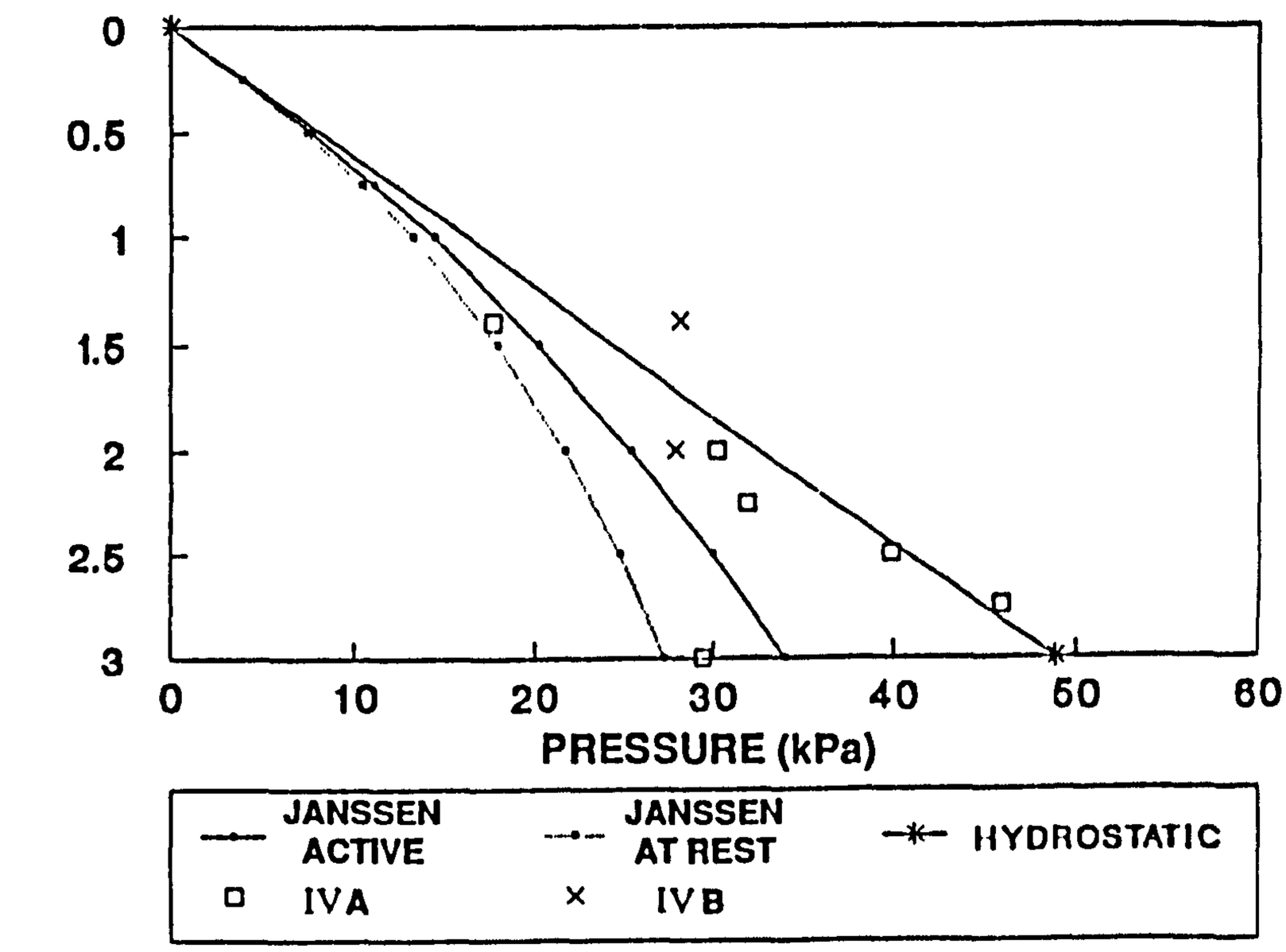

Figure 10.3

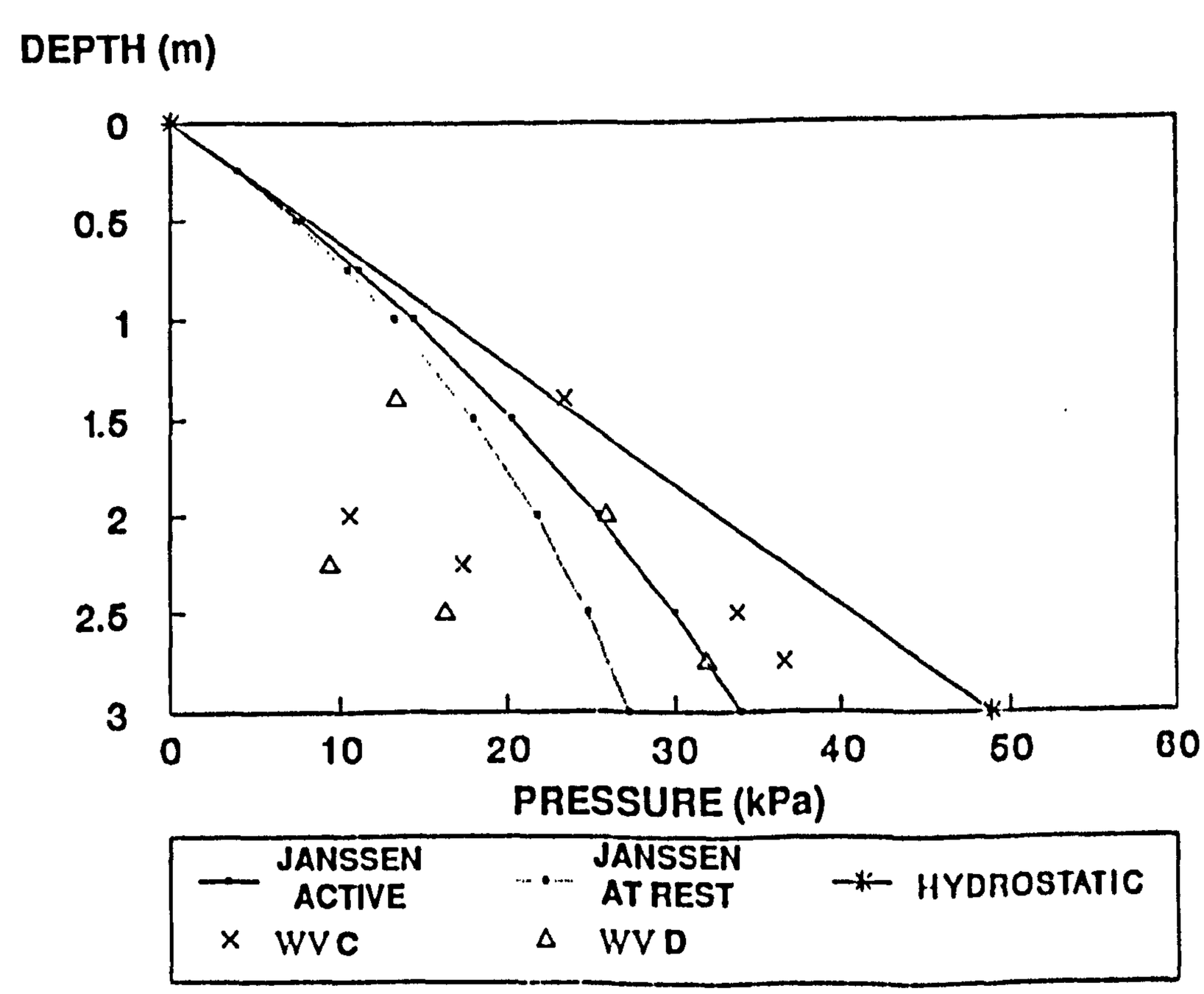

Figure 10.4

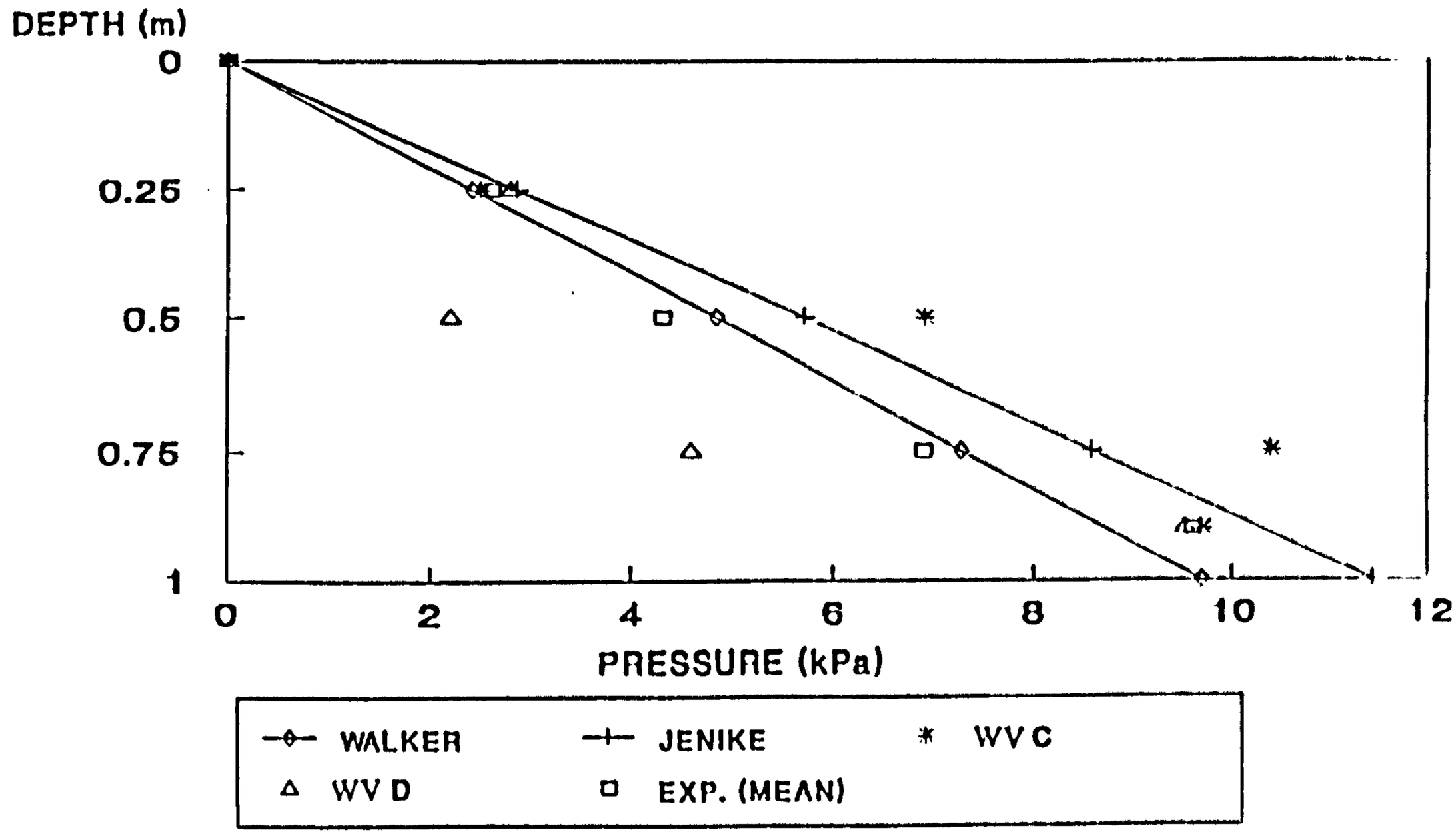

Figure 10.5

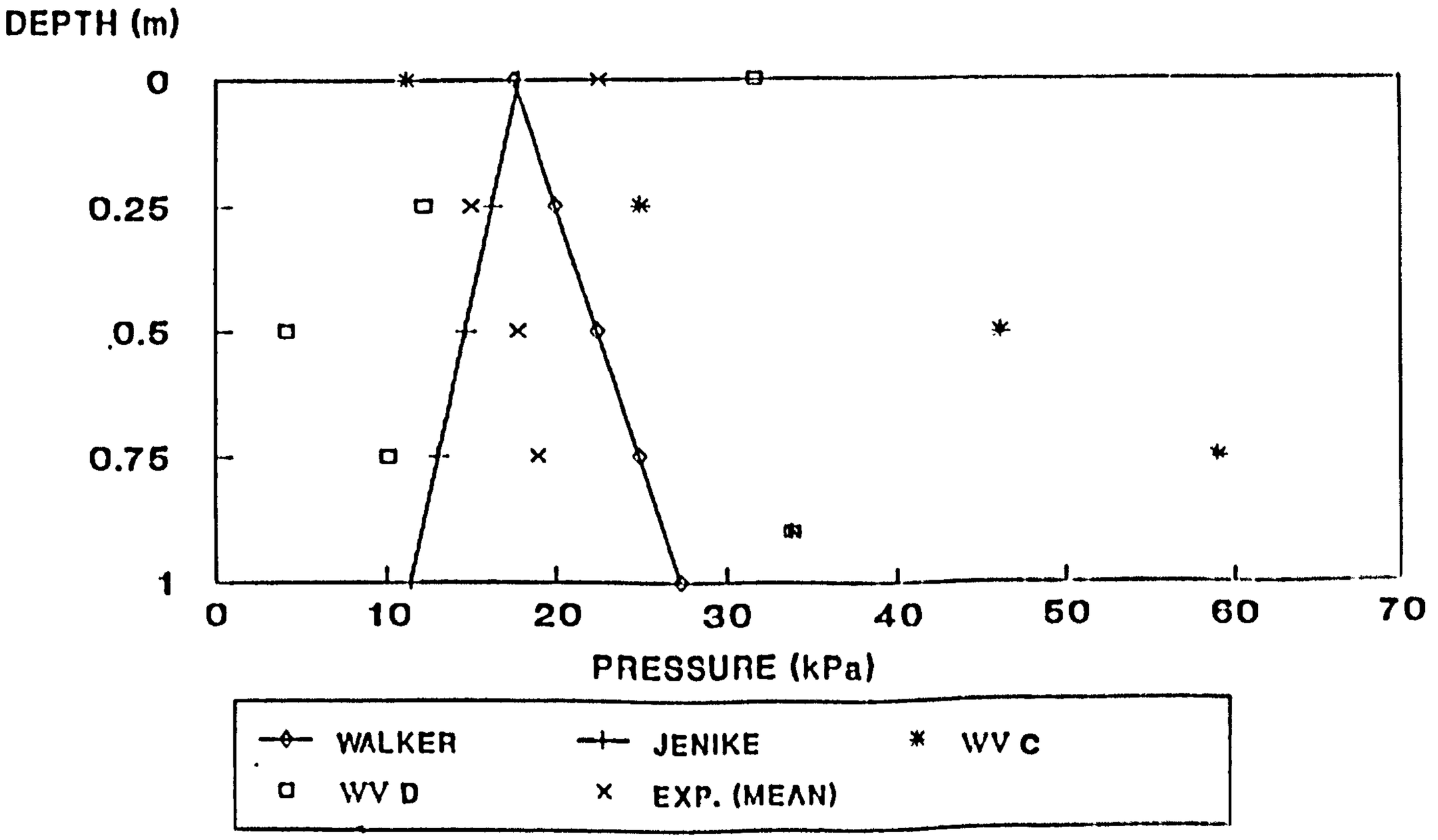

Figure 10.6

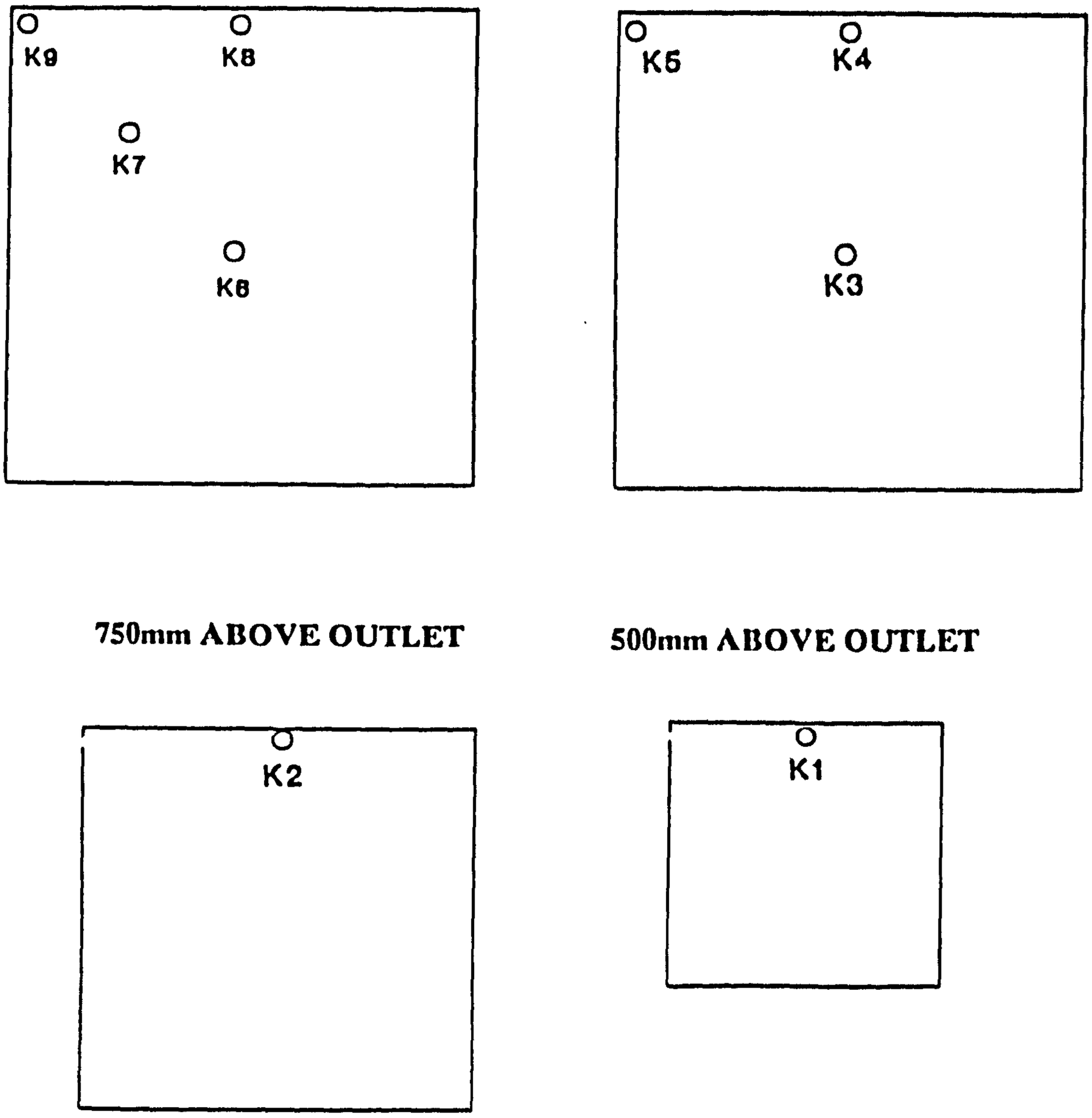

Figure 10.7 KEY TO CELL POSITIONS FOR K

RATIO OF HORIZONTAL TO VERTICAL PRESSURE

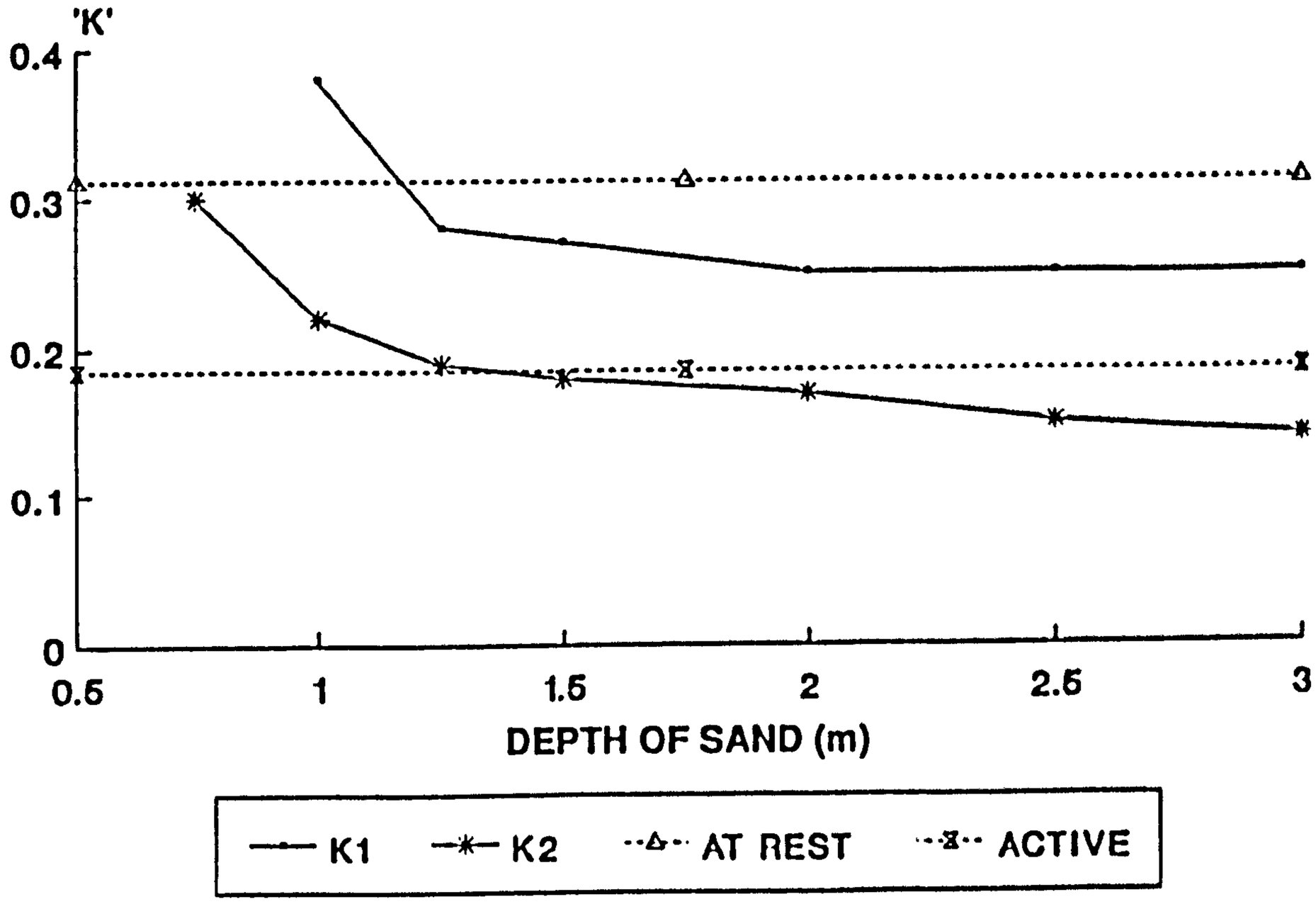

Figure 10.8

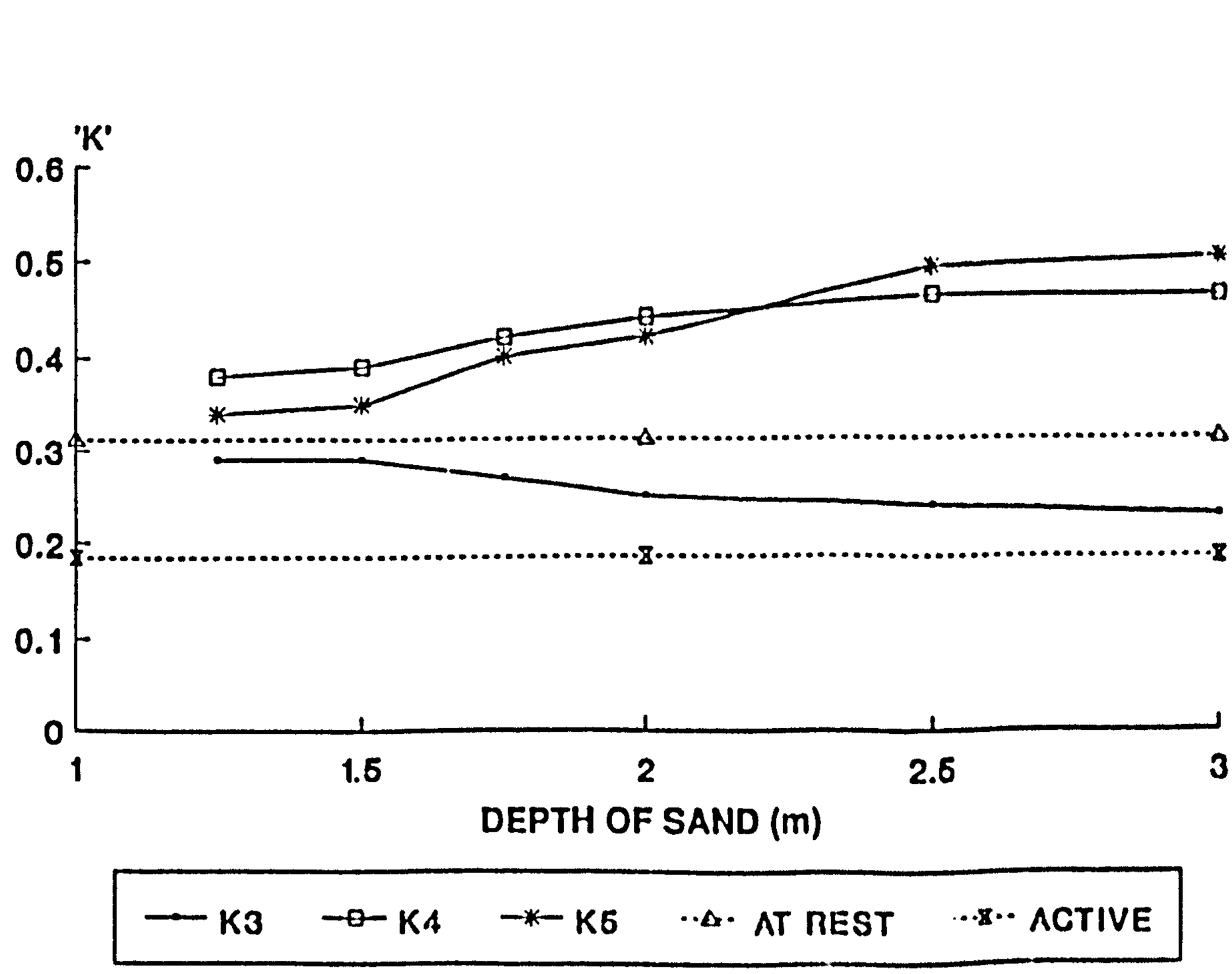

Figure 10.9

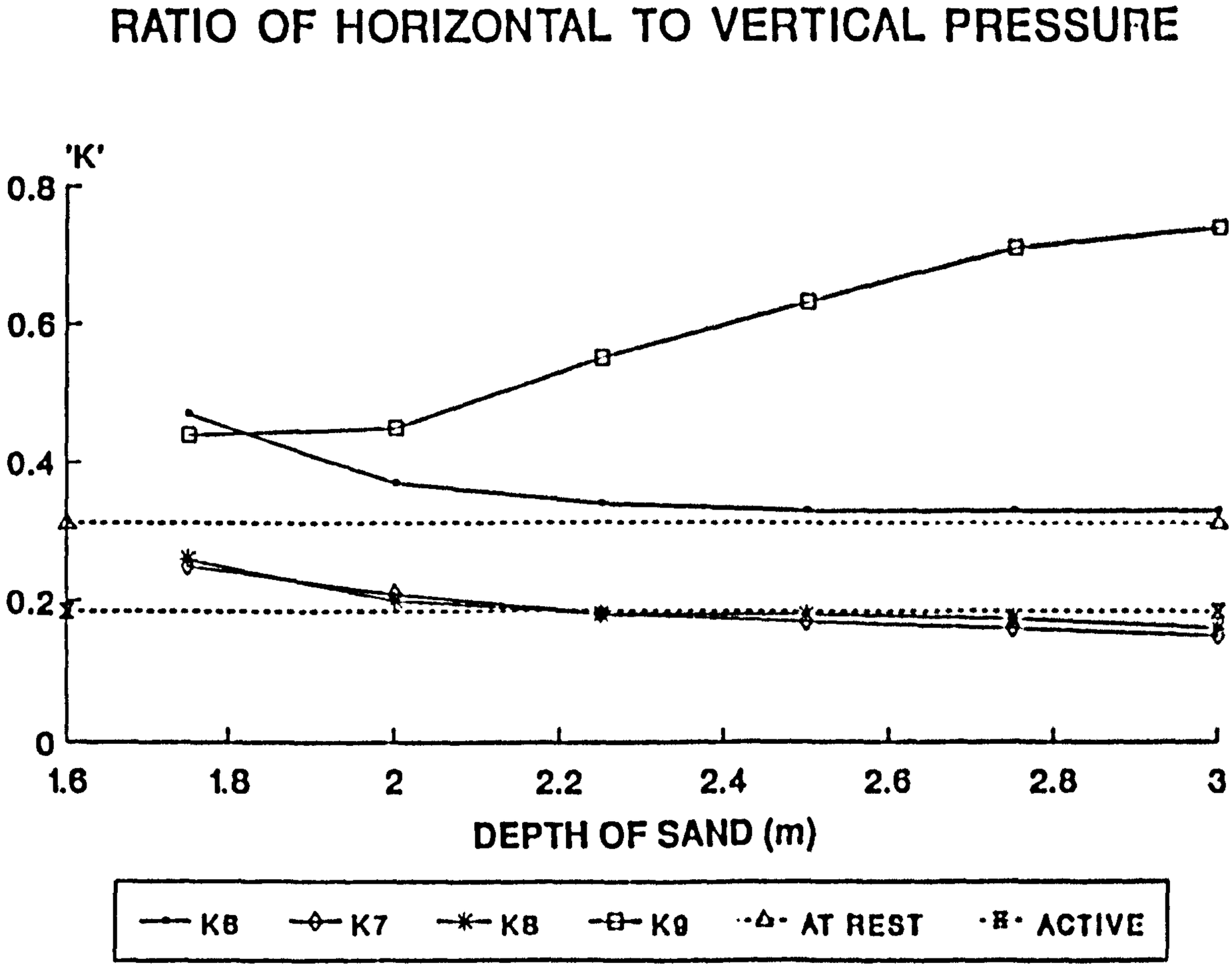
RATIO OF HORIZONTAL TO VERTICAL PRESSURE
'K'
0.8
0.6
0.4
0.2
0
1.6
1.8
2
2.2
2.4
2.6
2.8
3
DEPTH OF SAND (m)
K6
K7
K8
K9
AT REST
ACTIVE

Figure 10.10

11. Summary of the stored material stress state

A summary of the stress state within the stored material during filling is given below. The bin, ring beam and hopper are discussed separately. The stress block shown in Figure 11.1 defines a set of Cartesian axes and stress directions relative to the bin. Compressive stresses are positive. When considering the stored material behind one wall only, σ_z is the stress component aligned with the vertical axis, σ_x is aligned normal to the wall and σ_y acts parallel to the wall.

11.1. Bin

Early in the filling process, the wall deformation is small and the stored material is close to the at-rest state of elastic equilibrium. Wall friction is only partially mobilised and so the direction of the maximum principal stress, σ_1, is close to the vertical axis. The magnitudes of the intermediate and minor principal stresses, σ_2, σ_3, are nearly equal and they are on a plane which is close to the horizontal plane. Continued filling increases the pressure. Consolidation of the stored material mobilises friction forces at the interface of the wall and stored material, and introduces shear stresses (τ_{xz}, τ_{zx}) in a region adjacent to the wall. The direction of the major principal stress is now inclined from the vertical axis.

Wall deformation results in yield of the stored material in a similar manner to that illustrated in Figure 11.2. (Wall flexibility leads to some difference in the length of the shear planes and degree of mobilisation of shear stress but the analogy is appropriate for this discussion). Shear stresses τ_{xz} and τ_{zx} are generated and they reduce the horizontal pressure σ_x in the manner described by Rankine [3] and discussed in Chapter 3. The intermediate principal stress σ_2 is approximately parallel to the wall and the minor principal stress σ_3 is approximately normal to the wall. The slip planes are inclined at an angle of $45 + \frac{\phi}{2}$ degrees to the direction of the minor principal stress.

The wall deformation produces a yield in the form illustrated in Figure 11.2. The figure shows a single layer of the stored material inclined at an angle of $\psi = 45 + \frac{\phi}{2}$ degrees to the horizontal and it is divided into several strips of equal width. The strips slide relative to each other mobilising shear stresses τ_{yz}, τ_{zy}, τ_{yx} and τ_{xy} whose magnitude is in proportion to the wall slope. The centre strips are restrained from movement by friction on adjacent strips and in the same manner, the adjoining strips are restrained from sliding by adjacent strips. To maintain horizontal equilibrium, pressure is transferred from the centre strips and ultimately, a certain part of the pressure from the central area of the wall is transferred through friction to the corners.

The shear stresses τ_{yz}, τ_{zy}, τ_{yx} and τ_{xy} constitute the horizontal arching phenomenon. Because of symmetry, the horizontal slope at the vertical centreline of the wall and τ_{yz}, τ_{zy}, τ_{yx} and τ_{xy} are zero. Shear stresses are generated between the corner and the centre of the wall wherever the wall slopes. The lengths of the shear planes are influenced by the magnitude of the wall deformation and the stiffness of the stored material. Shear planes are longest in areas of maximum wall slope. Towards the corners the shear planes are short but significant pressure transfer is still possible due to the higher horizontal pressure and consequently high shear strength of the stored material.

In the early stages of loading, the small wall deformation leads to a pressure relief from a small area near to the centre of the wall only. A rise in the surface of the stored material increases the wall deformation and hence the length of the shear planes. The shear strength of the stored material is also increased and more pressure is redistributed from point *c* (Figure 11.2) at the centre of the wall towards points *d* and *d'* at the corners. Continued filling reduces the rate of pressure increase in areas of high wall deformation. Eventually, the position of maximum deformation (point *c*) does not feel any further pressure increase since the shear strength of the stored material and wall deformation are sufficient to redistribute all the pressure away from the centre of the wall. Points away from the centre continue to feel a pressure increase at a progressively slower rate until they also are relieved of any further increase.

In the centre of the wall (point 'c' in Figure 11.2) the wall slope in a horizontal plane is zero and so the direction of the minor principal stress is normal to the wall and the intermediate principal stress is parallel with the wall. The stress state at this point by the wall of the silo model at 1600 mm. above the outlet with the silo full is represented by the Mohr's circle shown for Position 3 (Figure 11.3) in Figure 11.4. The minor principal stress is 1.6 kPa. and the major principal stress is approximately 11 kPa. The major principal stress is aligned with an axis that is slightly inclined to the vertical axis because of wall friction.

Between the corner and the centre of the wall, the shear stresses τ_{xy} and τ_{yx} swing the direction of the principal stresses away from a plane normal to the wall and towards a plane parallel to the wall. This stress state is represented by the Mohr's circle at position 2, Figure 11.4. The stress normal to the wall is approximately 8 kPa. and the minor principal stress is approximately 6 kPa. The shear stresses τ_{yz} and τ_{zy} swing the direction of the major principal stress away from the vertical axis.

The stress state at the corner is represented by the Mohr's circle at Position 1, Figure 11.4. The limited wall deformation prevents the stored material from moving from the elastic state. The minor and intermediate principal stresses are both equal to 17 kPa.

The influence of wall flexibility in the centre of the silo is negligible. The stress state at this point is displayed in the Mohr's circle shown in Figure 11.4, Position 5. The stored material is nearly in an at-rest state. The major principal stress aligns with the vertical axis and the minor and intermediate principal stresses are equal.

The vertical pressure close to the corners of the silo is influenced by a Terzaghi arch formation which increases the frictional drag on the wall at the corner of the silo and the vertical pressure at some distance between the corner and the centre of the silo. Close to the corner, the wall yield is not sufficient to mobilise the active plastic state of equilibrium. Small wall deformations will cause some downwards and outwards slip of the stored material near the wall. This is illustrated in Figure 11.5 (Section

AA). It shows inclined layers of deformed stored material against one wall only. The horizontal arch (described above) generates a high horizontal pressure at the silo corners, and this combined with the downwards yield of the stored material induces a high wall friction force near the corner. The stress state near to the non deformed stored material is illustrated by the Mohr's circle in Figure 11.4, at Positions 4. Vertical shear stresses τ_{xz} and τ_{zx} are mobilised at the silo wall and across any section through the yielded stored material. These shear stresses constitute the Terzaghi arch. They increase the vertical friction force on the wall near to the corner of the silo and in the non-yielded stored material behind the slip planes. To maintain vertical equilibrium, vertical pressure is reduced between these areas. The Terzaghi arch is only evident close to the silo corners because it requires a high horizontal pressure to increase the shear strength of the stored material and hence induce high shear stresses at the wall and throughout the yielded material.

11.2. Hopper

The hopper pressures are redistributed by the same arch mechanisms described above. The principal stress directions are also rotated in the manner described above. The Horizontal arch (described in Section 11.1) redistributes both horizontal and vertical pressure from the centre of the wall towards the corners. The hopper wall is stiffer than the bin wall and so the ratio of the area relieved to the area subjected to a pressure increase is less in the hopper than it is in the bin. In addition a vertical arch formation reduces vertical pressure from near the hopper corners and increases the friction force on the hopper wall near the corners and the vertical pressure behind the slip plane.

The stress state in the stored material in the hopper differs to that in the bin due to the restraint of the upper boundary from the ring beam. Wall deformation produces a yield of the stored material in the manner illustrated in Figure 11.6. The ring beam at the top of the hopper limits horizontal translation and the bottom is restrained by the stiff outlet. In the upper half of the top of the hopper layers move

outwards in relation to layers above them. Near the bottom, the movement of any layer is outwards in relation to any layer below it. The yield of the wall mobilises the shear stresses τ_{xz} and τ_{zz} and pressure is transferred from the centre strips to those above and below them.

In the bottom of the hopper, vertical pressure within the stored material is relieved over the entire cross section due to Janssen arching between opposite walls. The increased pressure normal to the hopper wall at the outlet increases the wall friction force and the shear strength of the stored material between the walls. Shear stresses (τ_{xz}) are mobilised across the silo and at the interface of the wall and stored material in a similar manner to Janssen's [1] description of arching between the walls of a deep silo. It is possible that the high shear strength of the stored material above the outlet of the hopper will lead to a strong arch formation and flow hold ups for some hopper geometry and stored material combinations.

11.3. Ring beam

At the ring beam level the stress pattern is complicated by rupture zones and arching action extending from the hopper, and inward deformation of the ring beam during filling of the hopper. Measurements show little variation in pressure across the section. They suggest that the stored material is in an at-rest state of elastic equilibrium except close to the corners where it is affected by the central ring beam deformation. Here, the hopper walls exert a downward and inward force on the ring beam. Deformation is a minimum at the corners and a maximum at the mid-span. It changes the stress state of the stored material from the at-rest state towards the passive state of equilibrium. Passive (ring beam) arches are formed which 'bridge' the corners and generate an increase in pressure on the ring beam at some distance between the corner and mid-span.

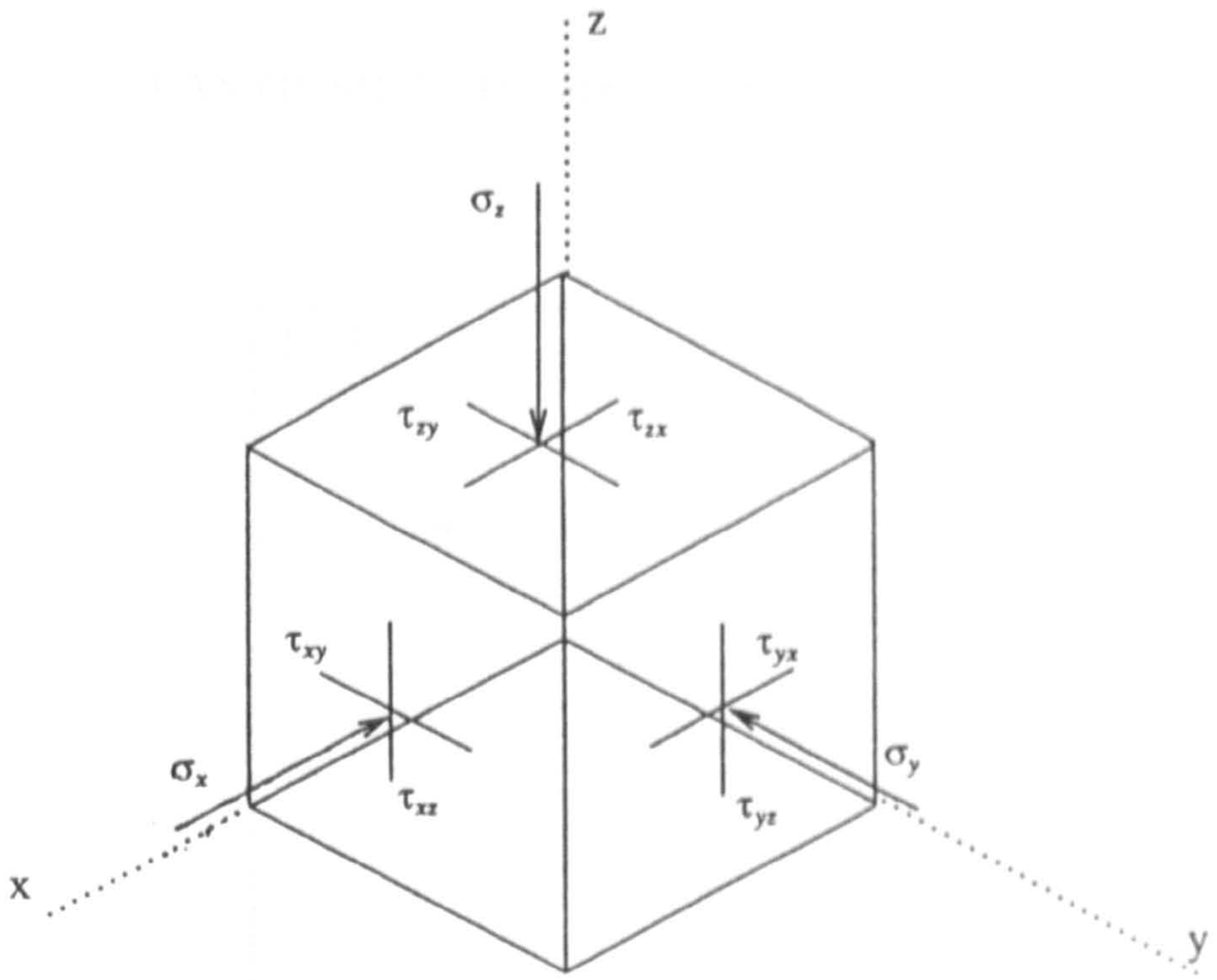

Figure 11.1 GENERAL STRESS COMPONENTS

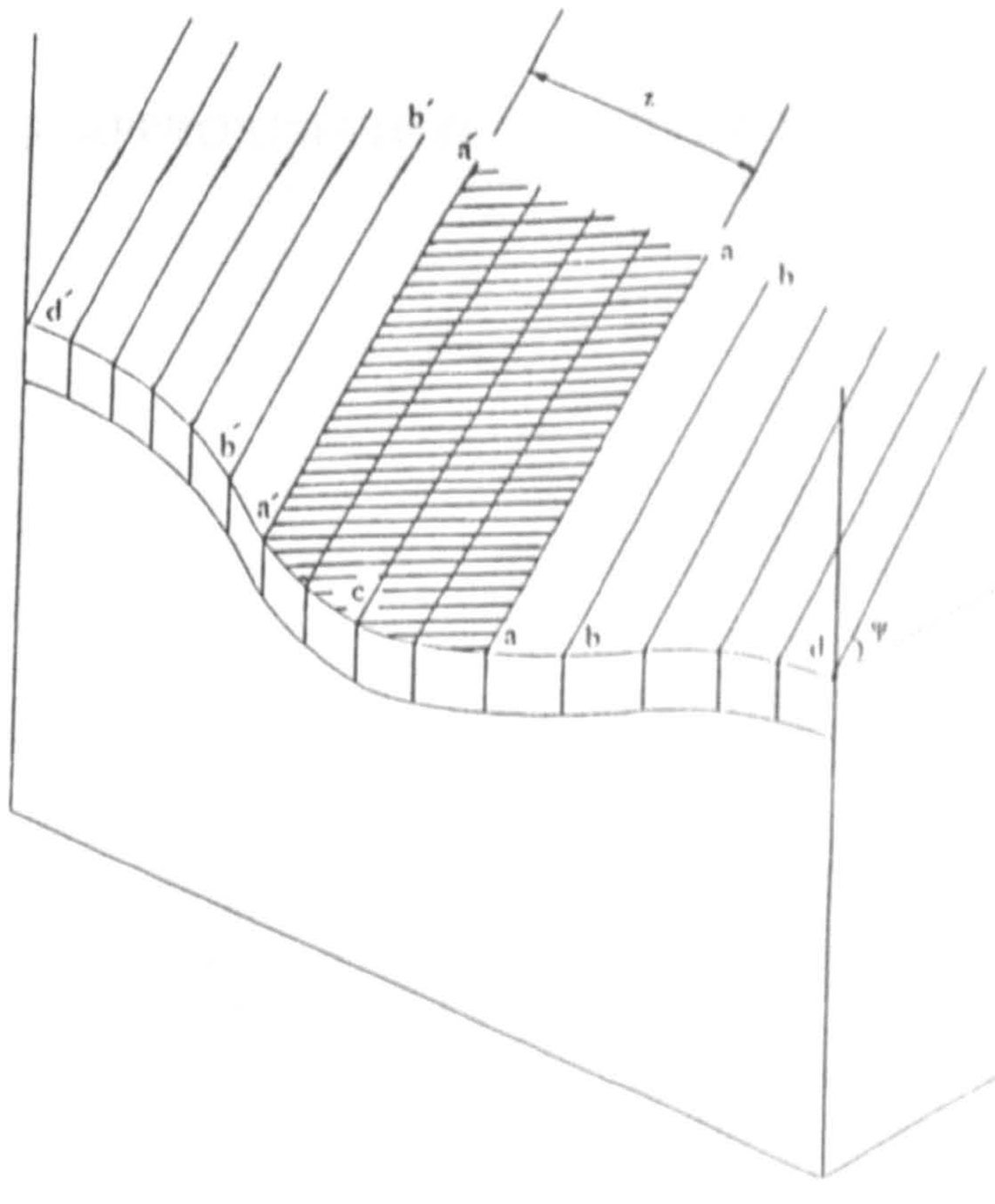

Figure 11.2 YIELD OF STORED MATERIAL

PLAN OF SILO - 1600mm ABOVE THE OUTLET

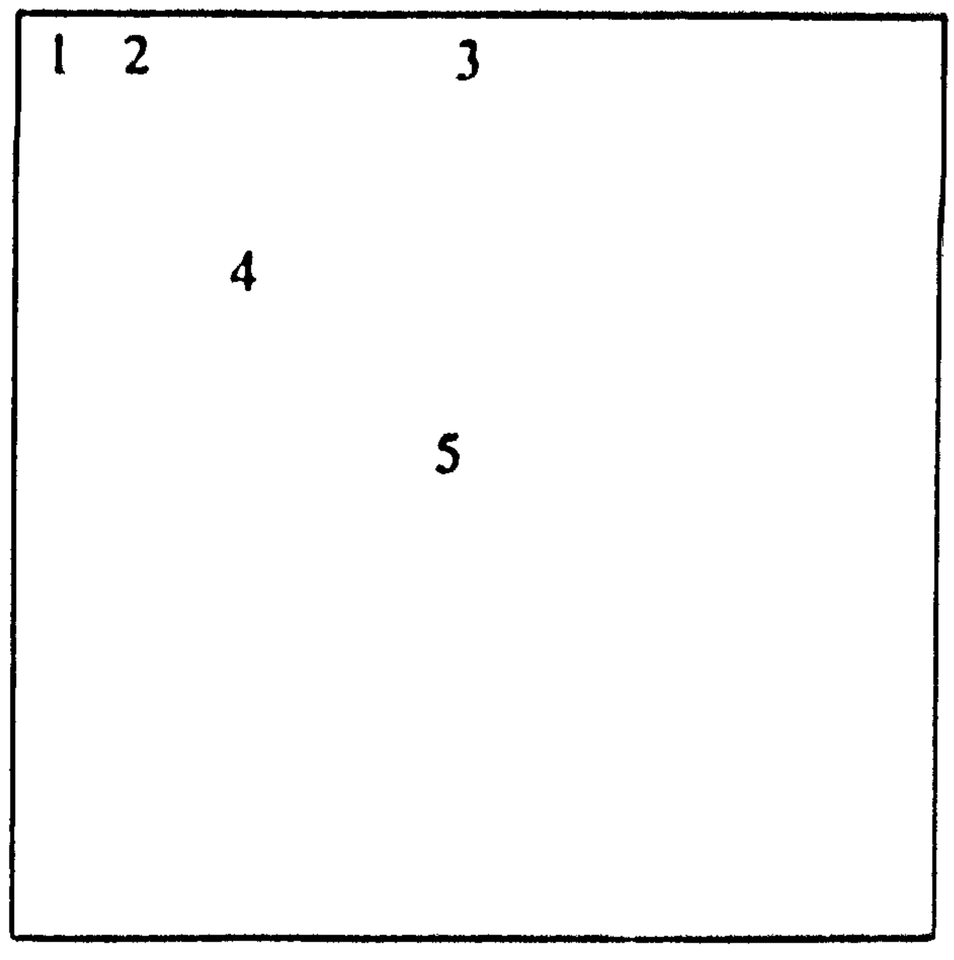

Figure 11.3 APPROXIMATE POSITIONS OF MOHR'S CIRCLES

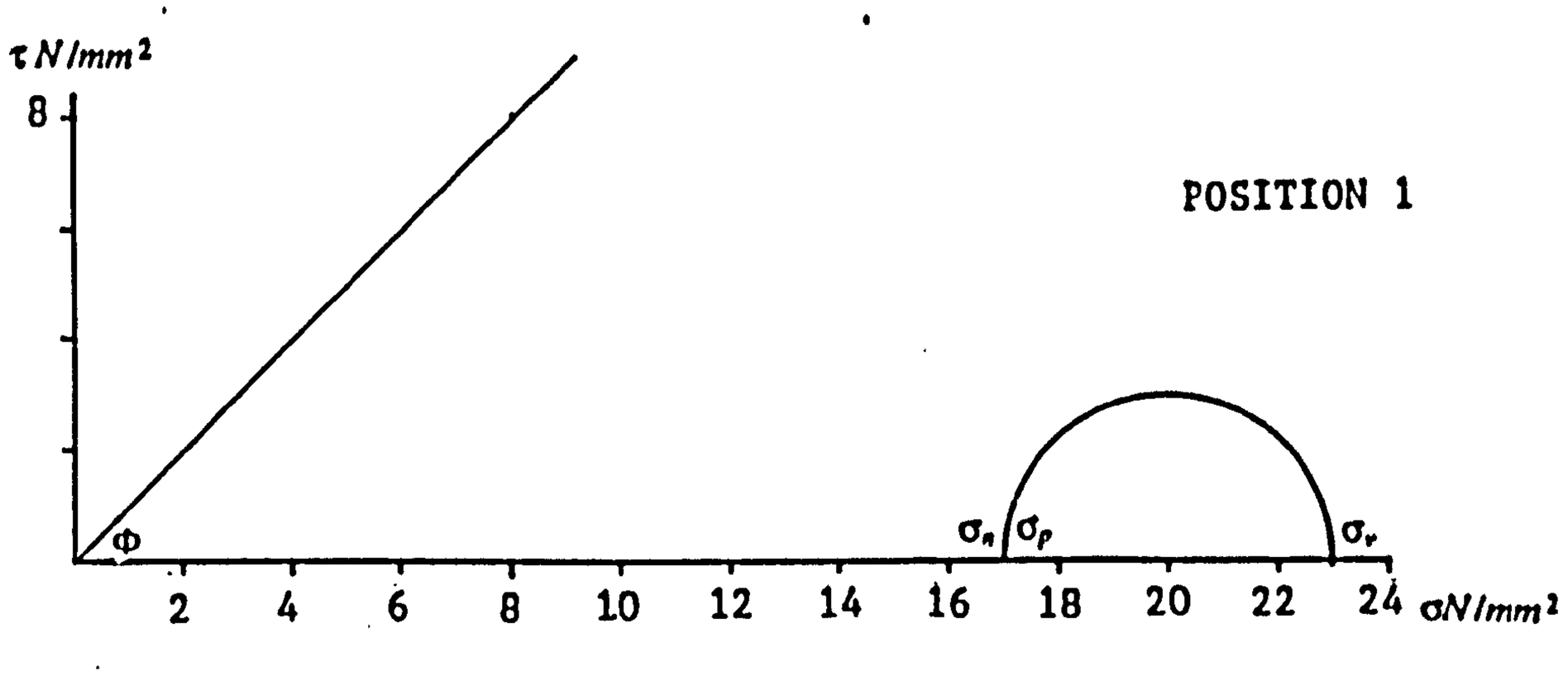

POSITION 1

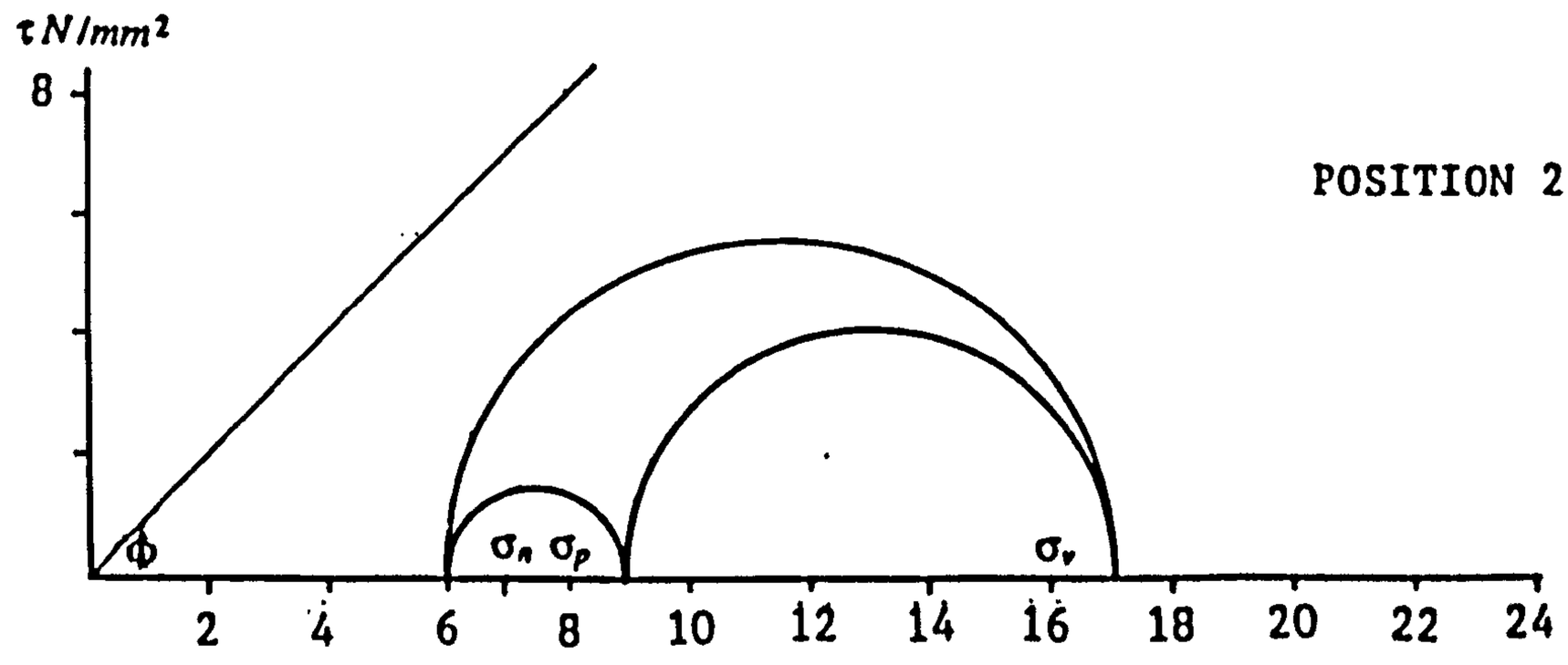

POSITION 2

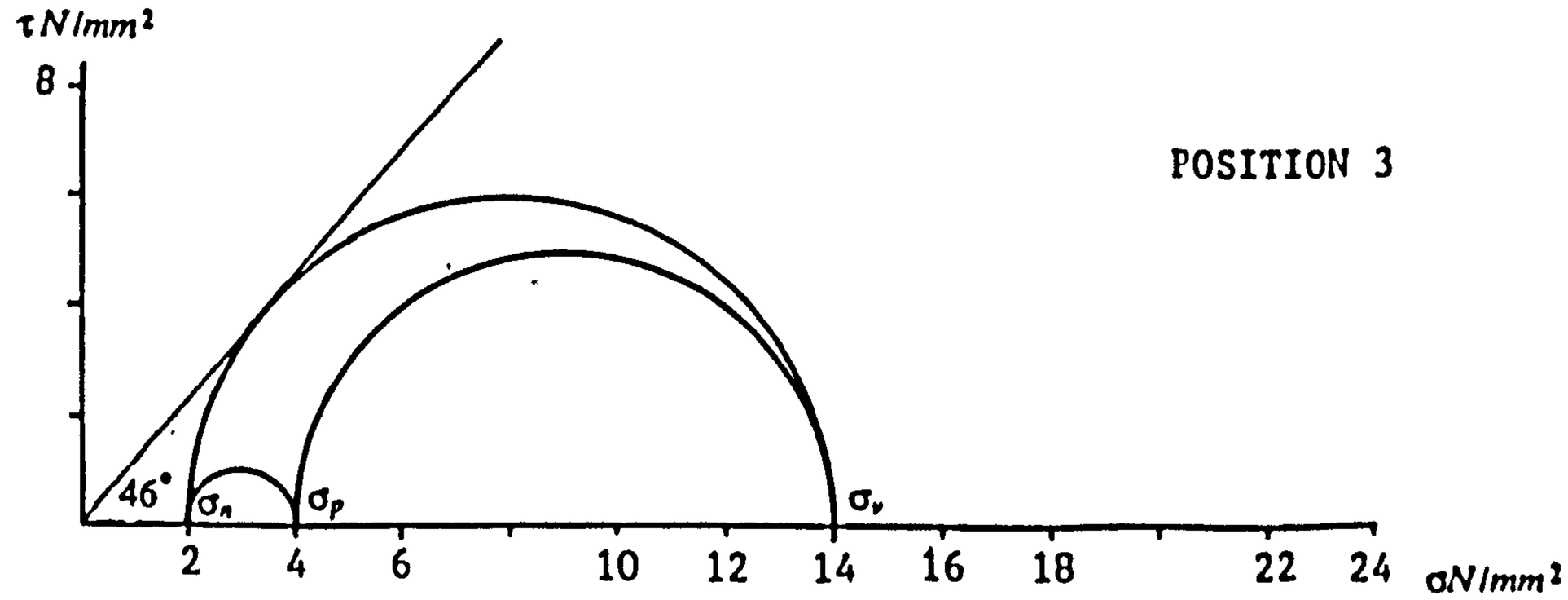

POSITION 3

Figure 11.4a MOHR'S CIRCLES OF STRESS STATES AT DIFFERENT POSITIONS IN THE SILO

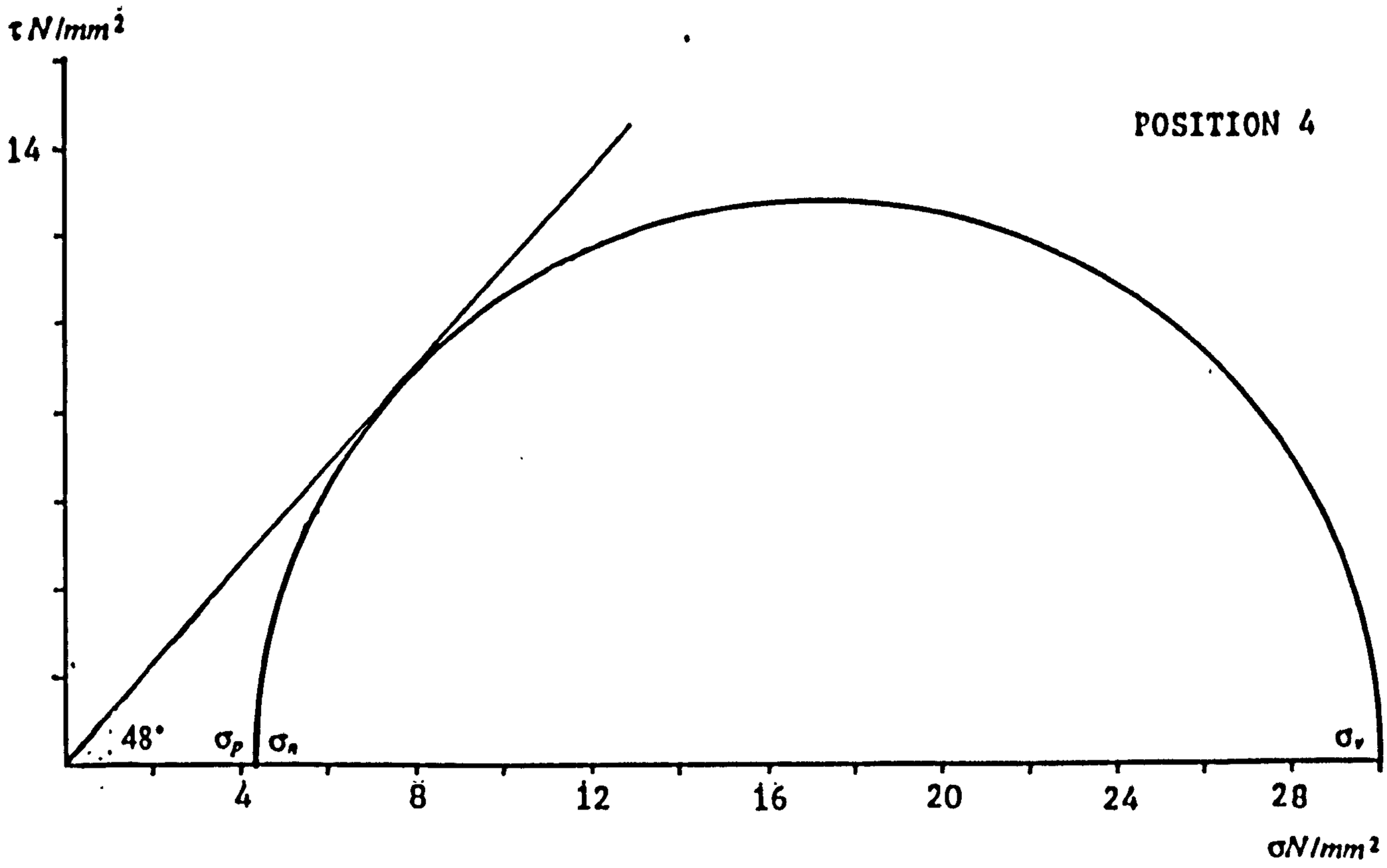

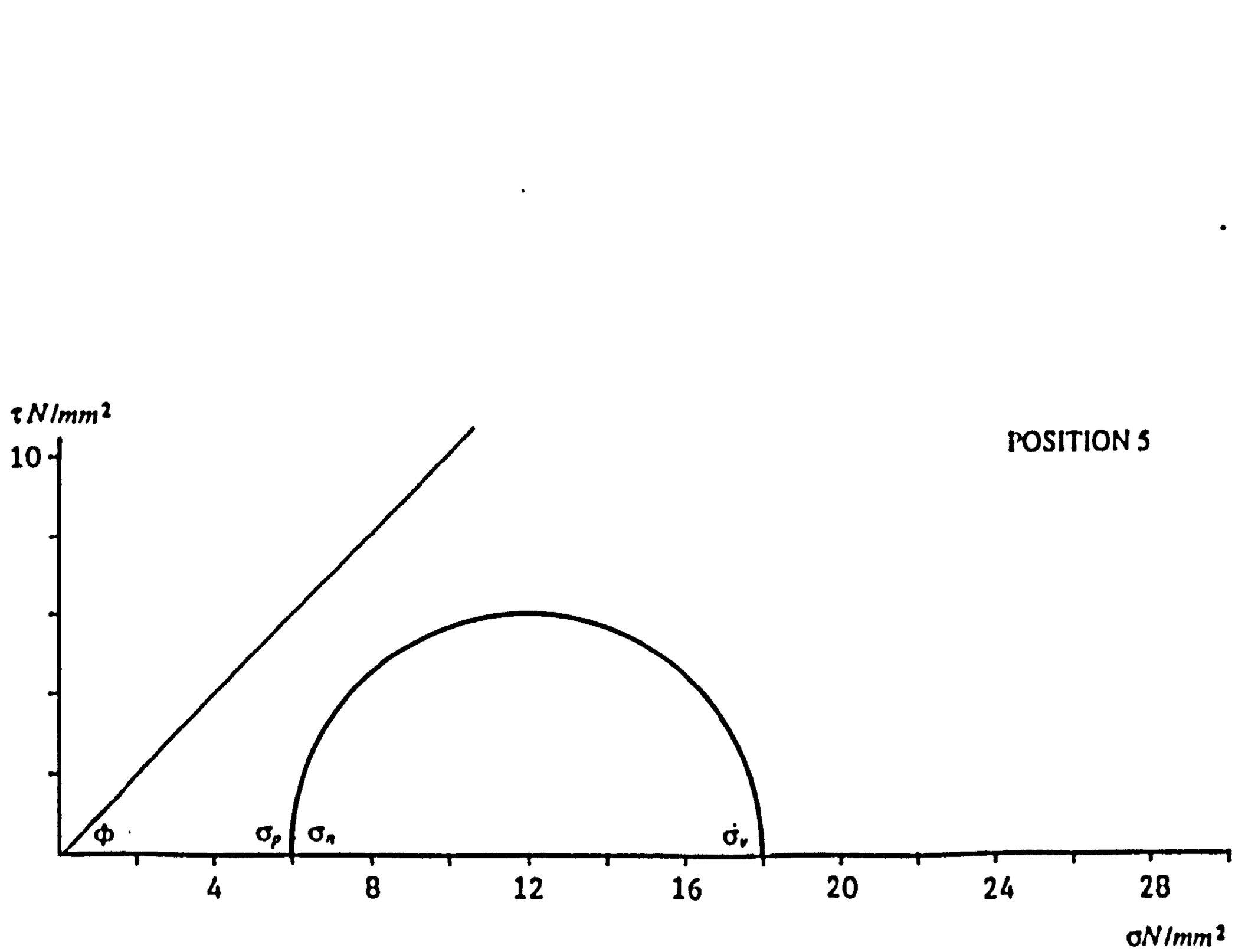

Figure 11.4b MOHR'S CIRCLES OF STRESS STATES AT DIFFERENT POSITIONS IN THE SILO

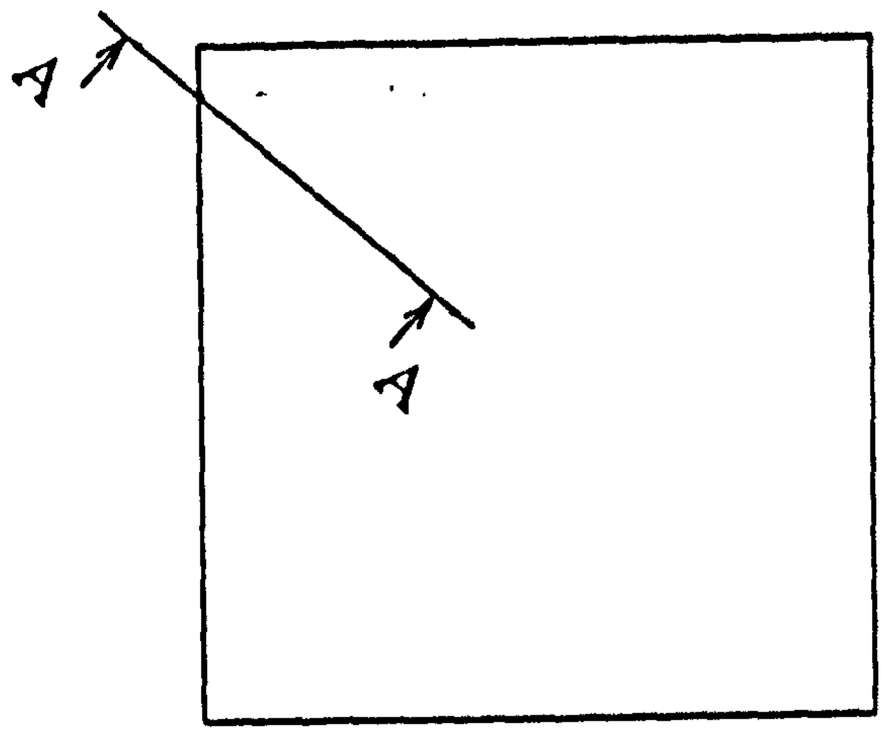

Plan view of bin

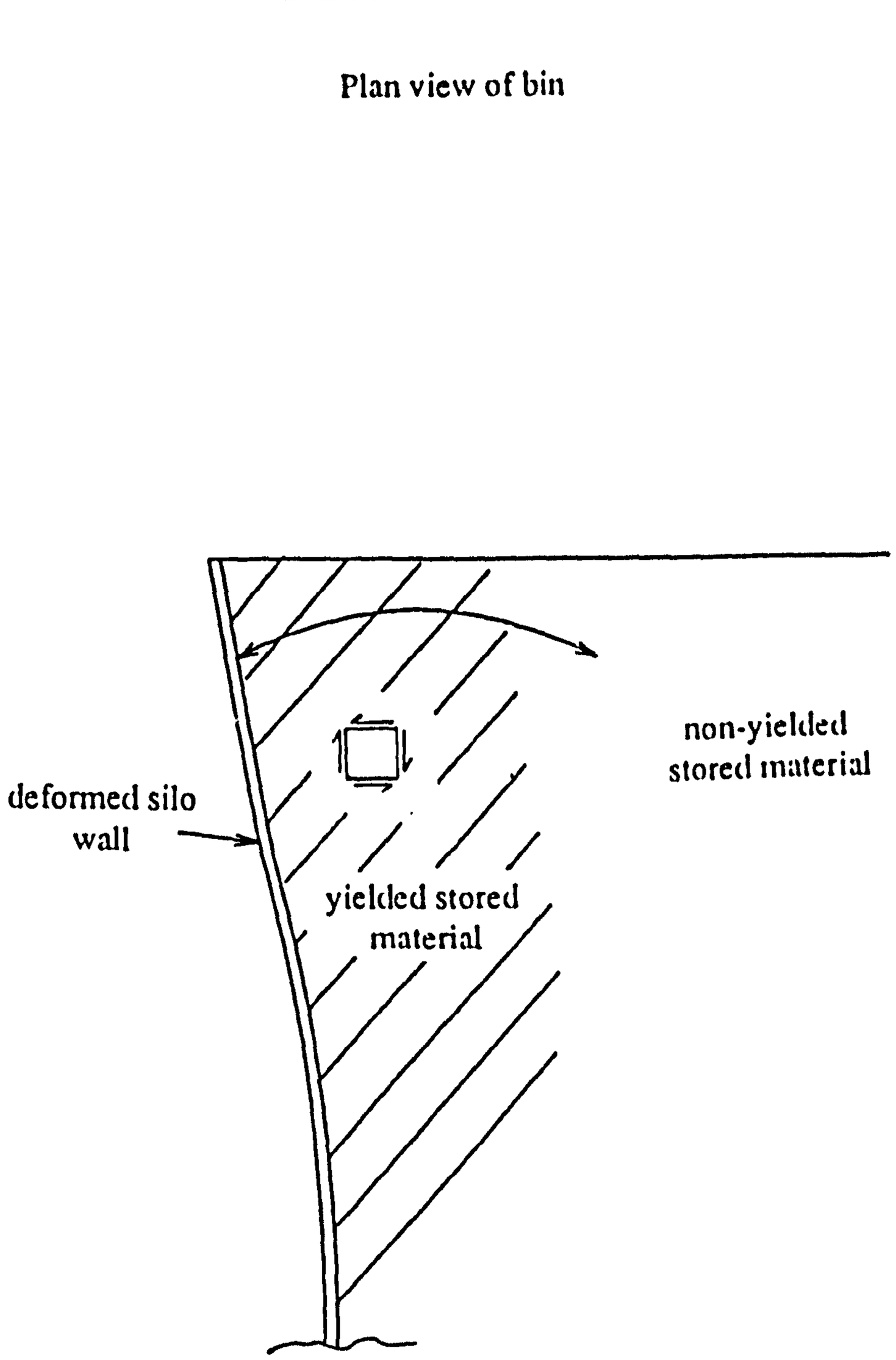

SECTION A-A

Figure 11.5 ARCHING AT THE CORNER BETWEEN THE WALL AND BEHIND THE SLIP PLANE

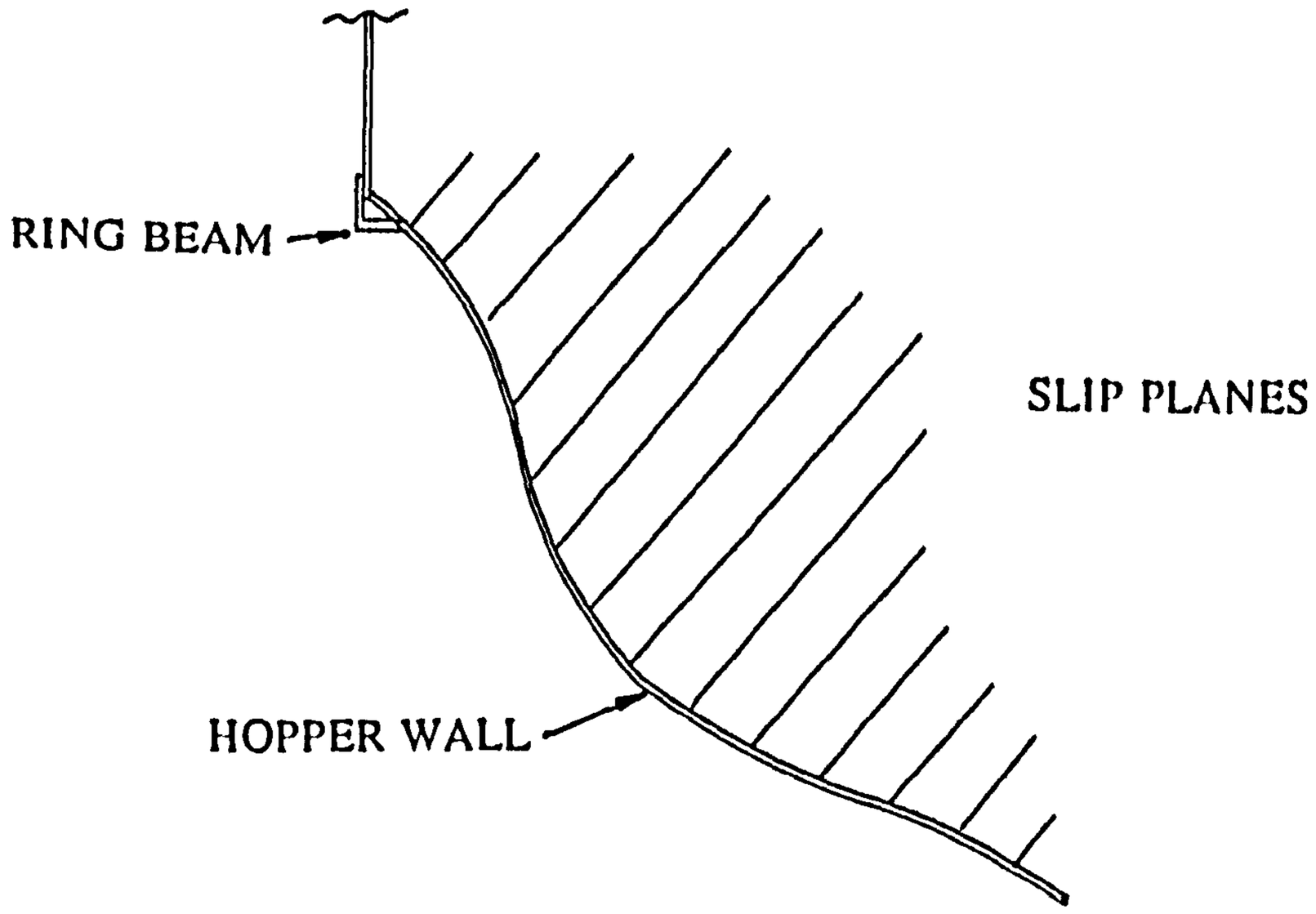

Figure 11.6 SLIP PLANES BEHIND THE DEFORMED HOPPER WALL

12. Summary and Conclusions

The tests in the square plan-form, flexible silo and pyramidal hopper have allowed the stress state to be described throughout the silo. This is the first time that extensive measurements have been carried out within the stored material behind a flexible silo wall. The tests have shown that accurate pressure measurements are possible if care is taken during the selection, calibration and placement of embedded cells.

The measurements of pressure within the stored material, wall strain and wall deformation suggest that existing design methods for the calculation of static pressure in square silos are conservative. They assume that the silo walls are rigid and do not deform or that they are rigid and rotate about their lower boundary. It has been shown that flexible plates with stiff boundaries produce a redistribution of pressure within the stored material. Internal arches are formed which increase the pressure in the vicinity of the stiff boundary and reduce it over most of the wall span, thus reducing the wall stresses. The boundary conditions of the silo wall as well as its flexibility and the stored material stiffness directly influence the pressure distribution. The existing theories are incorrect for the following reasons:

(a) The mobilisation of shear stresses between the stiff corners of a flexible silo reduces the vertical and horizontal pressure near to the centre of the deformed wall and increases pressure at the corners.

(b) The increased horizontal pressure in the corners allows a greater frictional force to be carried by the wall. Wall deformation mobilises shear stresses. They relieve vertical pressure close to the corner and increase it away from the corner and hence increase the in-plane force in the wall.

(c) The arch formations described in 'a' and 'b' are evident in the hopper. In addition, restraint to the upper boundary from the ring beam generates a third arch formation. Wall deformation mobilises shear stresses between the ring beam and the hopper outlet. If the

vertical consolidation force at the level of the hopper/cylinder transition is sufficient, pressure is reduced in the centre of the hopper wall and increased at the ring beam and the outlet.

(d) The loads on the inclined walls of the hopper lead to inward deformation of the ring beam. Deformation is greater in the centre of the beam than at the corners and so the centre will be subjected to the largest passive pressure. Since the inward deformation of the beam is small, any increase in pressure due to the move towards the passive pressure state will be small. A further increase is possible due to the inward deformation of the beam and subsequent arch formation over the corners. The arch relieves pressure from the corners and increases it towards the centre of the ring beam.

(e) The distance between opposite walls at the bottom of the hopper coupled with the high pressure normal to the hopper wall allow large shear stresses to be generated at the interface of the wall and stored material and within the stored material. A Janssen type arch is formed above the hopper outlet. It increases the force carried by wall friction and lowers the vertical pressure over the outlet.

(f) High pressures occur during discharge. This is partially due to the breakdown of the arches described above and partially due to the mobilisation of passive pressures due to inward deformation of the wall. In the areas of high wall deformation the inward movement is significant and passive pressures are generated that are up to twice the pressures measured during filling. A large proportion of the stored material is discharged before a passive pressure increase is incurred and so the total pressure felt by the wall and hence the wall stresses are at a maximum when the silo is full.

It is probably only necessary for simplified rules to include the pressure redistributions described in 'a' and 'c' since these have a significant effect upon the silo wall stresses. Silo designs which neglect to allow for the stored material/structure interaction can result in structures that could carry stresses that

are significantly greater than the actual maximum stresses.

12.1. Further Work

The complete stress state within the contents of a single flexible silo has been identified. Additional tests are required to quantify the effect of the following variables on the pressure distribution.

(a) Wall stiffness.

(b) Stored material stiffness.

(c) Wall aspect ratio and boundary conditions.

This Thesis has highlighted the need for design methods that utilise the benefits of stored material/structure interaction. A general explanation has been given which describes the wall pressure distribution in non-circular flexible silos. A rational theory is required which will predict this pressure distribution. Further tests are necessary to verify that a similar arching action is present in silos of different aspect ratios and stiffened silos. The theory may then be used to determine the effect of horizontal arching on the vertical walls of all flexible silos.

The effect of vertical arching between horizontal restraints such as horizontal stiffeners or ring beams should be quantified. The aspect ratio of the wall plate and the vertical confining pressures will influence the ratio of vertical and horizontal arching.

The tests showed that it is reasonable to assume that vertical pressure is constant at the transition between the cylinder and hopper. This simplifies the prediction of hopper pressures but it is still necessary to conduct tests on hoppers with different wall angles in addition to determining the effect of the stiffness properties, aspect ratio and boundary conditions.

13. References

1. Janssen H.A. , "Versuche uber Getreidedruck in Silozellen," *Zeitschrift des vereins deutscher ingenieure*, (1895).

2. Reimbert M. and Reimbert A. , "Silos: Theory and practice ," *Trans Tech publications*, (1976, Revised 1987).

3. Rankine W.J.M. , "On the stability of loose earth," *Transactions of the Royal Society of Engineers* 147 (1857).

4. Coulomb C.A. , "Essai sur une application des regles de maximis et minimis a quelques problemes de statique, relatifs a l'architecture," *Memoires de mathematique de l'Acadamie Royale des Sciences*, pp. 343-382 (1776).

5. Chandrangsu K. and Bishara A.G. , "Nonlinear finite element analysis of farm silos ," *Journal of Structural Engineering, A.S.C.E.* 104 (7)(1978).

6. Ibrahim A.G. and Dickenson R.P. , "Finite element analysis of the stresses in a silo storing powdered coal ," *International conference for powder and bulk solids flow and transportation, Illanois*, (1983).

7. Ooi J.Y. and Rotter J.M. , "Wall pressures in squat steel silos from simple finite element analysis," *University of Sydney Research Report No R538*, (1987).

8. Mahmoud A. and Abdel-Sayad G. , "Loading on shallow cylindrical flexible grain bins ," *International Journal of Powder and Bulk Solids Technology* 5 (3) pp. 12-19 (1981).

9. Mahmoud M.H. , "Practical finite element modeling of silo-material interaction," *International conference for powder and bulk solids flow and transportation, Illinois*, (1983).

10. Mahmoud M.H. , "Initial strain analysis of silo-material interaction ," *Powder Technology* 36 pp. 235-243 (1983).

11. Carder D.R. , Pocock R.G. and Murray R.T. , "Experimental retaining wall facility - lateral stress measurements with sand backfill," *Transport and Road Research Laboratory Report No. 766*, (1977).

12. Fang Y.S. and Ishibashi I. , "Static earth pressure with various wall movements," *Journal of Geotechnical Engineering, A.S.C.E.* **112** pp. 317-333 (1986).

13. Stroyer J. , "Earth pressure on flexible walls," *Min. of Proc. Instn. of Civil Engineers* **226 Pt.2** pp. 116-134 (1927-28).

14. Rowe P.W., "Anchored sheet-pile walls," *Proc. Instn. of Civil Engineers* **1 Pt.1** pp. 27-70 (1952).

15. Rowe P.W. and Peaker K. , "Passive earth pressure measurements," *Geotechnique* **15** pp. 57-78 (1965).

16. Pieper K. , "Investigation of silo loads in measuring models ," *Journal of Engineering for Industry, A.S.C.E.* , pp. 365-372 (1969).

17. Walker D.M. and Blanchard M.H. , "Pressures on experimental coal hoppers ," *Chemical Engineering Science* **22** pp. 1713-1732 (1967).

18. Tattersall C.G. and Schmidt L.C. , "Model studies of a plane converging hopper ," *Powder and Bulk Solids Technology* **5** (3) pp. 1-11 (1981).

19. Moran P. , "Design loads on retaining walls for granular material," *Journal of Agricultural Engineering Research* **39** p. 245 257 (1988).

20. Askegaard V. and Neilsen J. , "Measurements on silos," *B.S.S.M./I.C.E. joint conference "Measurements in Civil Engineering", Newcastle, England*, (1977).

21. Munch-Andersen J., "Measuring of internal stresses in granular media," *Euromech 157 Quality of mechanical observations on particulate media, Copenhagen*, (Aug 1982).

22. Lambert F.W. , "The theory and practical design of bunkers ," The British Constructional Steelwork Association Ltd. (1968).

23. Ronde L. , "Designing economical but reasonably safe silos," *Bulk Solids Handling* 5 (1) pp. 179-184 (1985).

24. Johnston F.T. , "Silo problems ," *International Journal of Powder and Bulk Solids Technology* , pp. 97-103 (1981).

25. Ravenet J. , "Silo Problems ," *Bulk Solids Handling* 1 (4) pp. 667-680 (1981).

26. Theimer O.F. , "Failures of reinforced concrete grain silos ," *Journal of Engineering for Industry, A.S.C.E.* 91 (2) pp. 460-469 (1969).

27. Safarian S. and Harris E.C. , *Design and construction of silos and bunkers* , Van Nostrand Reinhold Co. (1985).

28. Rotter J.M. , Jumikis P.T. , Fleming S.P. and Porter S.J., "Experiments on the buckling of thin-walled model silo structures," *University of Sydney Research Report No R570*, (1988).

29. Gaylord E.H. and Gaylord C.N. , *Design of steel bins for storage of bulk solids* , Prentice Hall, Englewood Cliffs (1984).

30. Lightfoot E. and Michael D. , "Prismatic coal bunkers in structural steelwork ," *The Structural Engineer* 44 pp. 55-62 (1966).

31. Nielsen J. , "Load distribution in silos influenced by anisotropic grain behaviour ," *Int Conf "Bulk Materials storage, handling and transportation" Newcastle, Australia*, (1983).

32. Jenike A.W. , "Stress and velocity fields in the gravity flow of bulk solids ," *Journal of Applied Mechanics, A.S.M.E.* 31 (1) pp. 5-11 (1964).

33. Terzaghi K. and Peck R.B. , *Soil mechanics in engineering practice*, John Wiley & Sons, New York (1967).

34. Walker D.M. , "An approximate theory for pressure and arching in hoppers ," *Chemical Engineering Science* **21** pp. 975-997 (1966).

35. Walters J.K. , "A theoretical analysis of stresses in axially- symmetric hoppers and bunkers ," *Chemical Engineering Science* **28** pp. 779-789 (1973).

36. Jaky J. , "The coefficient of earth pressure at rest," *Journal of the Society of Hungarian Architects and Engineers* **78**(22) pp. 355-358 (1944).

37. Mclean A.G. , "Initial stress fields in converging channels ," *Bulk Solids Handling* **5** (2) pp. 431-436 (1985).

38. Terzaghi K. , "General wedge theory of earth pressure," *Trans. A.S.C.E.* **106** pp. 68-97 (1941).

39. Clayton C.R.I. and Milititsky J. , *Earth pressure and earth retaining structures*, Surrey University Press, Glasgow (1986).

40. Costes N.C. , "Factors affecting vertical loads on underground ducts due to arching," *Highway Research Board Bulletin* **125** pp. 12-57 (1956).

41. Jenike A.W. , "Bin loads - parts 2,3 and 4," *Journal of Engineering for Industry, A.S.C.E.* **95** pp. 1-18 (1973).

42. Pieper K. and Wenzel F. , *Druckverhaltnisse in silozellen (Pressure conditions in silos)*, W. Ernst & Sohn, Berlin (1964).

43. Pieper K. and Wenzel F. , "Pressure conditions in silos," *Concrete and Constructional Engineering* **60**(4)(1965).

44. Hartlen J. et al, "The pressure condition in big grain silos. Inventory, stress measurement, material testing," *Rapport trykt af Byggforskningsradet*, (1981).

45. Nanninga N. , "Does the conventional method of calculating bin pressures give correct results? (In Dutch)," *Ingenieur* **44** pp. 190-194 (Nov 1956).

46. Enstad G. , "On the theory of arching in mass flow hoppers ," *Chemical Engineering Science* 30 pp. 1273-1283 (1975).

47. Van Zanten P.C. et al , "Wall pressures and flow design, Parts 1-4," *Journal of Engineering for Industry, A.S.C.E.* 99 (1977).

48. Hancock A.W. and Nedderman R.M. , "Prediction of stresses on vertical bunker walls," *Trans. Inst. Chemical Engineers* 52 pp. 170-179 (1974).

49. Jenkyn R.T. , "Calculation of material pressure for the design of silos ," *Proc.I.C.E.* 2(65) pp. 803-821 (1978).

50. Singh D. and Moysey E.B. , "Grain bin wall pressures - Theoretical and experimental ," *Can.Agricultural Engineering* 27 (1) pp. 43-48 (1985).

51. Turitzin A.M. , "Dynamic pressure of granular material in deep bins ," *Journal of the Structural Division, A.S.C.E.* 89 (2) pp. 49-73 (1963).

52. Bransby P.L. and Blair Fish P.M. , "Wall stresses in mass flow bunkers ," *Chemical Engineering Science* 29 pp. 1061-1074 (1974).

53. Deutsch G.P. and Schmidt L.C. , "Pressure on silo walls ," *Journal of Engineering for Industry, A.S.C.E.* , pp. 450-459 (1969).

54. Nielsen J. and Kristiansen N.O. , "Related measurements of pressure conditions in a full scale Barley silo and in a model ," *1st Conf. "Design of silos for strength and flow", Lancaster, England,* (1980).

55. Clague K. and Wright H. , "Pressure in bunkers ," *Iron and Steel International* 46 pp. 336-346 (1973).

56. Jenike A.W. , "Quantitive design of mass flow bins ," *Powder Technology* 1 pp. 237-244 (1967).

57. Munch-Andersen J. , "The boundary layer in rough silos," *2nd Int. conf."Bulk materials storage, handling and transportation" Wollongong, Australia*, pp. 160-163 (1986).

58. Abdel-Sayad G. , "Cold-formed steel farm structures Part I:Grain bins ," *Journal of Structural Engineering, A.S.C.E.* 111 (10) pp. 2065-2089 (1985).

59. Shamlou P.A., *Handling of bulk solids*, Butterworths, London (1988).

60. British Materials Handling board , *BMHB Draft code of practice for the design of silos.* 1987 .

61. Inst. of Engrs. Aust., "Guidelines for the estimate of loads on bulk solids containers ," , (1986).

62. Mclean A.G. and Bravin B. , "Wall loads in eccentric discharge silo ," *Bulk Solids Storage in Silos* 1 (1) pp. 12-24 (1985).

63. Jenike A.W. , "Denting of circular bins with eccentric draw points ," *Journal of the Structural Division, A.S.C.E.* 93 pp. 27-39 (1967).

64. Ooi J.Y. , Pham L. and Rotter J.M. , "Systematic and random features of measured pressures on full-scale silo walls," *University of Sydney Research Report No R590*, (1989).

65. Latincsics N.K. , "Silos and storage vessels - Influence of compressibility of the stored solids ," *Bulk Solids Handling* 5 (1) pp. 219-224 (1985).

66. Murfitt P.G and Bransby P.L. , "Pressures in hoppers filled with fine powders ," 1st Conf. "Design of silos for strength and flow", Lancaster, England (1980).

67. Arnold P.C. , *Bulk solids: Storage flow and handling* , TUNRA Ltd, Australia (1979).

68. Clague K., "The effects of stresses in bunkers," *PhD Thesis, University of Nottingham*, (1973).

69. Jenike A.W. and Johanson J.R , "Bin loads ," *Journal of the Structural Division, A.S.C.E.* 94 (4) pp. 1011-1040 (1968).

70. Lvin J.A. , "Analytical evaluation of pressures of granular materials on silo walls," *Powder Technology* 4 pp. 280-285 (1970).

71. Takami, A. and Syoten, O. , "A theory of the pressure distribution in powder in equilibrium in a cylindrical vessel," *Powder Technology* 10 pp. 295-301 (1974).

72. Koenan M. , "Berechnung des seiten-und bodendrucks in silos," *Zentralbl. Bauverwaltung* 16 pp. 446-449 (1896).

73. Cowin S.C. , "The theory of static loads in bins ," *Journal of Applied Mechanics, A.S.M.E.* 44 pp. 409-426 (1977).

74. Cowin S.C. , "The pressure ratio in the theory of bin pressures ," *Journal of Applied Mechanics, A.S.M.E.* 46 pp. 524-528 (1979).

75. Ingold T.S., "Some simplifications of Coulomb's active earth pressure theory," *Ground Engineering* 11(4) pp. 23-42 (1978).

76. National Coal Board, "The design of coal preparation plants," *National Coal Board Code of Practice*, (1970).

77. Jenike A.W. , "Why bins don't flow ," *Chemical Engineering Science* 10 pp. 150-156 (1958).

78. Horne R. and Nedderman R. , "Stress distribution in hoppers ," *Powder Technology* 19 pp. 243-254 (1978).

79. Arnold P.C. and McLean A.G. , "An analytical solution for the stress function at the wall of a converging channel ," *Powder Technology* 13 pp. 255-273 (1976).

80. Rotter J.M., "The structural design of light gauge silo hoppers," *Research report No R571*, University of Sydney, (1988).

81. Horne R. and Nedderman R. , "An analysis of switch stresses in two dimensional bunkers ," *Powder Technology* 19 pp. 235-241 (1978).

82. Arnold P.C. and McLean A.G. , "An evaluation of the radial stress field non-dimensional surcharge factor for mass flow hoppers ," *Powder Technology* 19 pp. 279-281 (1978).

83. Rotter J.M. , "On the significance of switch pressures at the transition in elevated steel bins ," *Proc. 2nd Int. Conf. on bulk materials storage handling and transportation Wollongong, Australia*, pp. 82-88 (1986).

84. Nielsen J. , "Model laws for granular media and powders with a special view to silo models ," *Archives of Mechanics* 29 (4) pp. 547-560 (1977).

85. Munch-Anderson J. , "Scale errors in model silo tests ," *2nd Conf. "Design of silos of silos for strength and flow", Stratford upon Avon, England*, (1983).

86. Nielsen J. and Askegaard V. , "Scale errors in model tests on granular media with special reference to silo models," *Powder Technology* 16 pp. 123-130 (1977).

87. Troitsky M.S. , "Design considerations for rectangular steel bins ," *Proc. Canadian Structural Engineering Conf*, (1980).

88. Troitsky M.S. , "On the structural analysis of rectangular steel bins ," *Powder and Bulk Solids Technology* 4 (4) pp. 19-25 (1980).

89. , "Steel Designers Manual ," *CONSTRADO, London*, pp. 489-503 (1960).

90. Skieller T. , "Structural design of silos ," *Powder and Bulk Solids Technology* 5 (1981).

91. Rotter M., "On the strength and stability of light gauge silos," *8th conf. on cold formed steel structures, St Louis, U.S.A.*, (Nov 1986).

92. Lichtarnikov J.M., Klykov V.M. and Ladyzhensky D.V., *Design of steel structures*. 1976.

93. Roark J. and Young C., *Formulas for stress and strain*, McGraw Hill, New York (1975).

94. Timoshenko S. and Woinowsky-Krieger S. , *Theory of plates and shells*, McGraw Hill, New York (1959).

95. Levy S. , "Simply supported long rectangular plate under combined axial load and normal pressure," *N.A.C.A. Tech. Note* 949(1944).

96. Brown C.J., "Elastic buckling of plates subjected to distributed tangential loads," *To be published*, ().

97. Potts D.M. , Dounias G.T. and Vaughan P.R. , "Finite element analysis of the direct shear box test," *Geotechnique* 37 pp. 11-23 (1987).

98. Morgenstern N.R. and Eisenstein Z., "Methods of estimating lateral loads and deformations," *Speciality conf. "Lateral stresses in the ground and design of earth-retaining structures", Cornell University, U.S.A.*, pp. 51-102 (June 1970).

99. Hvorslev, M.J., "The changeable interaction between soils and pressure cells; tests and reviews at the Waterways Experiment Station," *U.S. Army Engineer Waterways Experiment Station, Technical report S-76-7*, (1976).

100. Hanna T.H. , *Field instrumentation in Geotechnical Engineering*, Trans Tech Publications, Clausthal-Zellerfeld (1985).

101. Carder D.R. and Krawczyk J.V. , "Performance of cells designed to measure soil pressure on earth retaining structures," *Transport and Road Research Laboratory Report No. 689*, (1975).

102. Askegaard V., "The pressure cell problem," *Silos - Forschung und Praxis Tagung '88*, pp. 349 - 362 (Oct 1988).

103. Watts K.S. and Charles J.A. , "In situ measurement of vertical and horizontal stress from a vertical borehole," *Geotechnique* 38 pp. 619 - 626 (1988).

104. Marchant J.A. , "A pneumatic force transducer," *Journal of Physics E: Scientific Instruments* 10 pp. 1238 - 1240 (1977).

105. Blight G.E. , "Pressures exerted by materials stored in silos: Pt.1, coarse materials," *Geotechnique* 36 pp. 33-46 (1986).

106. Thomas H.S.H. and Ward W.H. , "The design, construction and performance of a vibrating wire earth pressure cell," *Geotechnique* 19 pp. 39 - 51 (1969).

107. Tory, A.C. and Sparrow, R.W., "The influence of diaphragm flexibility on the performance of an earth pressure cell," *Journal of Scientific Instruments* 44 pp. 781-785 (1967).

108. Askegaard V. and Munch-Andersen J. , "Results from tests with normal and shear stress cells in medium scale model silo," *Report no.191, Technical University of Denmark,* p. D1 4 (1984).

109. Askegaard V. , Bergholdt M. and Nielsen J. , "Problems in connection with pressure cell measurement in silos," *Byggningsstatiske Meddelelser,* pp. 33-73 (1971).

110. Nielsen J., "Pressure measurements in a full scale fly ash silo," *Particulate Science and Technology* 2 pp. 237-246 (1984).

111. Askegaard V., "Consequence of loading history on the measuring error of embedded stress cells," *2nd Int. Conf. on Bulk Materials Storage, Handling and Transportation, Wollongong, Australia,* (1987).

112. Bransby P.L. and Milligan G.W.E., "Soil deformations near a cantilever sheet pile wall," *Geotechnique* 25 pp. 175-195 (1975).

Appendix A The Finite Element model

The model silo was analysed using a linear elastic finite element model. Symmetry of the planform enabled the numerical model to be reduced to a quarter of the silo. The walls of the bin and hopper were modelled with triangular plate elements which have five degrees of freedom per node point. Preliminary analyses were carried out to determine the optimum mesh size and it is shown in Figure A1.

The boundary restraints were selected to ensure that the quarter model accurately represented a quarter of the full silo. The upper edges were left free and the ring beam between the bin and hopper was assumed to be restrained against vertical translation. The edges coinciding with the vertical centrelines of the silo walls were restrained against rotation about the vertical (y) axis and against translation in the in-plane direction of the plate.

Displacement output was in the form of three translations in the global 'x', 'y' and 'z' directions and two rotations in either the global 'y' and 'x' or the 'y' and 'z' directions. The values and directions of the principal stresses at each element centroid and each nodal point were given for the outer, middle and inner surfaces of each element.

The load from the stored material was simulated by applying a pressure to each element and converting this to a point load at each node. Load was applied normal to each element and in the plane of the plate to model the frictional drag. To maintain symmetry of the system, only some of the columns of nodes were subjected to an inplane force. To compensate, the force on the loaded nodes was increased in suitable proportions.

The material properties used in the finite element model were based on the results of tests carried out at the Building Research Establishment.

Three Finite Element models were developed.

1. A model of the Perspex silo shown in Figure 4.5. The finite element and physical models were subjected to a hydrostatic pressure. The principal stresses determined from the finite element model were compared with stresses calculated from experimentally measured strains and the accuracy of the finite element analysis and strain results were evaluated.

2. A finite element model of the large scale steel model silo (Figure 4.2b). A Janssen pressure distribution was used to determine the optimum wall thickness for the physical model at the design stage.

3. A numerical model of the bin section of the large scale model. The mesh spacing was reduced from the model described in '2' and the measured pressure distribution (determined from the tests described in Chapter 8) was applied to the silo. At two levels in the silo, pressure cells were placed close together to measure the steep pressure gradient. A similar distribution of pressure was assumed between the measurement points at other levels. The model provided a check on the accuracy of the measured pressure, displacement and strain data, and by comparison with the results from '2', it also allowed an assessment of the benefits of incorporating a realistic pressure distribution into design.

The Pafec 75 suite of programmes was used for the analysis. The data input files for '2' and '3' are given below. Diagrams showing the mesh generation for the models described in '2' and '3' are shown in Figures A2 and A3.

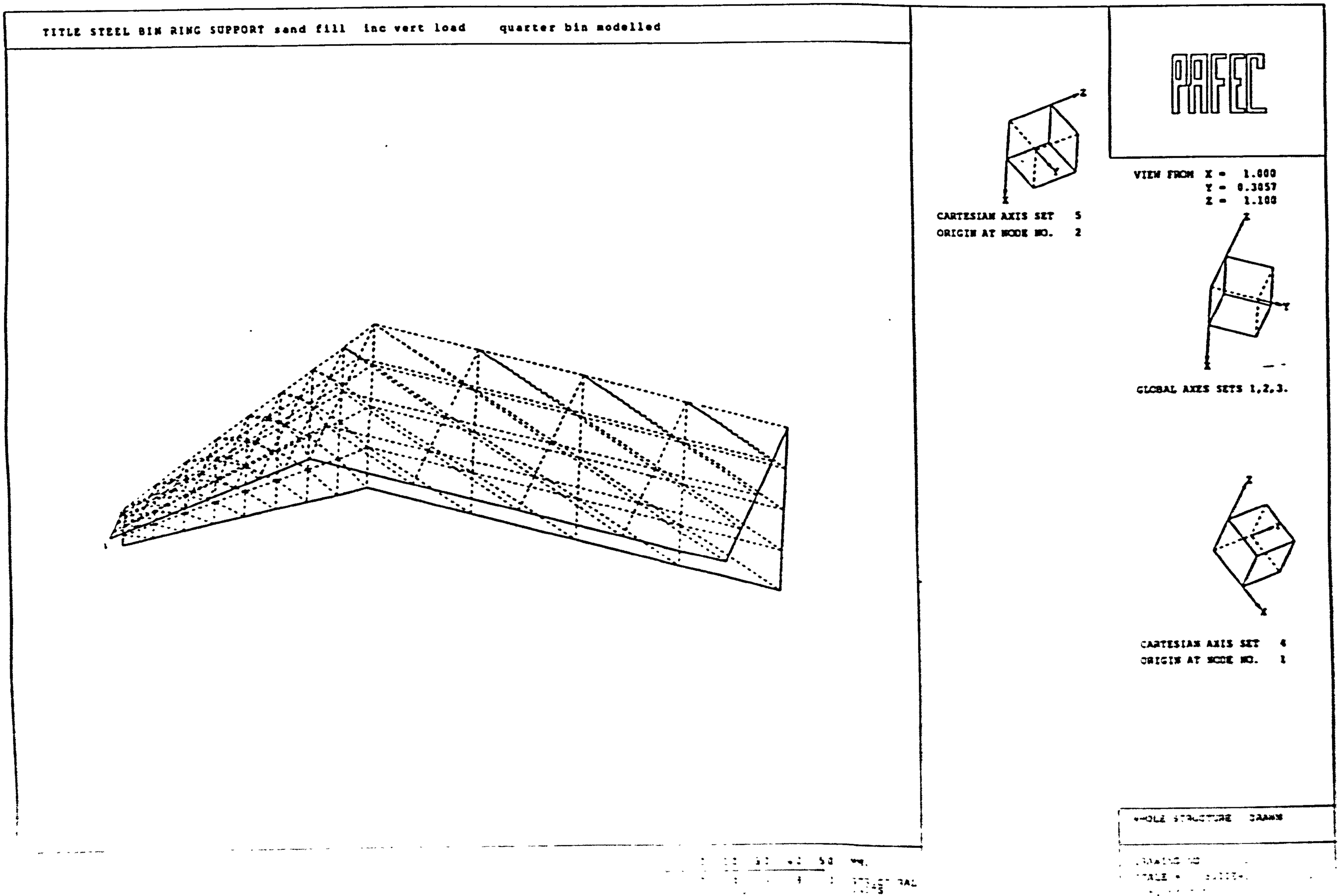

Figure A1 PAFEC MESH GENERATION OF THE SILO

PAFEC DATA INPUT FILE 1

```
CONTROL
FULL.CONTROL
PHASE=1
PHASE=2
PHASE=4
PHASE=6
PHASE=7
PHASE=9
STOP
CONTROL.END
TITLE STEEL BIN RING SUPPORT sand fill (inc vert load)   quarter bin modelled
nodes
node.number x y z
 1 1.00 0.000 0.000 // 2 1.00 0.000 0.300
 3 0.000 1.20 0.000 // 4 0.000 1.20 1.30
 5 1.30 0.000 0.300 // 6 1.30 1.20 1.30
 7 0.000 3.80 0.000 // 8 0.000 3.80 1.30
 9 1.30 3.80 1.30 // 10 1.00 0.000 0.750E-01
 11 1.00 0.000 0.150 // 12 1.00 0.000 0.225
 13 0.875 0.150 0.000 // 14 0.875 0.150 0.106
 15 0.875 0.150 0.212 // 16 0.875 0.150 0.319
 17 0.875 0.150 0.425 // 18 0.750 0.300 0.000
 19 0.750 0.300 0.137 // 20 0.750 0.300 0.275
 21 0.750 0.300 0.412 // 22 0.750 0.300 0.550
 23 0.625 0.450 0.000 // 24 0.625 0.450 0.169
 25 0.625 0.450 0.337 // 26 0.625 0.450 0.506
 27 0.625 0.450 0.675 // 28 0.500 0.600 0.000
 29 0.500 0.600 0.200 // 30 0.500 0.600 0.400
 31 0.500 0.600 0.600 // 32 0.500 0.600 0.800
 33 0.375 0.750 0.000 // 34 0.375 0.750 0.231
 35 0.375 0.750 0.462 // 36 0.375 0.750 0.694
 37 0.375 0.750 0.925 // 38 0.250 0.900 0.000
 39 0.250 0.900 0.262 // 40 0.250 0.900 0.525
 41 0.250 0.900 0.787 // 42 0.250 0.900 1.05
 43 0.125 1.05 0.000 // 44 0.125 1.05 0.294
 45 0.125 1.05 0.587 // 46 0.125 1.05 0.881
 47 0.125 1.05 1.17 // 48 0.000 1.20 0.325
 49 0.000 1.20 0.650 // 50 0.000 1.20 0.975
 51 1.22 0.000 0.300 // 52 1.15 0.000 0.300
 53 1.07 0.000 0.300 // 54 1.30 0.150 0.425
 55 1.19 0.150 0.425 // 56 1.09 0.150 0.425
 57 0.981 0.150 0.425 // 58 1.30 0.300 0.550
 59 1.16 0.300 0.550 // 60 1.02 0.300 0.550
 61 0.887 0.300 0.550 // 62 1.30 0.450 0.675
 63 1.13 0.450 0.675 // 64 0.962 0.450 0.675
 65 0.794 0.450 0.675 // 66 1.30 0.600 0.800
 67 1.10 0.600 0.800 // 68 0.900 0.600 0.800
 69 0.700 0.600 0.800 // 70 1.30 0.750 0.925
 71 1.07 0.750 0.925 // 72 0.837 0.750 0.925
 73 0.606 0.750 0.925 // 74 1.30 0.900 1.05
 75 1.04 0.900 1.05 // 76 0.775 0.900 1.05
 77 0.512 0.900 1.05 // 78 1.30 1.05 1.17
 79 1.01 1.05 1.17 // 80 0.712 1.05 1.17
 81 0.419 1.05 1.17 // 82 0.975 1.20 1.30
 83 0.650 1.20 1.30 // 84 0.325 1.20 1.30
 85 0.000 1.85 0.000 // 86 0.000 1.85 0.325
 87 0.000 1.85 0.650 // 88 0.000 1.85 0.975
 89 0.000 1.85 1.30 // 90 0.000 2.50 0.000
 91 0.000 2.50 0.325 // 92 0.000 2.50 0.650
 93 0.000 2.50 0.975 // 94 0.000 2.50 1.30
 95 0.000 3.15 0.000 // 96 0.000 3.15 0.325
 97 0.000 3.15 0.650 // 98 0.000 3.15 0.975
 99 0.000 3.15 1.30 // 100 0.000 3.80 0.325
 101 0.000 3.80 0.650 // 102 0.000 3.80 0.975
 103 1.30 1.85 1.30 // 104 0.975 1.85 1.30
 105 0.650 1.85 1.30 // 106 0.325 1.85 1.30
 107 1.30 2.50 1.30 // 108 0.975 2.50 1.30
 109 0.650 2.50 1.30 // 110 0.325 2.50 1.30
 111 1.30 3.15 1.30 // 112 0.975 3.15 1.30
 113 0.650 3.15 1.30 // 114 0.325 3.15 1.30
 115 0.975 3.80 1.30 // 116 0.650 3.80 1.30
 117 0.325 3.80 1.30
elem
numb group elem prop topo
 1 1 41320 1 1 10 13
 2 1 41320 1 14 13 10
 3 1 41320 1 10 11 14
 4 1 41320 1 15 14 11
 5 1 41320 1 11 12 15
 6 1 41320 1 16 15 12
 7 1 41320 1 12 2 16
 8 1 41320 1 17 16 2
 9 1 41320 1 13 14 18
 10 1 41320 1 14 19 18
 11 1 41320 1 14 15 19
 12 1 41320 1 15 20 19
 13 1 41320 1 15 16 20
 14 1 41320 1 16 21 20
 15 1 41320 1 16 17 21
 16 1 41320 1 17 22 21
 17 1 41320 1 18 19 23
 18 1 41320 1 19 24 23
```

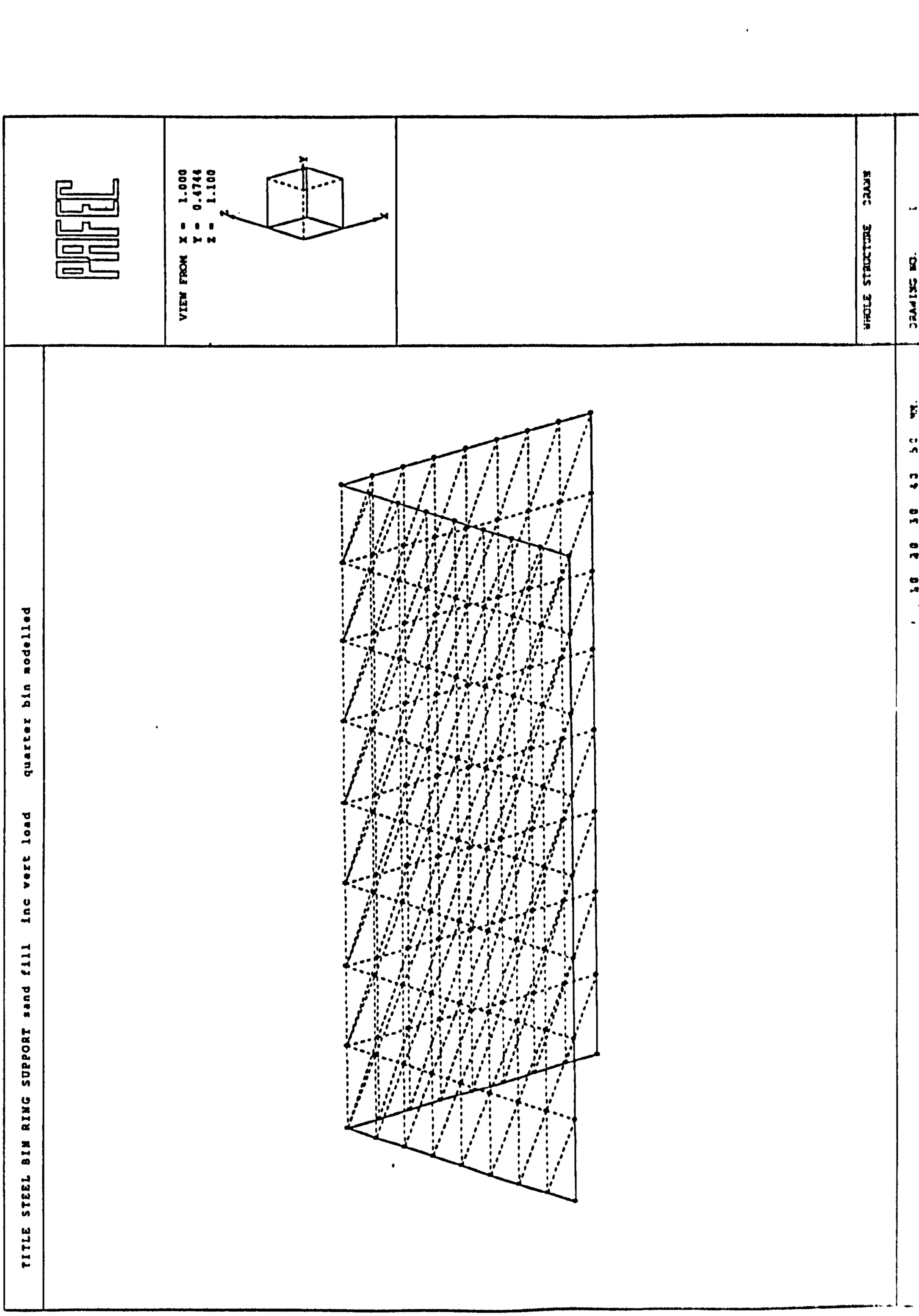

Figure A2 PAFEC MESH GENERATION OF THE BIN

PAFEC DATA INPUT FILE 1

```
CONTROL
FULL.CONTROL
PHASE=1
PHASE=2
PHASE=4
PHASE=6
PHASE=7
PHASE=9
STOP
CONTROL.END
TITLE STEEL BIN RING SUPPORT sand fill (inc vert load)   quarter bin modelled
nodes
node.number x y z
 1 1.00 0.000 0.000 // 2 1.00 0.000 0.300
 3 0.000 1.20 0.000 // 4 0.000 1.20 1.30
 5 1.30 0.000 0.300 // 6 1.30 1.20 1.30
 7 0.000 3.80 0.000 // 8 0.000 3.80 1.30
 9 1.30 3.80 1.30 // 10 1.00 0.000 0.750E-01
 11 1.00 0.000 0.150 // 12 1.00 0.000 0.225
 13 0.875 0.150 0.000 // 14 0.875 0.150 0.106
 15 0.875 0.150 0.212 // 16 0.875 0.150 0.319
 17 0.875 0.150 0.425 // 18 0.750 0.300 0.000
 19 0.750 0.300 0.137 // 20 0.750 0.300 0.275
 21 0.750 0.300 0.412 // 22 0.750 0.300 0.550
 23 0.625 0.450 0.000 // 24 0.625 0.450 0.169
 25 0.625 0.450 0.337 // 26 0.625 0.450 0.506
 27 0.625 0.450 0.675 // 28 0.500 0.600 0.000
 29 0.500 0.600 0.200 // 30 0.500 0.600 0.400
 31 0.500 0.600 0.600 // 32 0.500 0.600 0.800
 33 0.375 0.750 0.000 // 34 0.375 0.750 0.231
 35 0.375 0.750 0.462 // 36 0.375 0.750 0.694
 37 0.375 0.750 0.925 // 38 0.250 0.900 0.000
 39 0.250 0.900 0.262 // 40 0.250 0.900 0.525
 41 0.250 0.900 0.787 // 42 0.250 0.900 1.05
 43 0.125 1.05 0.000 // 44 0.125 1.05 0.294
 45 0.125 1.05 0.587 // 46 0.125 1.05 0.881
 47 0.125 1.05 1.17 // 48 0.000 1.20 0.325
 49 0.000 1.20 0.650 // 50 0.000 1.20 0.975
 51 1.22 0.000 0.300 // 52 1.15 0.000 0.300
 53 1.07 0.000 0.300 // 54 1.30 0.150 0.425
 55 1.19 0.150 0.425 // 56 1.09 0.150 0.425
 57 0.981 0.150 0.425 // 58 1.30 0.300 0.550
 59 1.16 0.300 0.550 // 60 1.02 0.300 0.550
 61 0.887 0.300 0.550 // 62 1.30 0.450 0.675
 63 1.13 0.450 0.675 // 64 0.962 0.450 0.675
 65 0.794 0.450 0.675 // 66 1.30 0.600 0.800
 67 1.10 0.600 0.800 // 68 0.900 0.600 0.800
 69 0.700 0.600 0.800 // 70 1.30 0.750 0.925
 71 1.07 0.750 0.925 // 72 0.837 0.750 0.925
 73 0.606 0.750 0.925 // 74 1.30 0.900 1.05
 75 1.04 0.900 1.05 // 76 0.775 0.900 1.05
 77 0.512 0.900 1.05 // 78 1.30 1.05 1.17
 79 1.01 1.05 1.17 // 80 0.712 1.05 1.17
 81 0.419 1.05 1.17 // 82 0.975 1.20 1.30
 83 0.650 1.20 1.30 // 84 0.325 1.20 1.30
 85 0.000 1.85 0.000 // 86 0.000 1.85 0.325
 87 0.000 1.85 0.650 // 88 0.000 1.85 0.975
 89 0.000 1.85 1.30 // 90 0.000 2.50 0.000
 91 0.000 2.50 0.325 // 92 0.000 2.50 0.650
 93 0.000 2.50 0.975 // 94 0.000 2.50 1.30
 95 0.000 3.15 0.000 // 96 0.000 3.15 0.325
 97 0.000 3.15 0.650 // 98 0.000 3.15 0.975
 99 0.000 3.15 1.30 // 100 0.000 3.80 0.325
 101 0.000 3.80 0.650 // 102 0.000 3.80 0.975
 103 1.30 1.85 1.30 // 104 0.975 1.85 1.30
 105 0.650 1.85 1.30 // 106 0.325 1.85 1.30
 107 1.30 2.50 1.30 // 108 0.975 2.50 1.30
 109 0.650 2.50 1.30 // 110 0.325 2.50 1.30
 111 1.30 3.15 1.30 // 112 0.975 3.15 1.30
 113 0.650 3.15 1.30 // 114 0.325 3.15 1.30
 115 0.975 3.80 1.30 // 116 0.650 3.80 1.30
 117 0.325 3.80 1.30
elem
numb group elem prop topo
 1 1 41320 1 1 10 13
 2 1 41320 1 14 13 10
 3 1 41320 1 10 11 14
 4 1 41320 1 15 14 11
 5 1 41320 1 11 12 15
 6 1 41320 1 16 15 12
 7 1 41320 1 12 2 16
 8 1 41320 1 17 16 2
 9 1 41320 1 13 14 18
 10 1 41320 1 14 19 18
 11 1 41320 1 14 15 19
 12 1 41320 1 15 20 19
 13 1 41320 1 15 16 20
 14 1 41320 1 16 21 20
 15 1 41320 1 16 17 21
 16 1 41320 1 17 22 21
 17 1 41320 1 18 19 23
 18 1 41320 1 19 24 23
```

```
19 1 41320 1 19 20 24
20 1 41320 1 20 25 24
21 1 41320 1 20 21 25
22 1 41320 1 21 26 25
23 1 41320 1 21 22 26
24 1 41320 1 22 27 26
25 1 41320 1 23 24 28
26 1 41320 1 24 29 28
27 1 41320 1 24 25 29
28 1 41320 1 25 30 29
29 1 41320 1 25 26 30
30 1 41320 1 26 31 30
31 1 41320 1 26 27 31
32 1 41320 1 27 32 31
33 1 41320 1 28 29 33
34 1 41320 1 29 34 33
35 1 41320 1 29 30 34
36 1 41320 1 30 35 34
37 1 41320 1 30 31 35
38 1 41320 1 31 36 35
39 1 41320 1 31 32 36
40 1 41320 1 32 37 36
41 1 41320 1 33 34 38
42 1 41320 1 34 39 38
43 1 41320 1 34 35 39
44 1 41320 1 35 40 39
45 1 41320 1 35 36 40
46 1 41320 1 36 41 40
47 1 41320 1 36 37 41
48 1 41320 1 37 42 41
49 1 41320 1 38 39 43
50 1 41320 1 39 44 43
51 1 41320 1 39 40 44
52 1 41320 1 40 45 44
53 1 41320 1 40 41 45
54 1 41320 1 41 46 45
55 1 41320 1 41 42 46
56 1 41320 1 42 47 46
57 1 41320 1 43 44 3
58 1 41320 1 44 48 3
59 1 41320 1 44 45 48
60 1 41320 1 45 49 48
61 1 41320 1 45 46 49
62 1 41320 1 46 50 49
63 1 41320 1 46 47 50
64 1 41320 1 47 4 50
65 2 41320 1 5 51 54
66 2 41320 1 55 54 51
67 2 41320 1 51 52 55
68 2 41320 1 56 55 52
69 2 41320 1 52 53 56
70 2 41320 1 57 56 53
71 2 41320 1 53 2 57
72 2 41320 1 17 57 2
73 2 41320 1 54 55 58
74 2 41320 1 55 59 58
75 2 41320 1 55 56 59
76 2 41320 1 56 60 59
77 2 41320 1 58 57 60
78 2 41320 1 57 61 60
79 2 41320 1 57 17 61
80 2 41320 1 17 22 61
81 2 41320 1 58 59 62
82 2 41320 1 59 63 62
83 2 41320 1 59 60 63
84 2 41320 1 60 64 63
85 2 41320 1 60 61 64
86 2 41320 1 61 65 64
87 2 41320 1 61 22 65
88 2 41320 1 22 27 65
89 2 41320 1 62 63 66
90 2 41320 1 63 67 66
91 2 41320 1 63 64 67
92 2 41320 1 64 68 67
93 2 41320 1 64 65 68
94 2 41320 1 65 69 68
95 2 41320 1 65 27 69
96 2 41320 1 27 32 69
97 2 41320 1 66 67 70
98 2 41320 1 67 71 70
99 2 41320 1 67 68 71
100 2 41320 1 68 72 71
101 2 41320 1 68 69 72
102 2 41320 1 69 73 72
103 2 41320 1 69 32 73
104 2 41320 1 32 37 73
```

```
105 2 41320 1 70 71 74
106 2 41320 1 71 75 74
107 2 41320 1 71 72 75
108 2 41320 1 72 76 75
109 2 41320 1 72 73 76
110 2 41320 1 73 77 76
111 2 41320 1 73 37 77
112 2 41320 1 37 42 77
113 2 41320 1 74 75 78
114 2 41320 1 75 79 78
115 2 41320 1 75 76 79
116 2 41320 1 76 80 79
117 2 41320 1 76 77 80
118 2 41320 1 77 81 80
119 2 41320 1 77 42 81
120 2 41320 1 42 47 81
121 2 41320 1 78 79 6
122 2 41320 1 79 82 6
123 2 41320 1 79 80 82
124 2 41320 1 80 83 82
125 2 41320 1 80 81 83
126 2 41320 1 81 84 83
127 2 41320 1 81 47 84
128 2 41320 1 47 4 84
129 3 41320 1 3 48 85
130 3 41320 1 86 85 48
131 3 41320 1 48 49 86
132 3 41320 1 87 86 49
133 3 41320 1 49 50 87
134 3 41320 1 88 87 50
135 3 41320 1 50 4 88
136 3 41320 1 89 88 4
137 3 41320 1 85 86 90
138 3 41320 1 86 91 90
139 3 41320 1 86 87 91
140 3 41320 1 87 92 91
141 3 41320 1 87 88 92
142 3 41320 1 88 93 92
143 3 41320 1 88 89 93
144 3 41320 1 89 94 93
145 3 41320 1 90 91 95
146 3 41320 1 91 96 95
147 3 41320 1 91 92 96
148 3 41320 1 92 97 96
149 3 41320 1 92 93 97
150 3 41320 1 93 98 97
151 3 41320 1 93 94 98
152 3 41320 1 94 99 98
153 3 41320 1 95 96 7
154 3 41320 1 96 100 7
155 3 41320 1 96 97 100
156 3 41320 1 97 101 100
157 3 41320 1 97 98 101
158 3 41320 1 98 102 101
159 3 41320 1 98 99 102
160 3 41320 1 99 8 102
161 4 41320 1 6 82 103
162 4 41320 1 104 103 82
163 4 41320 1 82 83 104
164 4 41320 1 105 104 83
165 4 41320 1 83 84 105
166 4 41320 1 106 105 84
167 4 41320 1 84 4 106
168 4 41320 1 89 106 4
169 4 41320 1 103 104 107
170 4 41320 1 104 108 107
171 4 41320 1 104 105 108
172 4 41320 1 105 109 108
173 4 41320 1 105 106 109
174 4 41320 1 106 110 109
175 4 41320 1 106 89 110
176 4 41320 1 89 94 110
177 4 41320 1 107 108 111
178 4 41320 1 108 112 111
179 4 41320 1 108 109 112
180 4 41320 1 109 113 112
181 4 41320 1 109 110 113
182 4 41320 1 110 114 113
183 4 41320 1 110 94 114
184 4 41320 1 94 99 114
185 4 41320 1 111 112 9
186 4 41320 1 112 115 9
187 4 41320 1 112 113 115
188 4 41320 1 113 116 115
189 4 41320 1 113 114 116
190 4 41320 1 114 117 116
191 4 41320 1 114 99 117
192 4 41320 1 99 8 117
plates.and.shells
mate thic
1 0.016
axes
```

```
axis relax type node ang1 ang2 ang3
4 1 1 1 39.806 0.0 0.0
5 1 1 2 0.0 0.0 -39.806
local
node loca
1 4
10 4
11 4
12 4
13 4
14 4
15 4
16 4
18 4
19 4
20 4
21 4
23 4
24 4
26 4
28 4
29 4
30 4
31 4
33 4
34 4
35 4
36 4
38 4
39 4
40 4
41 4
43 4
44 4
45 4
46 4
3 4
48 4
49 4
50 4
5 5
51 5
52 5
53 5
54 5
55 5
56 5
57 5
58 5
59 5
60 5
61 5
62 5
63 5
64 5
65 5
66 5
67 5
68 5
69 5
70 5
71 5
72 5
73 5
74 5
75 5
76 5
77 5
78 5
79 5
80 5
81 5
82 5
83 5
84 5
loads
node dire valu
10 2 -34040
12 2 -34040
51 2 -34040
53 2 -34040
14 2 -32340
16 2 -32340
55 2 -32340
57 2 -32340
19 2 -30660
21 2 -30660
```

```
59 2 -30660
61 2 -30660
24 2 -28960
26 2 -28960
63 2 -28960
65 2 -28960
29 2 -27260
31 2 -27260
67 2 -27260
69 2 -27260
34 2 -25560
36 2 -25560
71 2 -25560
73 2 -25560
39 2 -23860
41 2 -23860
75 2 -23860
77 2 -23860
44 2 -22160
46 2 -22160
79 2 -22160
81 2 -22160
48 2 -20480
50 2 -20480
82 2 -20480
84 2 -20480
86 2 -10200
88 2 -10200
104 2 -10200
106 2 -10200
91 2 -7540
93 2 -7540
108 2 -7540
110 2 -7540
96 2 -4200
98 2 -4200
112 2 -4200
114 2 -4200
pres
pres list
29480 1 10 11 12
-29480 5 51 52 53
28010 13 14 15 16
-28010 54 55 56 57
26550 18 19 20 21
-26550 58 59 60 61
25080 23 24 25 26
-25080 62 63 64 65
23610 28 29 30 31
-23610 66 67 68 69
22140 33 34 35 36
-22140 70 71 72 73
20670 38 39 40 41
-20670 74 75 76 77
19200 43 44 45 46
-19200 78 79 80 81
17730 3 48 49 50
-17730 6 82 83 84
8832 85 86 87 88
-8832 103 104 105 106
6536 90 91 92 93
-6536 107 108 109 110
3645 95 96 97 98
-3645 111 112 113 114
rest
node plan dire
3 2 2
1 6 1
2 4 3
1 3 53
5 1 51
end.of.data
```

PAFEC DATA INPUT FILE 2

```
CONTROL
PHASE=1
PHASE=2
PHASE=4
PHASE=6
PHASE=7
PHASE=8
PHASE=9
CONTROL.END
TITLE STEEL BIN RING SUPPORT sand fill Janssen dist.  quarter bin modelled
zero in-plane load
NODES
NODE X Y Z
1 0.0 0.0 0.0
2 0.0 0.0 1.0
3 0.0 2.0 0.0
4 0.0 2.0 1.0
5 1.0 0.0 1.0
6 1.0 2.0 1.0
PAFBLOCKS
GROUP ELEM N1 N2 INC
1 41320 1 2 1 2 3 4
2 41320 1 2 5 2 6 4
MESH
REFER SPAC
1 8
2 8
PLATES
MATER THICK
1 0.010
PRES
PRES LIST
10640 1 7 8 9 10 11 12 13 2
-10640 5 84 85 86 87 88 89 90
9735 14 15 16 17 18 19 20 21 22
-9735 91 92 93 94 95 96 97 98
8870 23 24 25 26 27 28 29 30 31
-8870 99 100 101 102 103 104 105 106
7745 32 33 34 35 36 37 38 39 40
-7745 107 108 109 110 111 112 113 114
6620 41 42 43 44 45 46 47 48 49
-6620 115 116 117 118 119 120 121 122
5175 50 51 52 53 54 55 56 57 58
-5175 123 124 125 126 127 128 129 130
3730 59 60 61 62 63 64 65 66 67
-3730 131 132 133 134 135 136 137 138
1900 68 69 70 71 72 73 74 75 76
-1900 139 140 141 142 143 144 145 146
REST
NODE PLANE DIRE
1 6 12
5 4 23
1 5 53
5 5 51
END.OF.DATA
```

Appendix B Strain Gauge Results

The primary reasons for the measurement of wall strains can be summarised as :-

a. To check the symmetry of loads within the silo.

b. To check the consistency of results throughout the test series.

c. To check the accuracy of the Finite Element analysis of the silo model and to appraise the benefits of using a realistic pressure distribution for silo design.

Only a limited selection of the strain gauge results has been presented during the discussion of each of these points. A full presentation of the results is given below.

The positions of strain gauges fixed to the external faces of the silo walls are shown in Figure 8.1. A three element rectangular rosette was bonded to the external surface of the wall at each point. The strain gauge positions were not selected to identify the stress distribution within the silo walls and so it was not necessary to fix gauges to the internal faces of the silo walls.

Figures B1 to B25 show the strain at each point of measurement throughout the filling process. The strain measured in three directions is given for each point: vertical, horizontal, and at 45° to the vertical and horizontal axes.

STRAIN GAUGE RESULTS
POSITION 'S1'

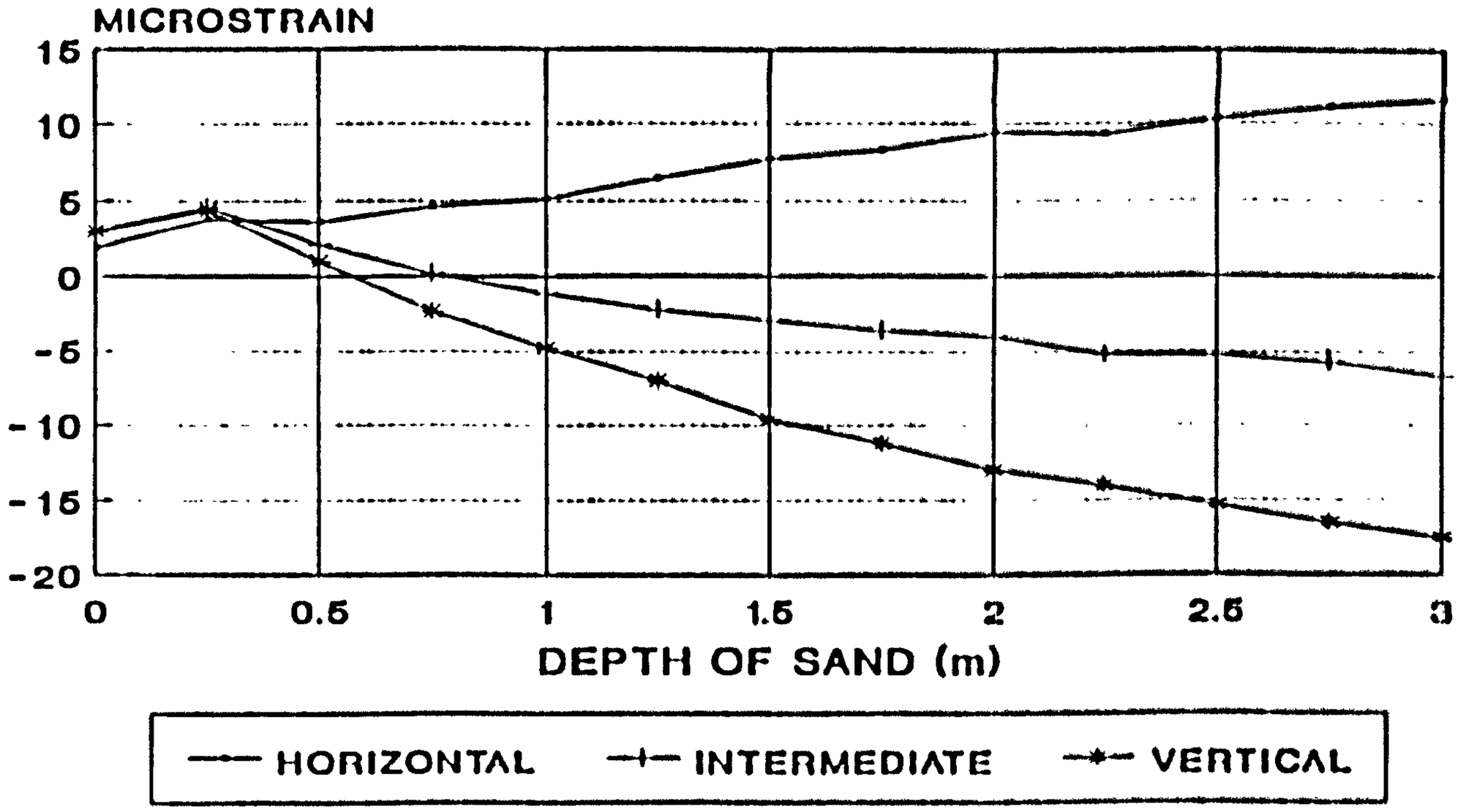

Figure B1

STRAIN GAUGE RESULTS
POSITION 'S2'

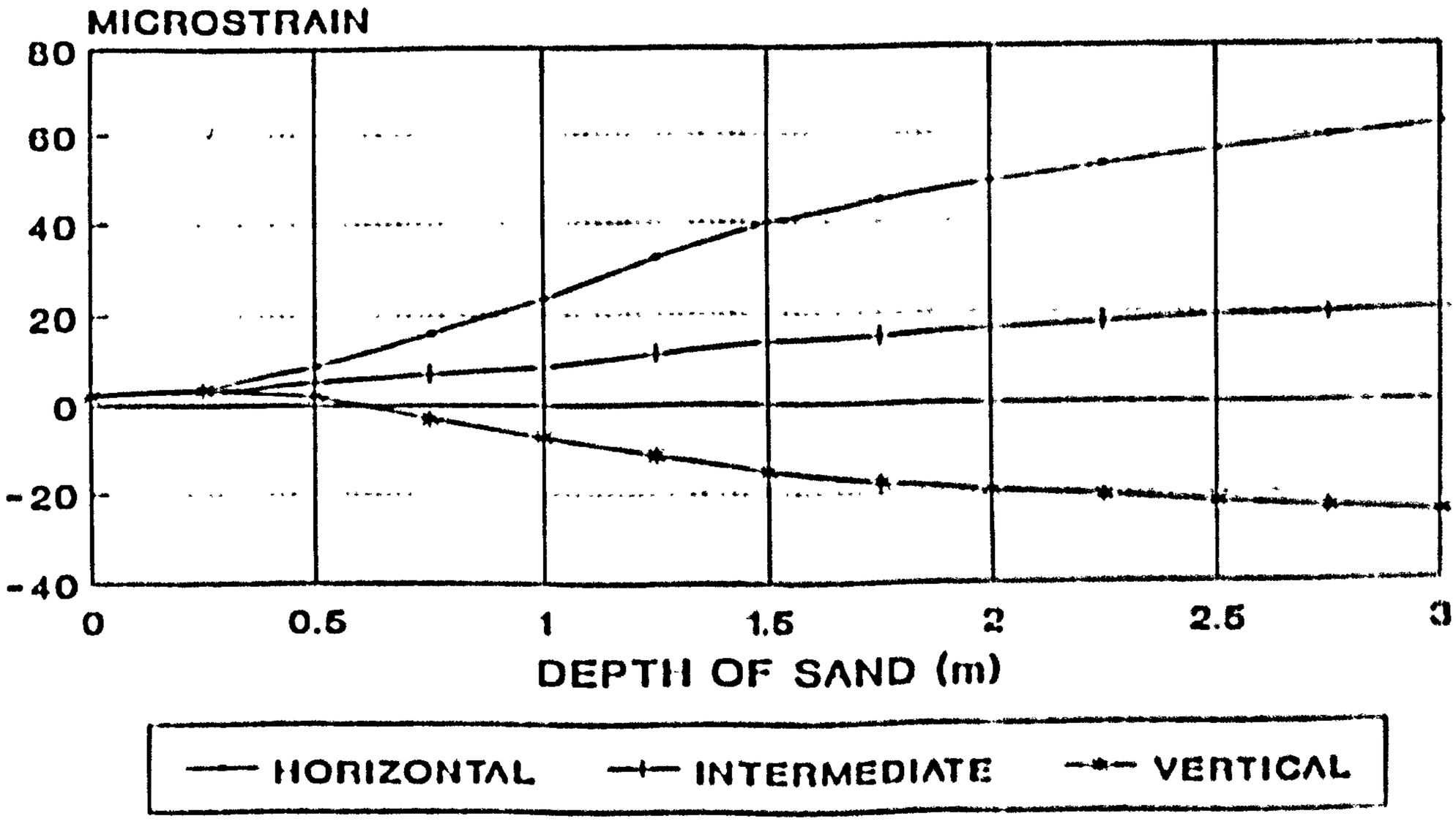

Figure B2

STRAIN GAUGE RESULTS
POSITION 'S3'

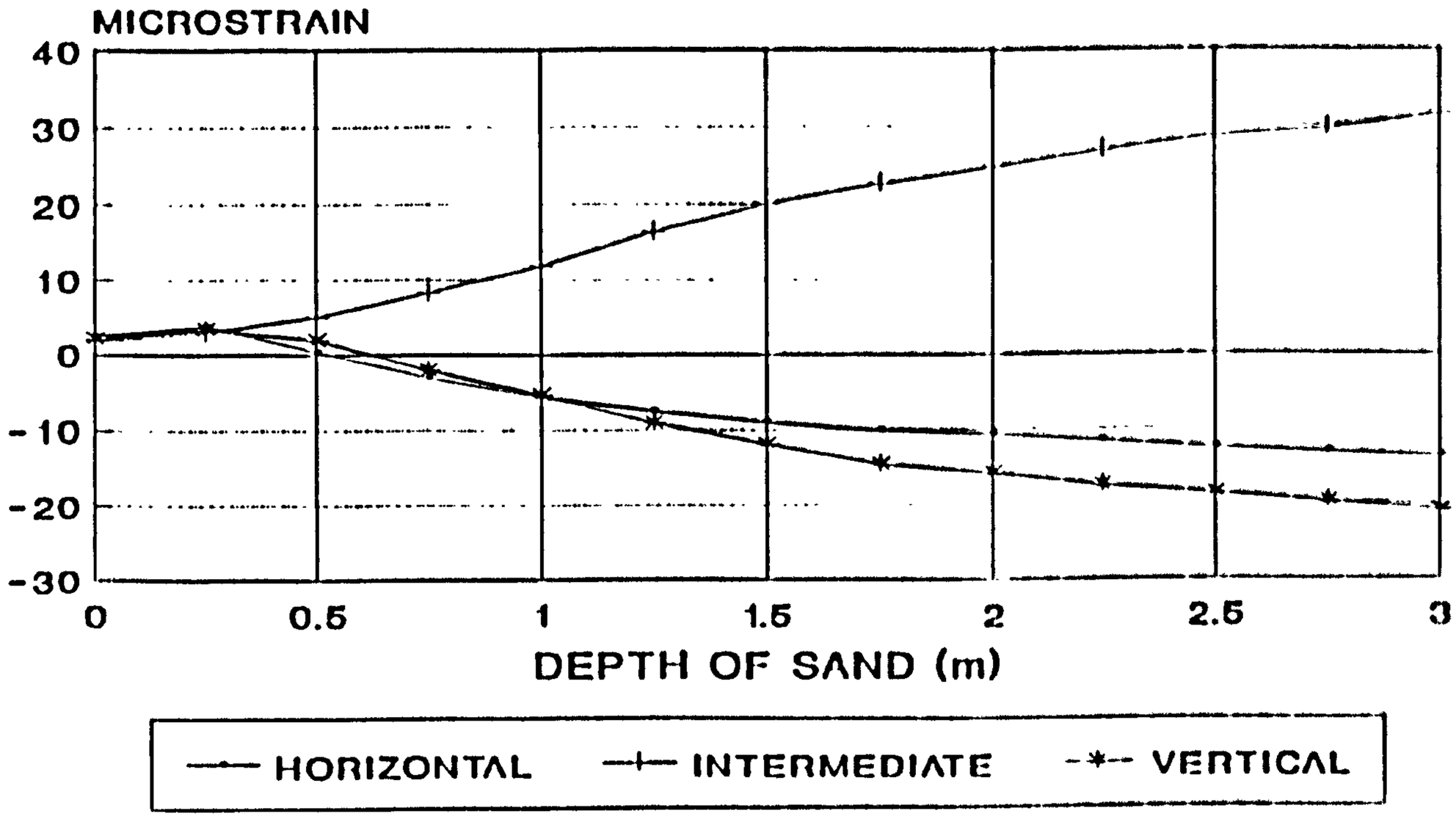

Figure B3

STRAIN GAUGE RESULTS
POSITION 'S4'

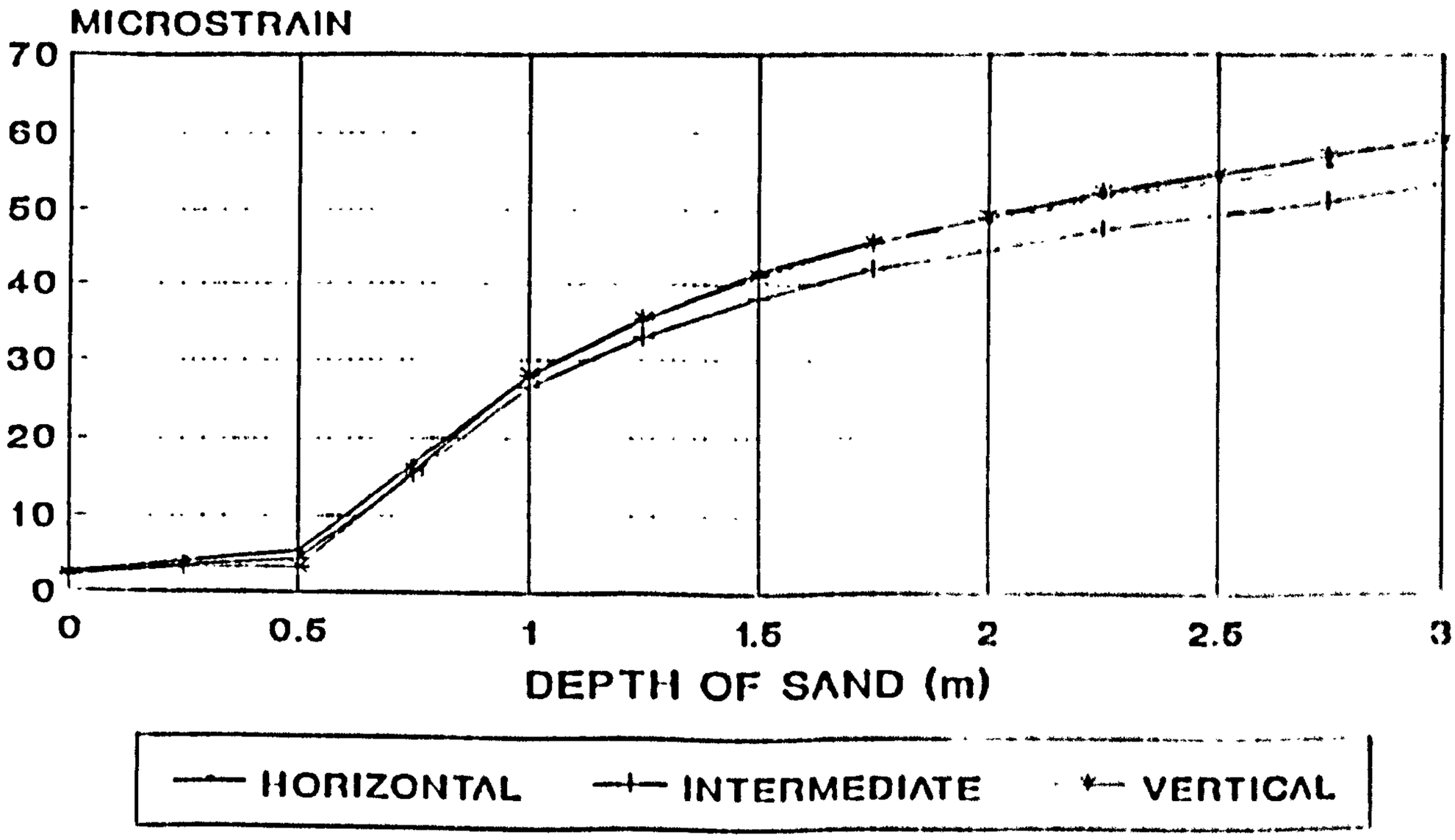

Figure B4

STRAIN GAUGE RESULTS
POSITION 'S5'

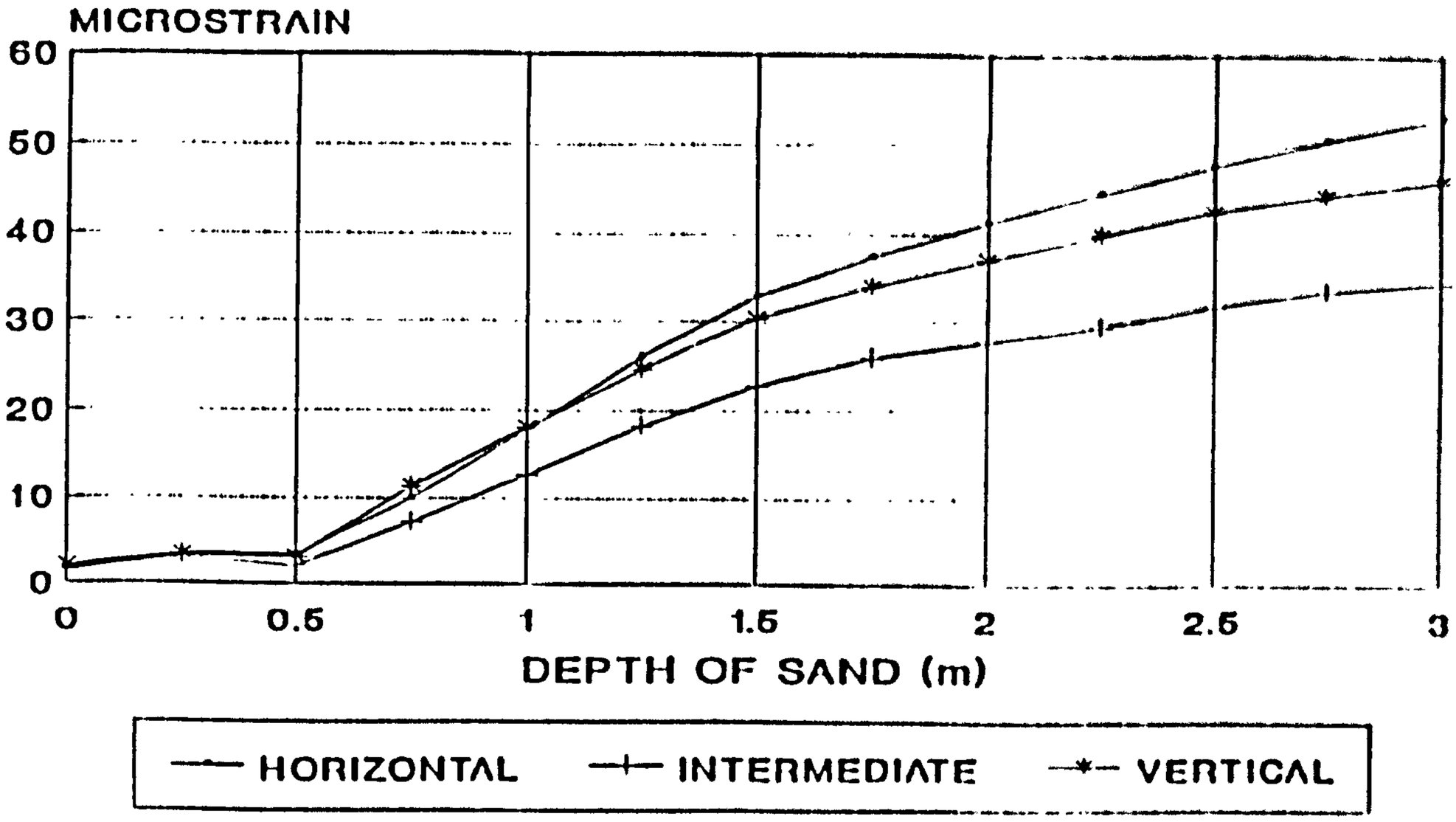

Figure B5

STRAIN GAUGE RESULTS
POSITION 'S6'

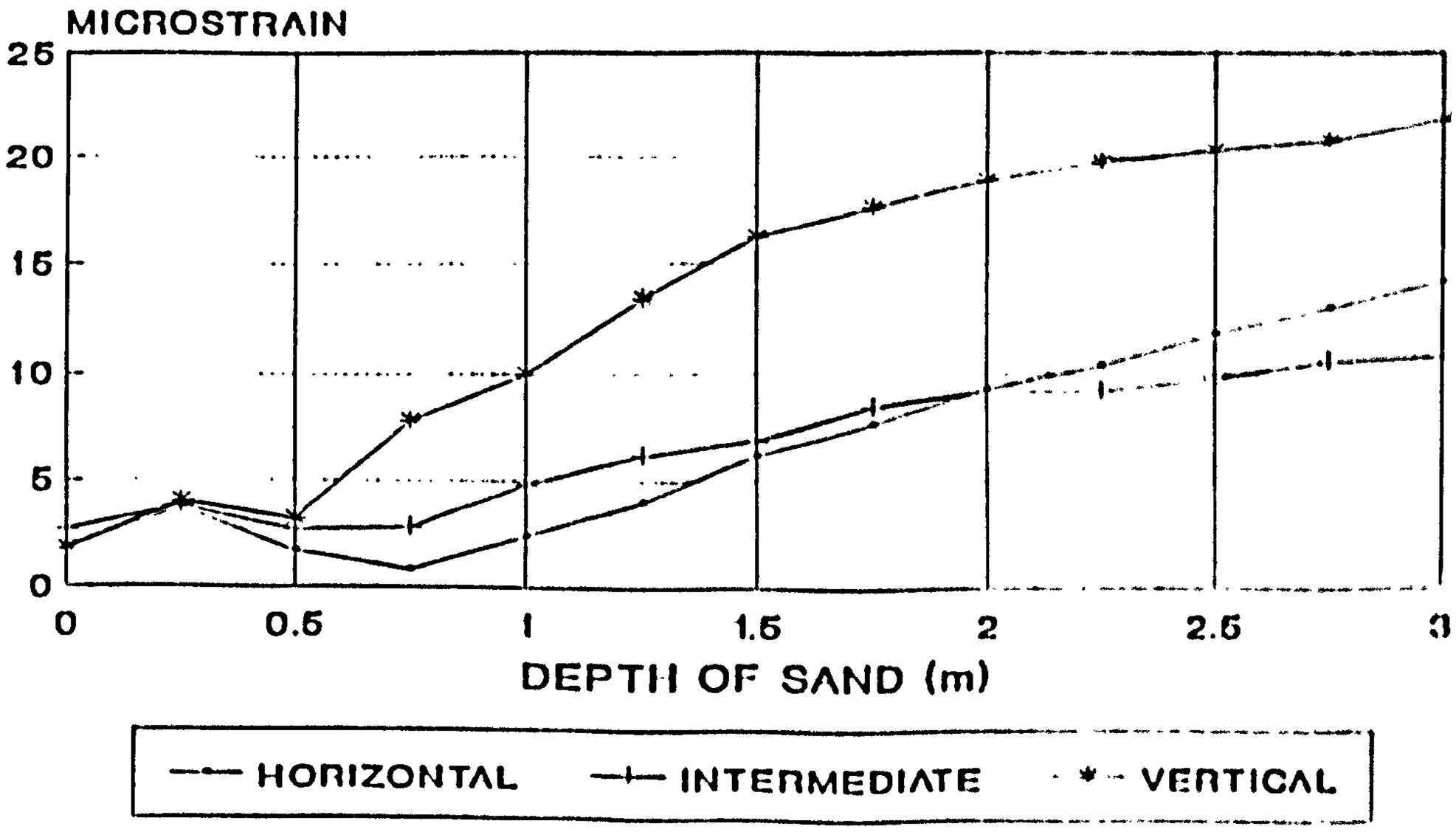

Figure B6

STRAIN GAUGE RESULTS
POSITION 'S7'

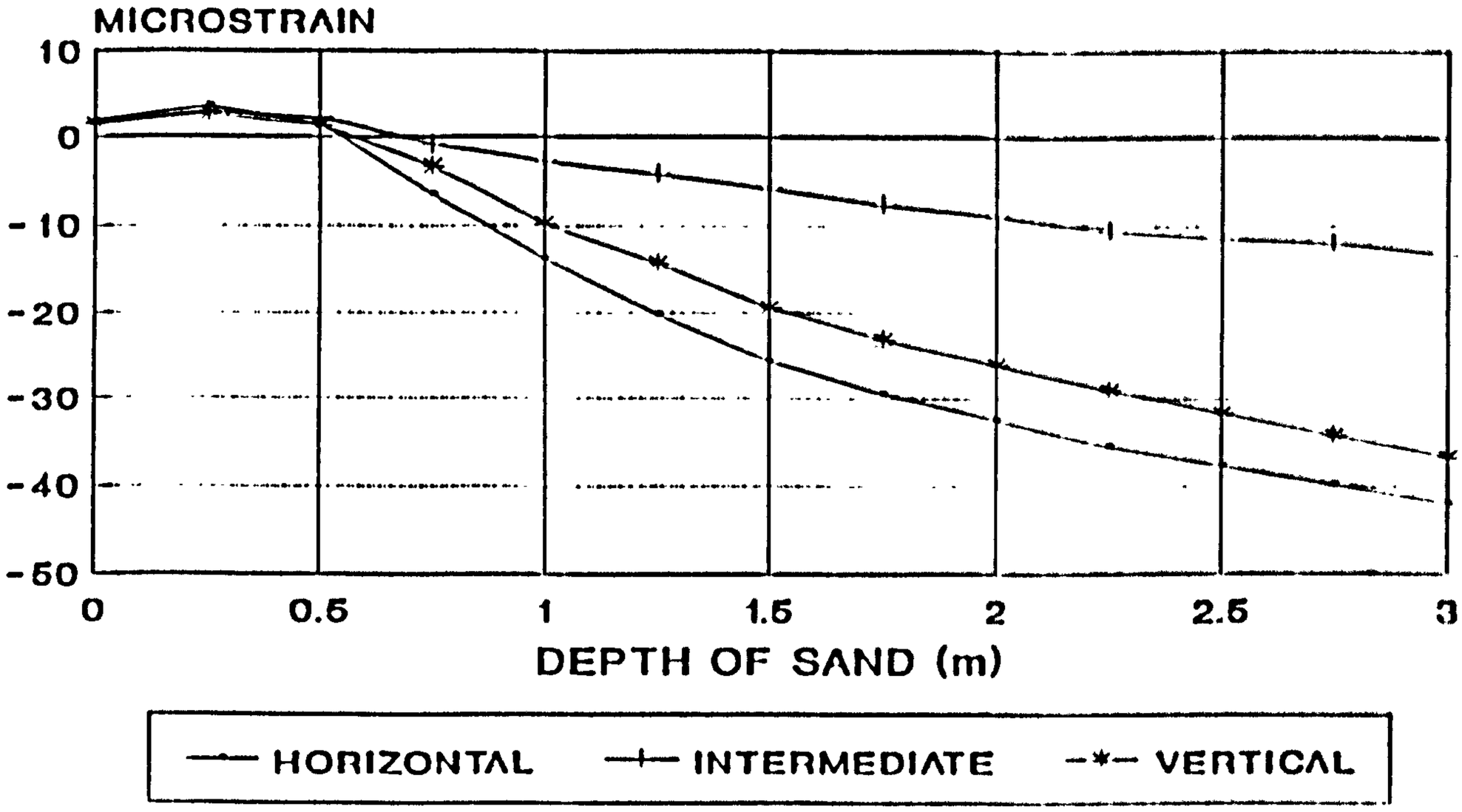

Figure B7

STRAIN GAUGE RESULTS
POSITION 'S8'

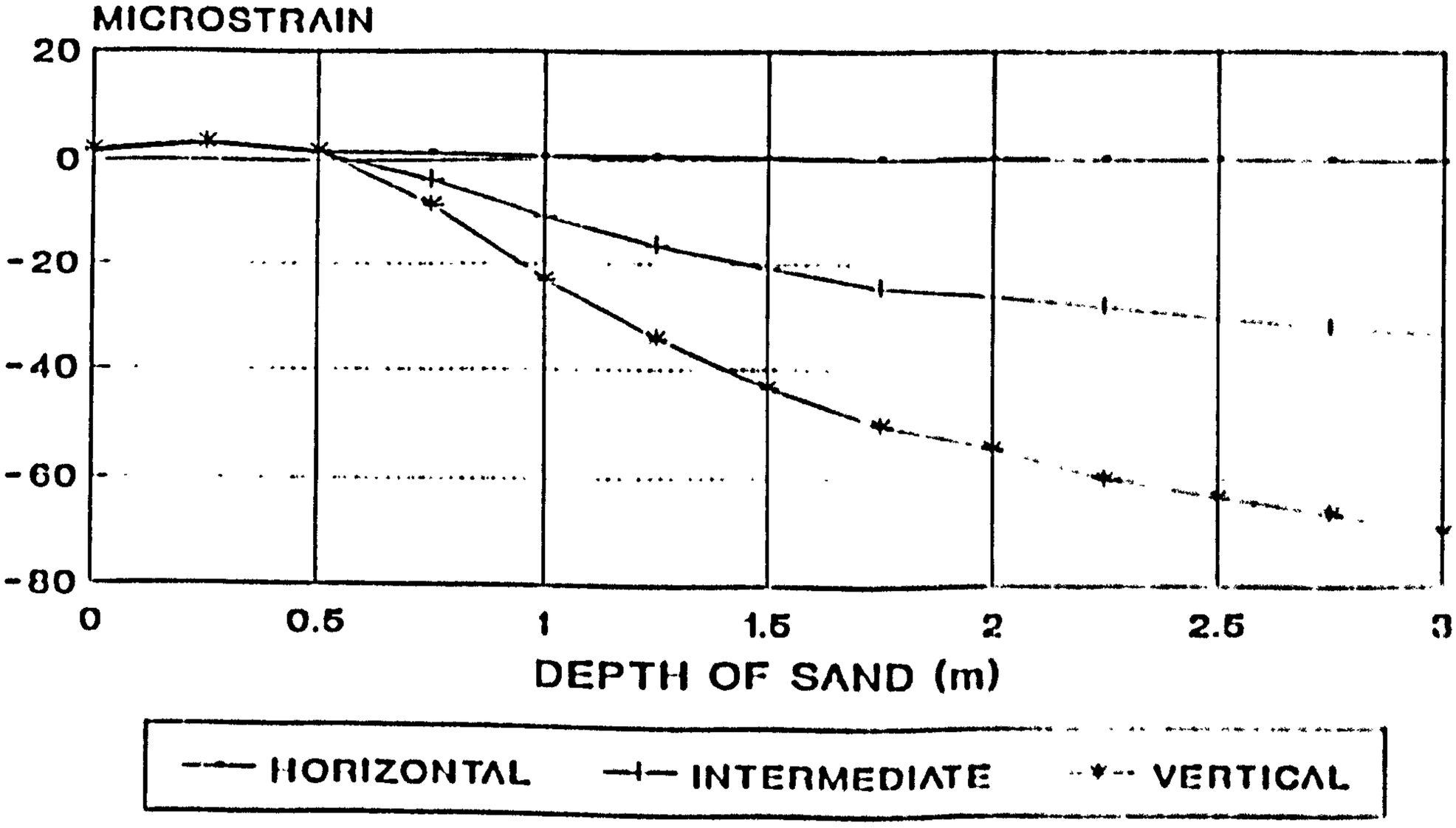

Figure B8

STRAIN GAUGE RESULTS
POSITION 'S9'

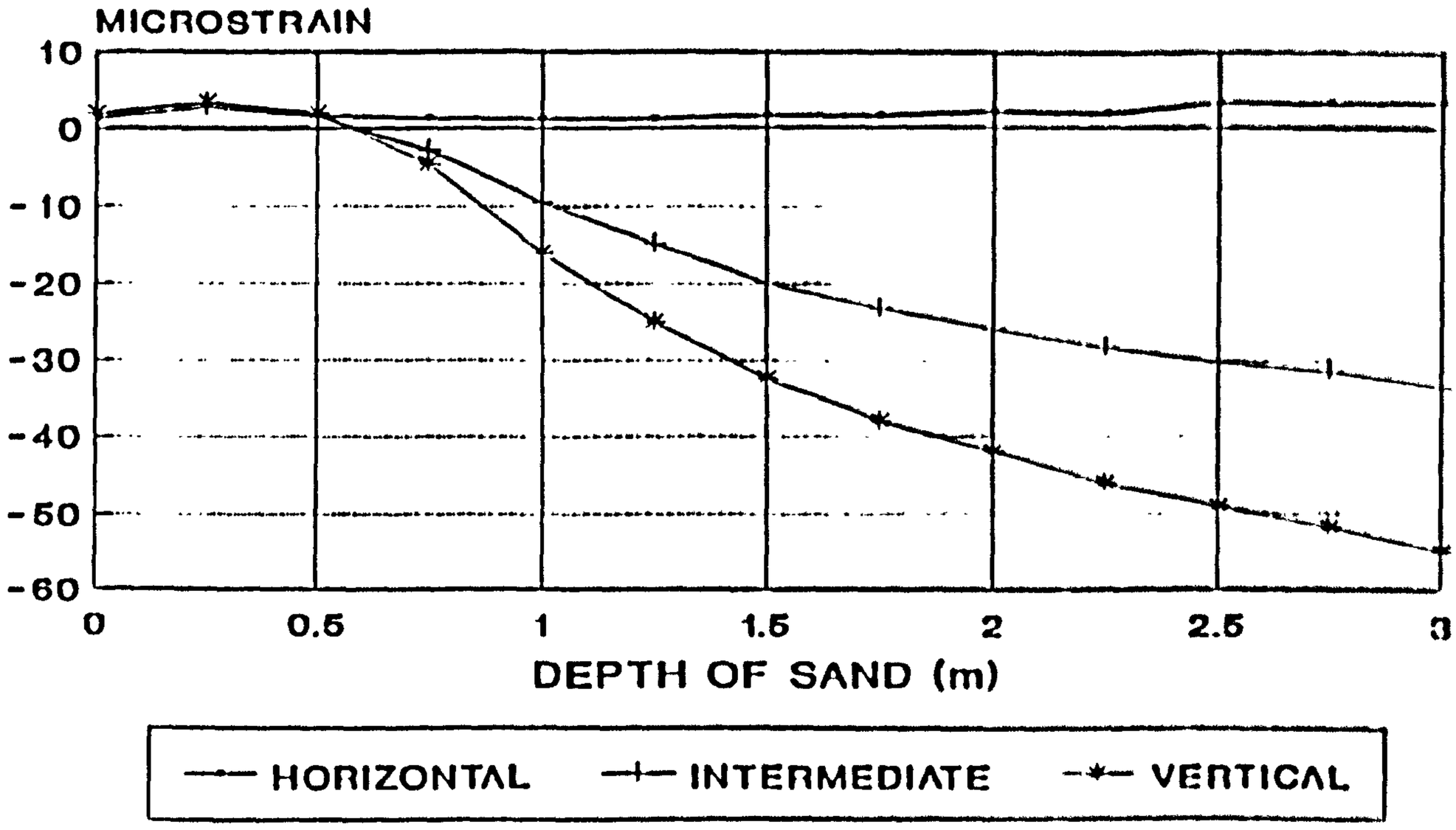

Figure B9

STRAIN GAUGE RESULTS
POSITION 'S10'

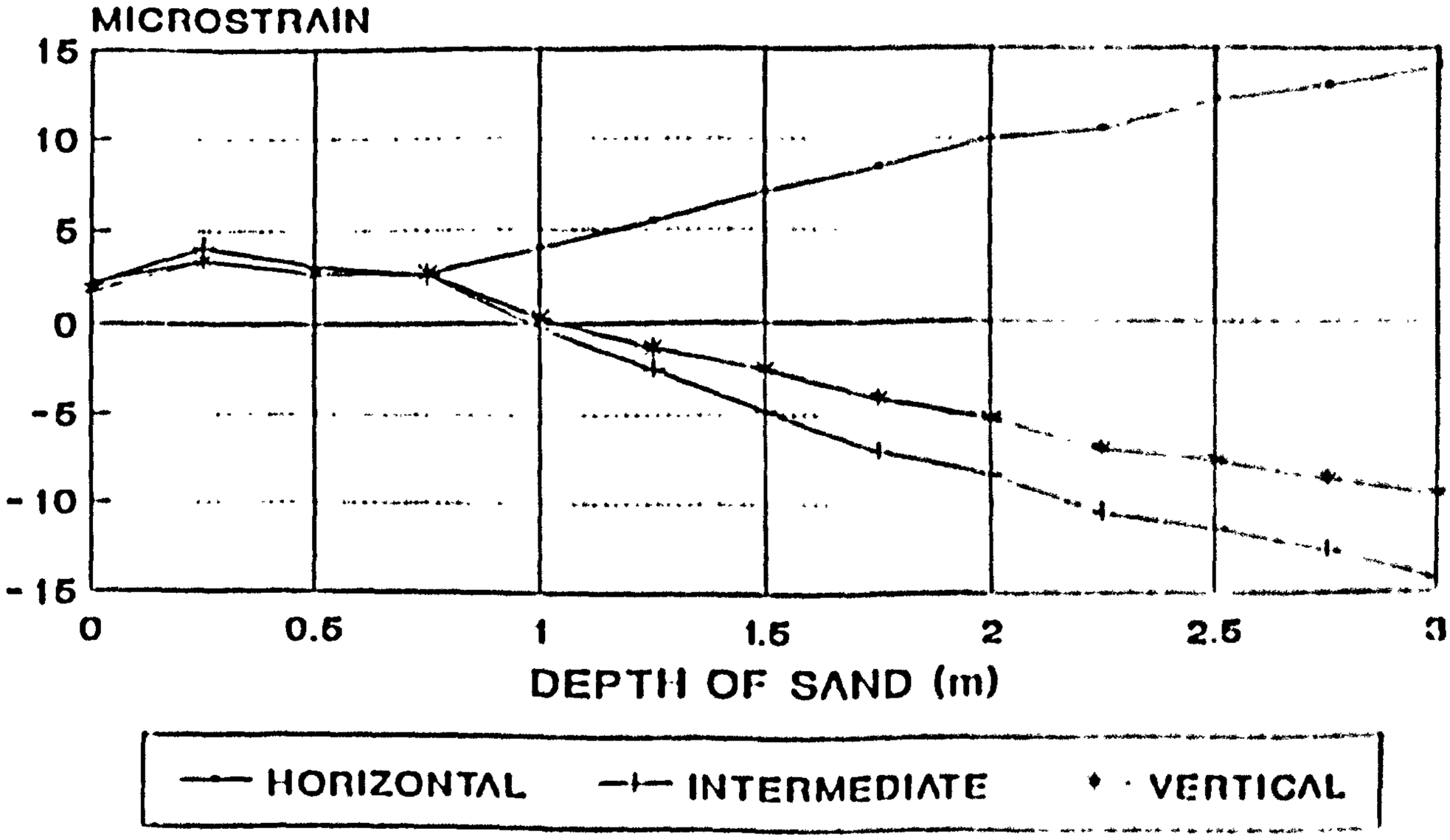

Figure B10

STRAIN GAUGE RESULTS
POSITION 'S11'

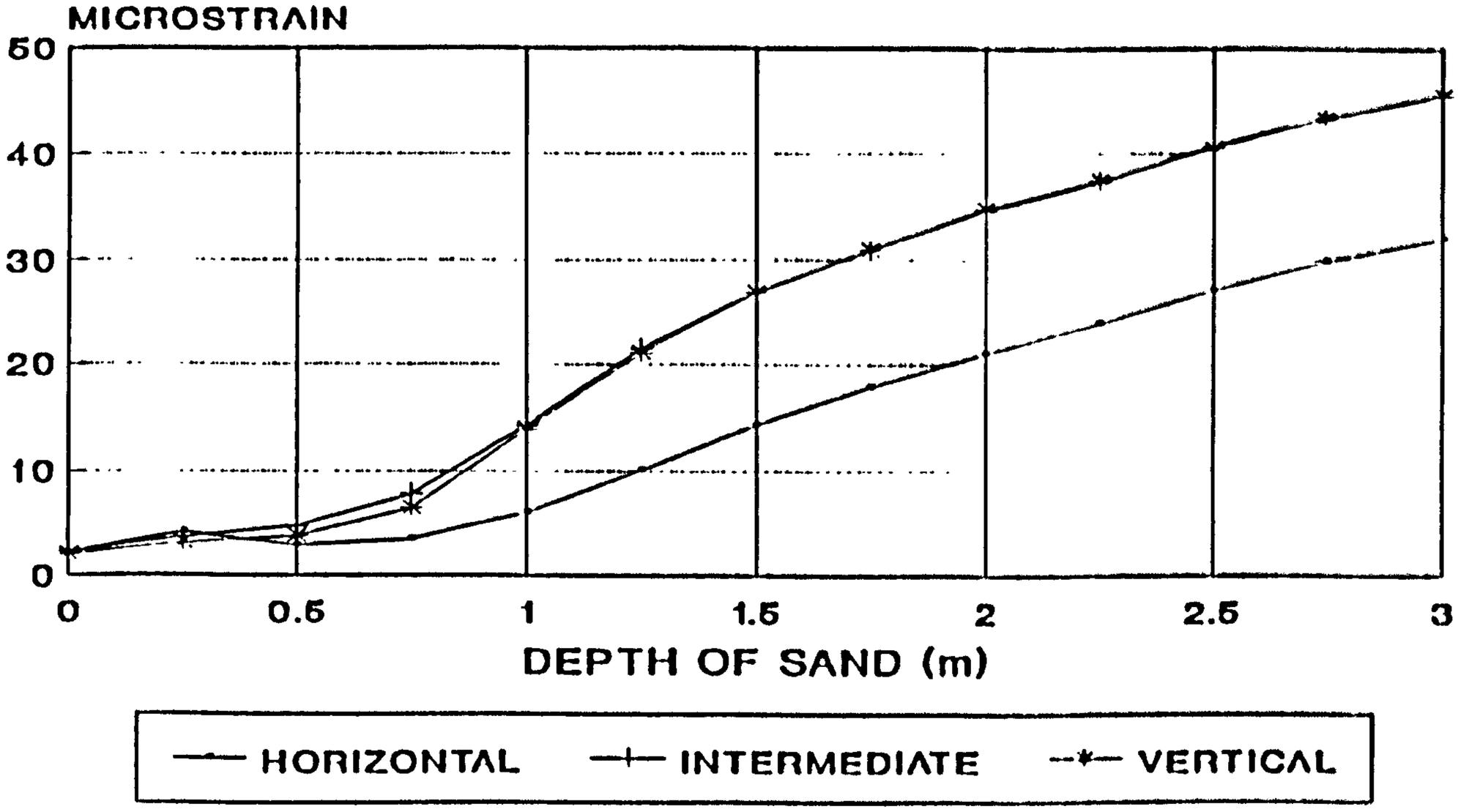

Figure B11

STRAIN GAUGE RESULTS
POSITION 'S12'

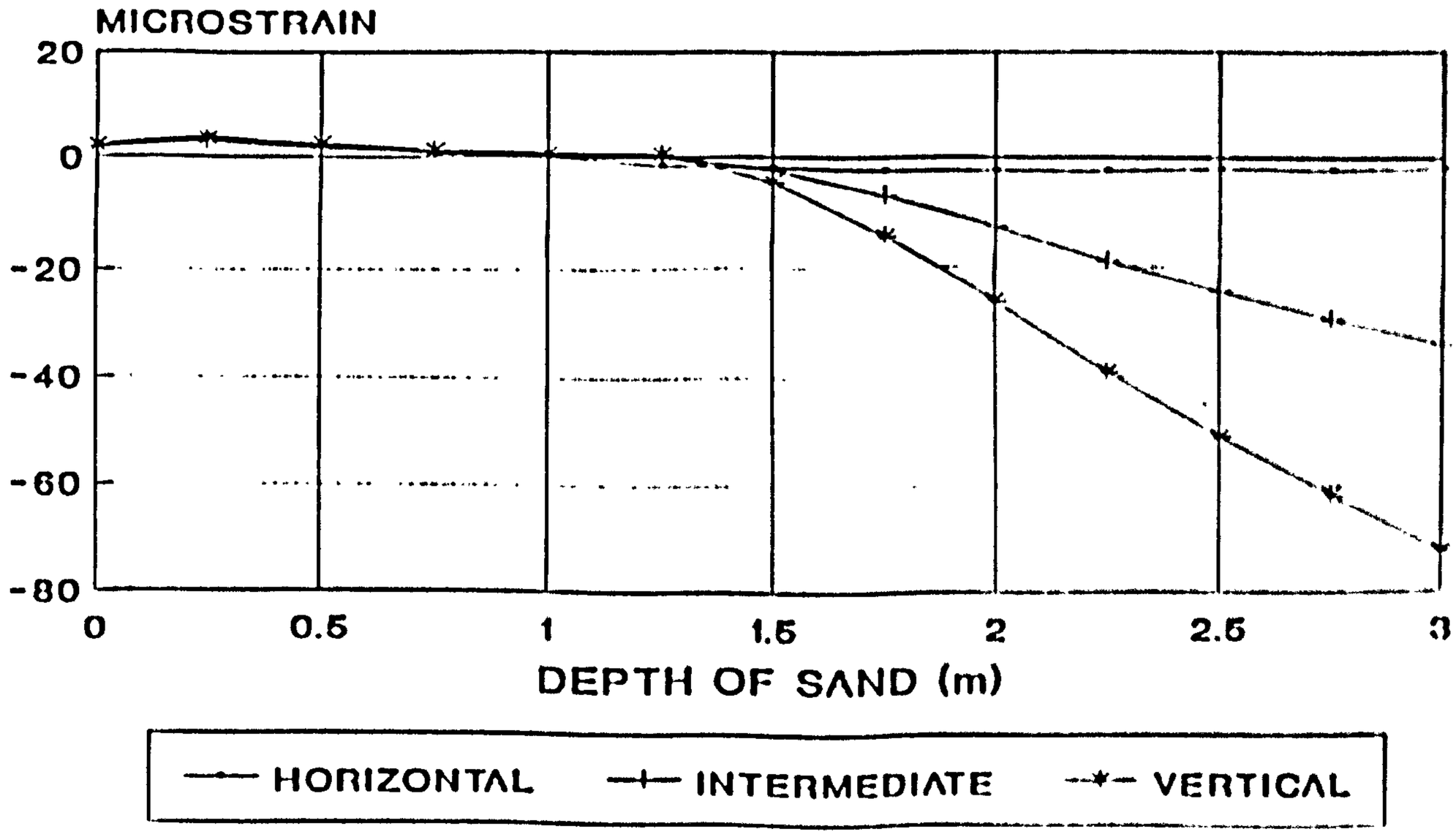

Figure B12

STRAIN GAUGE RESULTS
POSITION 'S13'

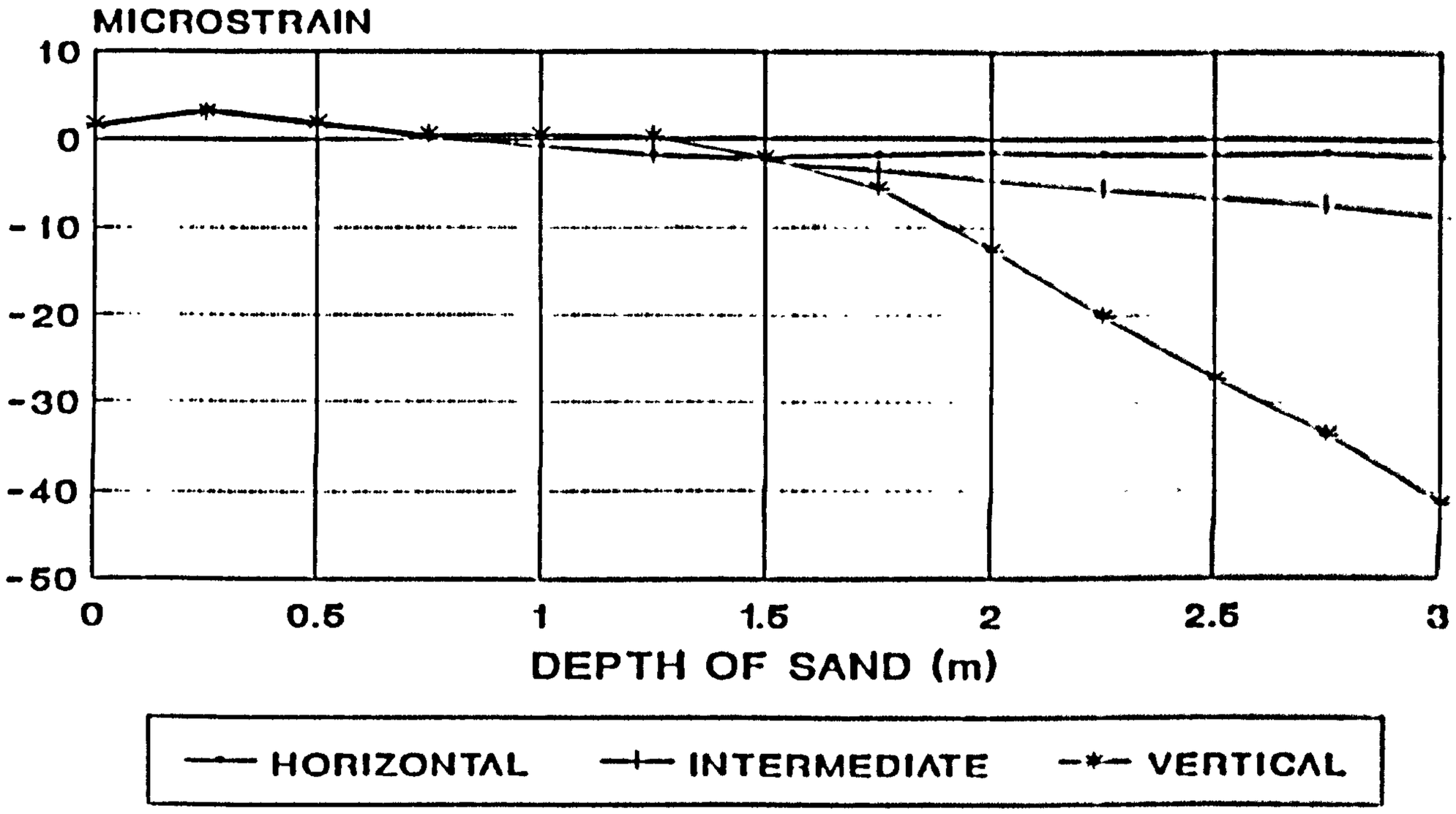

Figure B13

STRAIN GAUGE RESULTS
POSITION 'S14'

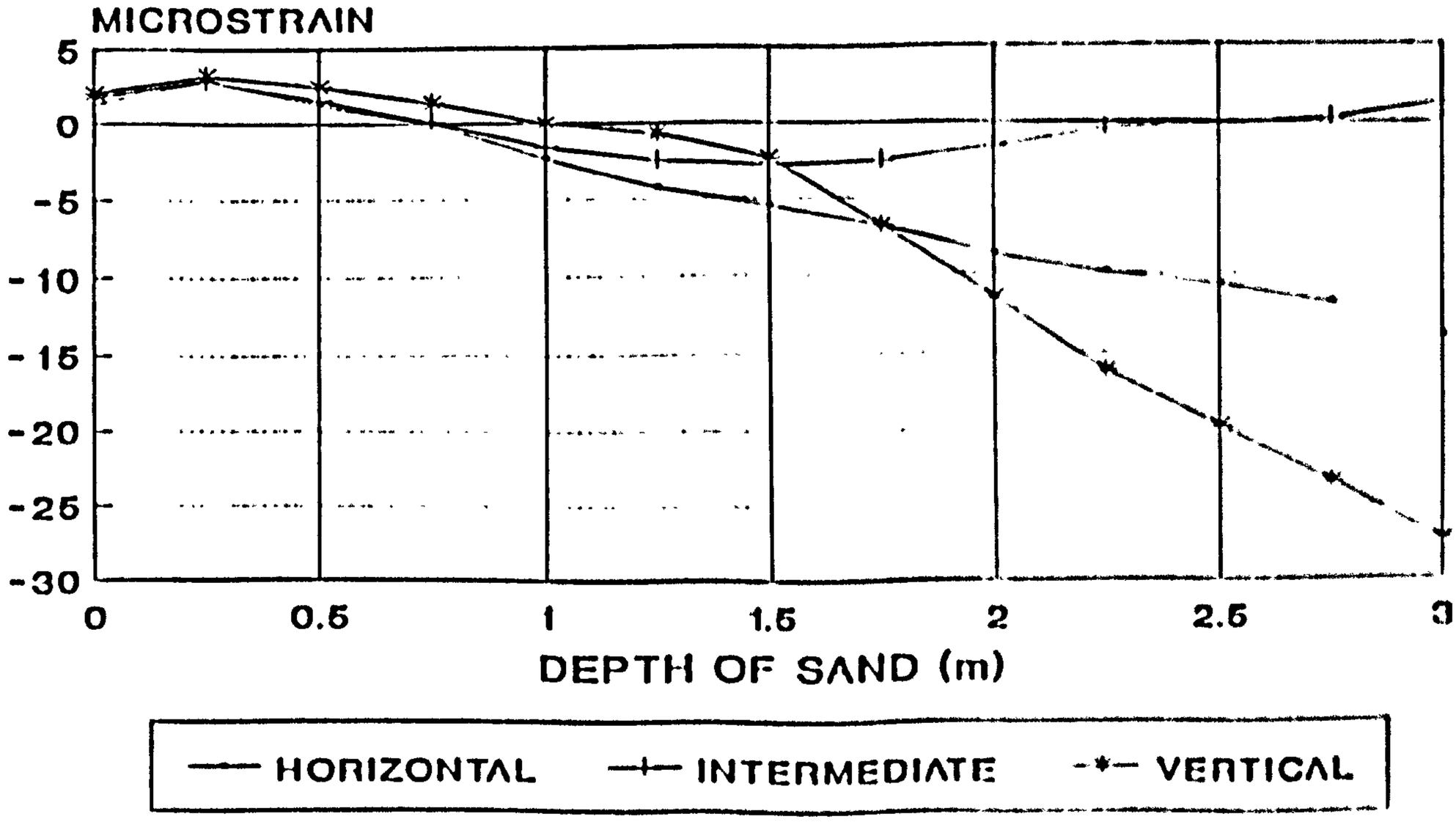

Figure B14

STRAIN GAUGE RESULTS
POSITION 'S15'

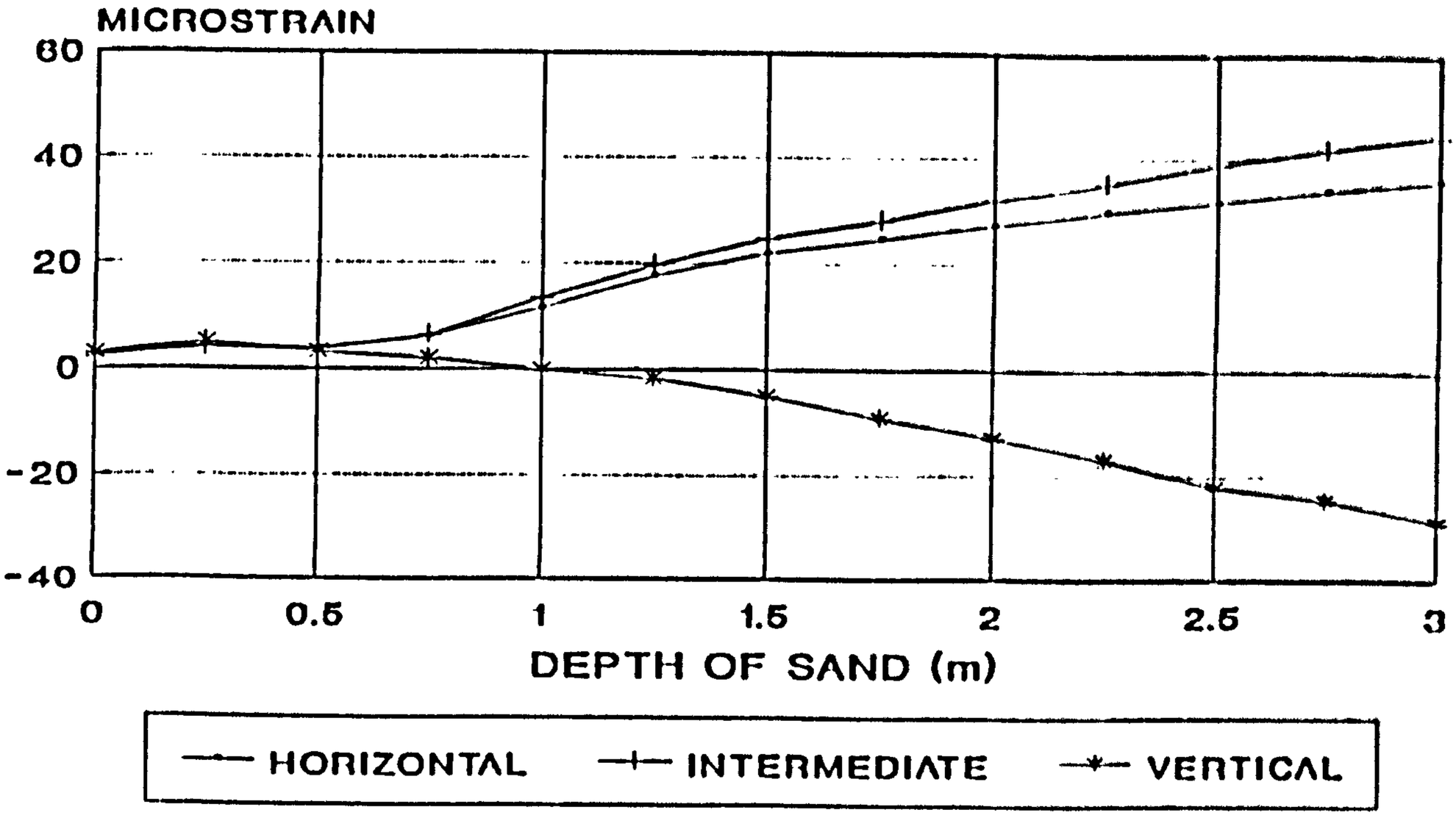

Figure B15

STRAIN GAUGE RESULTS
POSITION 'S16'

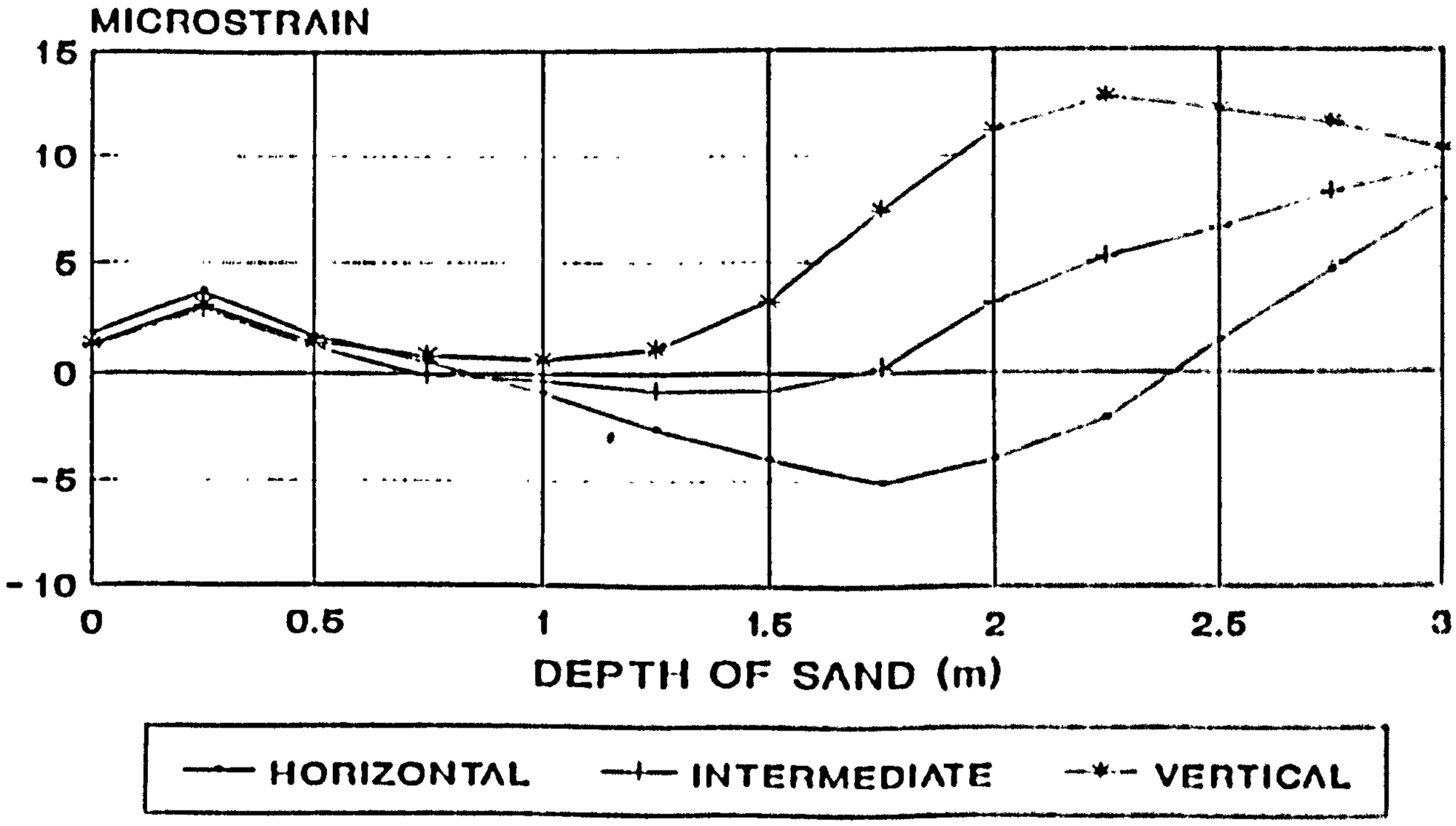

Figure B16

STRAIN GAUGE RESULTS
POSITION 'S17'

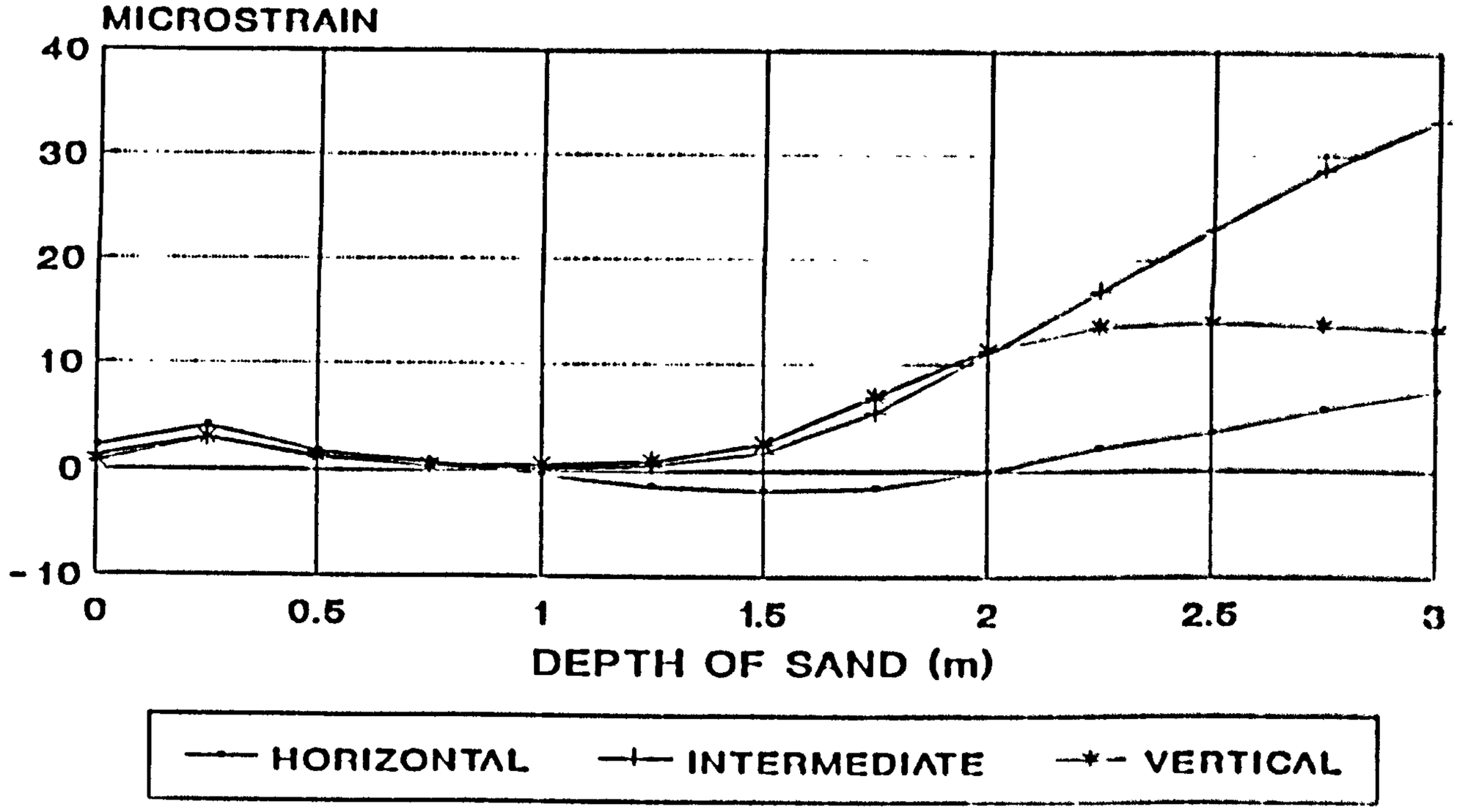

Figure B17

STRAIN GAUGE RESULTS
POSITION 'S18'

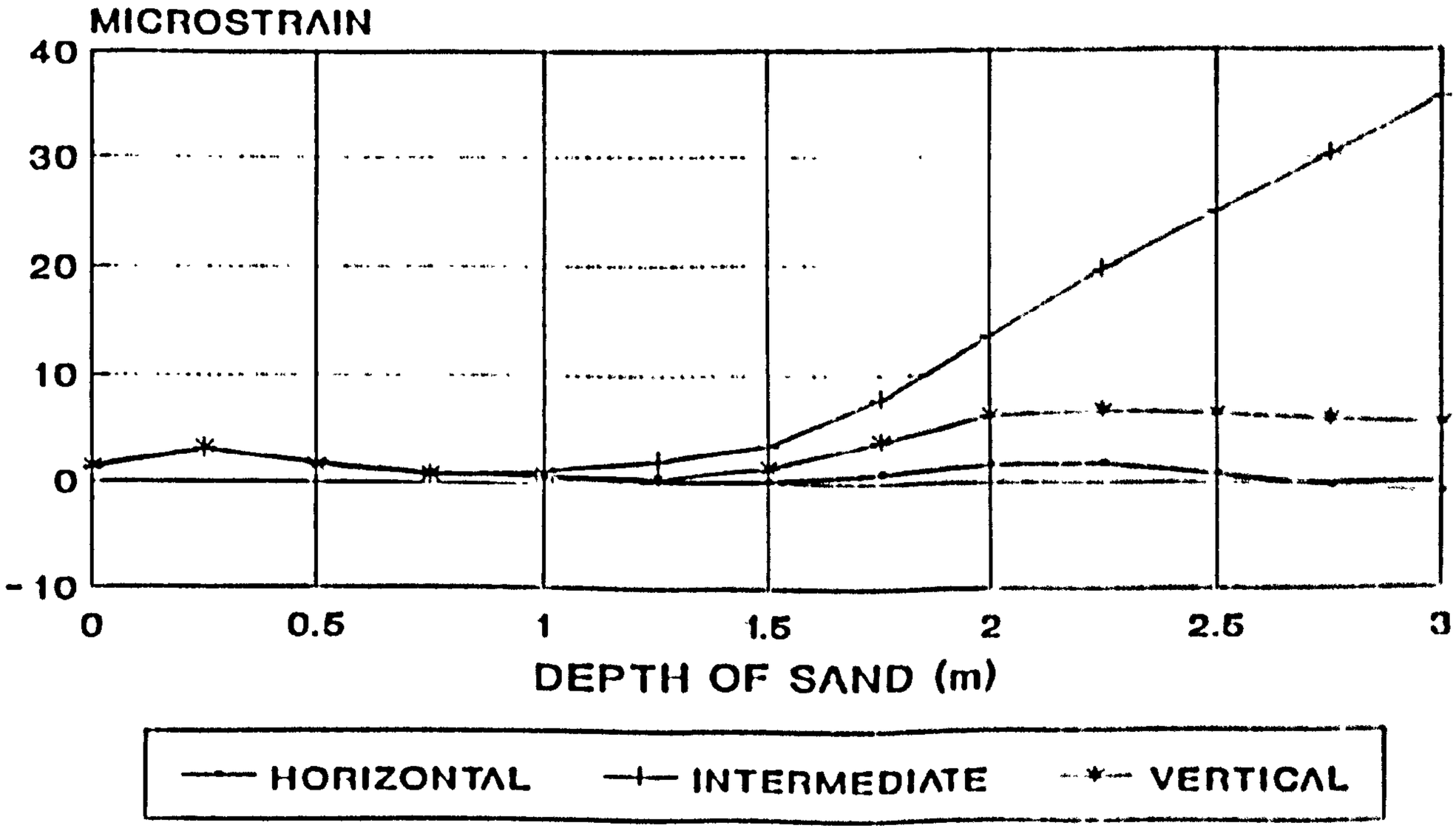

Figure B18

STRAIN GAUGE RESULTS
POSITION 'S19'

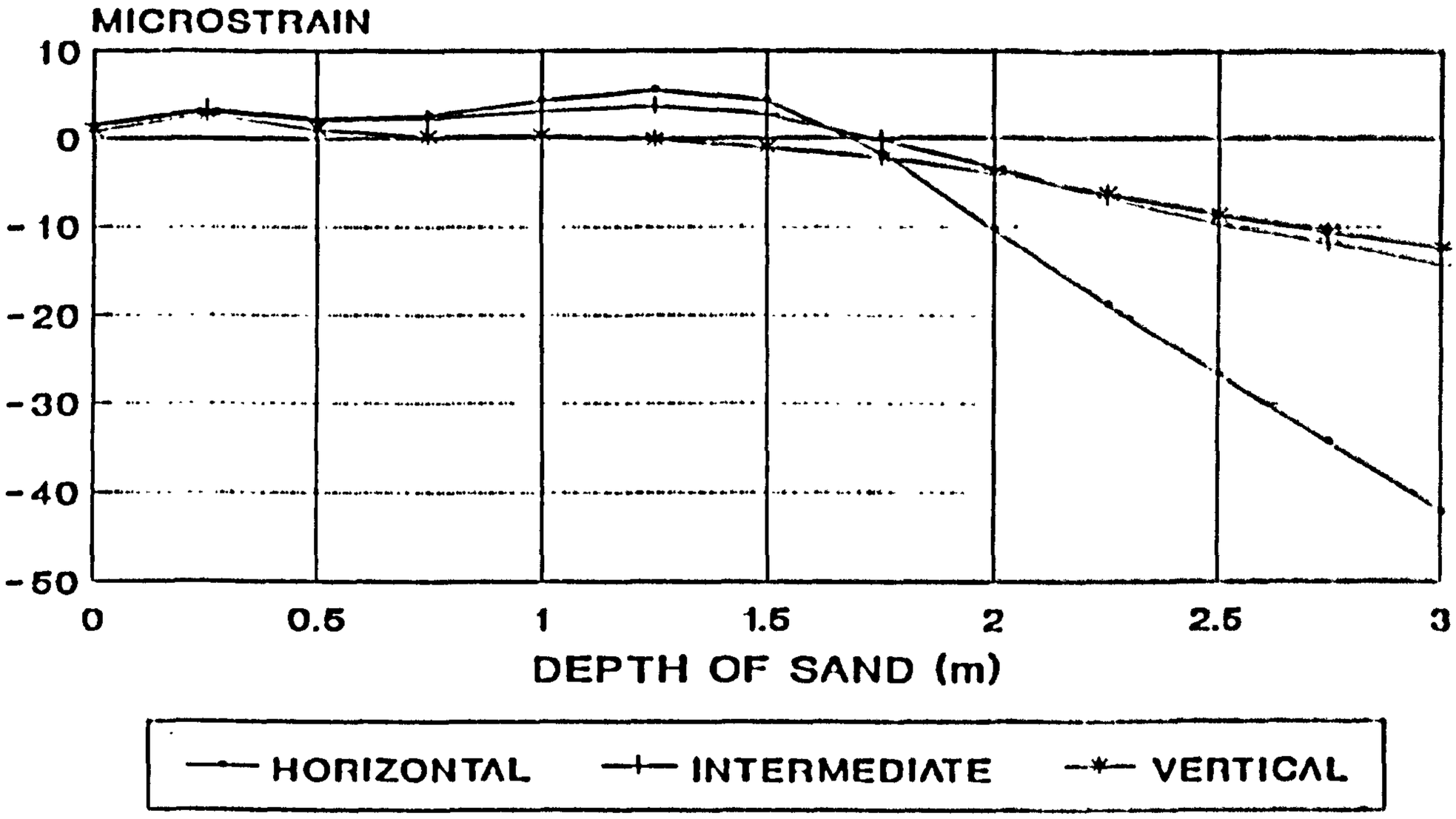

Figure B19

STRAIN GAUGE RESULTS
POSITION 'S20'

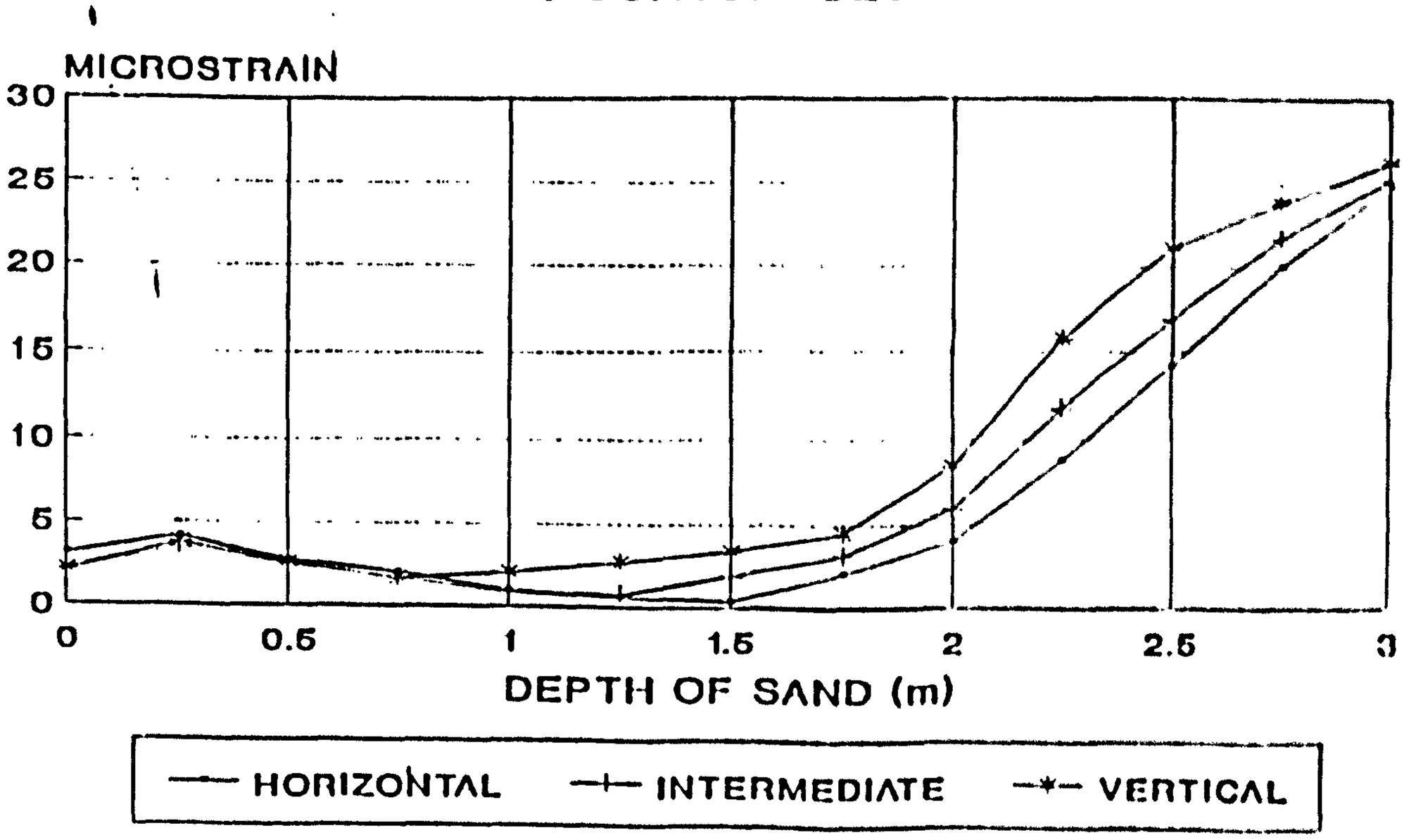

Figure B20

STRAIN GAUGE RESULTS
POSITION 'S21'

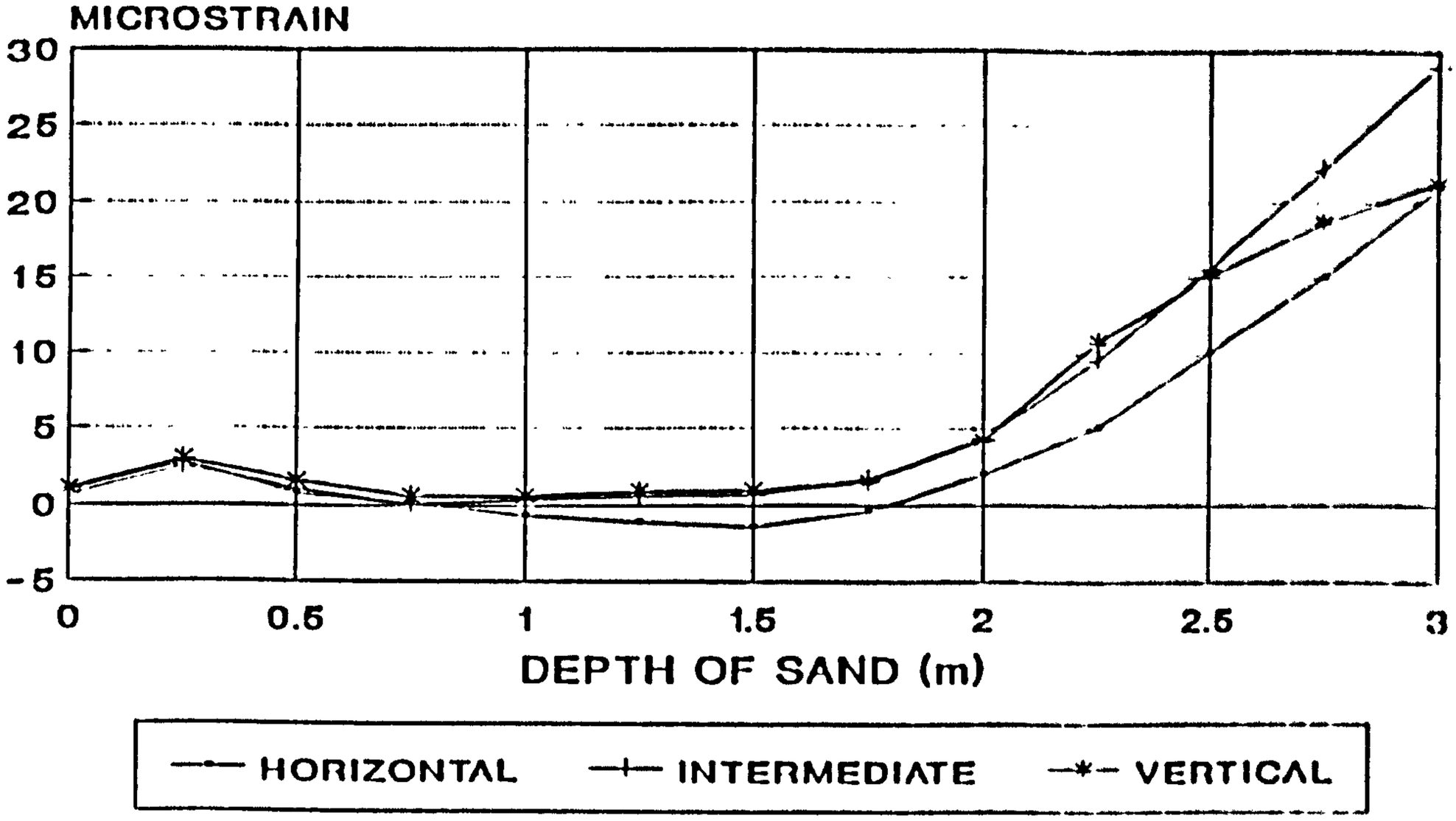

Figure B21

STRAIN GAUGE RESULTS
POSITION 'S22'

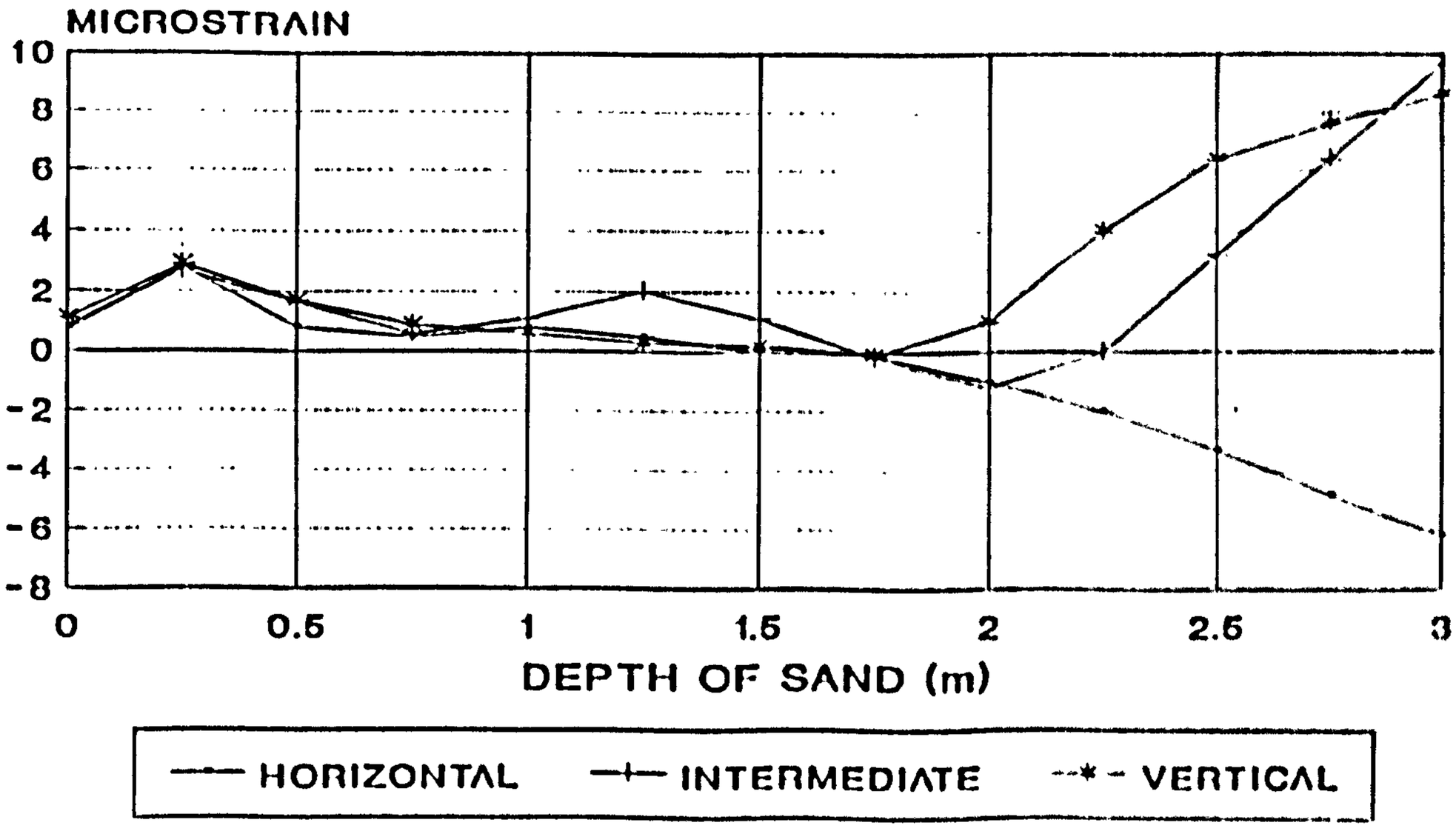

Figure B22

STRAIN GAUGE RESULTS
POSITION 'S23'

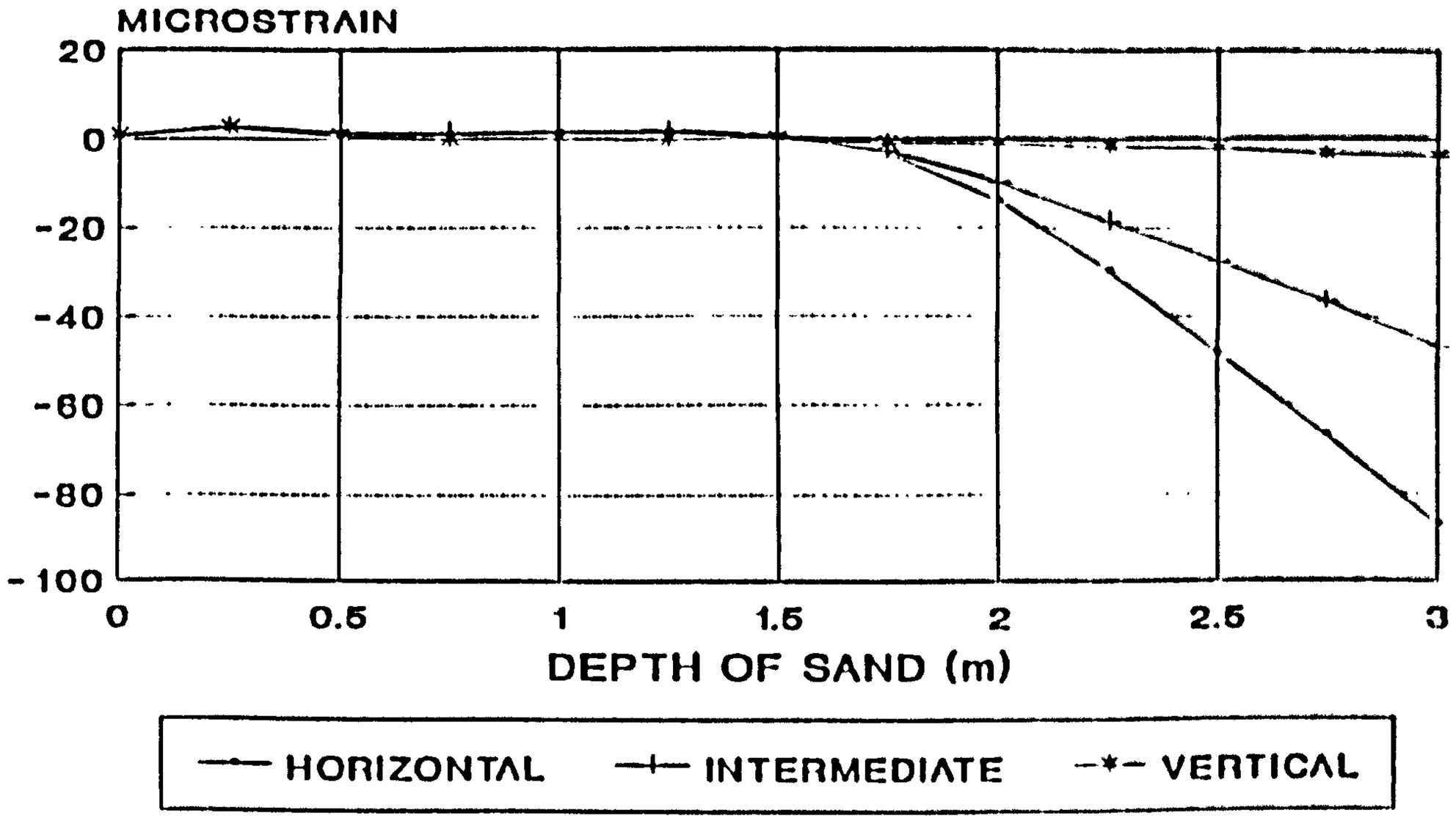

Figure B23

STRAIN GAUGE RESULTS
POSITION 'S24'

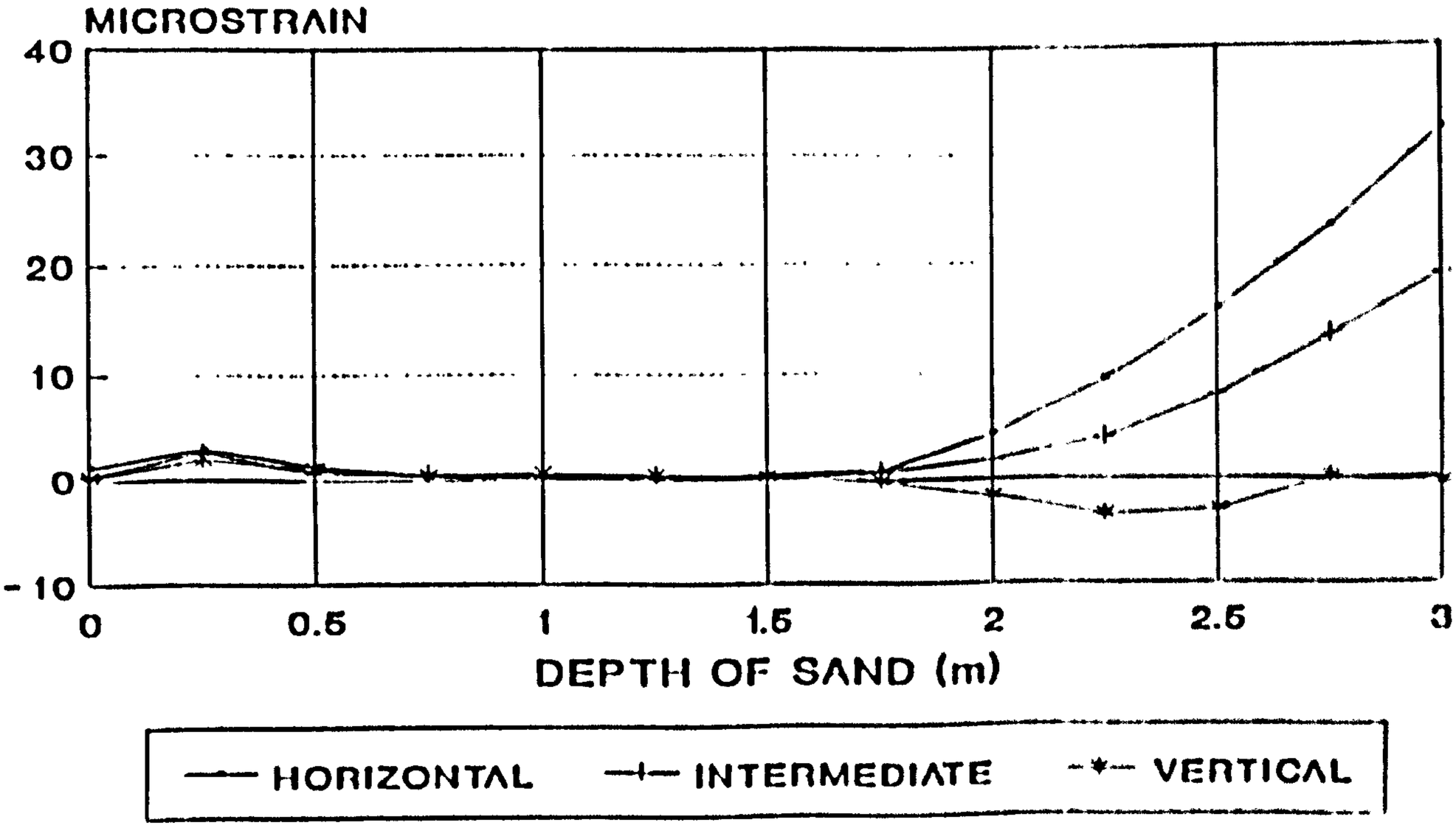

Figure B24

STRAIN GAUGE RESULTS
POSITION 'S25'

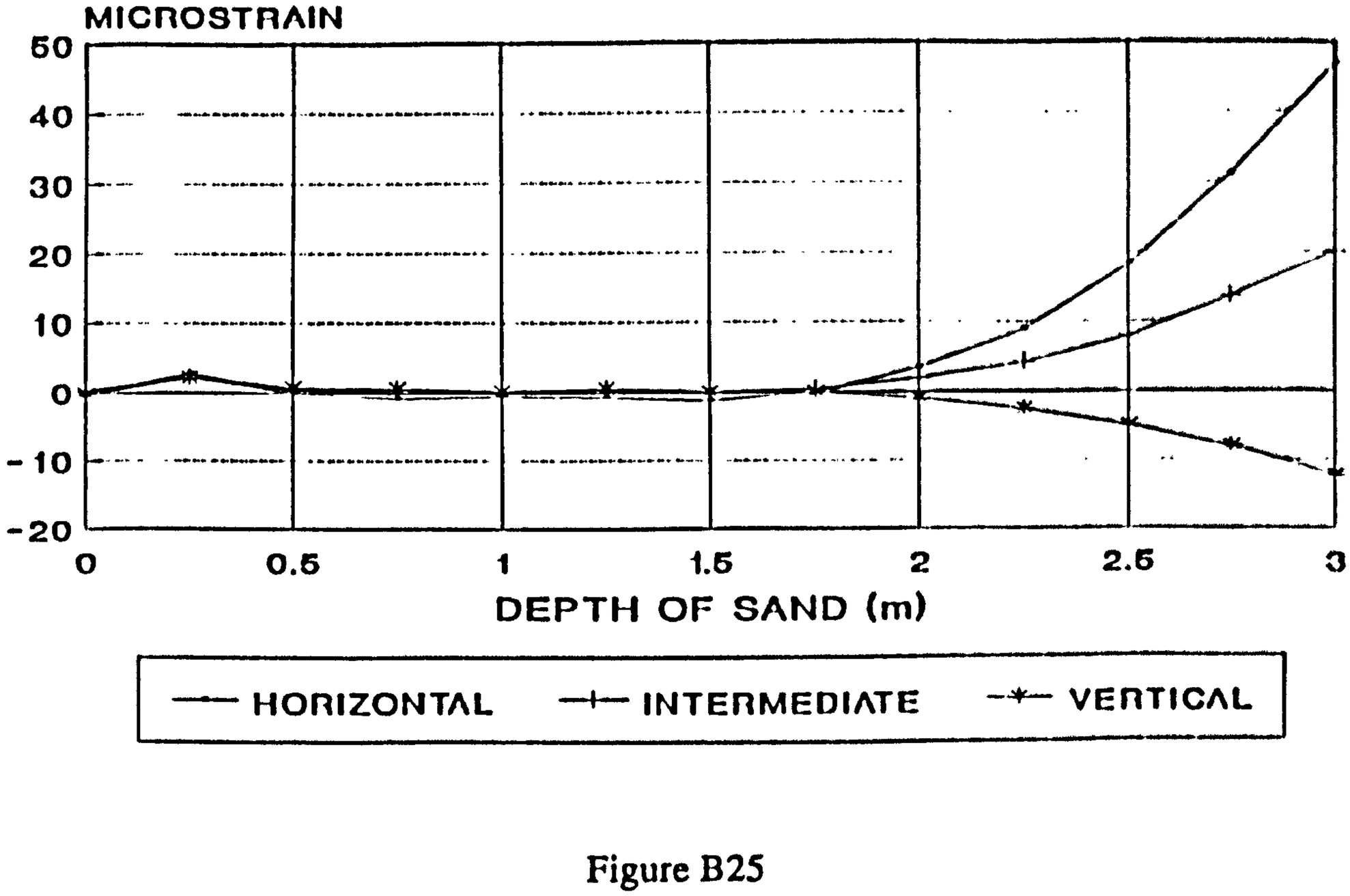

Figure B25